Bridge River Project Water Use Plan

Carpenter Reservoir Productivity Model Validation and Refinement

Implementation Year 2

Reference: BRGMON-10

Study Period: 2016-2017

Jennifer Harding, Roger Pieters, Chris Perrin, Dan Robb, Shauna Bennett and Greg Lawrence

April 7, 2017

ST'ÁT'IMC
ECO-RESOURCES

CARPENTER RESERVOIR PRODUCTIVITY MODEL VALIDATION AND REFINEMENT
PROGRESS IN 2016-2017

Bridge – Seton Water Use Plan Study Number BRGMON#10

April 7, 2017

LIMNOTEK

CARPENTER RESERVOIR PRODUCTIVITY MODEL VALIDATION AND REFINEMENT

PROGRESS IN 2016-2017

Bridge – Seton Water Use Plan Study Number BRGMON10

Submitted to
BC Hydro
Burnaby, B.C.

Prepared by:
Jennifer Harding, PhD, Roger Pieters, PhD, C.J. Perrin, MSc., RPBio., Dan Robb, PhD candidate,
Shauna. Bennett, MSc., RPBio, and Greg Lawrence, PhD.

April 7, 2017

Citation: Harding, J.N., R. Pieters, C.J. Perrin, D. Robb, S. Bennett, and G. A. Lawrence. 2017. Carpenter Reservoir Productivity Model Validation and Refinement (BRGMON10): Progress in 2016-2017. Report prepared for BC Hydro. 167p.

The study was managed by St'at'imc Eco-Resources Ltd.

Cover photo: Carpenter Reservoir, June 17, 2015: C. Perrin photo

EXECUTIVE SUMMARY

This report provides information for sample collection, laboratory work, and analyses from 2015 and 2016 that is required to answer four management questions addressing uncertainties about relationships between water management actions and biological production in Carpenter Reservoir. Statistical modeling and a hydrodynamic model called CE-QUAL-W2 both using empirical data from 2015 and 2016 were developed in 2015-16, refined in 2016-17 for this report and will undergo further refinement and finalization in 2017-2018 to answer the questions for BRGMON10. Progress in 2016-17 is as follows.

Question 1: Is light the primary factor regulating productivity of littoral habitat in Carpenter Reservoir?

Littoral production was assessed using a novel yet basic study design that was meant to capture the variation in algal accrual on substrata installed in Carpenter Reservoir. Multiple arrays of polystyrene balls were deployed at various depths in the reservoir as well as in Anderson and Seton Lakes. The polystyrene balls were meant to simulate stony substrate common amongst all three water bodies while sand pails were deployed in Carpenter Reservoir only, to simulate growth on smaller substrate unique to Carpenter. Based on an initial analysis of the 2015 and 2016 data, light was an important driver of littoral periphyton production on stony substrates as was water temperature and dissolve inorganic nitrogen (ammonium (NH_4-N) plus nitrate (NO_3-N) concentration. Light was less important in driving variation in periphyton accrual on sand. Temperature, turbidity and dissolved inorganic nitrogen concentration were better predictors of periphyton accrual on sand.

The periphyton community was different between the polystyrene and sand samples. The former mainly comprised attached chlorophytes and diatoms while taxa on sand were primarily chryso-cryptophytes (flagellated organisms more commonly found in the pelagic habitat). Entrainment during sample removal may have introduced pelagic species to the sand samples and could explain the low explanatory power of the models for chlorophyll-a on sand in Carpenter Reservoir. There was also 2-20x more biomass collected from the polystyrene balls than from the sand samples. The variation in community composition and size are likely responsible for the different responses to environmental variables tested in the regression models.

Next steps include integrating the CE-QUAL-W2 model results (see Question 3) once they are complete. A final version of the periphyton regression model will be presented in the 2018 final report.

Question 2: Is light the primary factor regulating productivity of pelagic habitat in Carpenter Reservoir?

Pelagic production was measured as phytoplankton and zooplankton production and biomass. This report includes a regression analysis for phytoplankton primary productivity and biomass as well as zooplankton biomass.

Phytoplankton productivity and biomass were measured monthly from May to October in Carpenter Reservoir and May to September in Anderson Lake and Seton Lake at 6 to 7 depths throughout the euphotic zone in 2015 and 2016. Primary productivity in the pelagic zone increased with increasing light and water temperature but decreased with increasing water residence time, turbidity, dissolved inorganic nitrogen concentration and soluble phosphorus concentration. From this initial analysis, PAR was a primary factor regulating productivity in the pelagic zone having at least 2x the effect on primary productivity compared to other predictor variables included in the analysis. Interestingly, phytoplankton biomass was negatively correlated with light, temperature as well as water residence time, turbidity and dissolved forms of nitrogen and phosphorus. Despite chlorophyll-a concentration being a measure of phytoplankton biomass, which requires light for photosynthesis, figures for each predictor variable by depth and time revealed the chlorophyll-a maxima occurred between 3 and 30 m depending on the reservoir or lake, which explains the negative correlation between biomass and PAR. The relationship between chlorophyll-a and the environmental predictor variables will be further investigated as the modeling approach is refined.

Zooplankton biomass was measured monthly from May to October in Carpenter Reservoir and May to September in Anderson and Seton Lakes along with environmental variables deemed important for zooplankton biomass. We found that zooplankton biomass increased with increasing water residence time and temperature but declined with the smaller size class of phytoplankton and turbidity.

Of the variables found to be important determinants of phytoplankton and zooplankton production, water residence time is one measure that can be altered through water use plans by increasing or decreasing the outflow in Carpenter Reservoir. The averaged models showed there was a weak negative relationship between phytoplankton and water residence time while zooplankton biomass increased with residence time. Despite zooplankton biomass increasing with water residence time by approximately 70 mg dry weight/m^2 over a doubling in water residence time, the effect of water temperature was much more pronounced. A 77% increase in zooplankton biomass was correlated with a 2.8 °C increase in water temperature. This correlation may be due to the seasonal patterns in species phenology, which will be further explored in subsequent analyses.

Based on the model fits (r^2) and coefficients for each response variable, it is possible that by including data from Anderson and Seton Lakes with data from Carpenter Reservoir, we have introduced too much variation in the predictor variables to

accurately explain the processes in Carpenter Reservoir. We will address this in the coming year by exploring the statistical implications of removing data from Anderson Lake and modelling the data for Carpenter Reservoir and Seton Lake separately. We will also continue to refine the CE-QUAL-W2 model and incorporate output for key scenarios with the final regressions in 2018.

Question 3: Is light penetration in Carpenter Reservoir impacted by changes in reservoir operations?

Simulation modeling supported with empirical data is being used to answer questions 3 and 4. The simulation model is CE-QUAL-W2, which is a hydrodynamic and water quality model for rivers, lakes, reservoirs and estuaries. CE-QUAL-W2 laterally averages calculations (across channel) with segments along the length of the water body, and bins from the surface to the bottom.

An interface was developed in MATLAB for reading and writing data to and from CE-QUAL-W2. The simulation model was set up to simulate conditions measured in 2015 and was adjusted to include the 2016 data.

Three model scenarios were developed and are presented as examples in this report. The first two scenarios simulated conditions in 2015 and 2016, which were used to validate the model against the field data. The third scenario was developed using the flow and water level data from 2009 but because meteorological forcing and tributary water quality data were not available for 2009, data from 2015 were used. We selected 2009 because the water level in Carpenter and inflow through La Joie dam were very low compared to 2015 and 2016. The 2009 conditions were only used as an example of how very different flows may influence endpoints. Output from these three scenarios were used to model phytoplankton biomass, measured as chlorophyll-a concentration, and compared against the actual model results for 2015 and 2016. Though the magnitude of the coefficients did not match, the direction did in all but two cases. Further refinement of the regression and CE-QUAL-W2 modelling will be required in 2017-2018 to improve their accuracy but the potential for using CE-QUAL-W2 to assist in predicting outcomes for response variables from management decisions is improving.

With this model, we will be able to show the sensitivity of biological production to various management actions and to natural processes in Carpenter Reservoir.

Question 4: Can suspended sediment transport into Seton be altered by changes in Carpenter Reservoir operation?

To answer this question, we will need to integrate all the information from the regression analyses for biological production and data from the CE-QUAL-W2 model, which will occur in 2017 and be ready for the final report in 2018.

A summary of the status of BRGMON10 study findings is listed in the following table:

Study objectives	Management questions	Status
Determine if light or other environmental variables affect periphyton production on sand or stony substrate in Carpenter Reservoir.	Is light the primary factor regulating productivity of littoral habitat in Carpenter Reservoir?	The study is on track to answering this management question with additional model refinement in 2017-2018 using the current approach/study design
Determine if light or other environmental variables affect phytoplankton and zooplankton production in pelagic habitat in Carpenter Reservoir.	Is light the primary factor regulating productivity of pelagic habitat in Carpenter Reservoir?	The study is on track to answering this management question with additional model refinement in 2017-2018 using the current approach/study design
Determine whether water management in Carpenter Reservoir affects light penetration or other environmental variables.	Is light penetration in Carpenter Reservoir impacted by changes in reservoir operations?	The study is on track to answering this management question with additional model refinement in 2017-2018 using the current approach/study design
Determine if changes to reservoir operation affect the inflow of suspended sediment into Seton Lake.	Can suspended sediment transport into Seton be altered by changes in Carpenter Reservoir operation?	The study is on track to answering this management question with additional model refinement in 2017-2018 using the current approach/study design

ACKNOWLEDGEMENTS

This project was performed under contract to BC Hydro as part of the Bridge River Water Use Plan Studies. The authors thank many people who contributed to the project as follows. Bonnie Adolf (Project Coordinator), Gilda Davis (contract manager), and Jude Manahan (bookkeeper) with St'at'imc Eco-Resources Ltd. (SER) are thanked for contract administration. Dave Marmorek (ESSA Technologies Ltd.) is thanked for discussions about study design in early phases of the project.

We thank the 2015 and 2016 field crew including Annika Putt, Marc Laynes, Tyler Creasey, Allison Hebert, Jeff Sneep, and Allison James for energy and enthusiasm to complete long and often complicated days in the field. Allison Hebert worked with Shannon Harris to complete lab work and calculations for the primary production measurements. The field crew was assisted by L.J Wilson and Caroline Melville who were safety check-in people on most field days.

Chemical analyses of stream and lake water samples and periphyton biomass were completed at ALS Environmental under the management of Courtney Duncan. Chemical analysis of passive samplers and ion exchange columns was completed by Dr. Julian Aherne and Jaime Morrison of Trent University. Danusia Dolecki performed the zooplankton enumerations and biomass measurements and Lech Dolecki completed the algal cell identifications, enumerations, and bio-volume measurements.

Odin Scholz (Split Rock Environmental Ltd.) and Brad Oleman (BC Ministry of Forests Lands and Natural Resource Operations) are thanked for support on access to meteorological data from the 5-Mile Forest Service weather station. We are grateful to Dr. David Levy, Fisheries Advisor to SER for numerous discussions regarding study scope and integration with other SER projects. Joes Goes in 2015 and Frank Richings in 2016 are thanked for organizing access for our crew to use the boat ramp at the east end of Anderson Lake. Mike Chung is thanked for assisting with data entry from field and lab sheets.

Several people from BC Hydro are thanked for attention to contract management with SER and for the provision of hydrology data from BC Hydro Power Records. They included Teri Neighbour, Dr. Ahmed Gelchu, Darin Nishi, and Jeff Walker. Jim Coles (Area Manager, BC Hydro), Rick Enegren (Dam Safety Engineer, B.C. Hydro), and Mark Thorsteinson (Dam Safety Engineer, B.C. Hydro) are thanked for approving our installation of meteorological instruments and samplers on the Terzaghi Dam and for approving our installation of samplers on the trash boom in Carpenter Reservoir. Eduardo Martins provided valuable feedback on the 2015-2016 Annual Progress Report, which was used to improve the draft report for this year.

GIS analysis and mapping in support of the CE-QUAL modeling was completed by Nicole Fink (GIS Specialist, BC Hydro) and Faizal Yusuf (Hydrotechnical Engineer, BC Hydro). Meaghan Leslie-Gottschligg produced the site location map. Special thanks

goes to Dorian Turner of BC Hydro for arranging a location on grounds of the BRG1 generating station for us to install a solar radiation sensor and for organizing building space on the same property for our field crew to set up and operate a field lab. We would also like to thank Adjoa Quanioo and Alex Huang, UBC co-op students, who helped with the CE-QUAL-W2 modelling as well as Thea Rodgers and Melanie Mewhort who helped with instrument servicing and data analysis and whose salaries were subsidized by the UBC Work Learn program.

TABLE OF CONTENTS

Page

LIST OF FIGURES

Page

LIST OF TABLES

Page

1 INTRODUCTION

The Bridge-Seton Water Use Plan Consultative Committee (CC) developed aquatic ecosystem objectives for the Bridge River watershed that included efforts to maximize the abundance and diversity of fish populations while establishing flow controls for hydroelectric power generation, among other interests (Bridge River WUP CC, 2003). The Bridge River watershed provides habitat for resident fish species, which are valued from commercial, recreational, and cultural perspectives. Tradeoffs occurred in the water use planning, resulting in decisions to set water elevations in reservoirs of the Bridge River watershed (Downton, Carpenter, Seton), manage spills from the reservoirs, and define flows in rivers (Middle and Lower Bridge River, Seton River). The complete package of flow controls is collectively known as N2-2P. While N2-2P was accepted, the Bridge River WUP CC (2003) was constrained in making decisions by lack of information about the effects of change in flows on fish populations and biological production that support those populations. Despite this uncertainty, N2-2P was implemented on March 30, 2011 (Water Act Order 2011, Bridge River Power Development Water Use Plan, 17 March 2011) with a commitment to fund monitoring studies to fill data gaps and better inform people tasked with water management decisions in future years, including the St'át'imc people and St'át'imc Eco-Resources Ltd. (SER).

Uncertainty among members of the Consultative Committee included unknown effects of low water temperature and turbidity produced by flow from upper reaches of the Bridge River on biological production in Carpenter Reservoir and the effect of the diversion of that cool and turbid water on sockeye salmon and Gwenis in Seton Lake. A small diversion of water from the Bridge River to Seton Lake started in 1934. The diversion increased in 1954 to power four turbines at Shalalth (located on the north shore of Seton Lake, Figure 1) and it was fully developed by 1960 with the installation of four more turbines. Effects of this diversion on fish populations were first investigated by the International Pacific Salmon Fisheries Commission (Geen and Andrew 1961) and later by Fisheries and Oceans Canada (Shortreed et al. 2001). Those studies suggested the diversion of cold and turbid water from the glacial Bridge River and Carpenter Reservoir, reduced water temperature, increased light attenuation, and decreased primary productivity in Seton Lake. These observations imply the existence of a "footprint" impact on fish production in Seton Lake due to the diversion that is being further investigated in water use plan monitoring study number BRGMON6 (Limnotek 2017).

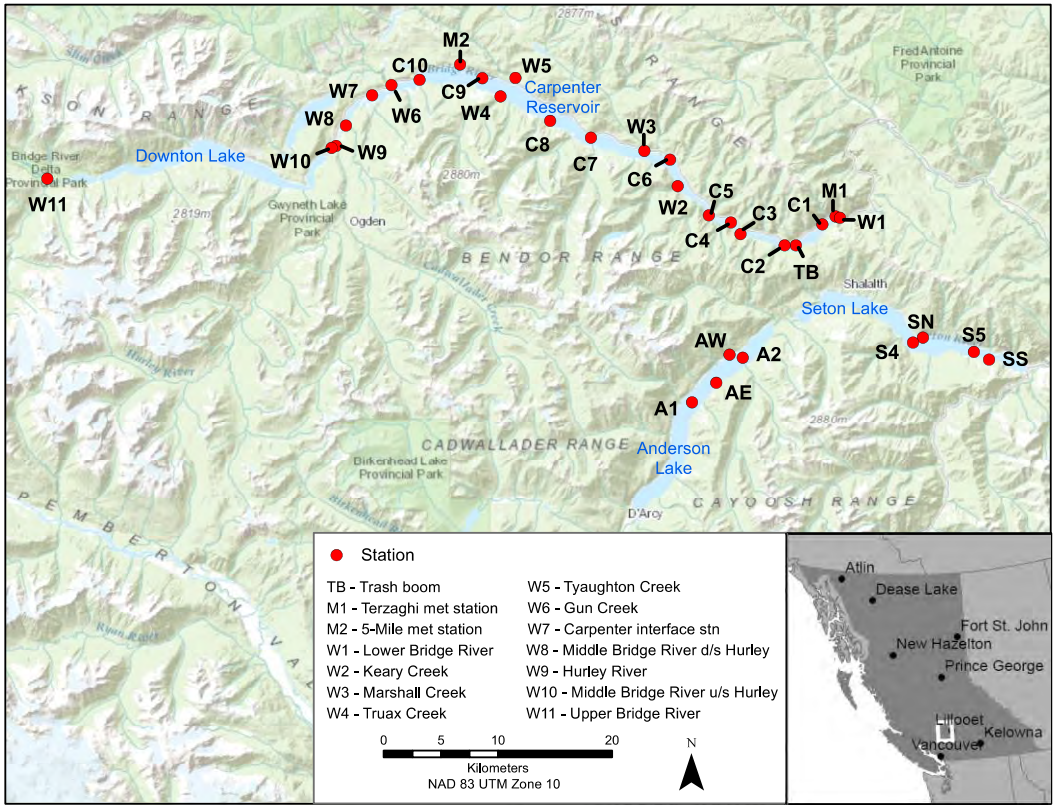

Figure 1. Sampling stations and landmarks in Carpenter Reservoir, Anderson Lake and Seton Lake. Stations C1 through C10 were stations for physical and chemical profiling along the longitudinal axis of Carpenter Reservoir. The "W" stations were tributary inflows and the "M" stations were meteorological stations. Periphyton moorings in Anderson Lake were labelled AW and AE and in Seton Reservoir they were labelled SN and SS. Chemistry and biological sampling stations in Anderson Lake were labelled A1 and A2 and in Seton Reservoir they were labelled S4 and S5.

Light was a focus of what is known as the Carpenter Reservoir Productivity Model (CLRPM) that was produced earlier for the Consultative Committee (Bridge River WUP CC. 2003). In that model, light solely limited biological production. There is no question that light or more correctly photosynthetically active radiation (PAR) limits photosynthesis that drives biological production in lakes and reservoirs (Wetzel 2001). A general rule is that photosynthesis is active where PAR occurs at intensities of more than 1% of irradiance at the water surface (Wetzel 2001). In addition to the basic physics of light attenuation in clear water, PAR attenuation is also affected by particles in water. In Carpenter Reservoir, those particles most notably include inorganic fines that are carried in suspension from upstream erosion by glaciers and snow fields in the headwaters of the Bridge River and potentially within the drawdown zone of Downton and Carpenter Reservoirs. The particles, measured as turbidty, increase PAR attenuation in the reservoirs, resulting in a smaller depth of photosynthetic production and shallower euphotic zone than would occur if turbidity was not present. However, the influx of organic and inorganic material, for example after a storm event, would increase turbidity in the reservoir, which could also benefit primary and bacterial production by increasing limiting nutrients (Guadayol et al. 2009; Liess et al. 2015). The assumption about light limitation of biological production in CLRPM was a statement about turbidity affecting the amount of habitat in Carpenter Reservoir where photosynthesis can occur but there are instances where turbidity could enhance primary productivity.

Within a water column where the amount of PAR is sufficient to support photosynthesis, production of algae can be limited by nutrient supply (Biggs 2000, Bothwell 1989, Guildford and Hecky 2000, Wetzel 2001), and temperature (Bothwell 1988, Goldman and Carpenter 1974) within available habitat, which is determined by water residence time, area of habitat, and volume of habitat that is influenced by reservoir filling and drawdown.

The CC found that uncertainties about the relative importance of the several habitat attributes that potentially drive biological production in pelagic and littoral habitats of Carpenter Reservoir and the influence of reservoir operations versus natural hydrology on those processes could not be resolved with existing information. Studies were recommended to fill data gaps and determine what water management actions, if any, could be used to mitigate effects of reservoir operations on biological production in pelagic and littoral habitat.

Four management questions resulted from analysis by the CC. They are listed as follows:

1) Is light the primary factor regulating productivity of littoral habitat in Carpenter Reservoir?
2) Is light the primary factor regulating productivity of pelagic habitat in Carpenter Reservoir?
3) Is light penetration in Carpenter Reservoir impacted by changes in reservoir operations?

4) Can suspended sediment transport into Seton be altered by changes in Carpenter Reservoir operation?

This report summarizes information from two years of data collection and analyses from Carpenter Reservoir as well as supporting information from Anderson and Seton Lakes. Using phytoplankton and zooplankton in pelagic habitat as examples, this report highlights the methods and analyses used thus far and it provides recommendations for subsequent analyses that are required to answer the above management questions as part of final reporting in 2018.

2 STUDY DESIGN AND METHODS

2.1 Study site description

2.1.1 Location, dimensions and geographic characteristics

Carpenter Reservoir is situated within the original Bridge River floodplain between the Bendor Range of the Coast Mountains to the south and the Shulaps Range, Pearson Ridge, and Marshall Ridge of the Chilcotin Ranges to the north. The reservoir was formed with construction of the Mission Dam on the Bridge River in 1960. In 1965 it was renamed the Terzaghi Dam. The dam is located 40 km upstream of the confluence of the Bridge River and the Fraser River near Lillooet. The width of the original flood plain and the present reservoir at the top water surface elevation is up to 1.5 km. Substrata within the draw down zone consists of a thin sediment veneer overlying glacial silts and sand with localized gravel and cobble remnants. At drawdown, the river typically erodes a profile of approximately 1 m below floodplain elevation, re-suspending substratum materials in the process. Deposits of organic debris including small branches and forest litter that is transported from upstream are evident in most locations where cut banks have been formed.

The Terzaghi Dam is located at a narrows between bedrock outcrops at the eastern extent of the original Bridge River floodplain. The dam was constructed over an original diversion dam that was built in 1948 (BC Hydro 1995). The dam is an earthfill structure, 60 m high with a crest length of 366 m. A spillway with two gates and a free overflow section is in rock on the right abutment. A low-level outlet tunnel is located below the spillway.

The Carpenter Reservoir, formed by the Terzaghi Dam, is 50 km long and has an average width of 1 km at full pool with a longitudinal axis lying east west. It extends westward from the Terzaghi Dam along the Bridge River floodplain. In 2016, the maximum reservoir surface elevation was 646.11 m on 14 October (BC Hydro Power Supply Operations). This elevation was 13.38 m higher than the elevation at complete drawdown that occurred on 18 April 2015 (BC Hydro Power Supply Operations). The reservoir surface area at full pool is 46.2 x 10^6 m^2 but it declines to approximately half this area at full drawdown. The dewatered area at drawdown occurs along 25 km of the

Bridge River floodplain in the western half of the reservoir. From the reservoir shorelines, ridges to the north rise to 2,445 m and peaks to the south are at elevations of more than 3,000 m.

Access to the reservoir is via a well-maintained gravel road on the north side. It connects the community of Gold Bridge with Lillooet. The road is maintained year-round.

Boat access to the reservoir is available at ramps located at Tyaughton Creek, a BC Hydro recreation site at Big Horn Creek, at Marshall Creek, and at the Terzaghi Dam. Ice cover develops over the reservoir in winter months thus preventing boat access at that time.

The dam is used to store water for power generation. Water is diverted through two tunnels located 3 and 4 km respectively upstream of the dam. The intake tunnels pass through Mission Mountain to the south and through penstocks to powerhouses called BRG1 and BRG2 located at Shalalth. Water discharges from BRG1 and BRG2 directly into Seton Reservoir (Figure 1).

2.1.2 Catchments and Tributaries

Main catchments that drain into the Carpenter Reservoir include the upper Bridge River (via Downton Reservoir), the Hurley River, Gun Creek, Tyaughton Creek, Marshall Creek and numerous other streams (Table 1). The Upper Bridge River upstream of the Hurley River confluence represents 26.7% of total catchment area for the reservoir. The Tyaughton Creek and Hurley River drainage are 20.5% and 18.2%, respectively, of the total catchment area. Other local drainages represent 34.6% of the catchment area.

Table 1. Catchment areas that drain into Carpenter Reservoir.

Drainage Name	Area (ha)	Percent of total area
Upper Bridge River	99,069	26.7
Tyaughton Creek	75,973	20.5
Hurley River	67,640	18.2
Marshall Creek	9,352	2.5
Gun Creek	58,988	15.9
Other local drainages	60,007	16.2
TOTAL (to Terzaghi Dam and tunnel intakes)	371,029	100

Most inflow is from the Upper Bridge River system that drains the Coast Mountains. Although Tyaughton Creek has a relatively large catchment area, it is all within the relatively dry Chilcotin Mountains and water yield is low compared to that from the upper Bridge and the Hurley Rivers. Water from the west and south originates as glacial meltwater at alpine elevations of the Coast Mountains (1,800 to 3,000 m). Parent materials in much of the headwater areas are granitic and volcanic and they have the potential to contribute phosphorus from rock weathering to drainage streams. The Bridge River is a 6th order system at the Carpenter Reservoir.

2.1.3 Reservoir Morphometry

Daily surface elevation and live storage volume were downloaded directly from BC Hydro, System Control Centre (Power Supply Operations). The storage data were from a regression model produced by BC Hydro that determines live storage volume as a function of water surface elevation. Volumes for the model were determined from interpretation of air photos taken at a low water surface elevation. Water surface area determined at several elevations on the air photo using planimetry multiplied by depth interval between elevations provided volumes for those selected elevations. For a given elevation, the sum of strata volumes below that elevation provided live storage volume. The calculated model is run daily to determine live storage volume from measurements of water surface elevation in the dam forebay at midnight.

The intake gates to the Seton Lake tunnels limit the lowest water surface elevation at 600.61m and 599.54 m (to bottom of gate). In 2016, the reservoir water surface elevation ranged from 632.73 m on April 18 to a maximum of 646.11 m on October 14 (BC Hydro Power Supply Operations). The original riverbed elevation immediately downstream of Terzaghi dam is approximately 609 m (Topographic map 92 J/16, 1992). Thus, the tunnels are located at approximately as low as the original riverbed and virtually the entire storage volume is available as live storage. Typical water depths in the region of the tunnels at full pool are 30-50m. A summary of morphometric features of the reservoir is shown in Table 2.

Table 2. Morphometric and bathymetric measures for Carpenter Reservoir.

Measure	Value at Maximum Water Elevation in 2016 (646.11 m)
Reservoir Length (km)	50
Average Reservoir Width (km)	1
Reservoir Area (ha)	46.2×10^6 m^2
Maximum water depth (m)	55
Live storage volume (m^3)	91.13×10^7 m^3
Dead storage volume	0
Total storage (m^3)	91.13×10^7 m^3

2.2 Study design and overview

Biological production is defined as algal production because photosynthetic algae are the only part of the food web that use PAR (the main variable of interest among management questions) as an energy source for production of organic matter. For question 1, algal production is measured as periphytic algal accrual in units of µg chl-a$\cdot cm^{-2}$ (Perrin et al. 1987, Bothwell 1988) where chl-a is chlorophyll-a, a primary plant pigment that is commonly used as a measure of biomass in algae (Wetzel 2001, Behrenfeld et al. 2005). Chlorophyll-a can be approximately converted to carbon (e.g. Riemann et al. 1989, Cloern et al. 1995, Li et al. 2010, Behrenfeld et al. 2005) to yield units of mg C$\cdot m^{-2}\cdot d^{-1}$. For question 2, algal production is the production of phytoplankton measured as the amount of ^{14}C incorporated into algal biomass in a 1 m^2 column of water, per unit time and expressed in units of mg C$\cdot m^{-2}\cdot d^{-1}$ (Steemann Nielsen 1952, Wetzel 2001). Phytoplankton biomass measured as chl-a concentration was also

measured because it is needed in calculations of algal production from the ^{14}C data. These measurements of algal production in each of littoral and pelagic habitats are standard procedures. They show the amount of carbon fixed per unit area per unit time, allowing direct comparison of amounts of algal production between pelagic and littoral habitats.

Fish populations that are of ultimate interest by the consultative committee ingest invertebrates or other fish as food sources. Invertebrates ingested by fish include zooplankton, benthic invertebrates that use bottom sediment as habitat and emerge through the water column during transition from larval and pupal stages to adults, benthic invertebrates that drift into the reservoir from tributary streams, and terrestrial insects that land on the water surface and fail to escape the surface tension. To facilitate bridging the gap between algal production and fish, zooplankton biomass was measured and modeled. Zooplankton are an important food source for Gwenish in the reservoir that in turn can be prey for the piscivorous bull trout (Griffiths 1999). In addition, zooplankton are sensitive to the hydrology of Carpenter Reservoir (Perrin and MacDonald, 1999). Hence, zooplankton are a good indicator of interactions between water management actions, natural hydrology, and food web processes supporting fish populations making them ideal for providing insight into links between primary production and fish.

2.3 Questions 1 & 2: Is light the primary factor regulating productivity of littoral habitat in Carpenter Reservoir and is light the primary factor regulating productivity of pelagic habitat in Carpenter Reservoir?

2.3.1 Periphyton production in the littoral habitat

Algal production in littoral habitat was measured as periphyton (algae growing on substrates) accrual on installed substrates (Bothwell, 1989, Perrin et al. 1987) using a novel and simple substrate sampling system. There are two common types of substrata in Carpenter Reservoir: stony materials that occur on steeper benches and sand flats that occupy most of the original river valley and dominate the drawdown zone. We used a customized sampler for each type of substrata. To represent stony sites, we deployed a sampler that consisted of six arrays of two replicate 2.5-cm diameter polystyrene balls attached at equidistant positions on a vertical mooring line over a depth that was 1.5 times the depth of the euphotic zone using horizontal line clips (Figure 2). To represent sand sites, six pairs of pails containing sand were suspended at different depths from vertical lines with the depth again being 1.5 times the depth of the euphotic zone (Figure 3). Sand for the pails was collected in early April 2015 from depths >10 cm among exposed sand flats within the Carpenter drawdown zone. Enough sand was stock piled for use in samplers for the duration of April through October. That sand was exposed for most of the previous winter. Collection of sand from below the sand surface was required to avoid presence of algal biomass in the samplers at the start of an incubation.

Figure 2. Polystyrene array used to represent periphyton growth on stony substrate in Carpenter Reservoir (Photo Credit: C. Perrin, 2015).

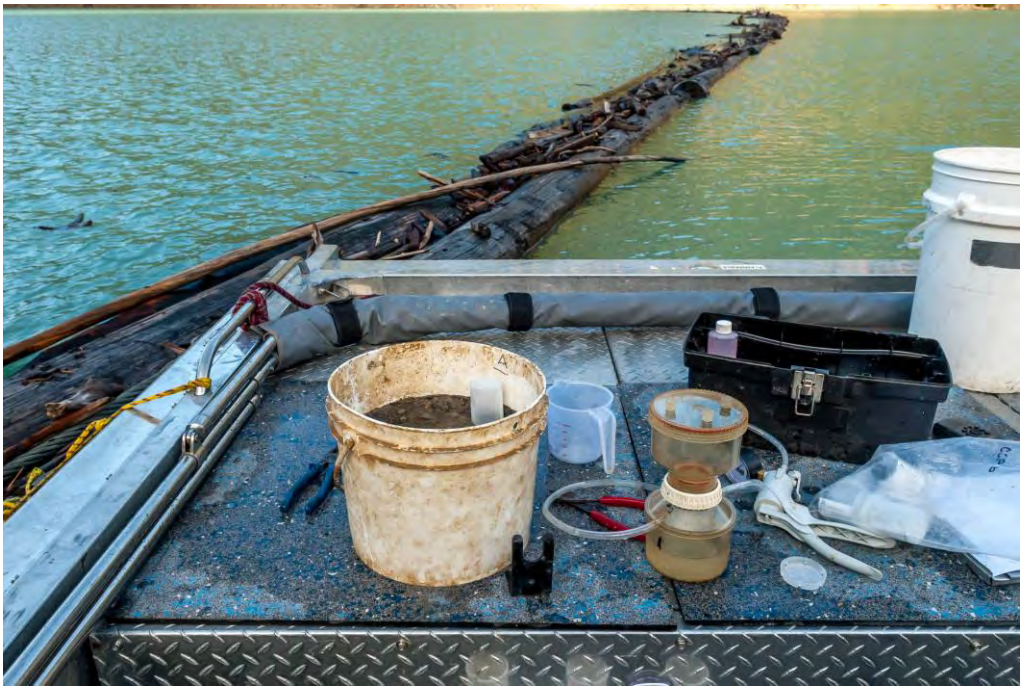

Figure 3. Sand pail used to represent periphyton growth on sand in Carpenter Reservoir (Photo Credit: C. Perrin, 2015).

The samplers were deployed during three time series. In 2015 Series 1 (spring) was April 16 to June 18, Series 2 (summer) was June 18 to August 12, and Series 3 (fall) was August 12 to October 20. In 2016 Series 1 (spring) was April 14 to June 16,

Series 2 (summer) was June 16 to August 11, and Series 3 (fall) was August 11 to October 13. A sampling time series involved installation of the samplers on the first day and removal on the last day, a period of approximately 2 months. On the transition day between sampling series in June and August, samples from the preceding series were collected and new substrata for the following series were installed.

The polystyrene and sand samplers were installed on moorings in each of the three reservoirs/lakes. Duplicate samplers of each type were installed at the trash boom in Carpenter Reservoir (C2; Figure 1). In each of Seton Lake (S4 and S5; Figure 1) and Anderson Lake (A1 and A2; Figure 1) a polystyrene sampler was installed on each of opposite shores in close proximity to stations used for measurements of algal production that was part of BRGMON6. Sand samplers were not installed in Seton or Anderson Lakes because they do not have sand substrata in littoral zones. In Seton and Anderson Lakes where there is little change in water surface elevation, the mooring line was secured between an anchor and submerged float. Depth of the samplers were recorded based on their distance from the anchor and depths recorded by a depth logger that was attached to the anchor. In Carpenter Reservoir where there was a continuous increase in water depth in spring through fall, mooring lines were secured to the trash boom that crosses the reservoir (Figure 1). This approach ensured that the sampler arrays maintained constant depth during incubation in Carpenter Reservoir.

2.3.1.1 Chlorophyll-a

Each polystyrene sampler was deployed with clean polystyrene balls. One polystyrene ball (surface area = 19.63 cm^2) from each of the duplicate samplers from each depth was retrieved after the approximate 60-day incubation period (mean $\pm$ standard deviation; 61.83 days $\pm$ 4.67). Each ball with adhered biomass was placed into a labelled plastic vial and packed on dry ice for shipment to the lab. Each ball was analyzed for biomass measured as chlorophyll-a concentration (corrected by sample surface area). Chlorophyll-a was extracted in 5 ml of 90% acetone and stored in the dark for 20 to 24 hours at –20 ^{o}C. The polystyrene dissolved in the acetone leaving only the chlorophyll extract in solution. Fluorescence of the acetone extract was measured before and after the addition of three drops of 10% HCl in a Turner Designs™ Model 10-AU fluorometer that was calibrated with a solution of commercially available chlorophyll-a. Calculations to determine chlorophyll-a concentration were made using equations reported by Parsons et al. (1984). Three blank balls that were not deployed at sampling sites were processed the same way to measure starting biomass. In each case, biomass on the blank replicates were below the detection limit of the fluorometer and assumed to be zero.

Each sand sampler was a pail with a surface area of 551.5cm^2 filled to 2/3 of total volume with new sand. After approximately 60 days of incubation (61.59 days $\pm$ 4.97) a sample (8-15.9 cm^2) was removed from each of the duplicate pails with a separate plastic vial. As with the polystyrene balls, the vials were capped, packed on dry ice for

shipment to the lab and analyzed for chlorophyll-a concentration (corrected by sample surface area) using the same methods as for the polystyrene samples.

2.3.1.2 Species composition

An additional sample was collected from each of the polystyrene and sand samplers closest to the surface for analysis of species composition.

In the laboratory, each sand sample was shaken vigorously for 1 minute, emptied into a graduated cylinder and the volume of the sample solution was recorded. Then the sample was diluted according to the amount of sediment in the sample to avoid covering the algal cells by the sediment. The different volumes of aliquots were pre-settled in settling chambers to determine proper concentration of subsamples used for counting.

Processing of the polystyrene ball periphyton samples first required the modification of an existing sample jar lid for adaptation to a “Waterpik Flossing System”. This system was used for accurately clearing the porous polystyrene surface of algae and debris using high-pressure water injection. The modification of the sample jar lid required the drilling of two small holes. One hole (approximately 3mm in size) was needed for a snug fit of rubberized Waterpik system injection nozzle. The other smaller hole on the opposite end of the lid was made to allow for air to escape as the sample jar would fill up with water without allowing the splash of sample contents to escape.

After a modified sample jar was prepared, a sample with an original and unmodified lid was shaken vigorously for 30 seconds and had its contents emptied into a graduated cylinder. The volume of the liquid contents was then recorded. Next, the polystyrene ball was taken out using forceps and mounted onto a skewer and placed back in the jar. The skewer prevented the polystyrene ball from spinning and moving around during Waterpik pressure wash. The jar was then closed using the modified pressure wash lid.

The Waterpik flossing system was set to its maximum setting of 12 PSI spray and the nozzle was then inserted through the larger hole in the lid. While observing the direction of spray, the nozzle was adjusted accordingly to pressure wash the entire hemisphere of the polystyrene ball. After one hemisphere had been thoroughly power washed, the lid was opened and the position of the skewer mounted polystyrene ball was inverted. The pressure washing procedure was the repeated to wash the other hemisphere of the polystyrene ball.

Once the polystyrene ball had been thoroughly washed, the lid was removed and the polystyrene ball was then held by the skewer within the sample jar. Lastly, the ball was gently scrubbed using an electric toothbrush to remove any remaining visible debris off and rinsed into sample jar using the gentle spray of filtered water from a squeeze bottle.

Algal cell counts and measurement of biovolume by species was conducted the same way for each of the sand and polystyrene samples once sample was prepared in

the settling chambers. Chamber contents were settled for 24 hours. Cell counts and biovolume measurements were completed at 500x magnification under an Olympus CK20 Inverted Microscope. Only cells containing cytoplasm were enumerated. A minimum of 100 cells of the most abundant species and a minimum of 300 cells in total were counted per sample. Biovolume, by species, was determined by multiplying cell counts by the volume of representative geometric shapes or combination of shapes that most closely approximated cell shape.

2.3.2 Phytoplankton production in the pelagic habitat

In 2015 and 2016, monthly chlorophyll-a concentration was measured at 6 to 7 depths through the euphotic zone at site C2 from May through October on Carpenter Reservoir as part of BRGMON10 and at sites A1 and S4 from May to September on Anderson and Seton as part of BRGMON6. Integrated samples were collected over the entire euphotic zone for sites C6 (Carpenter), A2 (Anderson) and S5 (Seton) in 2015 and 2016.

The algal production measurements were done *in situ* as the amount of ^{14}C incorporated into particulate organic carbon. Discrete water samples collected with a Van Dorn water bottle from the six depths over the profile of the euphotic zone were transferred directly into two light and one dark 300 ml acid-cleaned BOD glass bottles assigned as a group of bottles to each depth; hence there were six sets of two light and one dark bottle. Each BOD bottle was rinsed three times with the sample before filling. The water samples were maintained under low light conditions during all manipulations until the incubation was started within 1 h of the water collections. Water in the BOD bottles were inoculated with 0.185 MBq (5 µCi) of $NaH^{14}CO_3$ New England Nuclear (NEC-086H). The cluster of BOD bottles for each depth were attached to an acrylic plate and suspended at each of the six depths from which the water samples were taken. These samples were then incubated *in situ* for 4-5 h between the hours of 1000 and 1500 to allow the carbon uptake to proceed. Following retrieval of the incubation array, the BOD bottles were transported to facilities at BC Hydro in Shalalth in a cool dark box.

The incubations were terminated by parallel filtration of 100 ml of sample onto 0.20 and 0.75 µm polycarbonate Nucleopore™ filters, the same pore sizes used for primary production measurements on Seton and Anderson Lakes. Each folded wet filter and retained biomass were placed in a 7 mL scintillation vial and stored in the dark until processing at the University of British Columbia.

In the fumehood, 100 µL of 0.5 N HCl was added to each vial to eliminate the unincorporated inorganic $NaH^{14}CO_3$. The scintillation vials were then left uncapped in the fumehood for approximately 48 h until dry. After 5 ml of Scintisafe® scintillation fluor was added to each vial, and stored in the dark for >24 hours, the samples were counted using a Beckman® Model #LS 6500 liquid scintillation counter. Each vial was counted

for 10 minutes in an external standard mode to correct for quenching. The specific activity of the stock was determined by adding 100 μL ^{14}C-bicarbonate solution to scintillation vials containing 100 μL of ethanoalamine and 5 ml Scintisafe® scintillation cocktail. Calculation of rates of carbon incorporation followed methods reported by Parsons et al. (1984). Primary productivity values were vertically integrated according to procedures of Ichimura et al. (1980) for calculation of annual rates of primary production and each value from a discrete depth were considered to be independent observations for the regression modeling. Daily rates of primary production were calculated by multiplying the hourly primary productivity by the incubation time and by the ratio of the solar irradiance during the incubation to the solar irradiance of the incubation day where solar irradiance was measured using a Li-Cor irradiance meter. Corrections for solar irradiance over periods of time were determined from ambient irradiance logged using a sensor and data logger installed at a meteorological station at the Terzaghi Dam for the during sampling (May – October). The difference between the ^{14}C incorporation in the light bottles (includes photosynthetic and non-photosynthetic uptake) and the ^{14}C incorporation in the dark bottle (includes only non-photosynthetic ^{14}C uptake) indicated carbon uptake by photosynthesis.

Chlorophyll-a concentration was determined by *in vitro* fluorometry (Yentsch and Menzel, 1963) in aliquots from each of the six water samples that were used for primary production analysis. The aliquots were parallel filtered through 0.20 and 0.75 μm polycarbonate Nucleopore™ filters as was done for the aliquots used for primary production analysis using a vacuum pressure differential of <100 mm of Hg. Care was taken to limit light exposure of the chlorophyll samples during field handling of water samples and laboratory analysis. The water filtrations were completed on the day of sample collection at the Shalalth field lab. The filters with phytoplankton biomass were stored in the dark at –20°C prior to analysis at the University of British Columbia. Chlorophyll-a was extracted in 5 ml of 90% acetone and stored in the dark for 20 to 24 hours at –20°C. Fluorescence of the acetone extract was measured before and after the addition of three drops of 10% HCl in a Turner Designs™ Model 10-AU fluorometer that was calibrated with a solution of commercially available chlorophyll-a. Chlorophyll-a concentration was determined using equations reported by Parsons et al. (1984).

At the same stations where chlorophyll-a concentration was measured, aliquots from a depth integrated water sample were collected for phytoplankton cell enumeration by species. These data were used to describe the assemblage of algae that is contributing to the pelagic algal production. The depth integrated water sample was prepared by mixing equal aliquots of water from at least three depths in the euphotic zone. An aliquot was dispensed to a glass amber jar, preserved with acid-Lugol's solution, and stored in a cool and dark location until the algal cells were counted. Prior to the enumeration, the samples were gently shaken for 60 seconds and allowed to settle in 25 mL chambers for a minimum of 8 hrs (Utermohl 1958). Counts of algal cells, by taxa, were done using an inverted phase-contrast plankton microscope. Cells of large micro-plankton (20-200 μm) were counted at 250X magnification. All cells within

one 10-15 mm random transect were counted at 1560X magnification. In total, 250-300 cells were counted in each sample. The biovolume of each taxa were determined as the cell count multiplied by the volume of a simple geometric shape corresponding most closely with the size and shape of the algal taxon. Canter-Lund and Lund (1995) and Prescott (1978) were used as taxonomic references.

2.3.3 Zooplankton production in the pelagic habitat

Zooplankton biomass was measured monthly from May to October from duplicate vertical hauls of a 153 µm mesh Wisconsin net having a 30 cm intake opening. The depth of haul was 30m or the complete water column where and when water depths were <30m (28.35 m $\pm$ 3.76). The net was raised at a speed of approximately 0.5 $m \cdot s^{-1}$. The zooplankton was washed into the cod-end of the net and anaesthetized to prevent egg shedding in a wash of Club Soda before being added to a 10% sugared formalin solution. Each zooplankton sample was split using a Folsom plankton splitter to a subsample volume containing post-naupliar stages of >100 of the most abundant taxa of crustaceans. For each sub-sample, the species were enumerated at 5-100x magnification under a GSZ-Zeiss stereo microscope. The number of attached eggs were counted. Sub-sample counts were then extrapolated to the total sample. Biomass of zooplankton were determined from length-to-weight regressions reported by McCauley (1984) using lengths measured with a digitizing system. Up to 25 random length measurements per taxon were taken per sample, and the final biomass was expressed as µg dry weight per sample. The amount of zooplankton biomass per sample was converted to volumetric zooplankton biomass (µg dry $weight \cdot L^{-1}$) using the known volume of water that was filtered by the Wisconsin net. This value was corrected to the amount of biomass in a 1 m^2 column of water over the depth of water at the sampling site to yield areal biomass units of mg dry $weight \cdot m^{-2}$.

Zooplankton production was measured at C2 and C6 on Carpenter Reservoir, A1 and A2 on Anderson Lake and S4 and S5 on Seton Lake. Secondary production, in this case zooplankton (in units of $mass \cdot m^{-2} \cdot yr^{-1}$), is an indicator of food available to fish, and is the most commonly used indicator of ecological function, water quality, energy flow, disturbance, and recovery in freshwater ecosystems (Benke and Huryn 2010). Secondary production integrates several aspects of ecological performance including density, biomass, growth rate, reproduction, survivorship, and developmental time. Zooplankton production in Seton and Anderson Lakes was determined by re-organizing the equation:

$$\frac{P}{B} = y$$

Equation 1

where P is annual zooplankton production ($mass \cdot m^{-2} \cdot yr^{-1}$), B is mean annual dry weight biomass ($mass \cdot m^{-2}$) of the population of interest, and y is a rate in units of yr^{-1}

(Benke and Huryn 2006). Given that biomass can be measured and y, known as a production/biomass or P/B ratio, can be found in the literature for many taxa, the product of B and y gives P.

Production of zooplankton was determined from Equation 1, but P/B was calculated from a temperature dependent model reported by Shuter and Ing (1997) and shown to work well by Clarke and Bennett (2007):

$$[P{:}\,B]_{daily} = 10^{(\alpha_{taxon} + \beta T_{daily})}$$

Equation 2

where $[P{:}\,B]_{daily}$ is daily $P{:}\,B$, $\propto_{taxon}$ is -1.725 for cladocerans, -1.766 for cyclopoid copepods, and -2.458 for calanoid copepods, β is 0.044 for cladocerans, 0.040 for cyclopoid copepods, and 0.050 for calanoid copepods, and T is average water temperature (ºC) measured over the depth that zooplankton were collected on each sampling day. Zooplankton biomass and $[P{:}\,B]_{daily}$ was linearly interpolated between the six sample dates distributed between May and October, and the product of $[P{:}\,B]_{daily}$ and zooplankton biomass was summed over the sampling period May through October to estimate annual zooplankton production. In this approach, zooplankton production in the active growing season of May through October was considered to include most production for the calendar year and was called annual zooplankton production.

2.3.4 Environmental variables

Environmental variables (predictor variables for statistical regression modeling) were measured once per month, corresponding with the time of primary production measurements in pelagic habitat at C2 and C6 and over the time series of periphyton sampler incubation in littoral habitat also at C2 and C6. The same data from S4 and S5 on Seton Lake and A1 and A2 on Anderson Lake where biological production was measured as part of BRGMON6 were also used as part of the regression analyses.

We prioritized five abiotic variables that have been shown to affect periphyton production in littoral habitats and one biotic and six abiotic variables known to affect zooplankton production in pelagic habitats. Hypotheses for each variable included in the periphyton, phytoplankton and zooplankton analyses are detailed in Table 3, Table 4 and Table 5, respectively.

Table 3. Hypotheses for predictor variables included in the polystyrene ball and sand pail periphyton analyses.

Predictor Variable	Unit	Hypothesis	Predicted Response	Level[a]	Reference
PAR (accumulated over incubation time)	μMol·m^{-2}	PAR limits growth and production of photosynthetic algae	Positive	By depth, station and sampling day	(Lamberti and Steinman, 1997)

Predictor Variable	Unit	Hypothesis	Predicted Response	Level[a]	Reference
Temperature	°C	Affects metabolic activity and consequently periphyton growth	Positive	By depth, station and sampling day	(Allan and Castillo, 2007c; Bothwell, 1988; Lamberti and Steinman, 1997)
Phosphorus (soluble reactive phosphorus)	$mg{\cdot}L^{-1}$	Phosphorus limits periphyton growth	Positive to a threshold	By station and sampling day	(Perrin, Bothwell, and Slaney, 1987; Rosemond, Mulholland, and Elwood, 1993)
Nitrogen (dissolved inorganic nitrogen)	$mg{\cdot}L^{-1}$	Nitrogen limits periphyton growth	Positive to a threshold	By station and sampling day	(Perrin and Richardson, 1997; Rosemond, Mulholland and Elwood, 1993)
Turbidity	NTU	Turbidity increases light scatter and subsequently decreases light availability for algal production	Negative	By depth, station and sampling day	(Leland, 1995)

Note: [a] Level refers to the level at which the predictor variable was measured (e.g. by depth, station and sampling day means the predictor variable was measured once per depth, station and month coinciding with the response variable).

Table 4. Hypotheses for predictor variables included in the phytoplankton analysis.

Predictor Variable	Unit	Hypothesis	Predicted Response	Level[a]	Reference
PAR (accumulated over incubation time)	$\mu Mol{\cdot}m^{-2}$	PAR is a limiting factor for the growth and production of photosynthetic algae	Positive	By depth, station and sampling day	(Lamberti and Steinman, 1997)
Temperature	°C	Affects metabolic activity and consequently periphyton growth	Positive	By depth, station and sampling day	(Allan and Castillo, 2007c; Bothwell, 1988; Lamberti and Steinman, 1997)
Phosphorus (soluble reactive phosphorus)	$mg{\cdot}L^{-1}$	Periphyton growth can be limited by phosphorus	Positive to a threshold	By station and sampling day	(Perrin, Bothwell, and Slaney, 1987; Rosemond, Mulholland, and Elwood, 1993)
Nitrogen (dissolved inorganic nitrogen)	$mg{\cdot}L^{-1}$	Periphyton growth can be limited by nitrogen	Positive to a threshold	By station and sampling day	(Perrin and Richardson, 1997; Rosemond, Mulholland and Elwood, 1993)
Turbidity	NTU	Increases light scatter and subsequently decreases light availability for algal production	Negative	By depth, station and sampling day	(Leland, 1995)

Predictor Variable	Unit	Hypothesis	Predicted Response	Level[a]	Reference
Mean water residence time	Days	Longer residence time provides a longer growing period for phytoplankton within the reservoir	Positive	By reservoir and sampling day	(Korpelainen, 1986; Schwatz, and Ballinger, 1980)

Note: [a] Level refers to the level at which the predictor variable was measured (e.g. by depth, station and sampling day means the predictor variable was measured once per depth, station and month coinciding with the response variable).

Table 5. Hypotheses for predictor variables included in the zooplankton analyses.

Predictor Variable	Unit	Hypothesis	Predicted Response	Level[a]	Reference
Phytoplankton production (0.20 μm and 0.75 μm chlorophyll-a)	$\mu g \cdot L^{-1}$	Food source for zooplankton	Negative	By station and sampling day	(Burks, Lodge, Jeppesen, and Lauridsen, 2002)
Temperature	°C	Affects physiology and population ecology of zooplankton	Positive	By station and sampling day	(Burks, Lodge, Jeppesen, and Lauridsen, 2002)
Turbidity	NTU	Turbidity can reduce phytoplankton production and result in less food for zooplankton	Negative	By station and sampling day	(Burks, Lodge, Jeppesen, and Lauridsen, 2002)
78-day mean water residence time	Days	Longer residence time provides longer growing period for zooplankton within the reservoir	Positive	Reservoir and sampling day	(Korpelainen, 1986; Schwatz, and Ballinger, 1980)
78-day mean drawdown	m	Less habitat available for zooplankton as drawdown increases	Negative	Reservoir and sampling day	(Korpelainen, 1986; Schwatz, and Ballinger, 1980)
Station depth	m	Provides greater habitat availability for zooplankton.	Positive	Station and sampling day	

Note: [a] Level refers to the level at which the predictor variable was measured (e.g. by depth, station and sampling day means the predictor variable was measured once per depth, station and month coinciding with the response variable).

The monthly sampling dates spanned the complete algal growing season (May to October 2015 and 2016). Temperature, turbidity and PAR were measured over a vertical profile from surface to bottom using a Sea-Bird Electronics SBE19plusV2 CTD at C2, C6, A1, A2, S4 and S5 (Figure 1) at the time phytoplankton production measurements were done. Temperature and turbidity values were taken from the Sea-Bird profile at the

nearest depth to the periphyton and phytoplankton sample depths (± 0.5m). For the zooplankton analysis, mean values were calculated over the depth of the zooplankton haul at each station and sampling date. Means were deemed an acceptable surrogate given the samples were taken from a single haul on a single sampling day. Figure 4 and Figure 5 show the range in temperatures and turbidity in Carpenter Reservoir, Anderson Lake and Seton Lake.

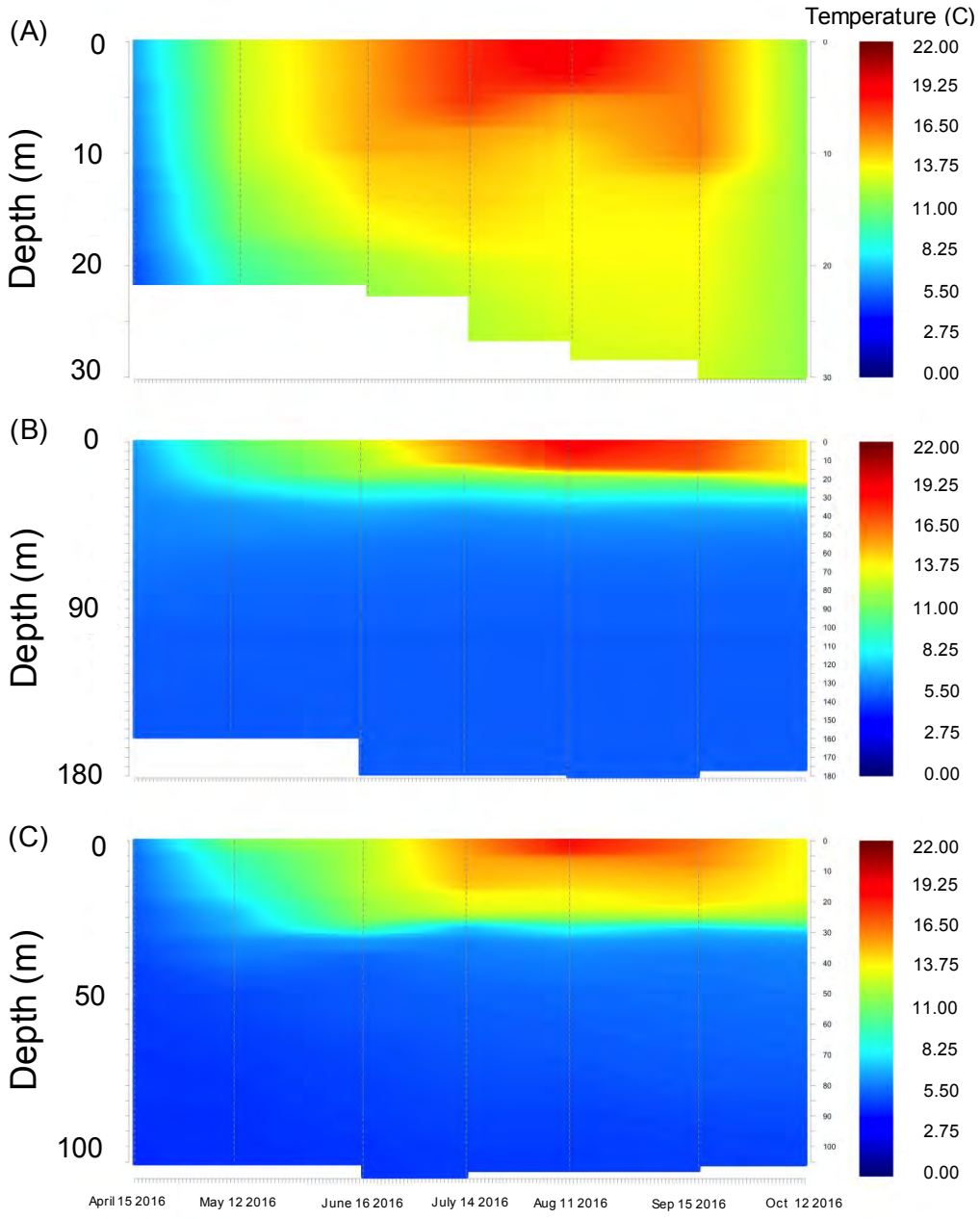

Figure 4. Temperature stratification in (A) Carpenter Reservoir at station C2, (B) Anderson Lake at station A1, and (C) Seton Lake at station S4 from May to October 2016. Note the difference in depths on the y-axis.

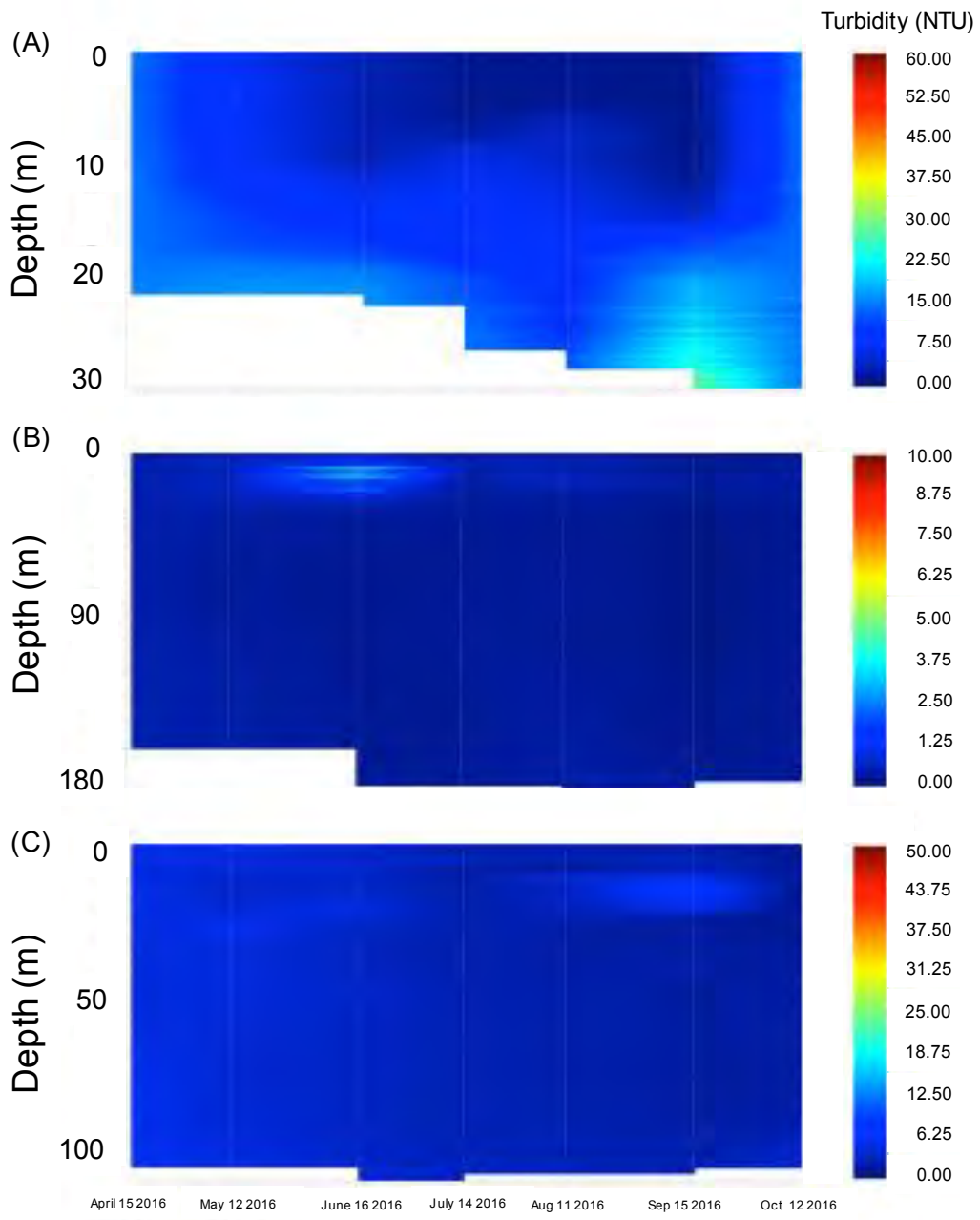

Figure 5. Turbidity in (A) Carpenter Reservoir at station C2, (B) Anderson Lake at station A1, and (C) Seton Lake at station S4 from May to October 2016. Note the difference in depths on the left and colour scales on the right.

The PAR data for the periphyton analysis was correlated with PAR that was continuously logged at a shore base station allowing the continuous measurements to be corrected for attenuation in water and used to calculate total accumulated PAR during incubation of the littoral periphyton samplers. Total accumulated PAR over the

incubation period for each series was used in the periphyton analyses and mean daily PAR by sampling depth, day and station was used in the phytoplankton analysis.

Temperature was also continuously measured at several depths along a thermistor chain installed at the trash boom (C2), providing continuous temperature data for each depth that periphyton samplers were deployed in Carpenter Reservoir. Temperature by station, sampling day and depth measured by the Sea-Bird CTD were used for Anderson and Seton Lakes whereas temperature for Carpenter Reservoir was the mean temperature measured by the logger on the thermistor chain over the incubation period at each depth.

Water residence times for Carpenter Reservoir and Seton Lake were calculated as rate of outflow (data from BC Hydro) divided by reservoir volume, which was determined from a digital elevation model (DEM) developed by BC Hydro for this project. Water residence time for Anderson Lake was derived from bathymetric data collected in 1961 (Geen and Andrew, 1961). The amount of drawdown by month was calculated as the difference between the maximum height and the daily height of the reservoir or lake. For this report, the mean water residence time and mean drawdown were calculated using the daily values for 78 days prior to each sampling day, corresponding to the maximum reported lifespan of common zooplankton species (Korpelainen, 1986; Schwartz and Ballinger, 1980). The station depth was measured at each station on each sampling day using the depth sounder on the boat.

Soluble reactive phosphorus (SRP) concentration, dissolved inorganic nitrogen concentration measured as the sum of ammonium (NH_4-N) and nitrate (NO_3-N) and pH were measured from one water sample collected from the surface and one from the hypolimnion using a VanDorn bottle each month, closely corresponding with the beginning and end of a periphyton sampling series and the dates of primary production measurements at C2, C6, A1, A2, S4 and S5. If Carpenter Reservoir was not stratified, a sample was collected from the reservoir surface and another from 2m off the bottom. These analyses were completed using standard methods at the ALS Canada Lab in Burnaby, B.C. Mean SRP and DIN concentrations were calculated by station and sampling day for the periphyton and zooplankton regression analyses.

See Table 6 for the mean values for each of the environmental variables used in the periphyton and zooplankton analyses.

Table 6. Mean environmental variables by lake and station for 2015 and 2016.

Reservoir/ Lake		Station	Station Depth (m)	Mean Water Residence Time (days)	Mean Draw-down (m)	DIN ($\mu g \cdot L^{-1}$)	SRP ($\mu g \cdot L^{-1}$)	Accumulated PAR ($\mu Mol \cdot m^{-2}$)	Temperature (°C)	Turbidity (NTU)	Chl a 0.20 um filter size ($\mu g \cdot L^{-1}$)	Chl a 0.75 um filter size ($\mu g \cdot L^{-1}$)
Carpenter	2015	C2	37.5	92.86	4.21	10.43	1.04	521,565,699	15.97	3.55	0.97	0.80
		C6	26.4	92.86	4.21	16.09	1.23	-	12.92	14.82	1.29	0.87
	2016	C2	32.76	536.247**	8.80	10.98	1.02	94,203,441	12.93	8.80	1.19	0.86
		C6	20.4	536.247**	8.80	10.00	1.03	-	11.80	15.29	0.84	0.79
Anderson	2015	A1	206.2	1807.49	0.96	18.54	1.00	308,629,582	12.43	0.52	1.18	0.93
		A2	196.4	1807.49	0.96	32.00	1.00	201,319,510	9.29	0.40	0.97	0.87
	2016	A1	204.3	1709.96	0.85	20.65	1.01	270,286,782	12.30	0.73	1.25	1.19
		A2	195.5	1709.96	0.85	20.03	1.00	203,948,311	12.03	0.54	0.95	1.04
Seton	2015	S4	119.4	204.49	0.28	30.73	1.01	150,666,404	13.80	4.60	1.27	1.07
		S5	110.0	204.49	0.28	27.88	1.00	395,465,749	14.17	3.17	1.01	1.04
	2016	S4	119.5	544.01	.346	13.97	1.01	387,284,635	13.08	3.23	1.28	1.15
		S5	110.2	544.01	.346	13.01	1.00	519,433,692	13.36	2.46	1.55	0.95

Note: ** Only sporadic flow through BRG1 from 13 September 2016 and 12 October 2016 and no flow through BRG2 from 13 September 2016 and 12 October 2016.

2.3.5 Analytical approach for periphyton and zooplankton production

For this report, we focused our analyses on phytoplankton and zooplankton from 2015 and 2016. Periphyton results presented in Section 3.2 are from 2015 and will be updated with the methods described for phytoplankton and zooplankton for the final report due in 2018.

We used mixed effects models in the package lme4 (Bates et al. 2016) in R (R Core Team, 2016) to model nested relationship between phytoplankton, zooplankton and the predictor variables identified in Table 4 and Table 5.

For phytoplankton, the predictor variables, known as fixed effects included temperature, turbidity, PAR, DIN, SRP and water residence time. We also included four random effects; year, month, sampling site and phytoplankton filter size. For the zooplankton analysis, we included six fixed effects, temperature, turbidity, phytoplankton biomass measured as chlorophyll-a, mean water residence time over 78 days and maximum water depth and three random effects, year, month and sampling site. The mixed effect models took on the following form:

$$y_i = \beta_0 + \beta_1 x_{i1} + \ldots + \beta_j x_{ij} + \gamma_1 u_{i1} + \ldots + \gamma_j u_{ij} + \varepsilon_i$$

Equation 3

where

y_i is the value of biological response for an ith observation,

$x_{1\ldots j}$ is the value of independent variable 1 and j is the number of independent variables,

β_0 is the intercept when all predictor variables (e.g. variables describing habitat attributes) have a value of zero,

β_1 is the fixed effect parameter for y on x_1 when all other predictor variables (other x's) are held constant,

β_j is the fixed effect parameter for y on x_j when all other predictor variables (other x's) are held constant,

γ_1 is the random effect parameter for y on u_1,

γ_j is the random effect parameter for y on u_j,

ε_i is unexplained error associated with the $i$the observation.

We conducted four separate analyses, two for phytoplankton production and two for zooplankton production as example analyses for this report. We constructed separate models for phytoplankton primary productivity measured as mg $C \cdot m^{-3} \cdot d^{-1}$ and chlorophyll-a measured as $\mu g \cdot L^{-1}$ and two separate models for zooplankton production, measured as $mg \cdot m^{-2} \cdot yr^{-1}$, one including phytoplankton biomass (as a predictor variable) sampled with a 0.20 μm filter and the second for phytoplankton biomass sampled with a 0.75 μm filter (see Section 2.3.2 of this report for a detailed description of the

phytoplankton sampling procedure). We hypothesized that zooplankton would have a different response to different size classes of phytoplankton. These were labeled as zooplankton-0.20 and zooplankton-0.75.

For the phytoplankton samples, we assumed samples for each filter size and depth were independent observations because each sample was collected in succession and not from the same filter. Phytoplankton was collected from Carpenter Reservoir (C2 and C6), Anderson (A1 and A2) and Seton Lakes (S4 and S5) in 2015 and 2016 at 6 or 7 different depths, which resulted in 156 data points for each filter size for a total of 312 data points. Two replicate samples for zooplankton were collected from a 30m haul (or from 2m off the reservoir bottom in the case of Carpenter) from each lake, station and month, which resulted in 130 observations, which were treated as independent observations.

We checked for multicollinearity among the environmental variables using variance inflation factors (VIF) and correlation coefficients (Zuur, Ieno, and Elphick, 2010). The combination of variables used in each of the phytoplankton and chlorophyll-a regressions were not highly correlated (VIF scores ≤ 1.88 and correlation coefficients ≤ ± 0.4 Figure A-1 in APPENDIX A) so we did not need to exclude any variables from the phytoplankton and chlorophyll-a regression analyses. Turbidity and maximum water depth were highly correlated when tested for the zooplankton analysis (correlation coefficient = -0.8 Figure A-2 in APPENDIX A) and resulted in a VIF score for maximum water depth = 4.37. We removed maximum water depth from the analysis, which resulted in correlation coefficients ≤ ± 0.4 and VIF scores ≤ 1.33 for the remaining variables (Figure A-3 in APPENDIX A). Phytoplankton primary productivity, chlorophyll-a, and zooplankton biomass were $\log_{10}$-transformed to model growth rate exhibited in biological systems. Log transforming the response variable also satisfied assumptions of normality, which were verified by visually inspecting residual versus fitted and Q-Q plots.

We generated a list of models with various combinations of biotic and abiotic variables identified in Table 4 and Table 5, limiting the number of parameters in each model to approximately one for every 10 data points, to avoid spurious results due to overfitting (Harrell, 2001). This approach generated 62 models for phytoplankton primary productivity and chlorophyll-a, and 32 models for each zooplankton analyses. We used Akaike's information criterion for small sample sizes (AICc) to evaluate support for each model/competing hypothesis (Akaike, 1974; Burnham and Anderson, 2002). We relied on ΔAICc, model weights (w_i), evidence ratios (ER) and adjusted r^2 to aid in the interpretation of model rankings. Delta AICc is the difference in AICc values between model *i* and the top ranked model, w_i is the probability that model *i* is the best model given the model set and ER is $w_{top\ model}/w_i$, which indicates the likelihood that the top model is better than model *i.*

To account for model uncertainty, we used multi-model inference to average across a candidate set of models with a cumulative weight of 0.95 ("full" method) to

avoid biasing coefficients away from 0 (Burnham & Anderson, 2002; Grueber et al., 2011) using the MuMIn package in R (Barton, 2015). We standardized the independent data to a mean of 0 and standard deviation of 2 so that comparisons could be made among independent variables (Grueber et al., 2011) but report the unstandardized coefficients to maintain the original units of measure and allow for quantitative prediction of the dependent variable with estimated error.

2.4 Questions 3 & 4: Is light penetration in Carpenter Reservoir impacted by changes in reservoir operations and can suspended sediment transport into Seton be altered by changes in Carpenter Reservoir operation?

2.4.1 CE-QUAL-W2 model overview

Simulation modeling supported with empirical data will be used to answer questions 3 and 4 after all years of work. Over that time, we will explore the effect of a wide range of reservoir operation and natural inflow scenarios on PAR, temperature, nutrient concentrations, and water residence time that are predictors of algal production (Section 2.3.4) using a hydrodynamic simulation model. Output of PAR, temperature, and nutrient concentrations from that model will be input into the regression models described in Section 2.3.5 to predict algal production among scenarios of reservoir operation and natural inflow. The following paragraphs describe the modeling approach.

The simulation model will be CE-QUAL-W2, a hydrodynamic and water quality model for rivers, lakes, reservoirs and estuaries. CE-QUAL-W2 laterally averages calculations (across channel) with segments along the length of the water body, and bins from the surface to the bottom. This structure makes CE-QUAL-W2 particularly suited for modelling long and narrow water bodies such as Carpenter Reservoir. Lateral averaging reduces the model to 2-dimensions, capturing the important physics along the length of the reservoir while ensuring the run time for the model is reasonable for a desktop computer. This also makes it possible to explore a wide range of reservoir operation scenarios. CE-QUAL-W2 has been widely used, having been applied to over 200 reservoirs in the United States, and more than 100 other reservoirs worldwide (http://www.ce.pdx.edu/w2/). The source code for CE-QUAL-W2 is publicly available, and is currently being developed and maintained at Portland State University (http://www.ce.pdx.edu/w2/) for the US Army Corp of Engineers. In addition, CE-QUAL-W2 is widely accepted in the scientific literature, making it ideal for our purposes.

CE-QUAL-W2 solves laterally averaged equations of fluid flow for conservation of mass, and conservation of momentum along the length of the reservoir. The model assumes that the reservoir is well mixed across channel, a reasonable assumption in a narrow reservoir like Carpenter Reservoir. The model will solve transport equations for temperature, conductivity, turbidity, and nutrients in Carpenter Reservoir. Conductivity is not a predictor of algal production but it is needed for solving mass transport equations.

Turbidity is a measure of the cloudiness of the water, and is measured using light scattering. Turbidity is then used to determine the light extinction coefficient in each cell of the CE-QUAL-W2 model. With the incident PAR at the meteorological station, the light extinction coefficients are used to determine PAR in the CE-QUAL-W2 model. Values of turbidity in output from CE-QUAL-W2 will be approximately converted to PAR as input into the regression models described in Section 2.3.5 or prediction of algal production in the second part of simulation modeling described above in this section.

2.4.2 Input data

CE-QUAL-W2 requires data describing the physical and chemical state of the reservoir over time periods when it will be run. The time will be May through October in each of 2015 and 2016. This duration covers the time from lowest water surface elevation and volume (early spring) to highest water surface elevation and volume (fall) and the time of most annual algal production. Data describing wide ranging habitat conditions allows for diverse reservoir management scenarios to be run after the model is compiled. Several measurements were made in 2015 to set up and calibrate CE-QUAL-W2 and they will be repeated in 2016 to support testing of the model or provide data for further calibration if found necessary during model development. Existing chemical data from 1995 and 1996 (Perrin and MacDonald 1999) were accessed and appended to the new data collected in 2015.

A basic tool for setting up and running CE-QUAL-W2 is a digital elevation model (DEM) of the reservoir. The DEM supports calculations of water volumes in the whole reservoir and in various segments and bins for given water surface elevations. The production of a DEM was completed by BC Hydro as part of this study.

The physical and chemical measurements within the reservoir were completed among stations situated along the longitudinal axis. Detailed measurements were made at each of the 10 stations shown in Figure 1 during each of the monthly sampling episodes when water depth was a minimum of 10m at a given station. The stations overlapped those established for earlier nutrient budget studies (Perrin and MacDonald 1999), thus providing consistency between data sets. The measurements were as follows:

2.4.2.1 Tributary water quality

The water quality of tributaries to Carpenter Reservoir was sampled monthly from May to October 2015. The area draining to Carpenter Reservoir can be divided into five major components:

1. Drainage area to La Joie Dam 26.7%
2. Hurley River 18.2%
3. Gun Creek 15.9%
4. Tyaughton Creek 20.5%
5. Other local drainage 18.7%

Of these components, the outflows from the first four were sampled, representing 81.3% of the total drainage. In addition, two smaller tributaries that contribute to the balance of the local drainage were also sampled, one from the north side of Carpenter Reservoir, Marshall Creek, and one from the south side, Keary Creek.

Sampling of the Middle Bridge River was done at three locations:

- Middle Bridge River above the Hurley, sampling below La Joie dam but above the confluence with the Hurley River;
- Middle Bridge River below the Hurley; and
- Middle Bridge River at Confluence, sampled after the Middle Bridge River has crossed the drawdown zone and enters the wetted reservoir.

Data were also collected from the outflows from Carpenter Reservoir, and from the Upper Bridge River for comparison.

2.4.2.2 Continuous turbidity monitoring in tributaries

A turbidity recorder was moored in the Bridge River above Carpenter Reservoir (UTM 10U 511,946 Easting 5,634,532 Northing). The recorder consisted of a RBR Virtuoso, connected to a Seapoint optical backscatter sensor (OBS). The OBS was placed face up at the highest point to reduce fouling. Data was recorded every 2 minutes. In 2015, the OBS was deployed without a wiper; in 2016 a Zebra Hydro wiper was added.

2.4.2.3 Meteorological data

In 2015 and 2016, three sources of meteorological data were available near Carpenter Reservoir:

- BC Hydro sensors at Terzaghi Dam:
  - This station provided hourly wind speed, wind direction and air temperature.
- Limnotek station at Terzaghi Dam:
  - This station was setup close to the BC Hydro sensors and consisted of an Onset Hobo Micro Station Data logger (H21-002) with a Photosynthetically Active Radiation (PAR) sensor (S-LIA) and a Solar Radiation sensor (S-LIB). An Onset Hobo Pro (U23) was used to measure air temperature and relative humidity.
- BC Wildfire Service Fivemile site:
  - This weather station is approximately half way up the reservoir (50° 54’ 39” N, 122° 41’ 20” W, elevation 865 m), and recorded wind speed and direction, air temperature and relative humidity.

2.4.2.4 Monthly Sea-Bird profiles

2.4.2.4.1 Profiler Survey Data

Profiles were collected using a Sea-Bird Electronics SBE19plusV2 CTD (conductivity, temperature, depth) profiler. This instrument, designed for oceanographic work, provides high accuracy (0.005 °C), high resolution (0.0001 °C) and stable temperature. The particular design of the conductivity cell gives rise to unprecedented accuracy and stability at low conductivity, with excellent results in fresh water. As the profiler is lowered through the water column, it collects four samples a second which are recorded internally for upload after the survey. The profiler was equipped with a WETlabs EC0 combined fluorometer and turbidity meter, a Photosynthetically Active Radiation (PAR) sensor, and a SBE43 dissolved oxygen sensor.

Surveys of the reservoir were conducted monthly from May to October 2015, and April to October 2016. Seabird profiles were collected at up to 10 stations along the 50 km length of the reservoir, providing a snapshot of the reservoir each month, and giving a detailed view of the gradients along the reservoir.

2.4.2.4.2 Light Data

At each station, the Seabird profiler was lowered on the sunny side of the boat to record light data. The Secchi depth was also measured at each station. The Secchi depth was the mean of the depth at which the disk disappeared on the way down, and the depth it reappeared on the way up.

2.4.2.5 Moorings

2.4.2.5.1 Mooring hung from the log boom

The mooring consisted of a line with temperature recorders attached to the log boom upstream of the intakes to the Bridge 1 and 2 powerhouses. The mooring was attached to the boom at the location with greatest depth (UTM 10U 551,263 Easting; 5,624,112 Northing). The mooring was deployed from 16 April to 20 October 2015, and 13 April to 14 October 2016.

The line consisted of 1.8 m of ¼" galvanized chain at the top, and 5/8" Samson Quik-Splice for the remainder, a 12 strand single braid polyolefin rope with low stretch (specific gravity 0.94, weight 11.9 kg/100 m). At the bottom of the mooring, was attached 20 lbs of steel (2 X 10 lb weight lifting rings). To increase this weight and reduce the drag on the mooring, this was replaced with a combination of a 10 lb and 20 lb cannonball in 2016.

The depths of the temperature recorders are given in Table 7 (2015), Table 8 (winter 2015-2016), and Table 9 (2016). Most of the temperature recorders were Onset U22-001 Hobo Water Temp Pro v2 (HWTP) loggers with accuracy of ±0.2 °C and resolution of 0.02 °C. The Onset HWTPs recorded every 20 minutes. Also included were two high accuracy RBR Solo T recorders, with accuracy ±0.002 °C, resolution of <0.05 m°C, and recording every 3 seconds. At the bottom of the mooring a RBR Solo D

depth recorder was included to monitor movement of the mooring, recording every 6 seconds.

Table 7. Temperature mooring in Carpenter Reservoir, 16 April to 20 October 2015.

Depth (m)	Instruments (16 Apr - 20 Oct 2015)
0.5	HWTP 1068-5988
1	RBR Solo T 75933
2	HWTP 1068-5976
3	HWTP 1068-5977
5	HWTP 1068-5978
7	HWTP 1068-5979
10	HWTP 1068-5980
15	HWTP 1068-5981
20	RBR Solo T 76651
~20[1] 25[2]	HWTP 1068-5982
27[3]	RBR Solo T 76652 RBR Solo D 78474
30[2]	RBR Virtuoso 54153 with Seapoint turbidity 14839

Note: [1] Tied up near 20 m from 16 April to 18 June; these data not used.
[2] From 18 June to 20 October.
[3] From 16 April to 22 May; removed for service from 22 May to 18 June.

Table 8. Temperature mooring in Carpenter Reservoir, 20 October 2015 to 13 April 2016.

Depth (m)	Instruments (20 Oct 2015 – 13 Apr 2016)
0.5	HWTP 1011-0014
5	HWTP 1011-0083
10	HWTP 1011-0084

Table 9. Temperature mooring in Carpenter Reservoir, 13 April to 14 October 2016.

Depth (m)	Instruments 13 Apr – 14 Oct 2016
0.5	HWTP 1068-5988
1	RBR Solo T 75933
2	HWTP 1068-5976
3	HWTP 1068-5977
5	HWTP 1068-5978
7	HWTP 1068-5979
8	HWTP 1038-8898
9	HWTP 1038-8899
10	HWTP 1068-5980
11	HWTP 1038-8900
12	HWTP 1038-8901
13	HWTP 1038-8902
14	HWTP 1038-8903
15	HWTP 1068-5981
16	HWTP 1038-8904
18	HWTP 1039-4321
20	RBR Solo T 76651 RBR Solo D 78475
22	HWTP 1039-4322 [1]
25	HWTP 1068-5982 [1]

Note: [1] Bottom 5 m segment added 14 July 2016.

In 2015, the mooring line included an RBR Virtuoso turbidity recorder, connected to a Seapoint optical backscatter sensor (OBS) with a Zebra Hydro Wiper. Data was recorded every 2 minutes. The turbidity recorder was at the same depth as the Solo T and Solo D at the bottom of the mooring (Table 7). In 2016, the turbidity recorder was attached to the subsurface mooring (see below).

On 23 April 2015, the bottom Solo T sensor, along with the Solo D and turbidity recorder were deployed at 27 m depth, just above the bottom (28.5 m). After deployment in April, however, the water level in Carpenter Reservoir declined slightly. On the first sampling trip on 22 May 2015 (day 142) the mooring was inspected and the bottom sensors were found to have dragged along the bottom. The instruments were undamaged except for the wiper arm, which was badly bent. The bottom three instruments were removed for service, a replacement wiper arm was built, and the instruments were reattached at 30 m during the subsequent sampling trip on 18 June 2015 (day 169).

In 2015, the mooring was pulled up to the surface each month to inspect the turbidity sensor; data during these times were removed. Data from the depth recorder showed brief periods when the bottom of the mooring was shallower than expected; this could have resulted from the log boom shifting to a shallow location, or from drag on the mooring as the boom moved from one location to another. Data during the worst cases were removed.

Upon recovery of the main mooring line on 20 October 2015, three temperature recorders were attached to the log boom for the winter. The recorders were hung from individual lines consisting of chain to 1 m, and 3/8" static cord from 1 m to a steel weight ring (10 lb) at the bottom (Table 8).

In 2016, additional temperature sensors were added to the boom line between 8 and 16 m to better resolve the thermocline. At deployment on 13 April 2016, the line was only 20 m long to avoid the dragging on the bottom. On 14 July 2016, an additional 5 m of line was added with sensors at 22 and 25 m.

2.4.2.5.2 Subsurface mooring

To better measure turbidity and temperature near the bottom of the reservoir, a subsurface mooring was deployed in 2016 at a location approximately 1 km downstream of the log boom (10U 552,594 Easting; 5,624,640 Northing). At the bottom, this mooring had a 60 lbs steel anchor; then a 5/8" Samson Quik-Splice line ran from the anchor to a 12" trawl float 2 m above the bottom; finally a line of 3/8" static cord ran to an 8" trawl float at 12.5 m above the bottom. A 3/8" Samson double-braid nylon ground line, was connected from the anchor at the bottom of the mooring to a tree on the south shore of the reservoir; the mooring was recovered using this line. The instruments on the subsurface mooring are given in

Table 10.

Table 10. Subsurface mooring in Carpenter Reservoir, 13 April to 14 October 2016

Distance from bottom (m)	Depth[1] (m)	Instruments (13 Apr – 14 Oct 2016)
12	20.6	HWTP 1068-5985
7	25.6	HWTP 1068-5986
1.8	30.8	RBR Virtuoso 54153 with Seapoint turbidity 14839
1.7	30.9	RBR Solo T 76652 RBR Solo D 78474
0.3	32.3	HWTP 1068-5987
0	32.6	Bottom

Note: [1] From a water level of 633.45 m ASL on 13 April 2016.

2.4.3 CE-QUAL-W2 Modelling

The model was run from spring through to fall, to simulate the evolution of the biologically productive season. The model was started on the date of the first sampling trip, 22 May 2015 (day 142), and was ended on the date of the last sampling trip, 20 October 2015 (day 293).

The model requires initial conditions to specify the state of the reservoir at the start of the model run. Initial conditions for temperature and conductivity were determined from the Seabird profiles on 22 May 2015. The initial concentration of TSS and nutrients were determined from the bottle samples collected on 22 May 2015.

As the model runs through a computational grid (Figure 6), it requires boundary conditions such as river inflow and meteorological data. The model has been setup with inflow from Bridge River, inflow from the local drainage, outflow to the Bridge River powerhouses, and outflow from Terzaghi Dam. The local inflow is distributed along the length of the reservoir based on drainage area.

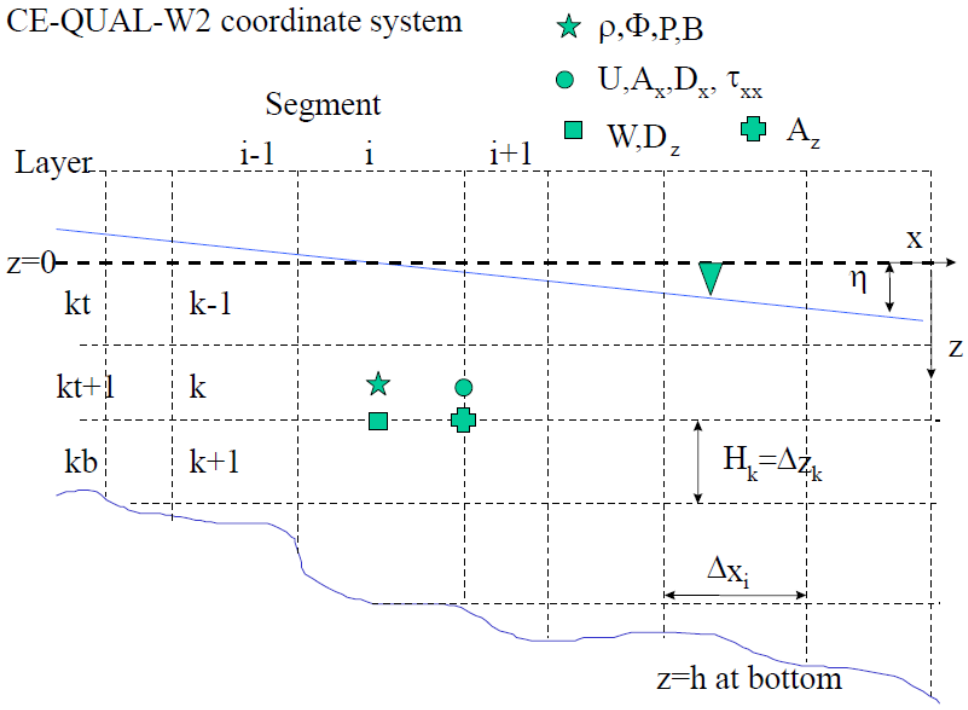

Figure 6. CE-QUAL-W2 computational grid. Width (B), density (ρ), pressure (P) and water quality state variables (Φ) are defined at cell centers. Horizontal velocity (U), longitudinal eddy viscosity (A_x) and diffusivity (D_x), and longitudinal shear stress (τ_{xx}) are defined at the right hand side of the cell. Vertical velocity (W) and vertical diffusivity (D_z) is defined at the bottom of the cell, and the vertical eddy viscosity is defined at the lower right corner of the cell. Adapted from Cole and Wells (2015).

2.4.4 Model Bathymetry

The Carpenter Reservoir model extends from Terzaghi Dam to the Middle Bridge River. The model consists of 56 horizontal segments along the length of the reservoir (Figure 7). The segment lengths vary from 700 m to 1000 m. Each segment is divided into vertical layers regularly spaced at 0.5 m intervals. The deepest segment, next to the dam, is divided vertically into 107 layers (Figure 8); the segment farthest from the dam has 15 vertical layers (Figure 9). A side view of Carpenter Reservoir showing all layers in each segment is shown in Figure 10. The model requires one additional inactive (empty) segment at the upstream and downstream boundaries and one inactive layer at the top and bottom boundaries.

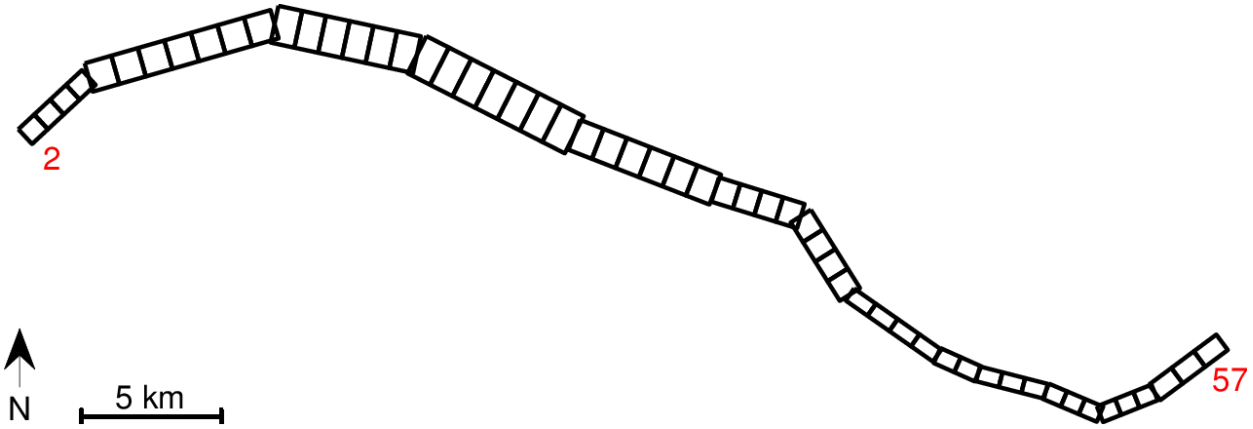

Figure 7. Plan view of model segments. The Bridge River flows into Segment 2. Terzaghi Dam is located at the east end of Segment 57. Segments 1 and 58 (not shown) are inactive boundary segments for use by the model.

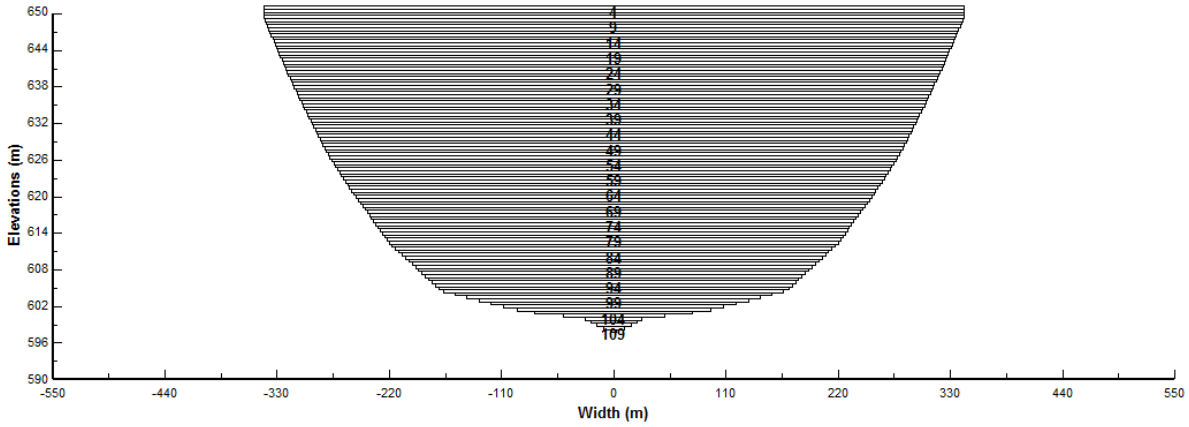

Figure 8. Cross channel profile of Segment 57, the last active segment before Terzaghi Dam. Shown are 107 active layers of 0.5 m each (layers 2 to 108). Layer 1 and 109 are inactive boundaries for use by the model. The top elevation of first active layer #2 is 651 mASL and the bottom elevation of the last active layer #108 is at 597.5 mASL.

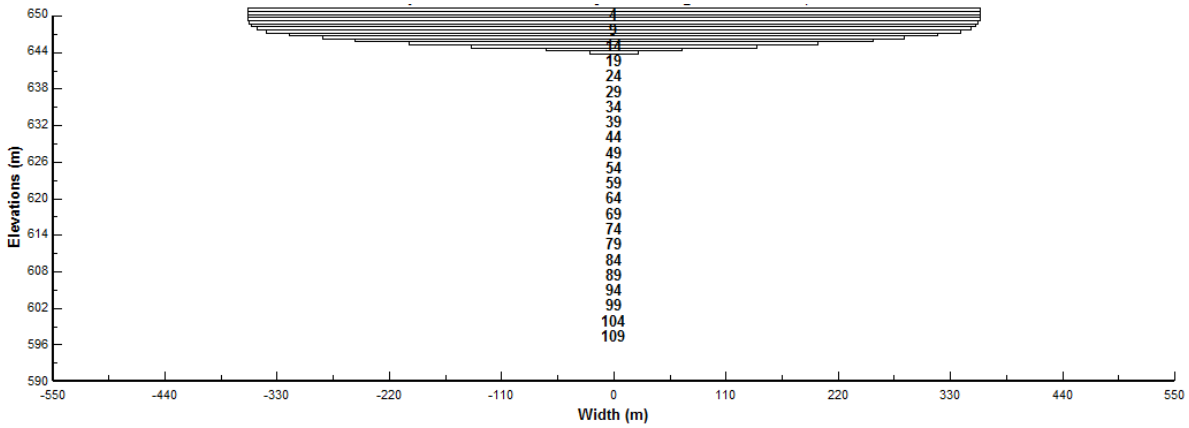

Figure 9. Cross channel profile of Segment 2, the shallowest active segment of the reservoir which received inflow from the Bridge River. The top elevation of first active layer #2 is 651 mASL and the bottom elevation of the last active layer is 643.5 mASL.

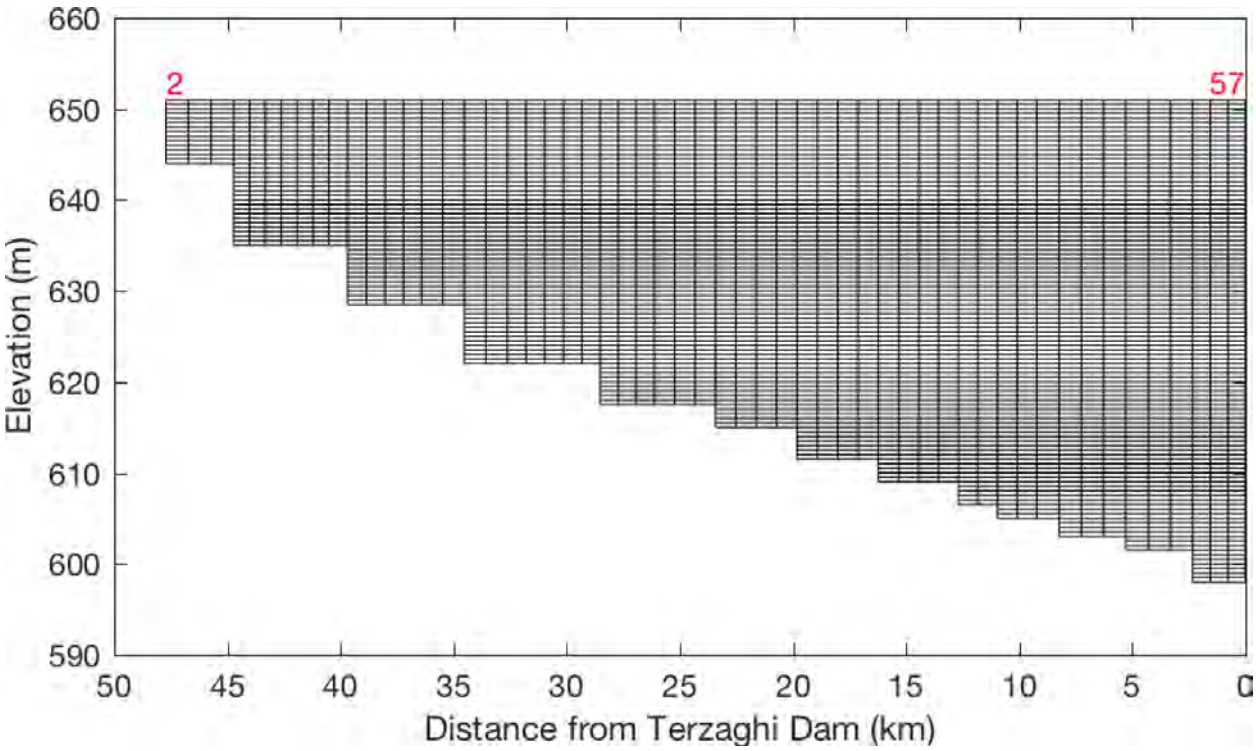

Figure 10. Side view of Carpenter Reservoir showing the 56 active segments along the length of the reservoir and the 107 active layers. Boundary (inactive) layers are not shown. The Middle Bridge River enters on the left, and Terzaghi Dam is adjacent to the deepest segment on the right.

Ten sampling stations are located along the length of Carpenter Reservoir. Based on the sampling stations the reservoir was divided into 13 drainage segments dividing the local drainage (Table 11). Each drainage segment was further divided into

model segments of equal length, with a maximum segment length of 1000 m. The model segments that are associated with each drainage segment are also given in Table 11.

Table 11. Drainage and model segments.

Drainage Segment	Model Segments	Comment
-	1	Upstream boundary segment (inactive)
C10B	2-5	Segment 2: Main inflow
C10A	6-12	
C9	13-18	
C8	19-25	
C7	26-31	
C6B	32-35	
C6A	36-39	
C5	40-43	
C4	44-45	
C3	46-48	
C2B	49-51	
C2A	52-54	Segment 53: Outflow to Bridge powerhouses
C1	55-57	Segment 57: Adjacent to Terzaghi Dam
-	58	Downstream boundary segment (inactive)

2.4.5 Initial conditions

The model requires initial conditions to specify the state of the reservoir at the start of the model run. Model runs were initialized with water temperature, total dissolved solids (TDS) and turbidity measurements from the Seabird profile at station C2 along with nutrient concentrations (SRP, TDP, TP and NO_3-N) from the bottle samples collected on the same date. Model runs started on the same date as the monthly Seabird profiles in May of the given field season. In 2015, the start date was 22 May and in 2016, it was 12 May.

2.4.6 Boundary conditions

As the model runs, it requires boundary conditions including hydrologic data, tributary temperature, tributary water quality and meteorological data.

2.4.6.1.1 Hydrologic data

Hydrologic data were obtained from BC Hydro for the period of 1961-2016 for flow data and 1960-2016 for water level. The data included inflows from La Joie Dam, outflows to the Bridge River powerhouses, outflows from Terzaghi Dam, inflows from local drainage, and reservoir water level. The model was set up with the following flow boundary conditions:

1. Main inflow to Carpenter Reservoir, consisting of the outflow from La Joie Dam plus the estimated flow from the Hurley River based on drainage area (25% of the local flow),
2. Outflow to the Bridge River powerhouses,
3. Outflow from Terzaghi Dam, and
4. Thirteen tributary inflows distributed along the length of the reservoir based on drainage area.

Tributary inflow was divided based on the areas of the drainage segments as shown in Table 12.

Table 12. Carpenter Reservoir local drainage segments.

Drainage Segment	Drainage Segment Area (ha)	% Local Drainage Area[1]	Sampled Tributaries[2]	% Coverage of Drainage Segment Area by Sampled Tributaries
C11	68,824	26	Hurley River (T, WQ)	99
C10B	3,881	1	Sucker Creek (T)	76
C10A	64,716	24	Gun Creek (T,WQ) McDonald Cr (T). Girl Creek (T)	90 3 1
C9	6,366	2	Truax Creek (T,WQ)	83
C8	78,753	30	Tyaughton Creek (T, WQ)	96
C7	12,756	5	-	-
C6B	12,213	5	Marshall Creek (T,WQ)	75
C6A	5,933	2	Keary Creek (T,WQ)	72
C5	6,803	3	-	-
C4	577	0.2	-	-
C3	1,989	1	-	-
C2B	1,476	1	-	-
C2A	714	0.3	-	-
C1	1,863	1	-	-
Total	266,864	100	-	-

Note: [1] Does not include drainage to La Joie Dam.
[2] Tributary was sampled for (T) temperature, and (WQ) water quality.

2.4.6.1.2 Tributary temperature and water quality

For drainage segments with one sampled tributary (Table 12), the temperature, turbidity, TDS and nutrient concentration data from that tributary was used for that entire drainage segment. For drainage segments with multiple tributaries, an area weighted average was used for that drainage segment. For drainage segments in which no tributaries were sampled, values were set to those of Gun Creek, which is generally representative of the other tributaries. Future work includes exploring the sensitivity to these assumptions.

2.4.6.1.3 Meteorological data

The model was forced with wind from the Fivemile site, along with air temperature, relative humidity, and solar radiation from Terzaghi Dam.

2.4.7 Testing and application of the model

The numerical model permits a detailed study of reservoir responses to a range of scenarios including both changes in reservoir operation and variation in natural

conditions. The field data collected in 2015 and 2016 enables an understanding of the present ecological function of Carpenter Reservoir without any modelling. The purpose of the model is to extend this understanding to hypothetical scenarios and to scenarios with less extensive field datasets.

The performance of the model relies heavily on the quality and extent of the field data. The model requires field data for two important purposes: (1) to impose initial and boundary conditions (Sections 2.4.5 and 2.4.6); and (2) for model calibration and validation. The approach taken herein is to calibrate the model to the first year of field data from 2015; then to demonstrate the model's predictive capability, it will be validated against the field data from 2016 without further adjustment of the model parameters. Following calibration and validation, the model will be used to simulate a variety of reservoir conditions (e.g. high flow year, low water level year) and a variety of reservoir operations. Model results from CE-QUAL-W2 will serve as input into the productivity model.

Model calibration, validation and a sensitivity analysis is in progress and results will be presented in the final report. Since model calibration and validation is still underway, the sections that follow do not contain calibration and validation results. Instead, we present model results for the 2015, 2016, and 2009 productive seasons to demonstrate changes in water quality (e.g., temperature, turbidity, nutrients) under different reservoir conditions.

2.4.8 CE-QUAL-W2 model validation with Phytoplankton Biomass (Chlorophyll-a)

To cross-validate the CE-QUAL-W2 model output data from 2015, 2016 and 2009, we regressed the actual chlorophyll-a data from phytoplankton samples in Carpenter Reservoir (Section 2.3.2) with the modeled CE-QUAL-W2 output. These variables included temperature, turbidity, PAR, SRP (measured as PO_4) and DIN (NO_3-N + NH_4-N). CE-QUAL-W2 does not model DIN but rather NO_3-N. To calculate DIN, we added 5 $\mu g \cdot L^{-1}$ (the method detection limit for NH_4-N) to the modelled NO_3-N from CE-QUAL-W2 because NH_4-N was often at or below the instrument method detection limit in Carpenter Reservoir. Finally, we included water residence time to the chlorophyll-a/CE-QUAL-W2 regression model to match the regression with actual data measured in Carpenter during 2015 and 2016.

3 RESULTS AND DISCUSSION

3.1 Overview

Data from 2015 and 2016 have been compiled to answer four questions about what environmental variables and reservoir activities affect productivity in Carpenter Reservoir. Section 3.2 on periphyton biomass in the littoral habitat remains unchanged from last year's report. We will revise this section for the final draft in 2018. This report now includes a section on phytoplankton primary productivity and chlorophyll-a concentration in the pelagic habitat (Section 3.3.2). We have also updated the

regression modelling and results for zooplankton (Section 3.3.3). Data in Sections 3.2 and 3.3 focus on data collected from Carpenter Reservoir but also include data from Anderson and Seton Lakes, where appropriate, to enhance the statistical power and biological interpretation of the results.

3.2 Question 1: Is light the primary factor regulating productivity of the littoral habitat in Carpenter Reservoir

3.2.1 Periphyton

3.2.1.1 Stony substrate community composition

Periphyton found on polystyrene balls in Carpenter Reservoir were comprised of 64%, 71% and 86% chlorophytes during spring, summer and fall incubation periods, respectively (Table B-1 in APPENDIX B; Figure 11A; Greens). The chlorophytes in these samples were predominantly *Spirogyra* spp. Diatoms were also prevalent in all three time series making up 12-33% of the total biovolume of periphyton. *Melosira* sp., *Nitzschia* sp., *Cymbella* sp., *Achnanthes* sp. and *Stauroneis* sp. were among the most common species found throughout the sampling period.

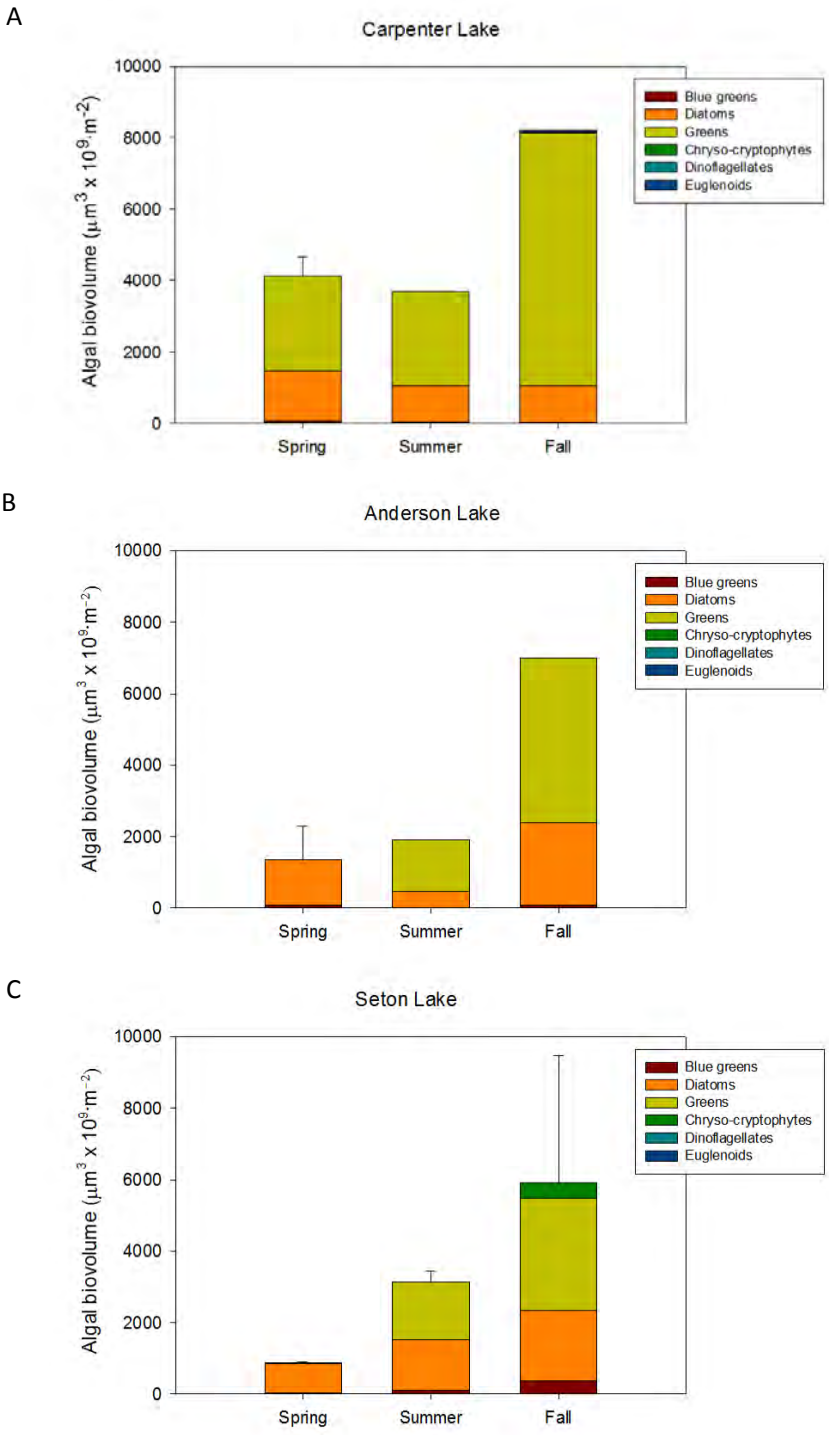

Figure 11. Algal biovolume by group found on polystyrene balls during each incubation period in (A) Carpenter Reservoir, (B) Anderson Lake and (C) Seton Lake. Standard deviations (error bars) were included where the mean of two samples was calculated.

The bulk of spring samples from both Anderson and Seton Lakes were comprised of diatoms (93% and 95%, respectively) with *Flagilaria* sp. *Nitzschia* sp. *Cymbella* sp. *Achnanthes* sp. and *Diatoma* sp. being the most abundant (Table B-1 in APPENDIX B; Figure 11B & C). A shift in composition occurred between spring and summer in both lakes where chlorophytes, specifically *Spirogyra* sp., became more abundant in the samples making up 75% and 51% of the periphyton community in Anderson and Seton Lakes, respectively. The remainder of the samples were composed of diatoms. This trend continued in Anderson Lake with a slight increase in blue-green algae, predominantly *Aphanisomenon* sp. In Seton Lake, while chlorophytes and diatoms still dominated the community, the biovolume of *Cryptomonas* sp., a chryso-cryptophyte, and blue-green algae, namely *Aphanisomenon* sp. increased (Figure 11B & C).

The chryso-cryptophytes, dinoflagellates and euglenoids identified from the polystyrene samples in Carpenter Reservoir and Seton Lake were likely not part of the samples as they are all free-living flagellated organisms, common to pelagic habitat (Table B-1 in APPENDIX B). These individuals were probably gathered from the water column as the polystyrene balls were pulled from the moorings.

3.2.1.2 Stony substrate regression analysis

Periphyton biomass, measured as chlorophyll-a, growing on polystyrene balls was higher in areas with greater accumulations of photosynthetically active radiation, warmer water and higher concentrations of dissolved inorganic nitrogen as shown by the top model in the AICc analysis (Equation 4). The top 10 of 40 models are shown in Table B-3 in APPENDIX B.

$$\log_{10}\text{Chlorophyll-a} = -0.58 + 2.08 \times 10^{9} * \text{PAR} + 0.05 * \text{Temperature} + 7.58 * \text{DIN} - 1.17 \times 10^{-10} * \text{PAR:Temperature}$$

Equation 4

The top model had an r^2 of 0.38 and was 1.29 and 2.27 times (ER) more likely than the next two models in the model set. Chlorophyll-a increased significantly with accumulated PAR to approximately 2.5×10^{8} μMol·m^{-2} and showed signs of saturation between 3 and 4×10^{8} μMol·m^{-2} (Figure 12A). Chlorophyll-a continuously increased with temperature between 6 and 20 °C and with dissolved inorganic nitrogen between 0.01 and 0.03 mg·L^{-1} (Figure 12B & C).

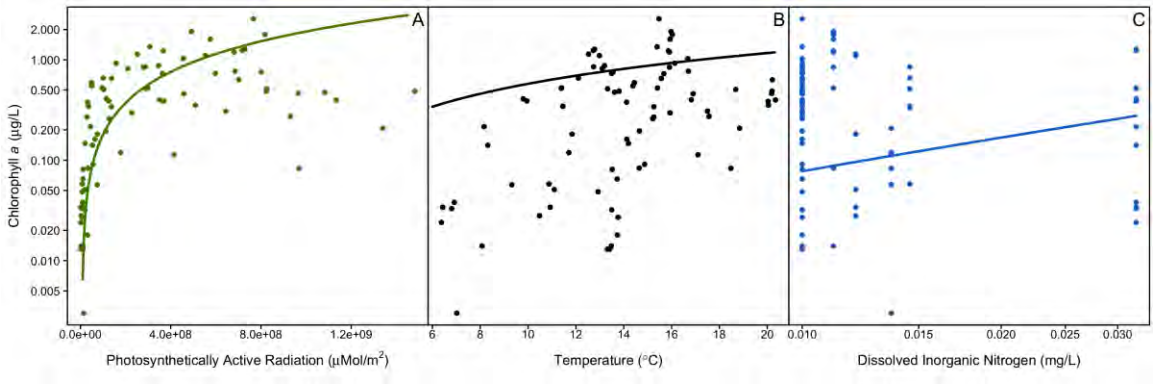

Figure 12. Relationship between chlorophyll-a, (A) photosynthetically active radiation (PAR), (B) water temperature and (C) dissolved inorganic nitrogen (DIN). The y-axis is log-transformed as is the x-axis for dissolved inorganic nitrogen but the data points are all untransformed so that units can be read from the figures. The model lines are derived from the intercept and coefficients from the top model selected by AICc and show the main effect of the environmental variable of interest while maintaining all other variables at their mean value.

There was a significant interaction between PAR and temperature such that the effect of temperature declined with increasing PAR and vice versa. Figure 13 shows a peak in chlorophyll-a concentration at values of PAR greater than 1.5×10^9 µMol·m^{-2} and water temperature less than 10 °C. A smaller peak also exists at PAR less than 5×10^8 µMol·m^{-2} and water temperature above 18 °C. The interaction between PAR and temperature may reflect the inherent seasonality between the two variables such that an increase in water temperature may lag behind increasing accumulated PAR in the spring and remain high into the fall as accumulated PAR declines with decreasing daylight.

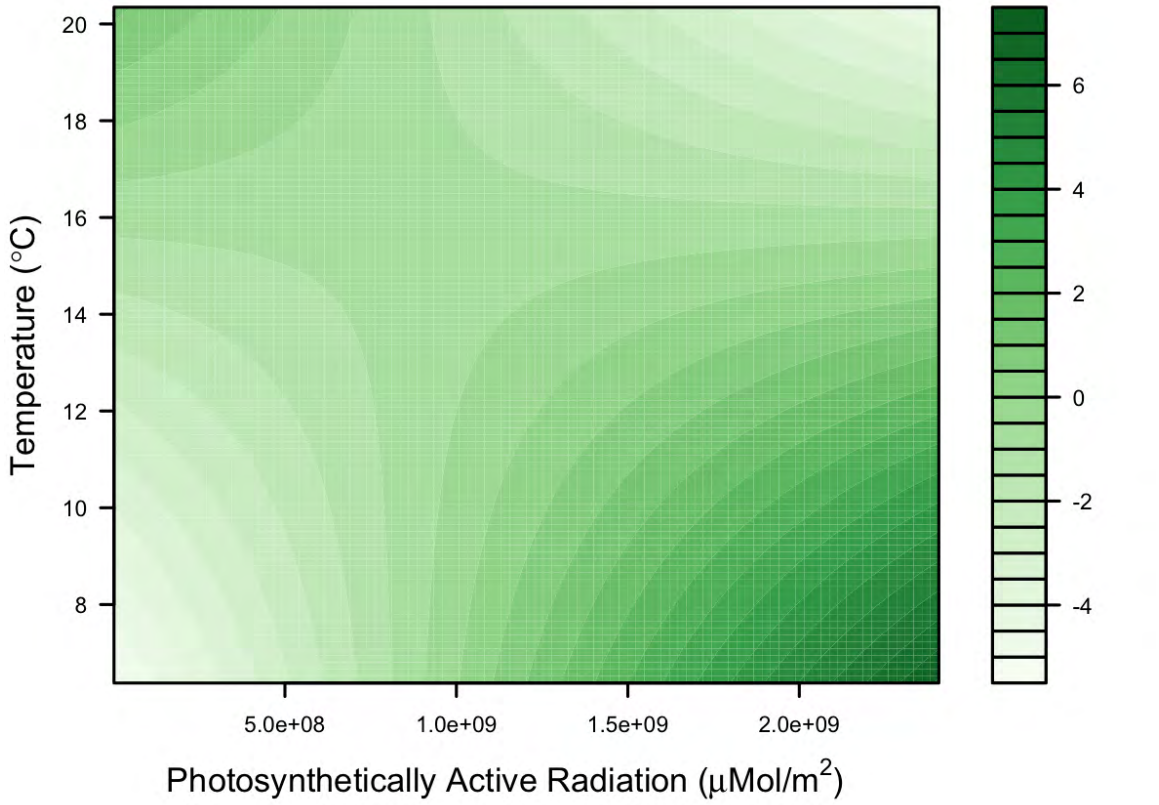

Figure 13. The combined effect of PAR and water temperature on chlorophyll-a concentration on polystyrene balls in the littoral habitat.

Interestingly, we did not see a peak in chlorophyll-a concentration at high temperatures and elevated levels of accumulated PAR as we might have expected based on the physiology of these organisms (Lamberti and Steinman, 1997). However, we know that *Spirogyra* spp. was the dominant species present on the polystyrene balls and that their biovolume increased throughout the 2015 growing season. Based on a study by Berry and Lembi (2000) certain forms of these chlorophytes are sensitive to high temperature and PAR. Consequently, the low chlorophyll-a concentration observed in Figure 11 might be a result of intolerance for these conditions.

Notably, the top ten models all included PAR and temperature suggesting these variables were primary factors regulating periphyton growth on the polystyrene balls in the 2015 growing season.

3.2.1.1 Sand substrate community composition

The periphyton community composition on sand was completely different and less dense than the community found on polystyrene balls in Carpenter Reservoir. Periphyton in the spring was entirely made up of *Cryptomonas* sp., a chryso-cryptophyte (Table B-1 in APPENDIX B; Figure 14). While in the summer, the community shifted to

100% diatoms dominated by *Stauroneis* sp. and some *Rhopalodia* sp. The community in the fall was approximately 5x larger than either of the previous seasons and was comprised primarily of *Cryptomonas* sp. (87%). The remaining portion was a combination of *Cymbella* sp. and *Stauroneis* sp., both diatom species. Chryso-cryptophytes are flagellated organisms suggesting that the individuals identified in the sand samples were likely from entrainment during the removal of the samples from the moorings. During analysis, we did not see any benthic algae attached to the sand particles but rather all free-living forms. This finding in part explains the low biomass observed in the sand samples compared to the polystyrene samples.

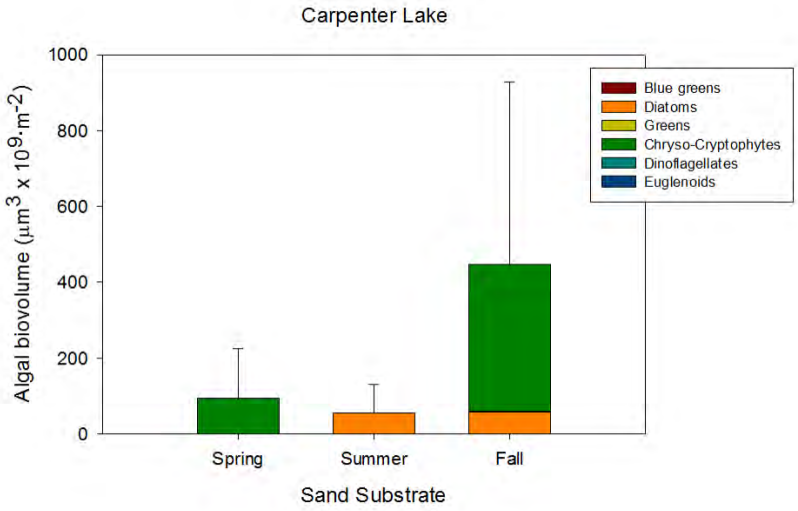

Figure 14. Algal biovolume, by group, found on sand substrate during each incubation period in Carpenter Reservoir. Error bars were included where the mean of two samples is shown.

3.2.1.2 Sand substrate regression analysis

The top four models for periphyton growth on sandy substrates had similar log-likelihoods, ΔAICc and evidence ratios but the amount of variation described by these models varied from 53% to 59% (Table B-4 in APPENDIX B). Given that the third model performed similarly to the other models with ΔAICc < 2, the magnitude and direction of the coefficients were similar among models and this model described the greatest amount of variation in the data (r^2 = 0.59), we selected the third model as the best descriptor of periphyton growth on sandy substrates (Equation 5),

$$\log_{10}\text{Chlorophyll-a} = -4.13 + 514.77 * \text{DIN} - 0.12 * \text{Turbidity} - 0.03 * \text{Temperature}.$$

Equation 5

This model showed that chlorophyll-a increased with higher concentrations of dissolved inorganic nitrogen but declined with increasing turbidity and water temperature (Figure 15).

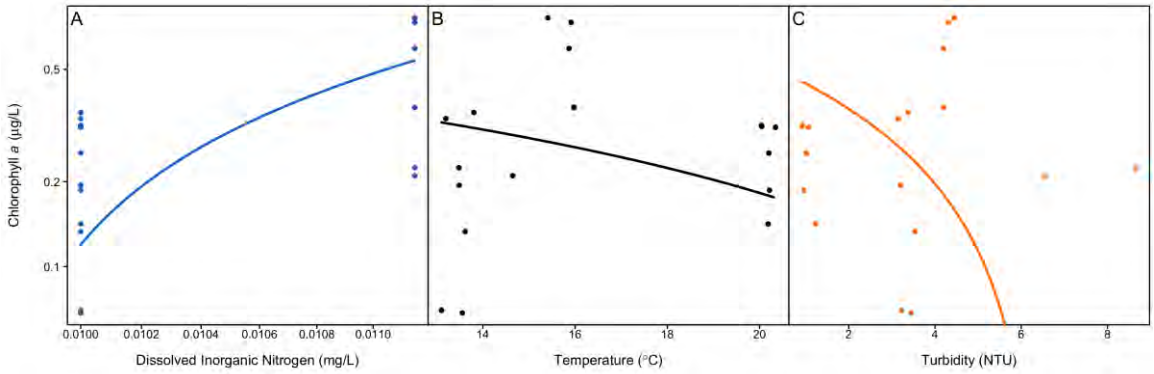

Figure 15. Relationship between chlorophyll-a, (A) dissolved inorganic nitrogen (DIN), (B) water temperature and (C) turbidity. The y-axis is log-transformed but the data points are all untransformed so that units can be read from the figures. The model lines are derived from the intercept and coefficients from the third model selected by AICc and show the main effect of the environmental variable of interest while maintaining all other variables at their mean value.

In this experiment, sand pails were deployed in Carpenter only as the other two lakes do not have sand bottoms. Sand offers less stability and surface area per particle for periphytic growth and can subsequently alter the metabolism in a system (Marcarelli, Huckins, and Eggert, 2015). This could explain the low biomass measured in the sand samples. Common disturbance in the reservoir may result from wave action in the littoral habitat but any effect of disturbance would be incorporated into the design of this experiment using sand pails. It is also worth noting that the majority of species found in the sand samples were chryso-cryptophytes, free-living flagellates that are common to the pelagic habitat. Therefore, the results for the sand samples in Carpenter may not be an accurate representation of the community residing in the littoral habitat on sand. This will be factored into the re-analysis of these data in 2017 when the 2016 data is incorporated.

With the above considerations and based on the results presented in Equation 5, periphyton growth, measured as chlorophyll-a, increased with dissolved inorganic nitrogen suggesting this community is nitrogen-limited. This is likely the case for all primary producers in these lakes as previous studies have identified Carpenter, Anderson and Seton as oligotrophic or ultraoligtrophic, meaning concentrations of dissolved nutrients accessible to primary producers are low (Limnotek, 2017) although shifts between nitrogen and phosphorus deficiency may occur between Carpenter Reservoir and Seton Lake in relation to changes in molar N:P supply ratios. For Carpenter Reservoir, the present model shows that the sand periphyton community is sensitive to change in inorganic N concentration. This finding means that change in DIN

concentration would be expected to have influence on areal biomass of algae on sand substrata. Potential changes in DIN concentration may originate from atmospheric sources (to be examined in 2017 data analysis) and from fluxes in transport of nitrogen from upstream and terrestrial sources (Allan and Castillo, 2007a). Further insight into the role of nitrogen on the algal assemblages having an affinity to sand will be further examined in upcoming data analyses in 2017.

The top model also showed that temperature and turbidity affected chlorophyll-a concentration on sand. While we expected that increased turbidity would have a negative effect on attached chlorophyll-a accrual as seen by Haven et al. (2001), it is interesting that temperature also had a negative effect, given it had a positive effect on chlorophyll-a concentration on the polystyrene balls. There is however, considerable variation in chlorophyll-a concentration with temperature and turbidity (Figure 15), which makes it difficult to discern a pattern in either direction. Additional data from 2016 will help resolve this uncertainty when the model is updated in 2017.

3.3 Question 2: Is light the primary factor regulating productivity of pelagic habitat in Carpenter Reservoir?

3.3.1 Overview

This section focuses on phytoplankton and zooplankton biomass. There were two regressions used to model phytoplankton: one for primary productivity measured as $mg \cdot C \cdot m^{-3} \cdot d^{-1}$ and biomass measured as µg chlorophyll-$a \cdot L^{-1}$. We also modeled zooplankton biomass using two regression models: one having phytoplankton biomass as an independent variable filtered on a 0.20 µm filter (called zooplankton-0.20) and a second with phytoplankton filter on a 0.75 µm filter (zooplankton-0.75). The 0.20 µm filter would capture phytoplankton > 0.20 µm while the 0.75 µm filter would capture phytoplankton > 0.75 µm. We were testing the hypothesis that zooplankton responds differently to different phytoplankton size classes.

3.3.2 Phytoplankton

3.3.2.1 Community composition and distribution

Phytoplankton biovolume was higher in 2016 than in 2015 at all stations with exception to S4 on Seton where the biovolume sampled in 2015 exceeded the 2016 biovolume in each month sampled (Figure 16, Figure 17, Table B-2 in APPENDIX B). Over the course of the 2015 and 2016 growing seasons in Carpenter and Seton, phytoplankton biovolume was highest in May and either abruptly (e.g. Figure 16A, Figure 17E) or slowly (e.g. Figure 17A, Figure 17F) declined to its lowest values in October (except station S5 in 2015 and C6 in 2016; Figure 16A,B,E,F; Figure 17A,B,E,F; Table B-2 in APPENDIX B). Peak biovolume in Anderson typically occurred later in the growing season in either July or August each year (Figure 16C,D; Figure 17C,D).

In 2015 and 2016, the phytoplankton community in Carpenter Reservoir was comprised mostly (32-88%) of *Ochromonas* spp. and *Uroglena americana*, which are

flagellates, from May to October. There was an observable peak in diatom biomass in May 2015 when diatoms comprised 37% and 33% of the total biomass at C2 and C6, respectively. *Asterionella Formosa* was the dominant diatom species found in Carpenter in 2015 comprising of 88% of all diatoms present. While in 2016, diatoms were present throughout most of the growing season at both stations with *Asterionella Formosa* and *Flagellaria crotonensis* comprising 16% and 69% of the total diatom assemblage, respectively. A notable shift occurred in June 2016, when *Botryococcus* sp., a green algae, occupied between 38-51% of the phytoplankton assemblage (Figure 17A,B). Otherwise, green algae made up less than 16% of the total assemblage in 2015 and 2016 in Carpenter Reservoir.

Phytoplankton in Anderson was a mix of flagellates (27-66% of all phytoplankton) and green algae (9-50% of all phytoplankton) throughout the growing season in 2015 but like Carpenter, diatoms were more abundant in 2016 and made up 11-62% of the phytoplankton samples collected in 2016 compared to half that in 2015 (3-26%; Figure 16C,D; Figure 17C,D; Table B-2 in APPENDIX B). The dominant flagellate species in 2015 and 2016 were *Ochromonas* spp. (34-49% of flagellates) and *Uroglena americana* (16-20% of flagellates), while the most common green algae in 2015 were *Oocystis* sp. (28% of green algae) and Staurastrum sp. (27% of green algae). Green algae in Anderson in 2016 were mostly comprised of *Oocystis* sp. (27% of green algae), *Botryococcus* sp. (13% of green algae) and *Kirchneriella* sp (13% of green algae). In 2015, the most common diatoms were *Aulacoseira* sp. (53% of diatoms) and *Discotella* sp. (26% of diatoms) with a shift in 2016 to more *Flagellaria crotonensis* (38% of diatoms), *Cyclotella sp.* (34% of diatoms) *and Aulacoseira* sp. (17% of diatoms).

Phytoplankton was typically more abundant in Seton than in Carpenter and Anderson. In 2015, the phytoplankton assemblage was mix of flagellates, diatoms and green algae, while green algae were almost non-existent in 2016 (Figure 16E,F; Figure 17 E,F; Table B-2 in APPENDIX B). The dominant species in Seton in 2015 were *Ochromonas* spp. (29% of flagellates), *Flagellaria crotonensis* (63% of diatoms) and *Oocystis* sp. (40% of green algae) while in 2016, *Ochromonas* spp. (53% of flagellates), *Uroglena americana* (23% of flagellates), *Flagellaria crotonensis* (58% of diatoms) and *Chlamydomonas* sp. (39% of green algae) were the most common phytoplankton species present.

Blue-green algae (cyanobacteria) was typically equal to or less than 2% of the phytoplankton assemblage in Carpenter, Anderson or Seton except for on three occasions when it was 3% in Carpenter at station C2 in September 2015, 4% at station A2 in Anderson in May 2015 and 5% at A1 in Anderson in July 2015 (Table B-2 in APPENDIX B).

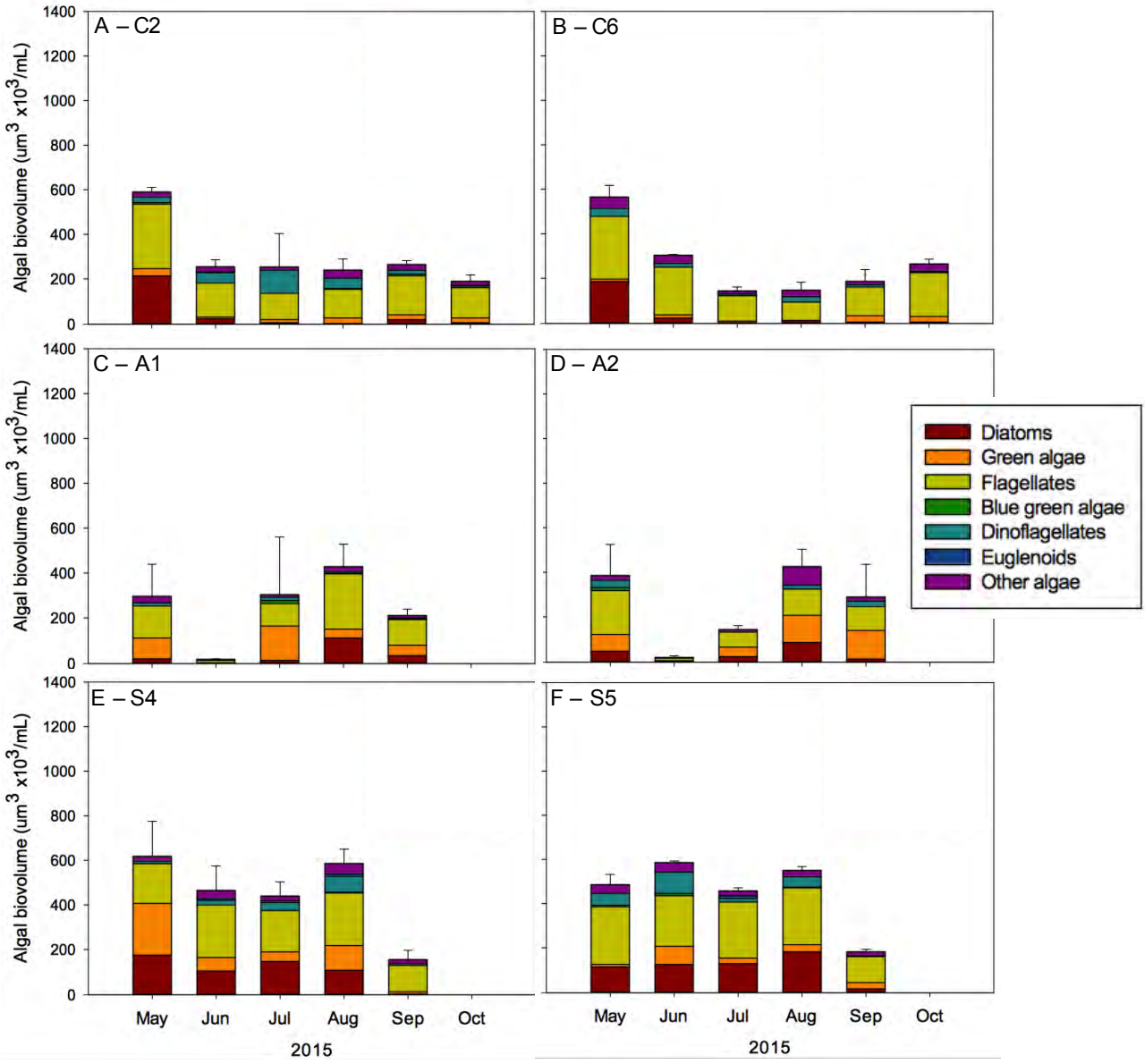

Figure 16. 2015 phytoplankton community composition by month in Carpenter Reservoir at station C2 and C6 (A & B), Anderson Lake at station A1 and A2 (C & D) and Seton Lake at station S4 and S5 (E & F).

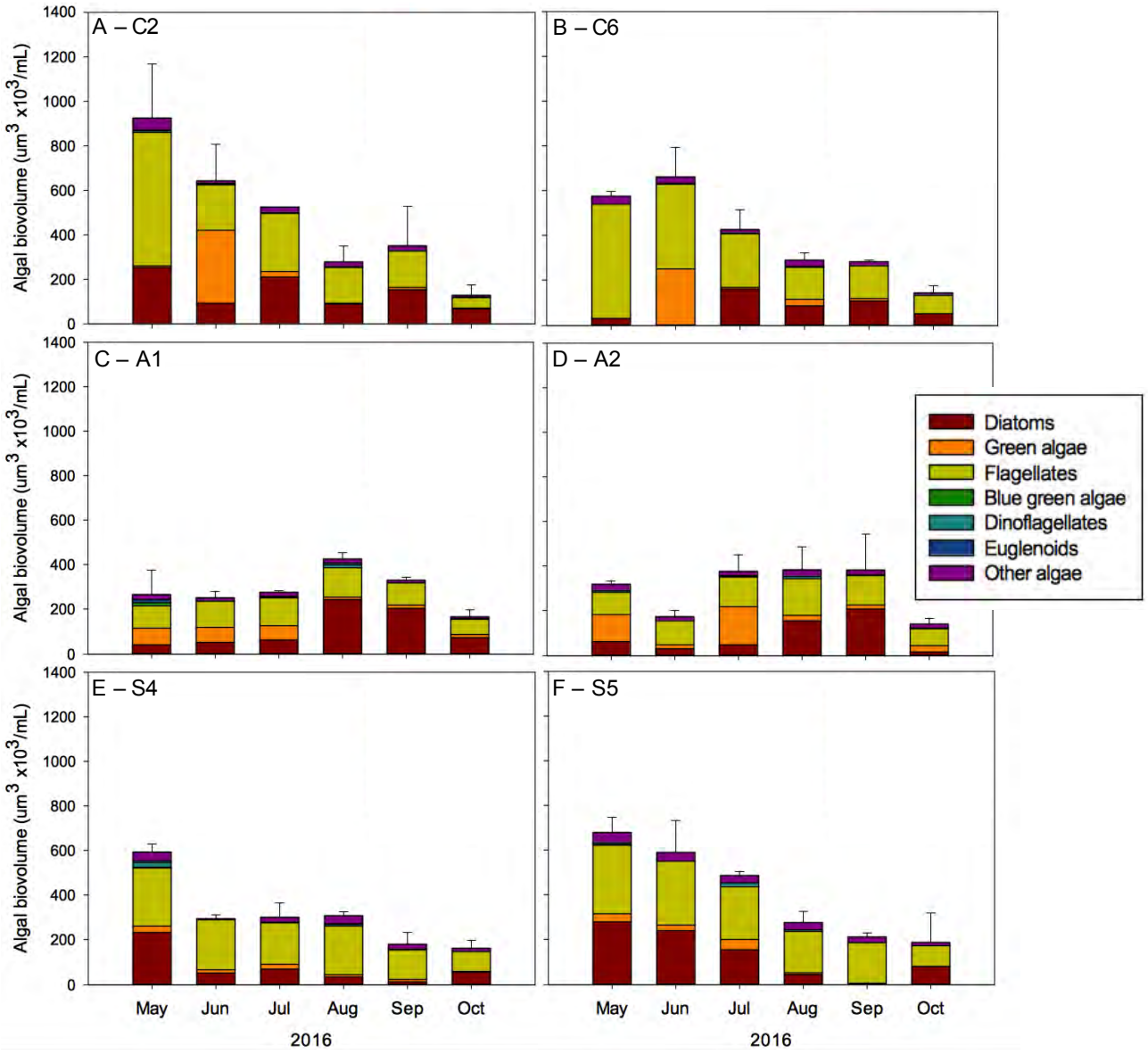

Figure 17. 2016 phytoplankton community composition by month in Carpenter Reservoir at station C2 and C6 (A & B), Anderson Lake at station A1 and A2 (C & D) and Seton Lake at station S4 and S5 (E & F).

3.3.2.2 Primary Productivity Regression Analysis

Primary productivity in Carpenter, Anderson and Seton was higher when there was more light (measured as a percent of surface PAR), shorter water residence time, less turbidity and warmer water temperature (Table 13). The averaged model is presented in Equation 6 and the standardized coefficients and other averaged model statistics are presented in Table 13. The candidate model set that was used to derive the averaged coefficients is presented in Table B-5 in APPENDIX B. These models had an r^2 of 0.18 to 0.21 and model weights that ranged from 0.01 to 0.9.

$$\log_{10}\text{Primary Productivity} = 0.705 + 0.004*\text{PAR} - 5.74 \times 10^{-5}*\text{Water Residence Time} - 0.019*\text{Turbidity} + 0.008*\text{Temperature} - 0.090*\text{SRP} - 0.001*\text{DIN}$$

Equation 6

Table 13. Averaged coefficients and statistics for 2015 and 2016 phytoplankton primary productivity in Carpenter, Anderson and Seton.

Variable	Standardized Coefficient	Estimate	Adjusted SE	z-value	p-value	RVI
(Intercept)	0.000	0.705	0.245	2.876	<0.001	
PAR	0.317	0.004	0.001	5.564	<0.001	1.000
Water Residence Time	-0.169	-5.74×10^{-5}	0.000	2.126	0.03	0.930
Turbidity	-0.176	-0.019	0.009	2.093	0.04	0.920
Temperature	0.074	0.008	0.008	0.938	0.35	0.620
SRP	-0.024	-0.090	0.170	0.530	0.60	0.380
DIN	-0.023	-0.001	0.002	0.461	0.64	0.340

Note: Estimate is the unstandardized coefficients that are presented in Equation 6.

RVI is the relative variable importance and is the percentage of models in the candidate set where the predictor variable was present.

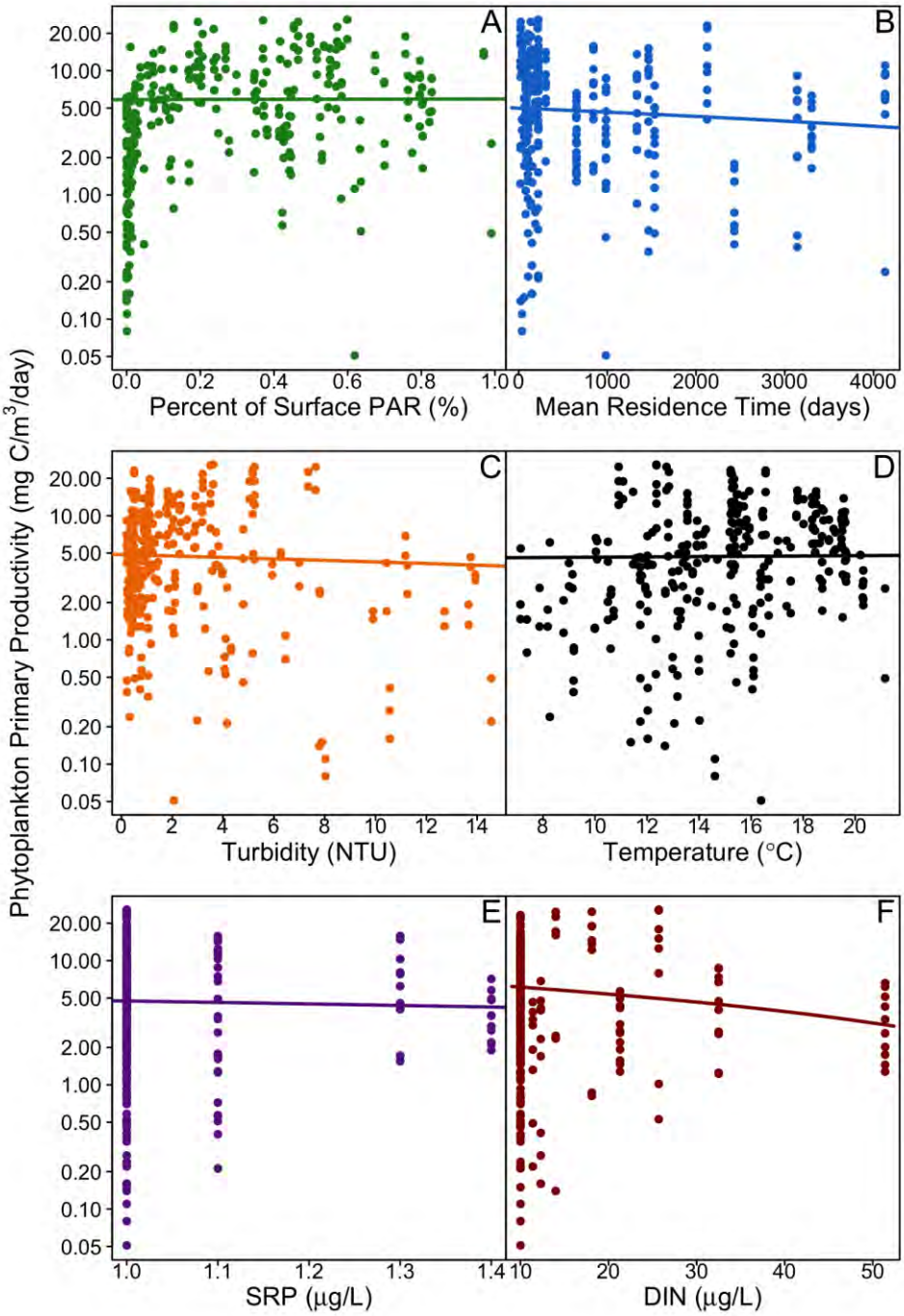

Figure 18. Relationship between phytoplankton primary productivity (A) percent surface PAR, (B) mean water residence time, (C) turbidity and (D) water temperature, (E) soluble reactive phosphorus (SRP) and (F) dissolved inorganic nitrogen (DIN). The model lines are derived from the intercept and coefficients from the averaged model coefficients in Table 13 and show the main effect of the environmental variable of interest while maintaining all other variables at their mean value. Each point represents a sample from each month and year sampled.

PAR was present in all the models in the candidate model set (RVI = 1; Table 13; Table B-5 in APPENDIX B) and had an effect size 1.87 and 1.77 times greater than the next two variables, water residence time and turbidity, on phytoplankton primary productivity. This shows the importance PAR has in explaining primary production in Carpenter, Anderson and Seton. PAR limits photosynthetic production in aquatic environments (Wetzel 2001), which can be affected by additional particles in the water measured as turbidity. Turbidity and PAR were not highly correlated (Figure A-1 in APPENDIX A) suggesting these two variables could explain different aspects of primary production. In this case, given the difference in turbidity between Carpenter, Anderson and Seton (Table 6; Figure 5), turbidity in the primary productivity model is likely explaining the differences between lakes that is unaccounted for in the global model.

Water residence time, like turbidity, may also help account for the inherent differences between Carpenter, Anderson and Seton. Water residence time does not directly affect the ^{14}C uptake measured in the bottles used to calculated primary productivity (Section 2.3.2) but was included in the analysis to account for water turnover time in the lakes and reservoir as well as differences between water bodies not accounted for by the other predictor variables.

Higher primary production in this case was associated with shorter water residence times. Despite the negative relationship with turbidity, which would suggest that primary production is higher in Anderson than in Carpenter, the negative relationship with water residence time implies the opposite. Including data from Anderson Lake (and possibly Seton Lake) may be confounding the relationships we are observing between primary productivity and the environmental variables in the current model structure. That is, food web relationships that exist in Anderson Lake (and possibly Seton Lake), such as rates of herbivory and nutrient concentrations, may be biasing the model results and not reflect the processes occurring in Carpenter Reservoir. This became apparent when assessing the direction and magnitude of the coefficients in Table 13 and Equation 6 against our predictions in Table 4 as well as the relatively low model fit (r^2) for the top models in the candidate set (Table B-5 in APPENDIX B). We will explore the implications of removing data from Anderson Lake and modelling data from Carpenter Reservoir and Seton Lake separately. It may be that the trophic interactions in a large lake like Anderson are not reflective of the interactions observed in a smaller reservoir such as Carpenter.

3.3.2.3 Chlorophyll-a Regression Analysis

Phytoplankton biomass, measured as chlorophyll-a, in Carpenter, Anderson and Seton, decreased with increasing PAR (measured as percent of surface PAR), DIN, SRP, water temperature, turbidity, and residence time Figure 19. The averaged model is presented in Equation 7 with unstandardized coefficients. Standardized model coefficients and other statistics are presented in Table 14 and the full candidate set used

to average the coefficients is presented in Table B-6 in APPENDIX B. The r^2 for the eight models in the candidate set was 0.30.

$$\log_{10}\text{Chlorophyll-a} = 0.565 - 0.006*\text{DIN} - 0.056*\text{PAR} - 0.011*\text{Temperature} - 0.002*\text{Turbidity} - 0.009*\text{SRP} - 1.60 \times 10^{-7}*\text{Water Residence Time}$$

Equation 7

Table 14. Averaged coefficients and statistics for 2015 and 2016 phytoplankton chlorophyll-a in Carpenter, Anderson and Seton.

Variable	Standardized Coefficient	Estimate	Adjusted SE	z-value	p-value	RVI
(Intercept)	0.000	0.565	0.066	8.564	<0.0001	
PAR	-0.132	-0.056	0.020	2.789	0.01	1.00
DIN	-0.502	-0.006	0.001	8.714	<0.0001	1.00
Temperature	-0.297	-0.011	0.002	4.984	0.00	1.00
Turbidity	-0.061	-0.002	0.002	0.986	0.32	0.63
SRP	-0.007	-0.009	0.040	0.237	0.81	0.28
Water Residence Time	-0.002	-1.60×10^{-7}	0.000	0.046	0.96	0.26

Note: Estimate is the unstandardized coefficients that are presented in Equation 7

RVI is the relative variable importance and is the percentage of models in the candidate set where the predictor variable was present.

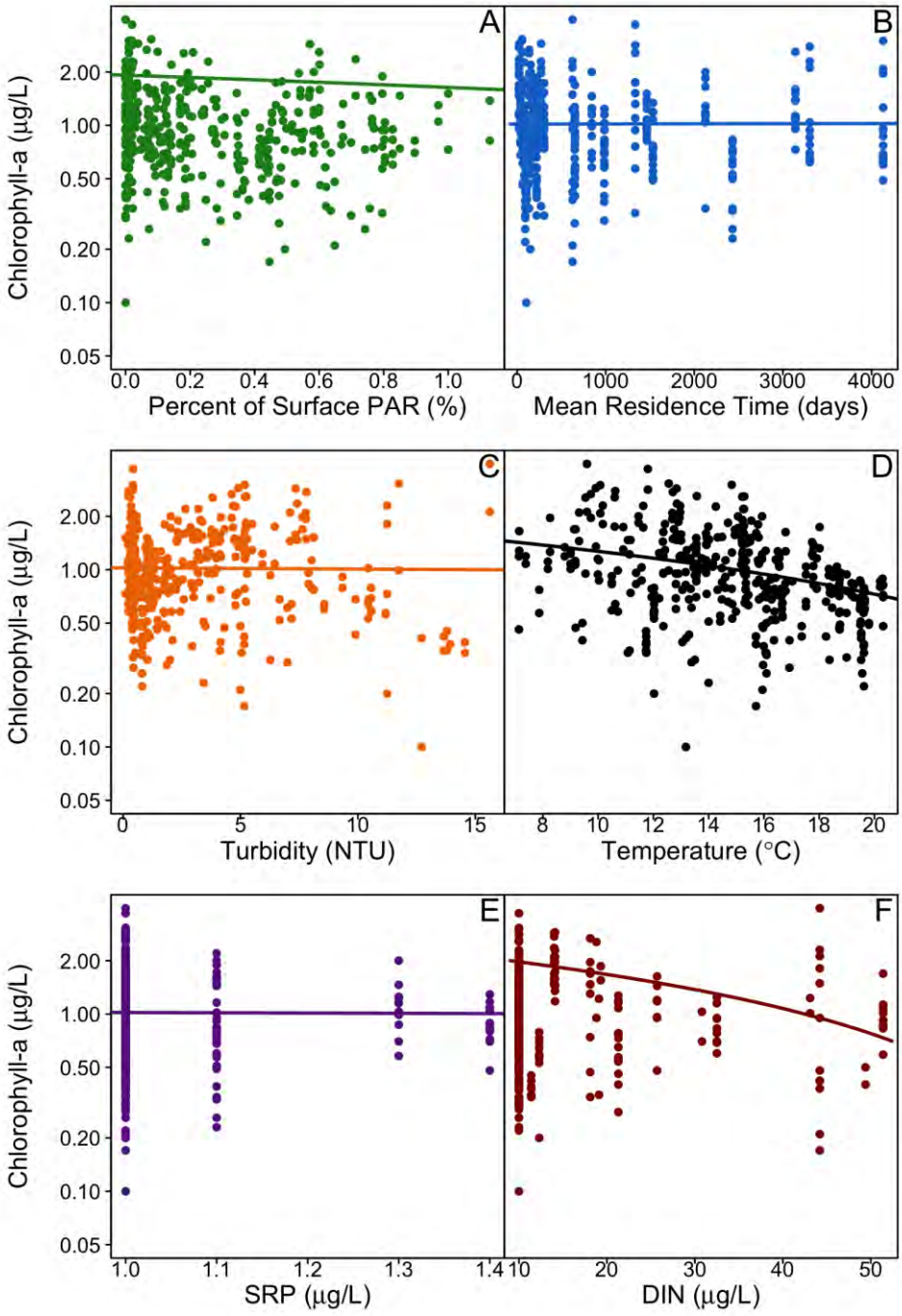

Figure 19. Relationship between phytoplankton biomass measured as chlorophyll-a (A) percent surface PAR, (B) mean water residence time, (C) turbidity and (D) water temperature, (E) soluble reactive phosphorus (SRP) and (F) dissolved inorganic nitrogen (DIN). The model lines are derived from the intercept and coefficients from the averaged model coefficients in Table 14 and show the main effect of the environmental variable of interest while maintaining all other variables at their mean value. Each point represents a sample from each month and year sampled.

The results for the averaged model (Equation 7) and models presented in the candidate (Table B-6 in APPENDIX B) for phytoplankton biomass seemed counter intuitive until further inspection revealed that the chlorophyll-a maxima occurred between 3-10 m deep in Carpenter, 5-30 m deep in Anderson and 3-25 m deep in Seton as shown by the fluorescence measured with the CTD profiler (Figure 20). This peak in biomass 3 m or below the surface, corresponded with lower water temperature, turbidity and fluorescence and explains the negative relationships with these variables in Equation 7 (Figure 21, Figure 22 and Figure 23). The deep chlorophyll-a maxima also suggest that to maintain current chlorophyll-a concentrations, drawdown would need to be managed accordingly to avoid displacing primary producers.

Finally, chlorophyll-a concentration also declined with water residence time. For similar reasons to primary productivity, we believe the data from Anderson Lake (and possibly Seton Lake) may be biasing the results. That is, food web interactions, such as predator-prey relationships, and nutrient dynamics occurring in Anderson Lake may be swaying the results and not be accurately representing the interaction between phytoplankton biomass and environmental variables in Carpenter. Originally included to increase the predictive power of the models, data from Anderson and Seton may not allow us to accurately model data from Carpenter Reservoir. As such water residence time and turbidity may be reflecting other processes in the lakes that are not being accounted for by the other variables in the models. For this reason, we will model data from Carpenter Reservoir and Seton Lake separately and explore the model statistics after removing data collected from Anderson. These changes may improve the fit (r^2) and consequently the predictive power of the models for both primary productivity and biomass.

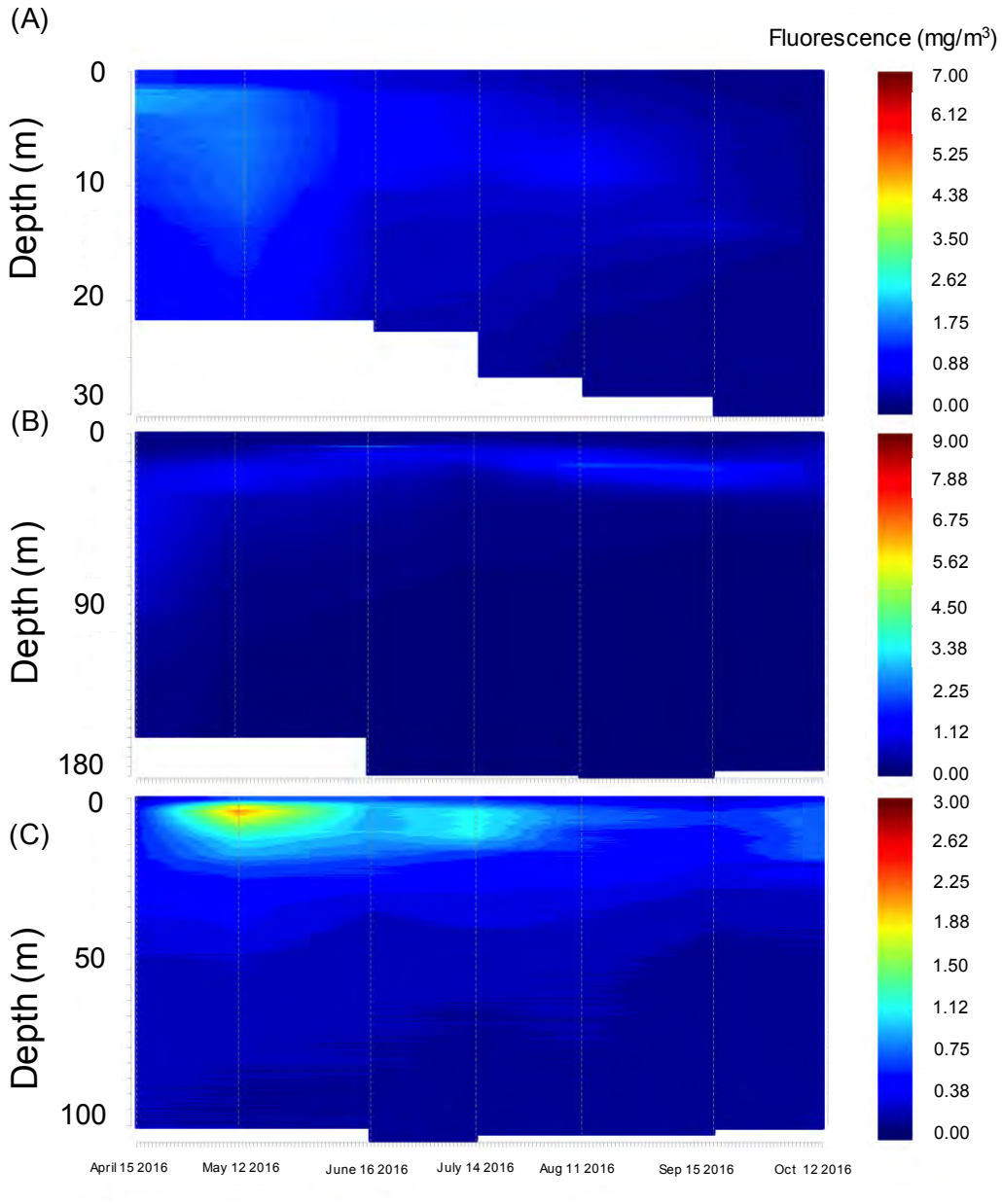

Figure 20. Fluorescence in (A) Carpenter Reservoir at station C2, (B) Anderson Lake at station A1, and (C) Seton Lake at station S4 from April to October 2016. Note the difference in depths on the left and colour scales on the right.

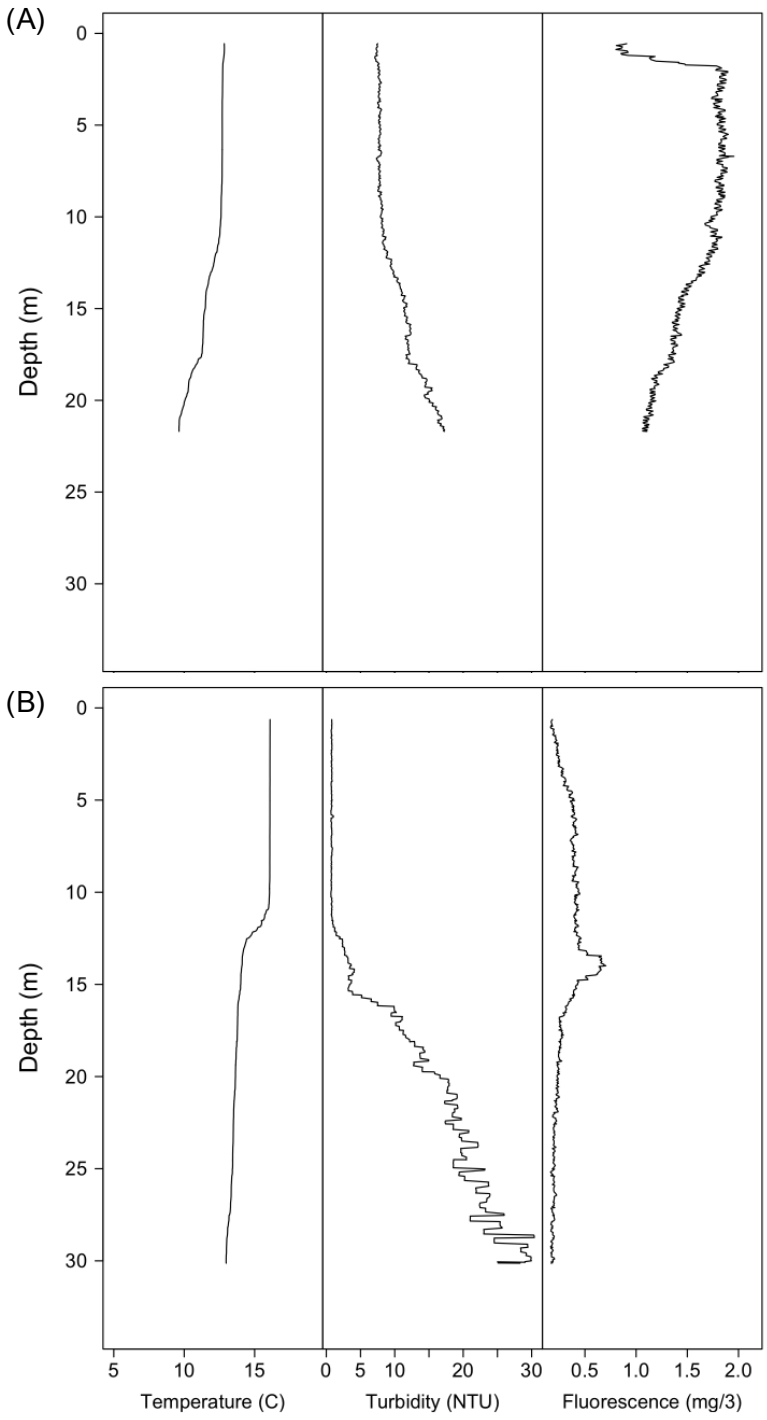

Figure 21. Temperature, turbidity and fluorescence from the CTD profiler in (A) May and (B) September 2016 in Carpenter Reservoir at station C2.

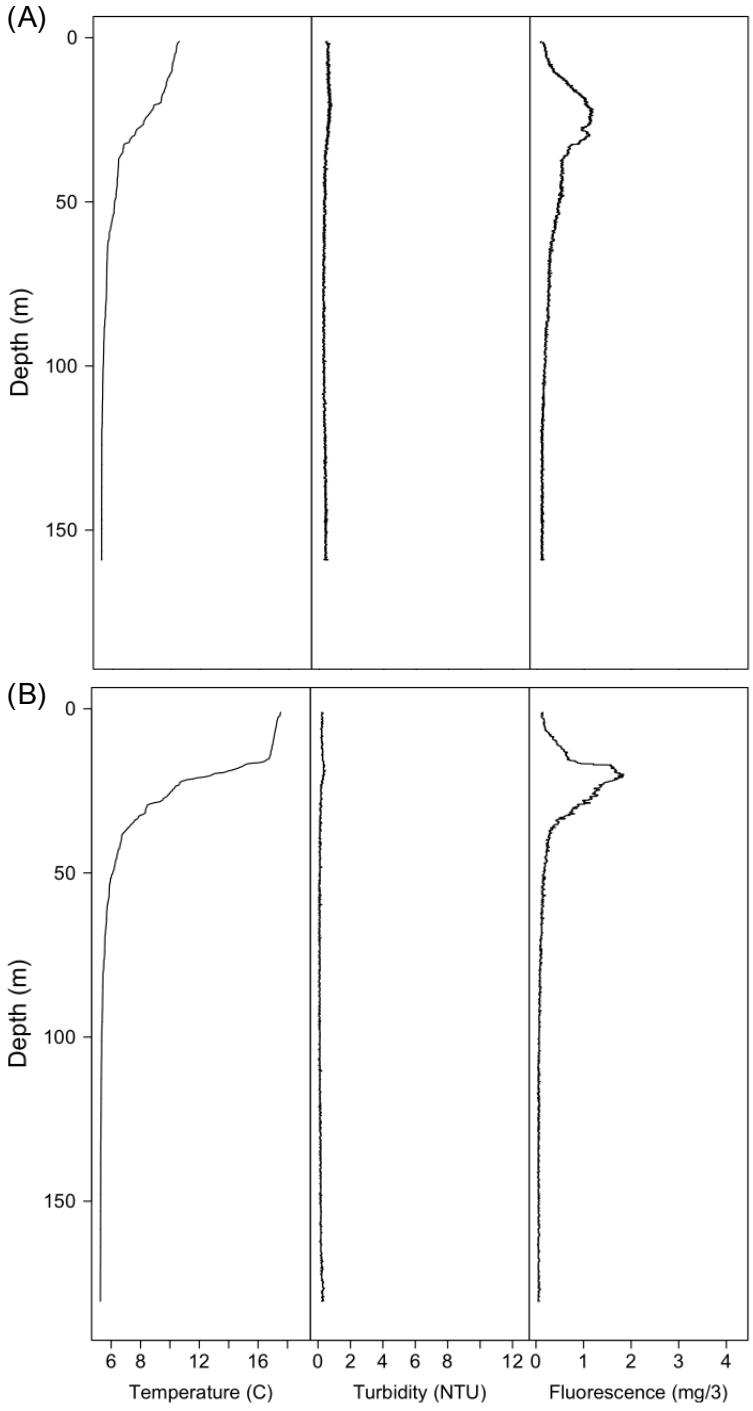

Figure 22. Temperature, turbidity and fluorescence from the CTD profiler in (A) May and (B) September 2016 in Anderson Lake at station A2.

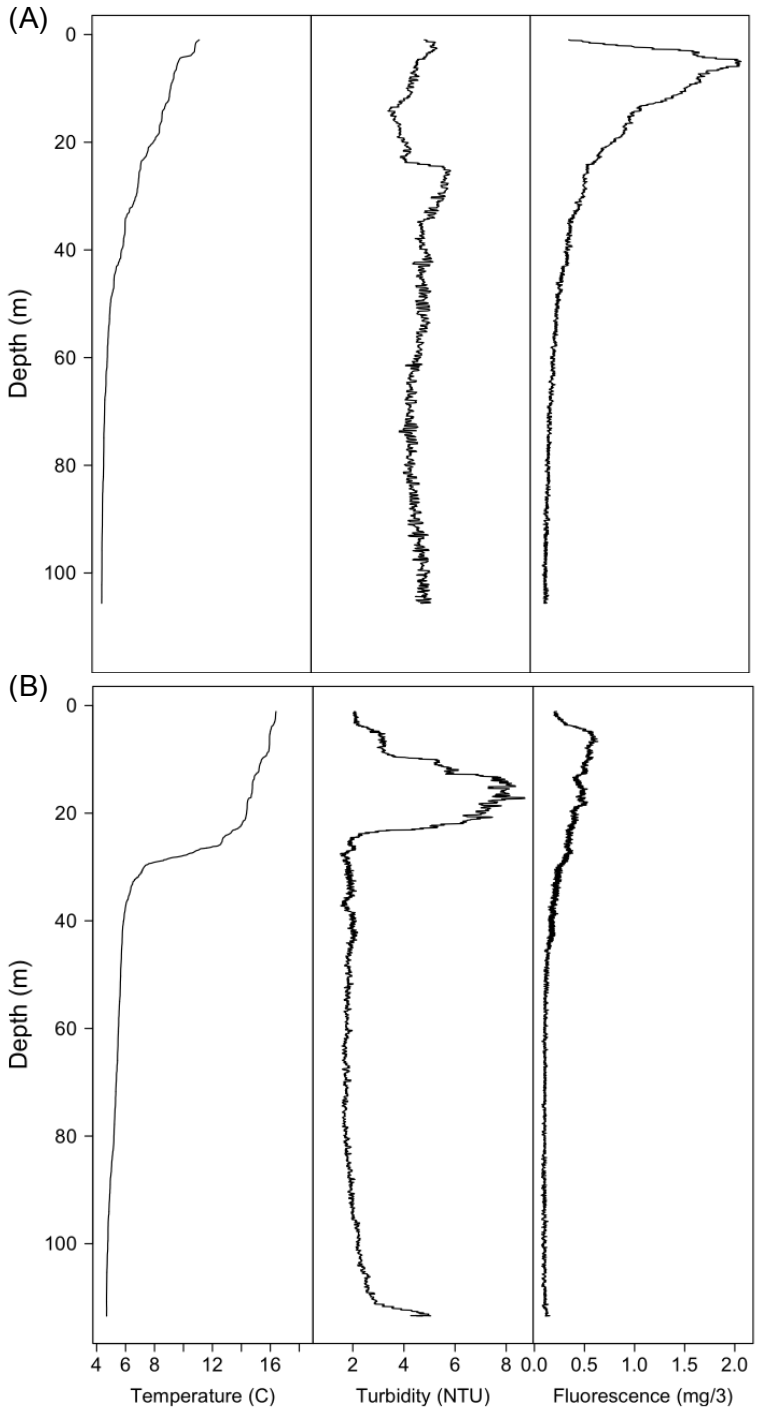

Figure 23. Temperature, turbidity and fluorescence from the CTD profiler in (A) May and (B) September 2016 in Seton Lake at station S4.

3.3.3 Zooplankton

3.3.3.1 Community composition

Zooplankton biomass in 2015 increased 10 fold from May to July at station C2 in Carpenter Reservoir to a peak biomass of 3,399 mg dry weight/m^2 (Table B-8 in APPENDIX B; Figure 24). Biomass declined back to spring values by October when the last sample was collected. There was a one-month lag in biomass at station C6 compared to C2 whereby peak biomass (3,504 mg dry weight/m^2) occurred in August and was 100x greater than in May at the same station. In 2016, zooplankton biomass was more variable than in 2015, with a notable peak in June at station C2. This peak was more than 4x the peak biomass observed at either station in 2015 and almost 5x larger than the next highest biomass in 2016 (Table B-8 in APPENDIX B; Figure 25).

Throughout the season, the zooplankton community was dominated by cladocerans at both stations and in both years (except for May and June 2016). *Daphnia* spp. made up 90% or more of the cladocerans present except in May when half the cladocerans were *Leptodora* sp. and half were *Daphnia* spp. At both stations, cyclopods peaked in June 2015 and 2016, making up approximately 35% and 95% of the zooplankton community, of which 95% or more were *Cyclops* spp. Peak calanoid biomass occurred in July and August 2015 at stations C2 and C6, respectively, making up approximately 20% of the samples and comprised primarily of *Acnathodiaptomus* spp. However, less than 13% of the total zooplankton biomass in 2016 was calanoids. Of the individuals present, 60% were *Epichura* spp. and 28% were copepod nauplii.

The zooplankton community in Anderson Lake was similar to Carpenter Reservoir with some notable differences. Total biomass was 1.5x to 60x (May, C6 vs. A2) higher in Anderson compared to Carpenter (Table B-8 in APPENDIX B; Figure 24). Zooplankton biomass in 2016 peaked at both stations in June, being 2-7x larger than at other times during the growing season.

Cyclopoida biomass in 2015 was higher throughout the sampling season at both stations in Anderson, with few calanoids compared to Carpenter (Figure 24). Peak cyclopoid biomass occurred in May at stations A1 and A2, in 2015 and 2016 with 794 to 1,271 mg dry weight/m^2. The proportion of cyclopoids declined in the middle of the season and rebounded by October to near spring values (Figure 24 and Figure 25). *Cyclops* spp. made up 91% or more of the total cyclopoids present. However, as in Carpenter, the zooplankton community was largely made up of cladocerans with 95% or more of those being *Daphnia* spp. (Table B-8 in APPENDIX B; Figure 24 and Figure 25). The only exception was at A1 in September 2015, where 30% of the community was Eubosmina spp.

Total monthly biomass at both stations in Seton were remarkably similar from month to month and year to year. The zooplankton in Seton was also lower in the summer compared to Carpenter and Anderson (Table B-8 in APPENDIX B; Figure 24

and Figure 25). Most of the community in May was comprised of cyclopoids (84-91%) and the bulk of these individuals were *Cyclops* spp. However, *Daphnia* spp. (Cladocera) quickly dominated the zooplankton community making up 70% or more of the samples from July to September in 2015 and 2016. Calanoids were present throughout the season but made up 12% or less of the total community (Table B-8 in APPENDIX B; Figure 24 and Figure 25).

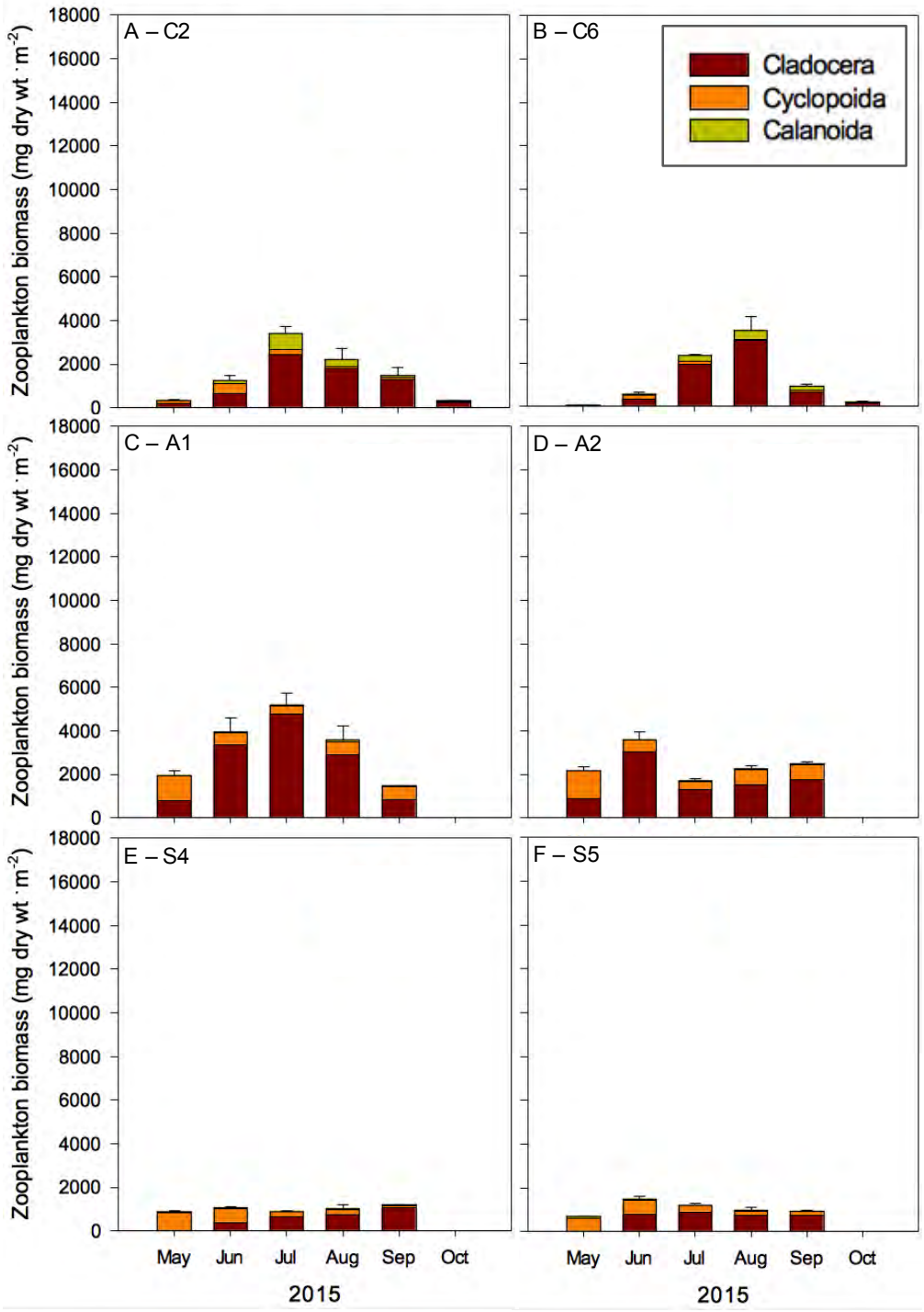

Figure 24. Zooplankton biomass by month and station in Carpenter Reservoir at stations C2 and C6 (A & B), Anderson Lake at stations A1 and A2 (C & D) and in Seton Lake at stations S4 and S5 (E & F). Error bars were included when the mean of two samples was calculated.

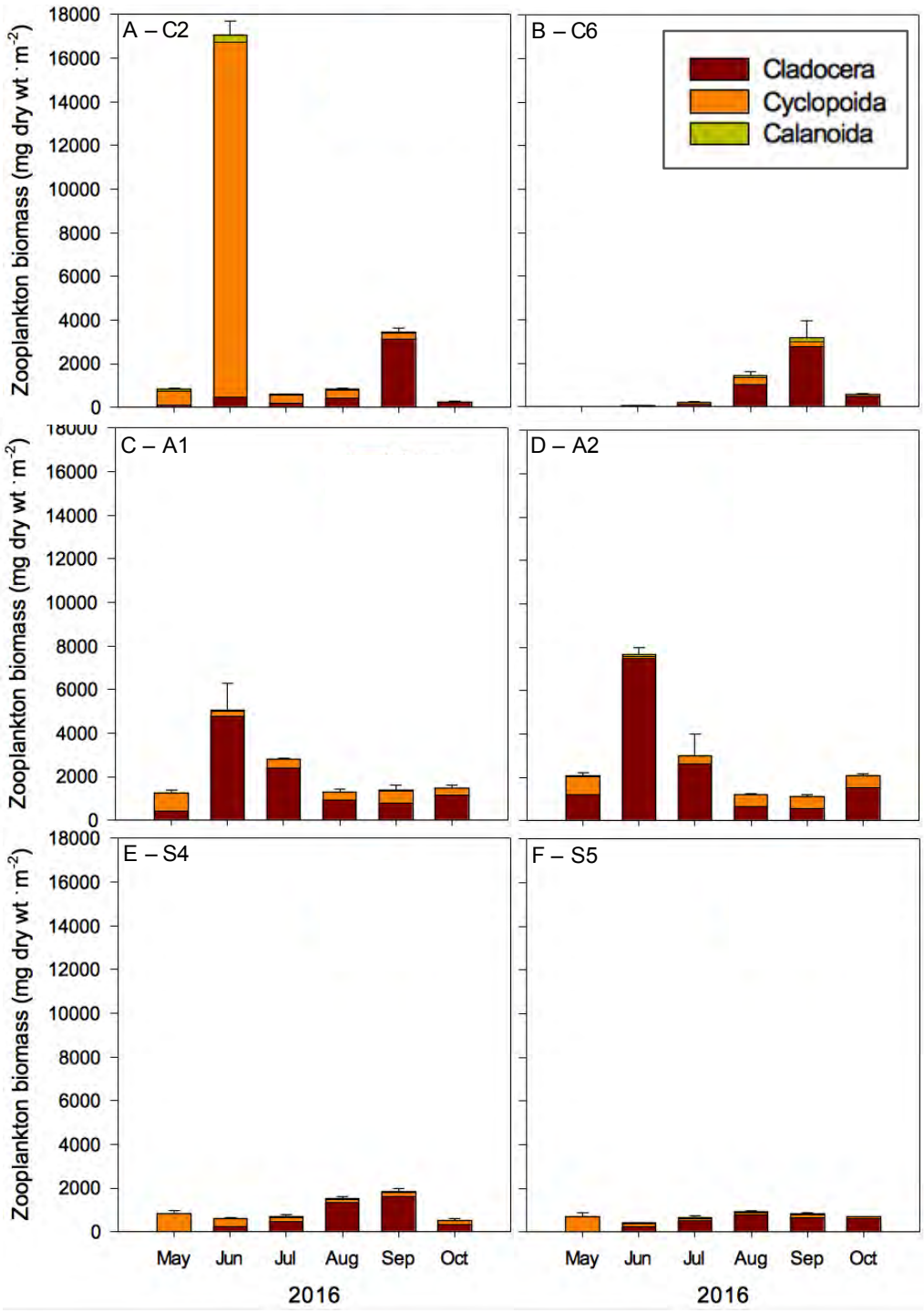

Figure 25. Zooplankton biomass by month and station in Carpenter Reservoir at stations C2 and C6 (A & B), Anderson Lake at stations A1 and A2 (C & D) and in Seton Lake at stations S4 and S5 (E & F). Error bars were included when the mean of two samples was calculated.

3.3.3.2 Regression analysis for zooplankton-0.20

There was more zooplankton biomass at stations with lower phytoplankton biomass as measured by chlorophyll-a from 0.20 μm filters, warmer water, less turbidity, and longer water residence time (Figure 26). The averaged model is presented in Equation 8 and the standardized coefficients and other averaged model statistics are presented in Table 13.

$\log_{10}$Zooplankton-0.20 = 0.1*Temperature - 0.579*Turbidity + 0.009*Mean Water Residence Time - 0.274*Chlorophyll-a-0.20.

Equation 8

The r^2 for the models in the candidate set were 0.39 to 0.49 with model weights up to 0.41 (Table B-9 in APPENDIX B). The effects of each environmental variable are clearly visible in Figure 26.

Table 15. Averaged coefficients and statistics for 2015 and 2016 zooplankton biomass including chlorophyll-a sampled with a 0.20 μm filter in Carpenter, Anderson and Seton.

Variable	Standardized Coefficient	Estimate	Adjusted SE	z-value	p-value	RVI
(Intercept)	0.000	0.000	0.000	NA	NA	
Chlorophyll-a	-0.274	-0.274	0.069	3.958	0.000	1.000
Temperature	0.100	0.100	0.106	0.946	0.344	1.000
Turbidity	-0.579	-0.579	0.103	5.601	<2.00E-16	0.630
Mean Water Residence Time	0.009	0.009	0.046	0.201	0.840	0.160

Note: Estimate is the unstandardized coefficients that are presented in Equation 6.

RVI is the relative variable importance

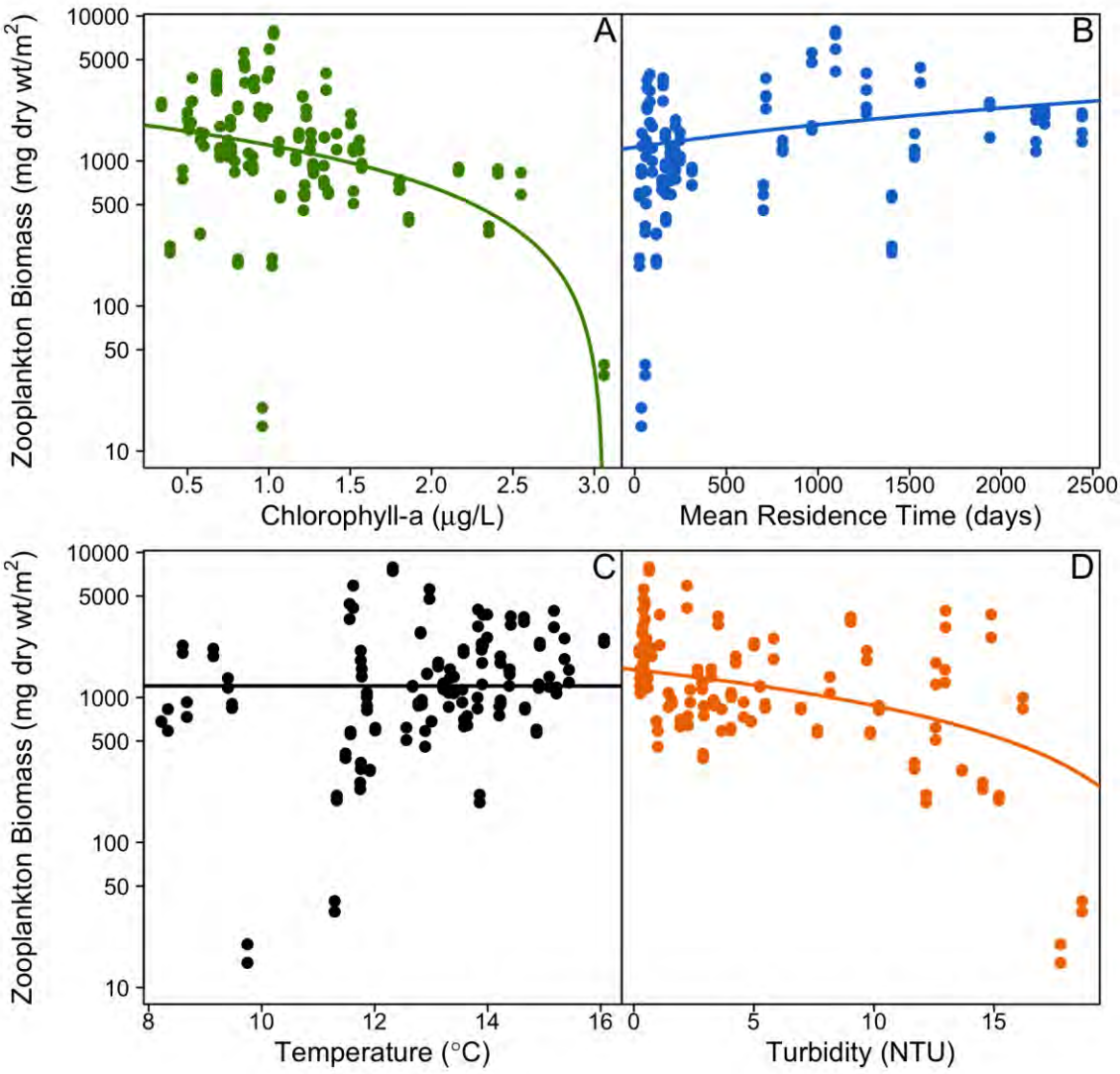

Figure 26. Relationship between zooplankton biomass (A) chlorophyll-a-0.20, (B) mean water residence time, (C) water temperature and (D) turbidity. The model lines are derived from the intercept and coefficients from the averaged model in Table 15 and show the main effect of the environmental variable of interest while maintaining all other variables at their mean value. Each point represents a replicate from each month and year sampled.

While there is considerable variation in zooplankton biomass at low levels of chlorophyll-a, zooplankton biomass was inversely related to phytoplankton biomass, which is what we would predict if grazing by zooplankton alone strongly affected phytoplankton biomass. That is, as zooplankton biomass increases, so would the amount of phytoplankton they consume. This relationship between herbivores and plants has been shown in a variety of habitats but is particularly strong in aquatic systems (Cyr and Face, 1993). It is not consistent among lakes, however, and in many cases zooplankton and phytoplankton biomass are positively related where top down

control of phytoplankton is not a factor determining phytoplankton biomass (Shuter and Ing 1997).

There was a positive relationship between mean water residence time and zooplankton biomass as seen in other studies on zooplankton (e.g. Basu, and Pick, 1996). The longer the water resided in the lake or reservoir the more zooplankton biomass that was present. Residence time ranged from approximately 2.5 months (80 days ± 9) in Carpenter Reservoir to almost 8 months (233 days ± 22) in Seton Lake and just over 4 years (1593 days ± 228) in Anderson Lake. For this analysis, we used a shifting 78-day mean based on the day zooplankton was sampled. This 78-day mean corresponds to the mean lifespan of common zooplankton species (Korpelainen, 1986; Schwartz and Ballinger, 1980); a water residence time less than this would potentially flush developing zooplankton from the system. This is particularly relevant in Carpenter Reservoir given that the mean water residence time at the beginning of the zooplankton growing season is typically less than 78 days (minimum mean recorded value = 56 days in May 2015). The low residence time in the reservoir would have important implications for pelagic food web interactions. Water residence time lower than time needed for cladocerans and cyclopoids to fully develop and reproduce would strongly limit availability of zooplankton as food for pelagic fish, potentially forcing a shift to food produced in benthic habitats. This kind of response was shown by Wu and Culver (1992), albeit for a different food web than in Carpenter, but still relevant with respect to potential shifts in trophic interactions caused by change in limitation of zooplankton production.

Zooplankton biomass increased with water temperature and decreased with turbidity. Temperature ranged between 8 and 16 °C, within the range of maximum lifespans reported for common *Daphnia* spp. (Korpelainen, 1986), which make up most these samples (Figure 24 and Figure 25). We would expect temperature to have a negative effect on zooplankton biomass if it were to increase beyond 24 °C (Korpelainen, 1986). Turbidity measures the amount of light scatter, which results from of organic (e.g. plankton, detritus) and inorganic (e.g. silt and clay) suspended solids in the water column (Jeppesen, Jensen, Søndergaard, and Lauridsen, 1999). Turbidity may not directly affect zooplankton production but rather phytoplankton production and result in less food for zooplankton. In fact, in Sections 3.3.2.2 and 3.3.2.3 we discussed the negative correlation between phytoplankton and turbidity in 2015 and 2016 in Carpenter, Anderson and Seton. These current findings further highlight the importance of temperature and turbidity in regulating biological production in these systems.

3.3.3.3 Regression analysis for zooplankton-0.75

There was a shallower slope between zooplankton and the larger size class of phytoplankton (Table 16; Figure 27) suggesting zooplankton were feeding more regularly on smaller phytoplankton. Otherwise the direction and magnitude of the other predictor variables included in the model had a similar effect on zooplankton as in the analysis present in Section 3.3.3.2. In this case, zooplankton biomass increased with

water temperature and mean water residence time but declined with increasing turbidity as seen in Figure 27 and shown by the averaged model presented in Equation 9. The standardized coefficients and other averaged model statistics are presented in Table 16 and the candidate model set that was used to derive the averaged coefficients is presented in Table B-10 in APPENDIX B. These models had an r^2 of 0.36-0.48 and model weights up to 0.38.

$$\log_{10}\text{Zooplankton-0.75} = 2.996 + 0.037*\text{Temperature} - 0.051*\text{Turbidity} + 3.85\text{x}10^{-5} *\text{Mean Water Residence Time} - 0.206*\text{Chlorophyll-a-0.75}.$$

Equation 9

Table 16. Averaged coefficients and statistics for 2015 and 2016 zooplankton biomass including chlorophyll-a sampled with a 0.75 µm filter in Carpenter, Anderson and Seton.

Variable	Standardized Coefficient	Estimate	Adjusted SE	z-value	p-value	RVI
(Intercept)	0.000	2.996	0.426	7.036	<2.00E-16	
Chlorophyll-a	-0.181	-0.206	0.075	2.765	0.006	1.00
Temperature	0.220	0.037	0.031	1.221	0.222	1.00
Turbidity	-0.604	-0.051	0.010	5.022	0.000	0.71
Mean Water Residence Time	0.161	3.85E-05	0.000	0.623	0.533	0.39

Note: Estimate is the unstandardized coefficients that are presented in Equation 6.

RVI is the relative variable importance

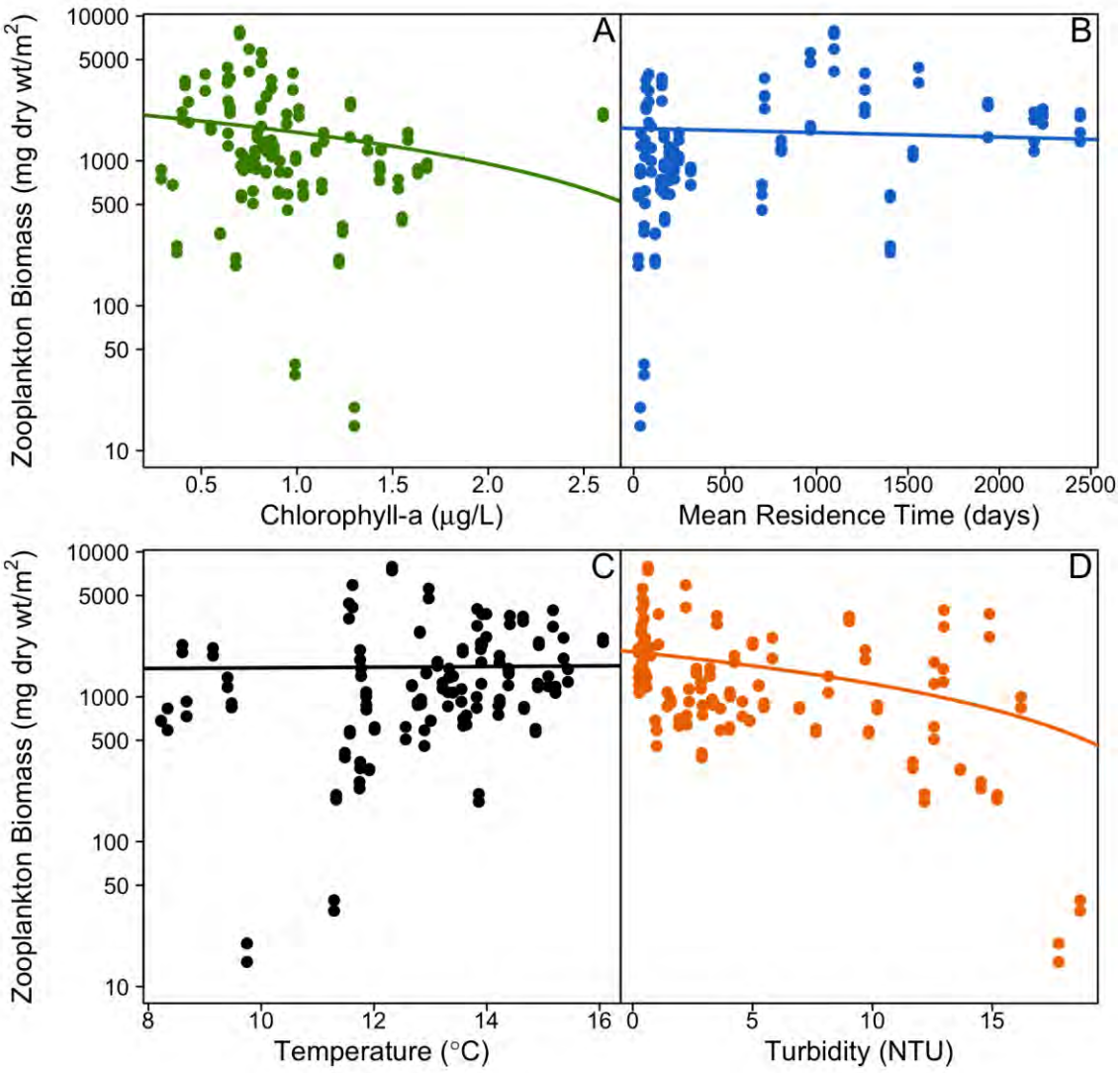

Figure 27. Relationship between zooplankton biomass (A) chlorophyll-a-0.75, (B) mean water residence time, (C) water temperature and (D) turbidity. The model lines are derived from the intercept and coefficients from the averaged model coefficients in Table 16 and show the main effect of the environmental variable of interest while maintaining all other variables at their mean value. Each point represents a replicate from each month and year sampled.

3.4 Question 3: Is light penetration in Carpenter Reservoir impacted by changes in reservoir operations?

The goal is to address this question by running the model CE-QUAL-W2, for reservoir operation scenarios. In this report, we set the reservoir operation observed in 2015 and 2016 into historic context (Sections 3.41), and describe the physical limnology of Carpenter Reservoir in 2015 and 2016 including observed light penetration (Sections 3.4.2 to 3.4.7). Then the results of running the model CE-QUAL-W2 for 2015 and 2016

are presented (Section 3.4.8). The next steps toward answering this question – which will be addressed in a future report - are running the model using a variety of reservoir operation scenarios. Here we present model results using the flow and water level for 2009, providing one example of a scenario.

3.4.1 Hydrology

3.4.1.1 Outflow from La Joie Dam

Outflow from La Joie Dam is shown in Figure 28. The average outflow for 1961-2016 was 41.1 m^3/s. The mean outflow is relatively uniform throughout the year with small increases in the mean outflow in February-March and August-September. The year to year variability in the outflow is greatest in August, at which time brief periods of high flows are not unusual. In 2015, the outflow from La Joie Dam generally followed the average through most of the year, except for with significantly above average flow from March to mid-April, and from mid-July to mid-August. In 2016, the outflow remained higher than average from late March to late September, and was a record high from late May to mid-July.

3.4.1.2 Local inflow

The local inflow to Carpenter Reservoir includes all drainage and tributaries below La Joie Dam. The average from 1961-2016 was 50.8 m^3/s. The local inflow shows a strong seasonal signal dominated by a peak of snowmelt in June (Figure 29). This peak shows a long tail through July and August driven by glacial melt. In 2015, freshet was early with above average flows from early May to early June, but below average inflows from mid-June to the end of August. Flow in fall 2015 was generally average, though there were three large peaks resulting from rainstorms. In 2016, freshet was also early with above average flows in April and May, but with below average inflows from mid-June to mid-July. In fall of 2016, inflows were generally average except for a November rainstorm which reached a record high for several days.

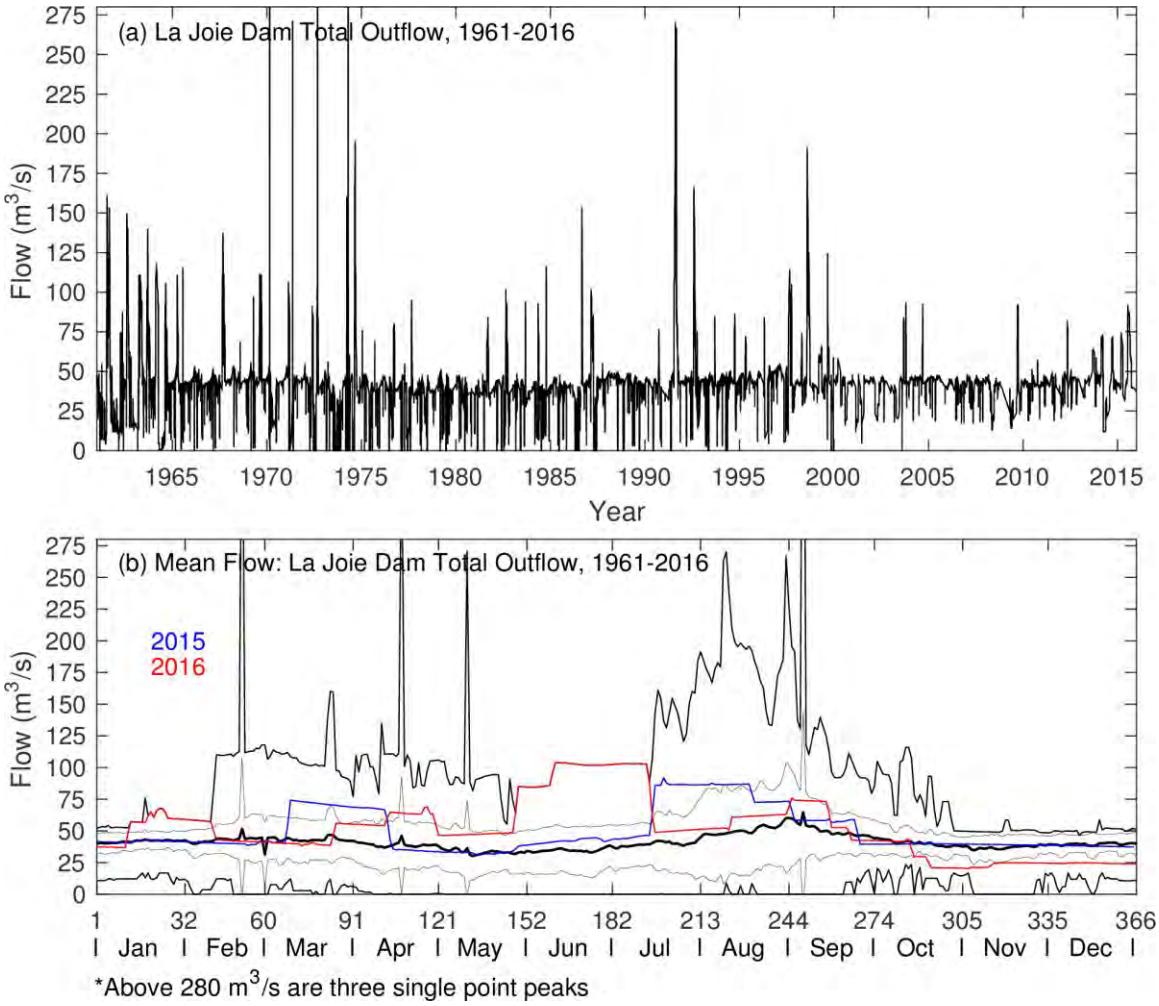

Figure 28. (a) Daily total outflow from Downton Reservoir at La Joie Dam, 1961-2016. (b) Total outflow from La Joie Dam averaged over 1961-2016 for each calendar day. Mean (heavy black line), maximum and minimum (medium black lines) and mean ± one standard deviation (light black lines). The total outflow is shown in blue for 2015 and in red for 2016. In (a) there are three off-scale peaks consisting of a single point each.

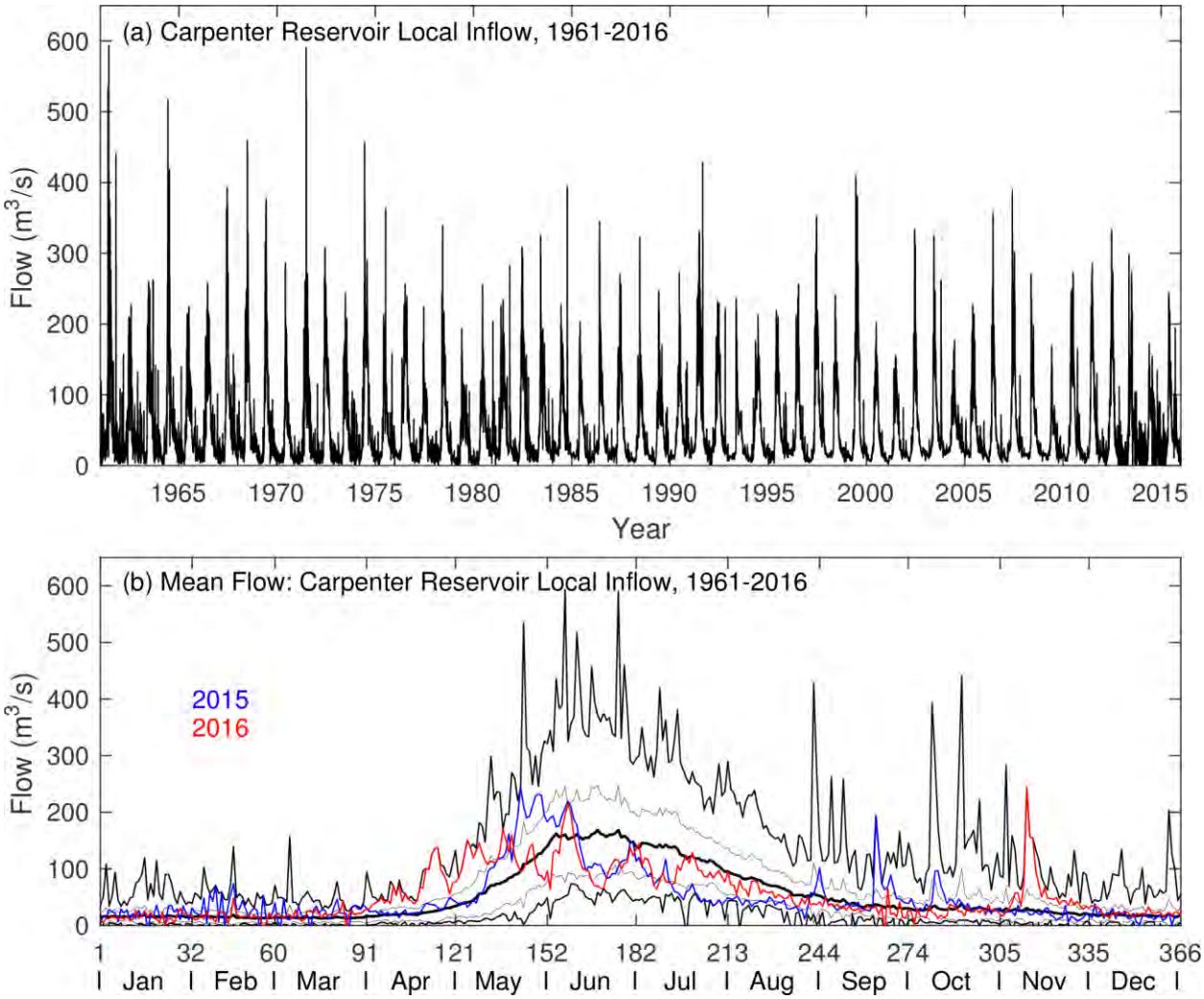

Figure 29. (a) Daily local inflow to Carpenter Reservoir, 1961-2016. (b) Daily local inflow to Carpenter Reservoir, averaged over 1961-2016. Mean (heavy black line), maximum and minimum (medium black lines) and mean ± one standard deviation (light black lines). The local inflow is shown in blue for 2015 and in red for 2016.

3.4.1.3 Outflow to Bridge 1 and 2 Powerhouses on Seton Lake

The vast majority of water (96%) exits Carpenter Reservoir through two tunnels to the Bridge powerhouses on Seton Lake. The flow to Seton Lake for 1961-2016 averaged 87.4 m^3/s. The flow is highest through winter, with another small but broad peak through August and September (Figure 30B). In 2015, the outflow was generally average, except for mid-June to mid-July when it was significantly higher than average. In 2016, flows were generally average from January to March and above average from April to June. The Bridge powerhouses were closed for 25 out of 30 days from 13 September to 12 October, 2016.

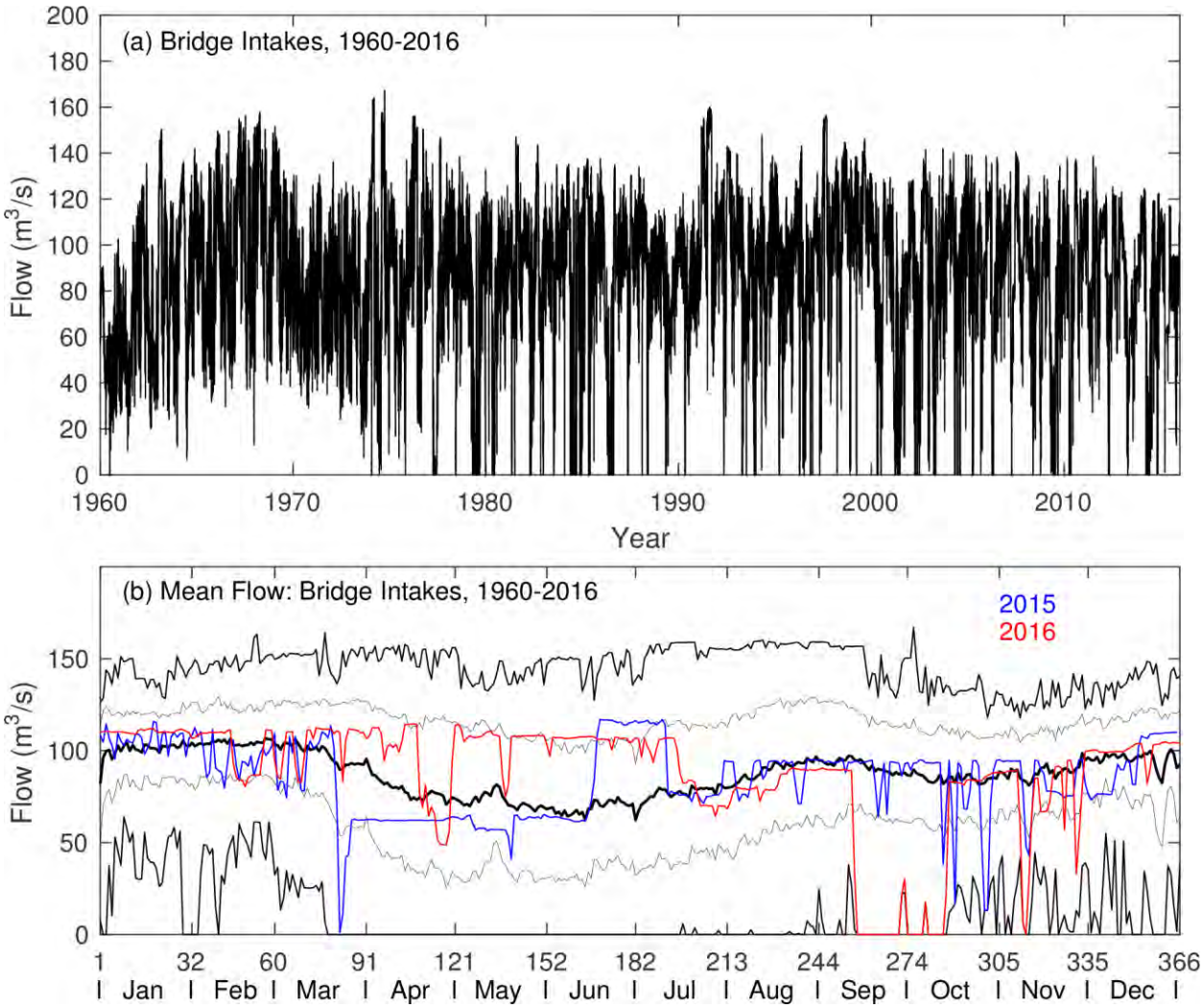

Figure 30. (a) Daily local outflow to Bridge powerhouses, 1961-2016. (b) Outflow to the Bridge powerhouses, averaged over 1961-2016. Mean (heavy black line), maximum and minimum (medium black lines) and mean ± one standard deviation (light black lines). The outflow is shown in blue for 2015 and in red for 2016.

3.4.1.4 Water level

Water level in Carpenter Reservoir is shown in Figure 31. The water level also shows a strong seasonal cycle, with the water level declining through fall and winter to sustain power generation, reaching a minimum in May, and rising rapidly through spring with storage of freshet inflow (Figure 31b). There is also inter-annual variability in the maximum water level, and this variability can go in cycles with periods of relatively high water level (e.g. 1982-1985), alternating with periods of relatively low water level (e.g. 2007-2009, Figure 31a). The water level in 2015 was generally average, except for above average water level from April to June, and slightly above average water levels in the fall. In 2016, the water level was above average from January to mid-May and significantly below average from early July to late September.

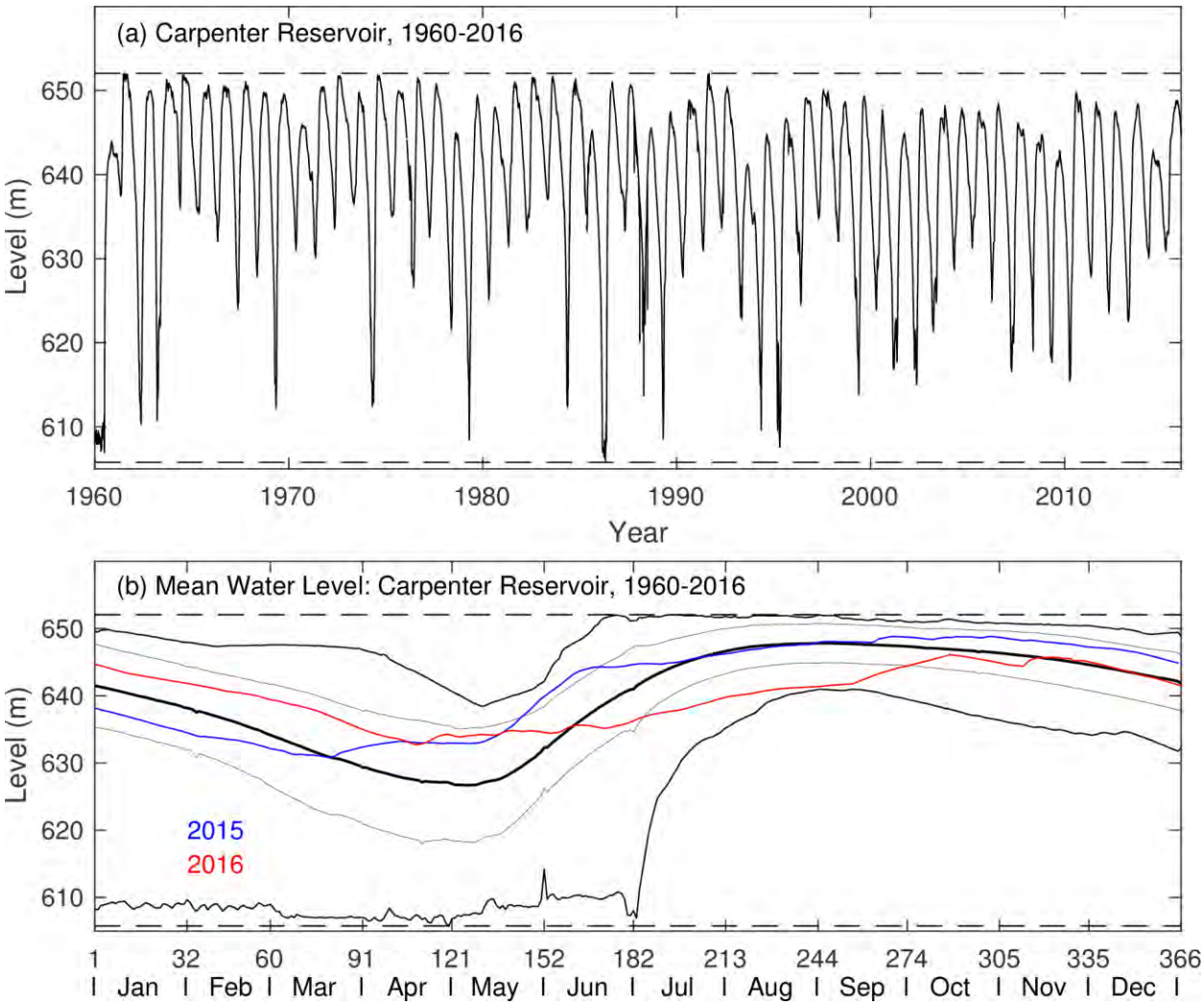

Figure 31. (a) Water level, Carpenter Reservoir, 1960-2016. (b) Average water level, Carpenter Reservoir, 1960-2016. Mean (heavy black line), maximum and minimum (medium black lines) and mean ± one standard deviation (light black lines). The water level is shown in blue for 2015 and in red for 2016. The dashed lines mark the normal minimum (606.55 m ASL) and maximum (651.08 mASL).

3.4.1.5 Flow climatology

The mean outflow from La Joie Dam from April to October (the productivity season) is shown in Figure 32. In 2015, the outflow from La Joie Dam was significantly higher than average and in 2016 it was even higher, the fourth highest on record. In contrast, the year before (2014) had relatively low outflow (Figure 32).

In both 2015 and 2016, the local flow was average, while in 2014 it was significantly below average (Figure 33). In 2015, the water level was somewhat above average from April to October, while it had been close to average for the previous five years and close to average in 2016 (Figure 34). These data will be used to select scenarios with extremes in climate and operating conditions. For example, April to

October in 2009 had low outflow from La Joie Dam (Figure 32), significantly low local flow (Figure 33), and significantly low water level (Figure 34).

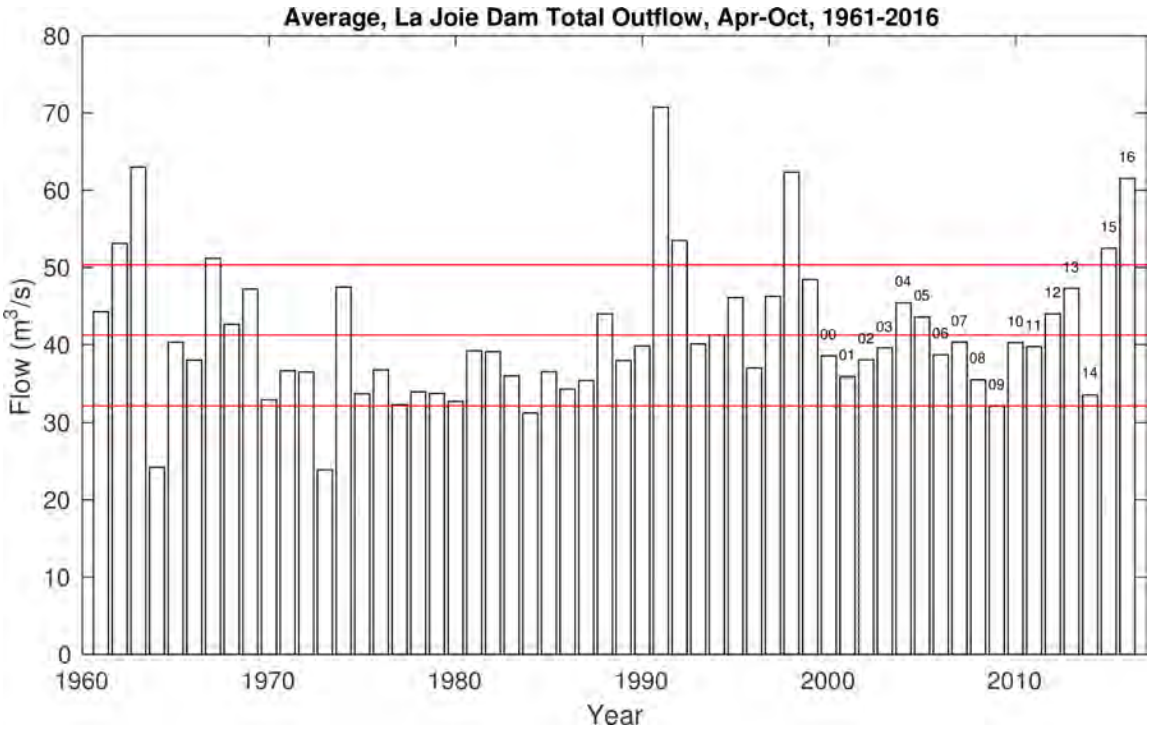

Figure 32. Average outflow from La Joie Dam, April to October, 1961 to 2016. The red lines show the mean and the mean ± one standard deviation.

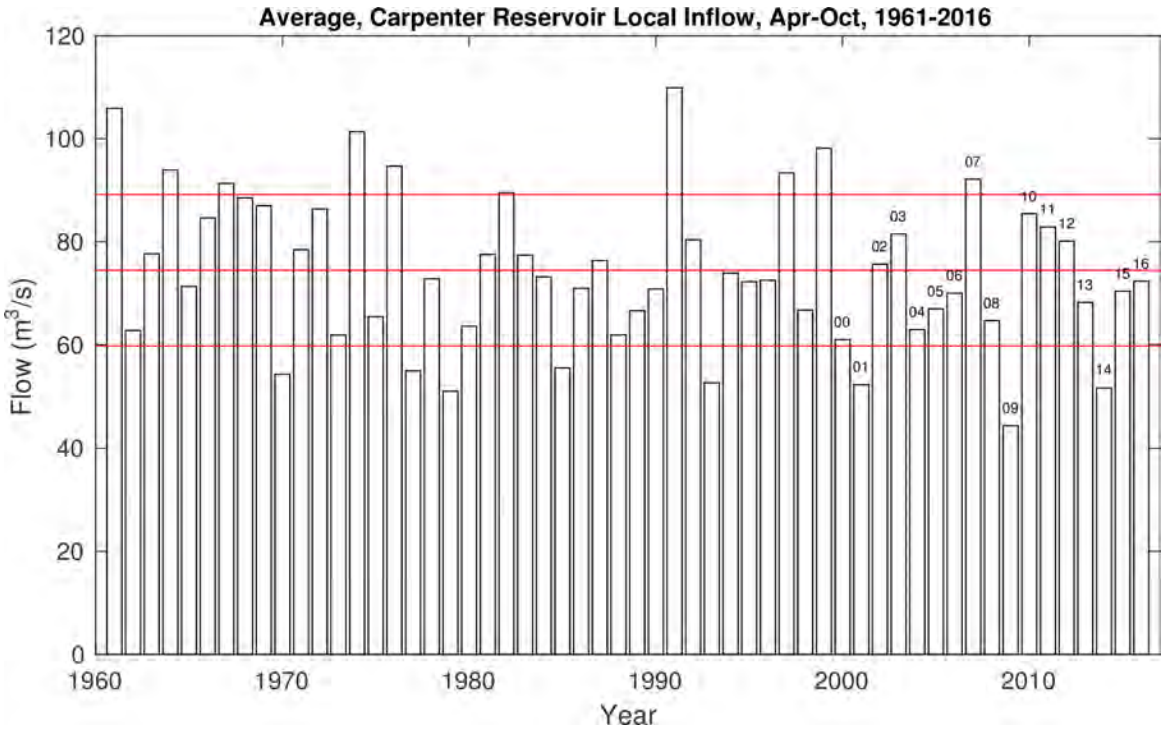

Figure 33 Average local inflow to Carpenter Reservoir, April to October, 1961 to 2016. The red lines show the mean and the mean ± one standard deviation.

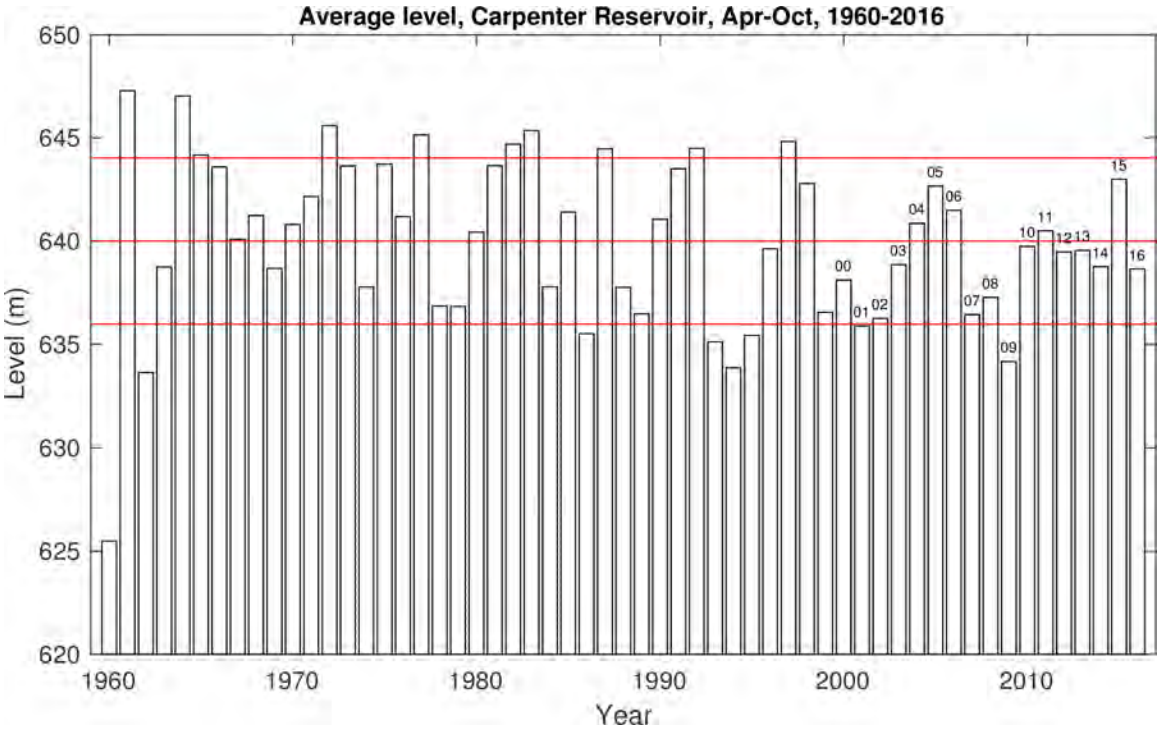

Figure 34. Average water level, Carpenter Reservoir, April to October, 1961 to 2016. The red lines show the mean and the mean ± one standard deviation.

3.4.2 Tributary temperature

From May to October, in both 2015 and 2016, the temperature of the outflow from La Joie Dam was relatively steady between 8 and 11 °C (blue, Figure 35a,b). In contrast, the temperature of the Hurley River showed strong seasonal, weekly and daily variations (red, Figure 35a,b). The mixing of the Hurley River into the outflow of the La Joie Dam resulted in an intermediate temperature (green, Figure 35a,b). The temperatures of the other two major inflows to Carpenter Reservoir, Gun and Tyaughton Creeks, are shown in Figure 35c,d. The temperatures of three smaller tributaries are shown in Figure 35e,f, and vary from warmer (Sucker Creek) to colder (Girl Creek).

Tributary temperatures in 2015 and 2016 followed the same seasonal trend except from late June to mid-July, when tributary temperatures in 2015 were higher than in 2016. This corresponds to a period of hot weather in 2015 with 15 consecutive days with air temperatures > 30 °C.

Given the low TSS and TDS observed in Carpenter Reservoir tributaries, temperature is the key parameter in determining the plunge depth into the reservoir (e.g. Pieters and Lawrence 2011). If the tributary is cold, and entrainment during plunging is low, then the tributary can plunge into the hypolimnion; however, if the tributary is warm, it will enter the epilimnion. If the tributary temperature is intermediate, it can slot in at the thermocline. In the summer, the tributary temperature can vary by over 5 °C in the course of a day, and the plunge depth will vary accordingly.

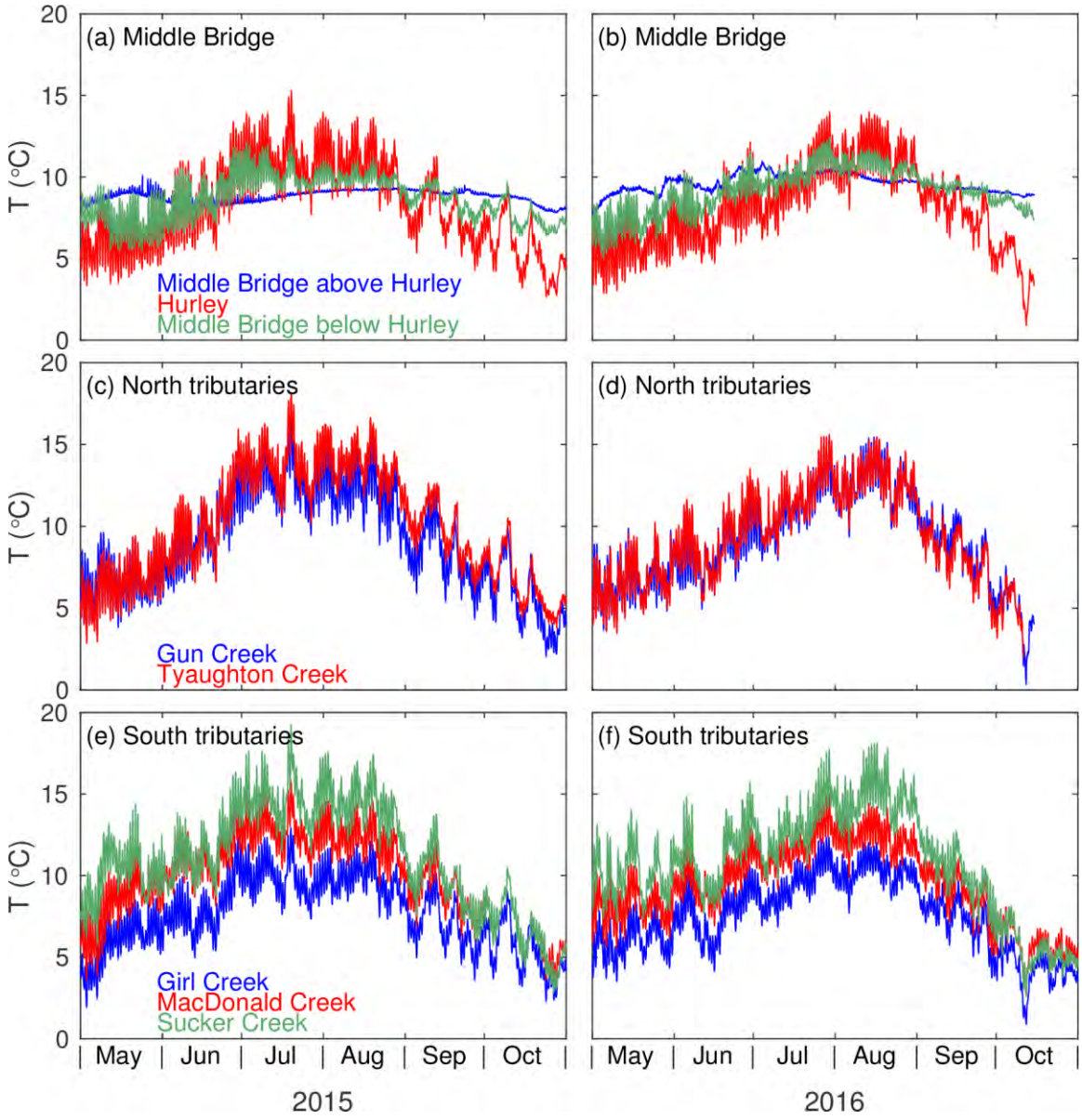

Figure 35. Tributary temperature for (a) Middle Bridge inflow (b) tributaries to the north side of Carpenter Reservoir, and (c) tributaries to the south side.

3.4.3 Tributary water quality

Total suspended solids (TSS) and turbidity data are shown for the Upper Bridge, Middle Bridge and Hurley Rivers in Figure 36, and for the other tributaries to Carpenter Reservoir in Figure 37. TSS and turbidity are important measures related to the penetration of light which is controlled by glacial fines in Carpenter Reservoir.

For the tributaries without an upstream reservoir - Hurley, Gun, Truax, Tyaughton, Marshall and Keary – three general observations can be made: the May 2015 samples which occurred right at the onset of freshet were elevated; with a few occasional exceptions, subsequent turbidity readings in these tributaries were low; and

TSS and turbidity were well correlated (Figure 36f and Figure 37a-e). In contrast, in the Upper Bridge River, the Middle Bridge River, and in the Bridge Tailrace, the values of turbidity and TSS were generally higher, and the values of TSS and turbidity show little correlation (Figure 36b-e and Figure 37f).

Total suspended solids and turbidity are complementary but different physical measurements. Total suspended solids are time consuming to measure: a filter is weighed, a water sample is passed through the filter, the filter is dried and weighed again, and the solids content is determined as the difference in the filter weights. The results have poor resolution at low suspended solids and for small particles.

In contrast, turbidity, which measures the amount of scattered light, is easy to measure with an optical sensor. However, the amount of scattered light depends on the size, shape, color and texture of the particles, which make turbidity an indirect measure.

Even a reservoir-specific relationship between TSS and turbidity usually shows significant scatter, and Carpenter Reservoir is no exception. For the local tributaries, there is a reasonable relationship between TSS and turbidity, though the fit is mainly controlled by the highest reading (blue, Figure 38). However, there is little correlation between TSS and turbidity for the other samples (red, Figure 38).

In a lotic environment, particles of all sizes are transported downstream. In a lentic environment, such as in the reservoir, the larger particles that contribute mass to TSS settle, while the small (<2 μm) glacial particles that contribute to light scattering remain suspended. For example, the settling rate for particles of 2 μm diameter is ~ 8 m/month. Because only small particles remain suspended in the reservoir, turbidity - which is a better measure of those small particles - is used in place of TSS in the CE-QUAL-W2 model. For the model runs shown here, we used a settling rate of 6 m/month; future work will include further analysis of the sensitivity of the model results to the settling rate.

Figures for other parameters (TDS and nutrients) are given in APPENDIX B.

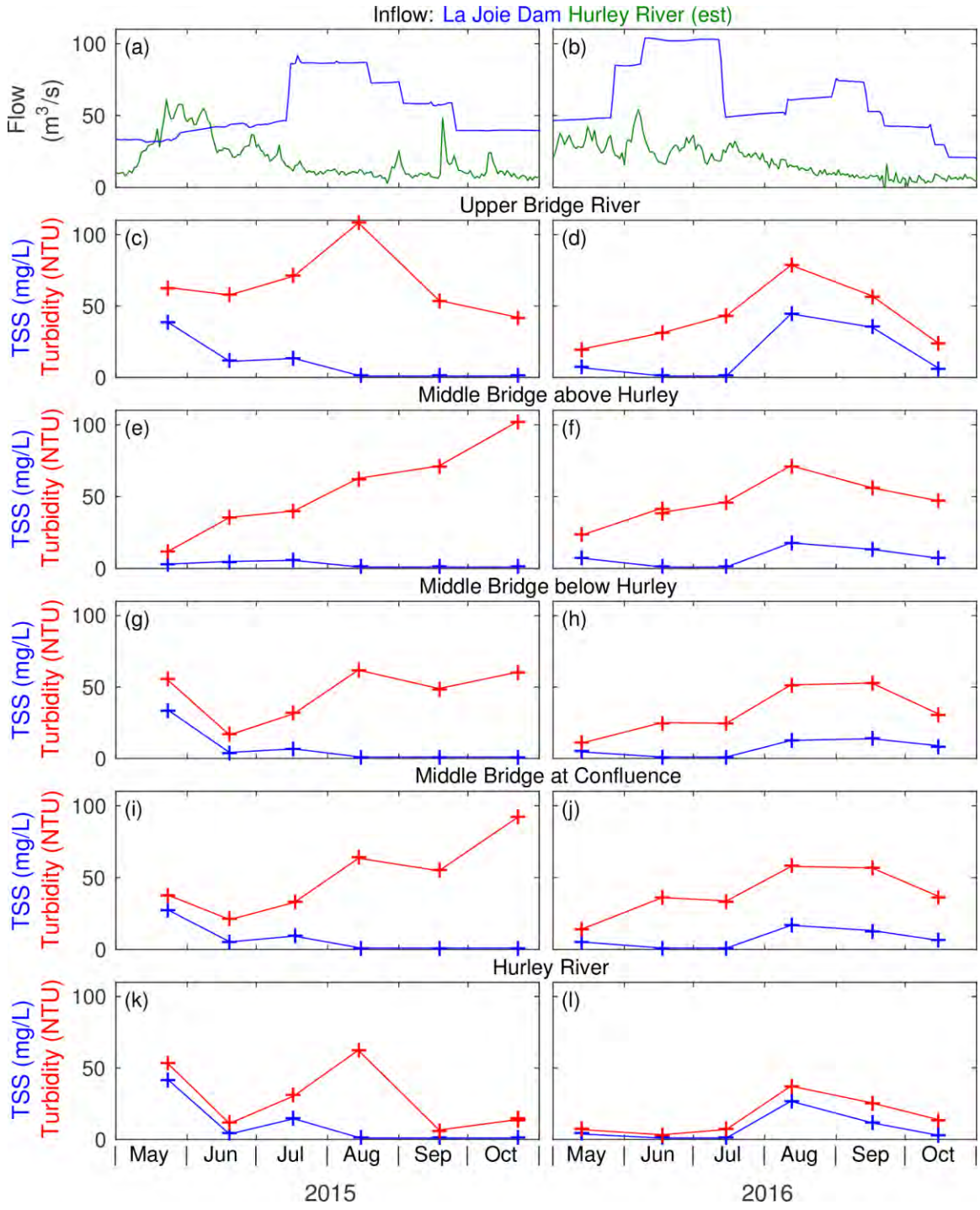

Figure 36. (a) Outflow from La Joie Dam, and inflow from the Hurley River (estimated as 25% of the local flow). (b-f) Total suspended solids (TSS) and turbidity, May to October, 2015 and 2016.

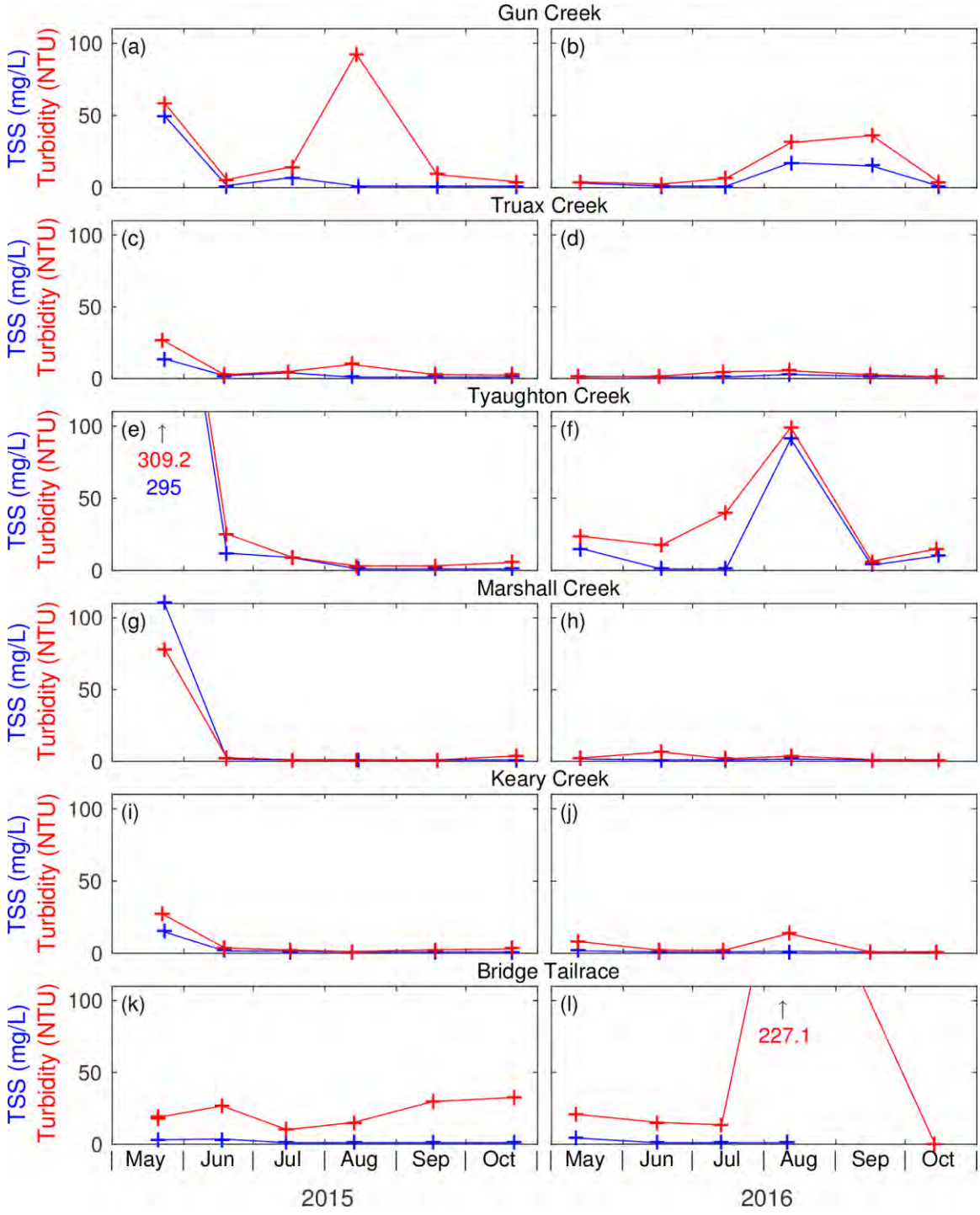

Figure 37. (a-f) Total suspended solids (TSS) and turbidity, May to October, 2015 and 2016.

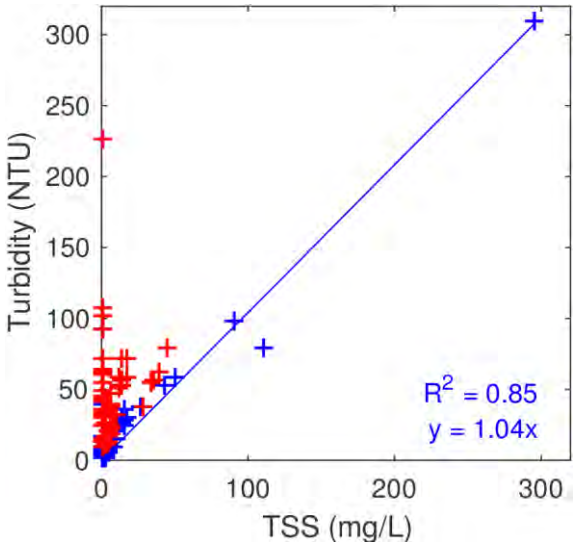

Figure 38. Turbidity versus total suspended solids (TSS) for tributaries to Carpenter Reservoir, 2015 and 2016. RED – Samples from Upper and Middle Bridge Rivers and the Bridge Tailrace. BLUE – Samples from the Hurley River and from Gun, Truax, Tyaughton, Marshall and Keary Creeks. The blue line gives the fit through zero to the blue data.

3.4.4 Continuous turbidity monitoring in the Middle Bridge River

Data from the turbidity recorder moored in the Middle Bridge River are shown in Figure 39c and Figure 41c. The sensor was deployed without a wiper in 2015, and with a wiper in 2016. In 2015, the sensor face was cleaned at the time of the spot readings (except for 22 October 2015 when the water was too deep to recover the mooring). At times, this monthly cleaning of the sensor resulted in a change in the turbidity (e.g. in May and September 2015, Figure 39c), which suggests fouling had affected the readings. In 2016, the data collected with a wiper shows better overall agreement with the monthly spot readings.

Turbidity in the Middle Bridge River above the Hurley represents outflow from La Joie Dam, and this turbidity increased through spring and summer and remained elevated in fall (red, Figure 39b and Figure 41b). The turbidity in the water coming from La Joie Dam was generally higher than the turbidity measured in the Hurley River (green, Figure 39b and Figure 41b). The exception was during the onset of spring freshet in May 2015, when the turbidity in the Hurley River was higher.

The Middle Bridge below the Hurley is the combination of the La Joie and Hurley outflows, and the turbidity of the Middle Bridge below the Hurley (blue, Figure 39b and Figure 41b) generally falls between that of the two sources. The turbidity of the Middle Bridge at confluence with Carpenter Reservoir (cyan, Figure 39b and Figure 41b) is close to that of the Middle Bridge below the Hurley (with the exception of October 2015),

which suggests that the Middle Bridge River did not pick up significant additional turbidity as it flowed through the drawdown zone.

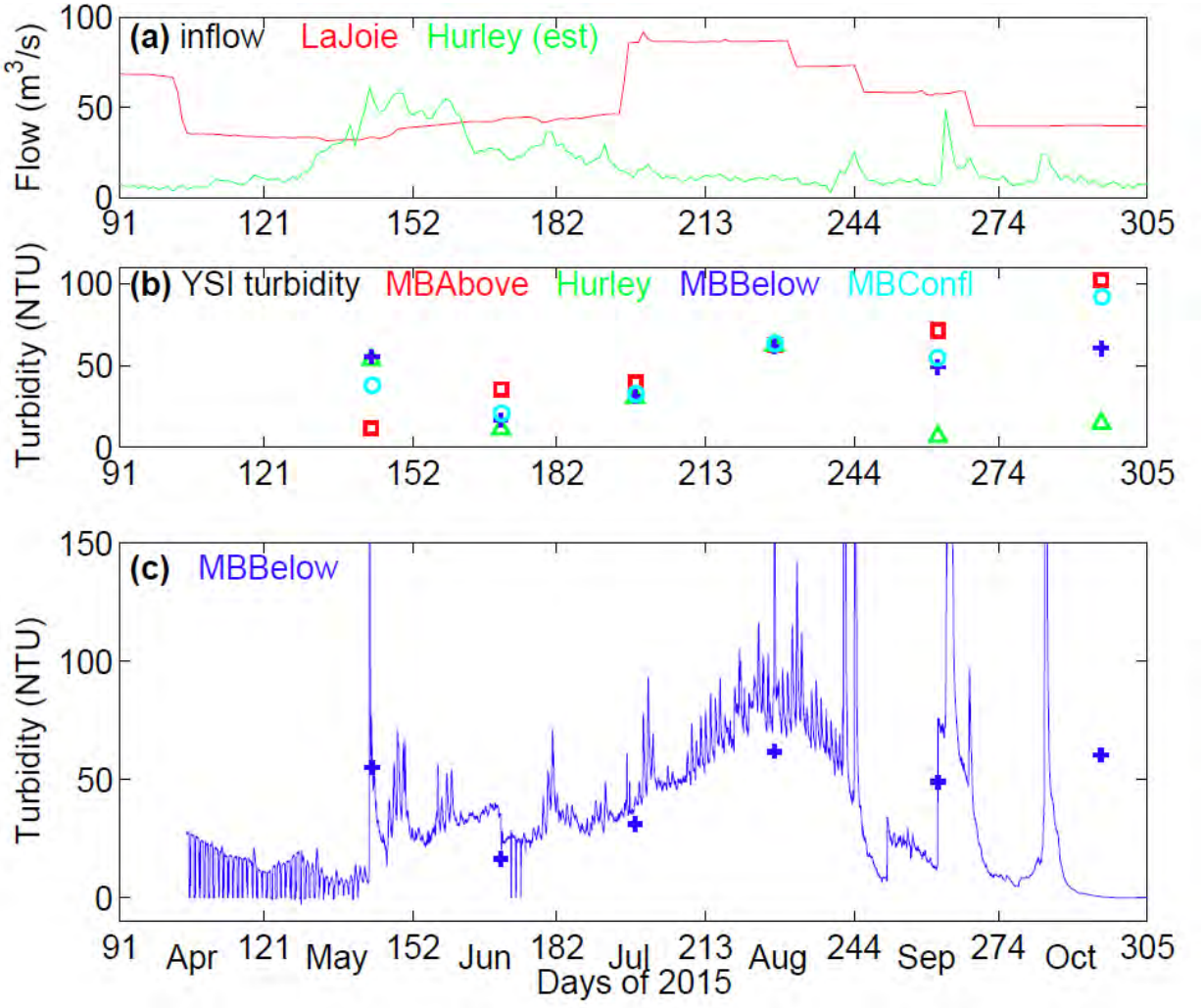

Figure 39. (a) Inflow, (b) YSI turbidity, and (c) hourly average turbidity from inflow to the top of Carpenter Reservoir, 14 April to 22 October, 2015. MBAbove marks the Middle Bridge River above the Hurley; MBBelow marks the Middle Bridge Below the Hurley, and MBConf marks the Middle Bridge at confluence with Carpenter Reservoir. Flow in the Hurley was estimated as 25% of the local flow.

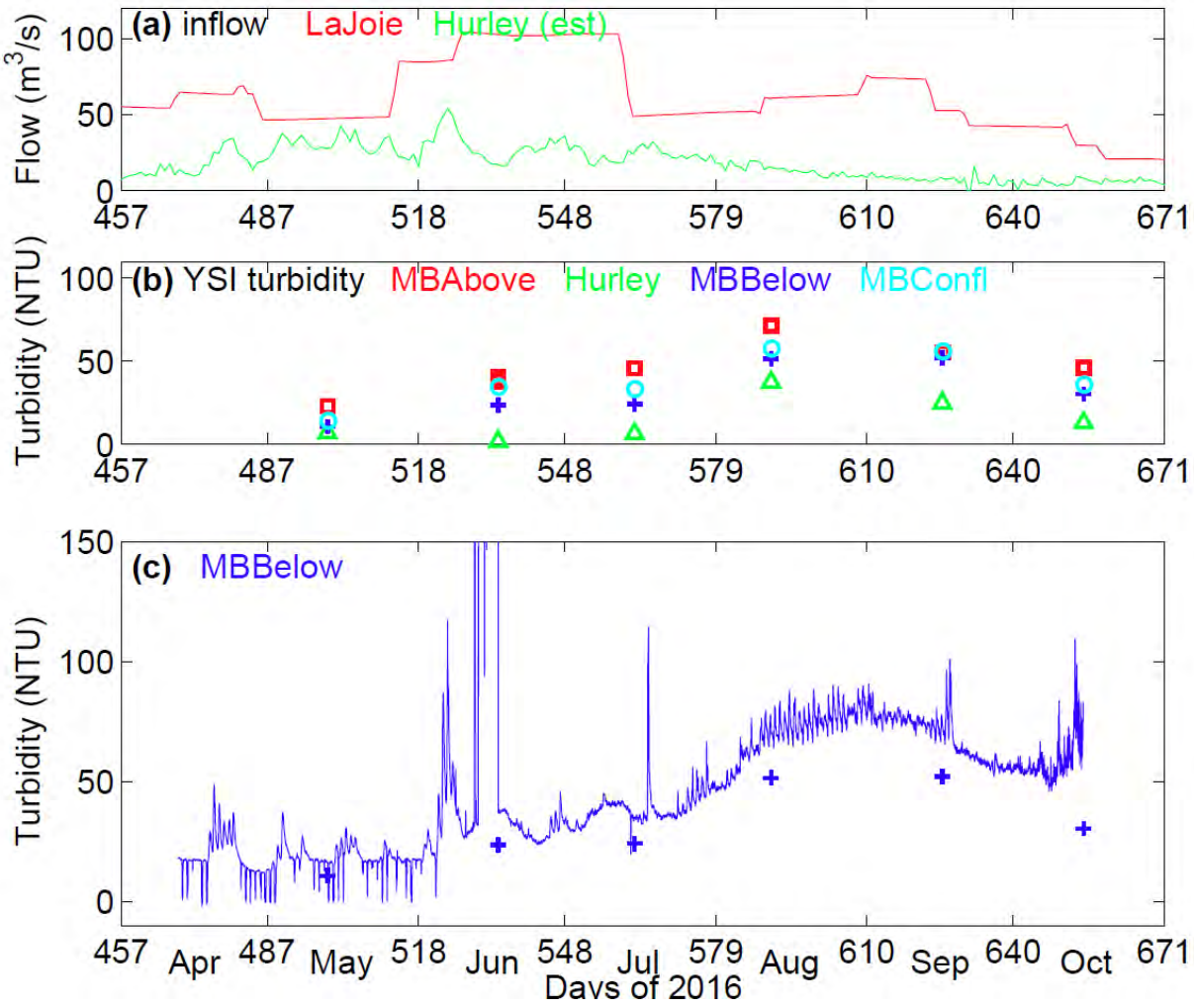

Figure 40. (a) Inflow, (b) YSI turbidity, and (c) hourly average turbidity from inflow to the top of Carpenter Reservoir, 13 April to 26 October, 2016. MBAbove marks the Middle Bridge River above the Hurley; MBBelow marks the Middle Bridge Below the Hurley, and MBConf marks the Middle Bridge at confluence with Carpenter Reservoir. Flow in the Hurley was estimated as 25% of the local flow.

3.4.5 Meteorological data

Meteorological data from both Terzaghi Dam and the Forest Service Fivemile site, located about half way up Carpenter Reservoir, are shown in Figure 41 and Figure 42 for years 2015 and 2016, respectively. The winds at Terzaghi Dam were relatively high, often reaching over 10 m/s, likely the result of funnelling in the narrow region near the dam. In contrast, the winds at Fivemile were modest, generally less than 10 m/s, and these will be used in the CE-QUAL-W2 model.

The air temperature is shown in Figure 41b for 2015; the three temperature records are generally consistent with each other. In 2015, there were 31 days with temperature > 30 °C, and, in particular, 15 consecutive days > 30 °C from 26 June to 10 July 2015. The maximum air temperature was 37 °C on 27 June 2015. In 2016, the

meteorological data followed similar seasonal trends as 2015, except for a cooler summer, having only 14 days with temperature > 30 °C.

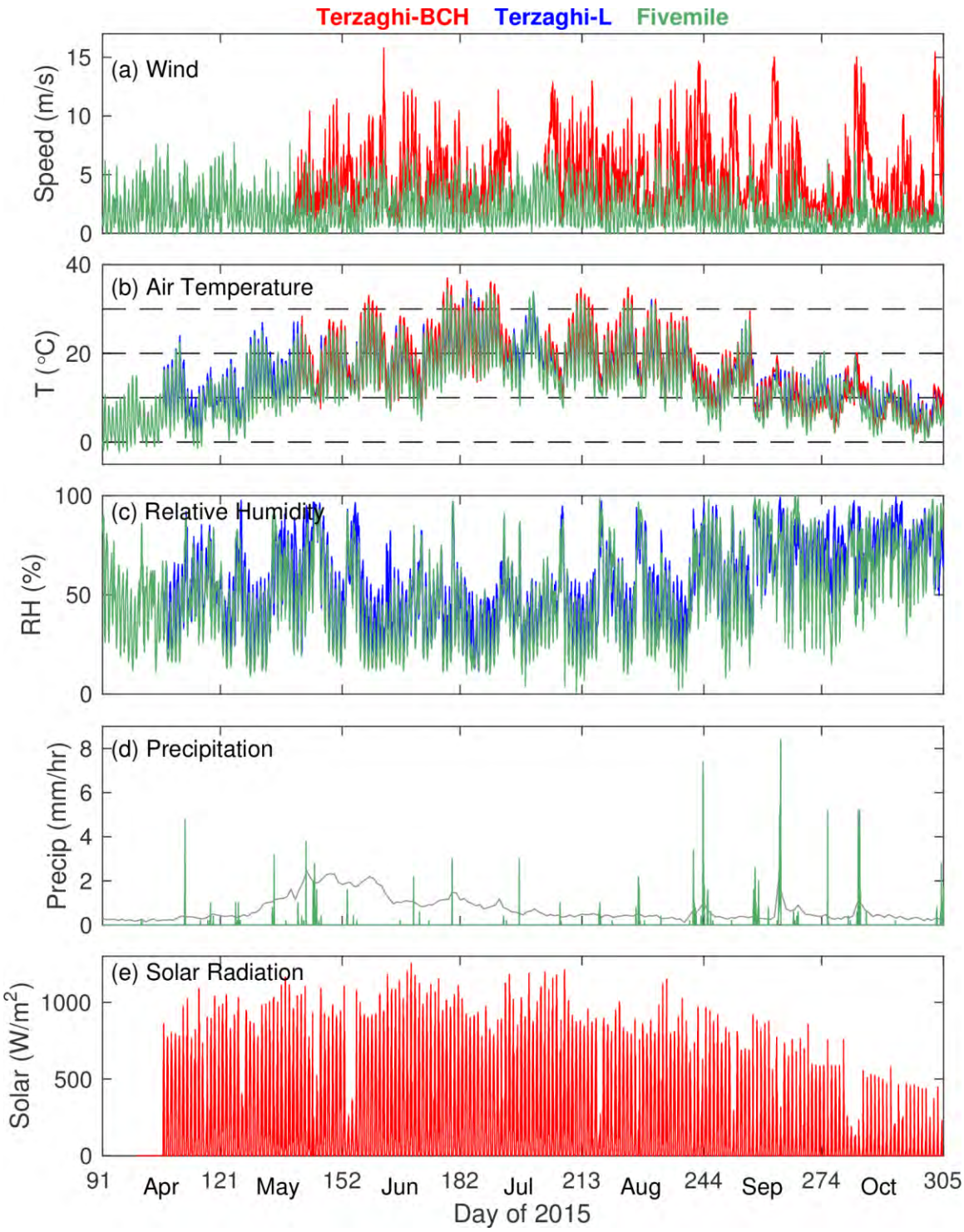

Figure 41. (a) Wind speed, (b) air temperature, (c) relative humidity, (d)precipitation and (e) solar radiation data available for Carpenter Reservoir, hourly, April to October 2015. The grey line in (d) is local inflow, (m^3/s)/100.

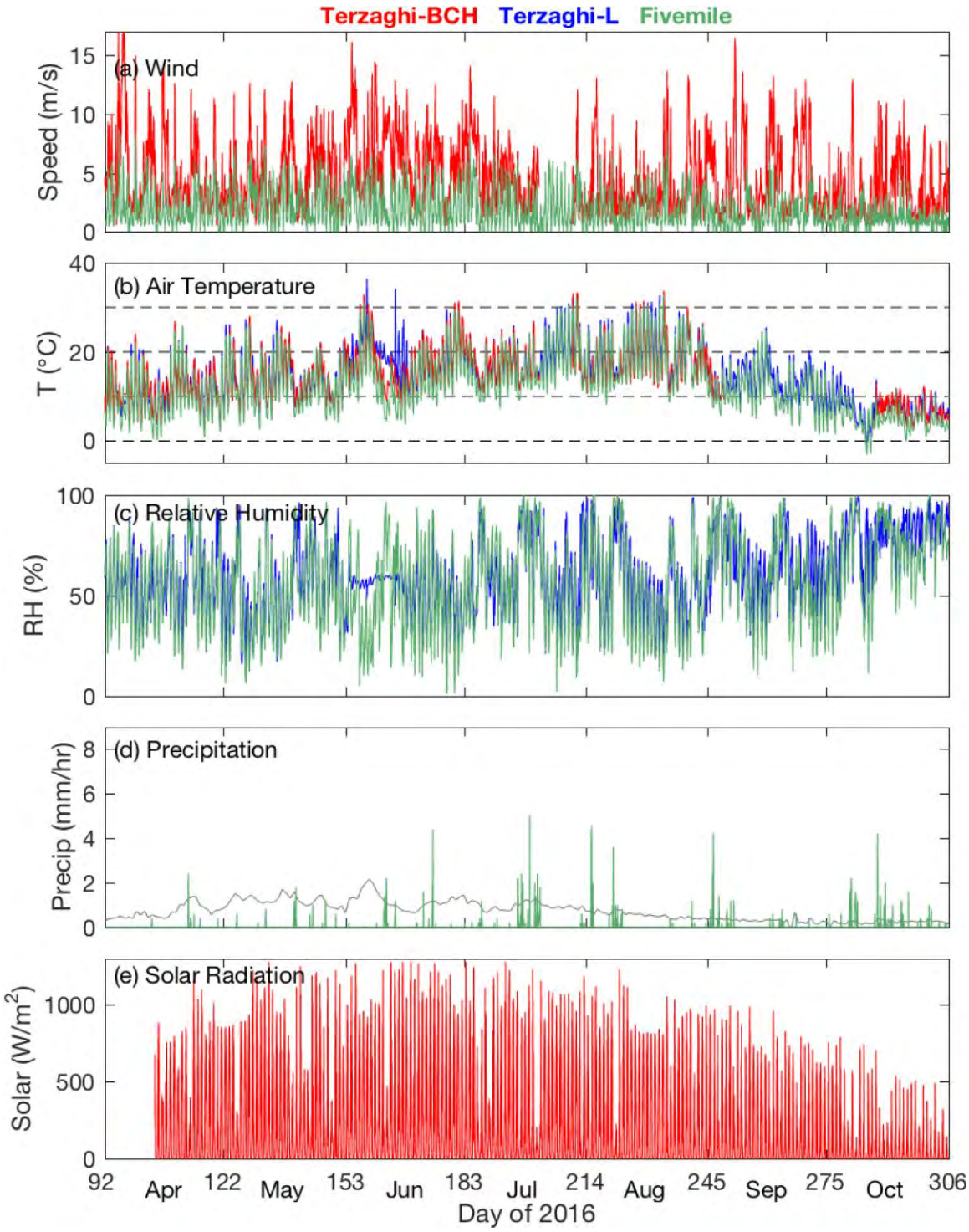

Figure 42. (a) Wind speed, (b) air temperature, (c) relative humidity, (d) precipitation and (e) solar radiation data available for Carpenter Reservoir, hourly, April to October 2016. The grey line in (d) is local inflow, (m3/s)/100.

3.4.6 Monthly Sea-Bird profiles

On 22 May 2015, the surface was 15 °C and the temperature stratification consisted of a broad gradient to the bottom (Figure 43a). By 18 June 2015, a typical two-layer stratification was observed, with a surface mixed layer (epilimnion), a sharp thermocline between 12 and 14 m, and cooler deep water (hypolimnion) below 14 m. On 16 July and 12 August 2015, the surface layer was close to 20 °C. By 17 September 2015, the surface layer had cooled to 15 °C. By 20 October, the surface layer had deepened to over 25 m and cooled to 12 °C, just above the temperature of the deep water, 11 °C. Fall turnover would be expected shortly after this last profile.

The conductivity at 25 °C (C25) declined from May to September 2015, particularly in the deep water because of freshet inflow (Figure 43b).

After May, the turbidity in the epilimnion was generally low (<2 NTU), while the turbidity in the hypolimnion remained elevated, up to 35 NTU (Figure 43c). The turbidity of the surface layer rose in October, the result of mixing with more turbid water at depth, and possibly the result of shallower plunging of turbid inflows.

The dissolved oxygen was high (Figure 43d) and close to saturation (Figure 43e), as would be expected for an oligotrophic system with short residence time. On 16 July, when the thermocline was in the photic zone, there was a small peak in oxygen (>120 % saturation) at the thermocline, and a corresponding small peak in chlorophyll fluorescence (Figure 43f), both suggestive of localized productivity.

Chlorophyll fluorescence was generally low (<2 µg/L) consistent with an oligotrophic system. In May, there was a broad peak to 1.7 µg/L at the base of the photic zone, suggestive of a spring bloom (Figure 43f). In the remaining months, the fluorescence was a little lower with smaller peaks near the 1% light level.

The CTD profiles in 2016 show a similar seasonal cycle as observed in 2015 (Figure 44). In 2016, profiles were also collected in April, at which time the reservoir had little temperature stratification (Figure 44a), and relatively uniform but high turbidity (Figure 44c). In June, July and August 2016, the thermocline was not as strong as in 2015, either a result of different weather conditions and possibly the result of higher outflow from La Joie Reservoir during June and July 2016 (e.g. Figure 36a,b).

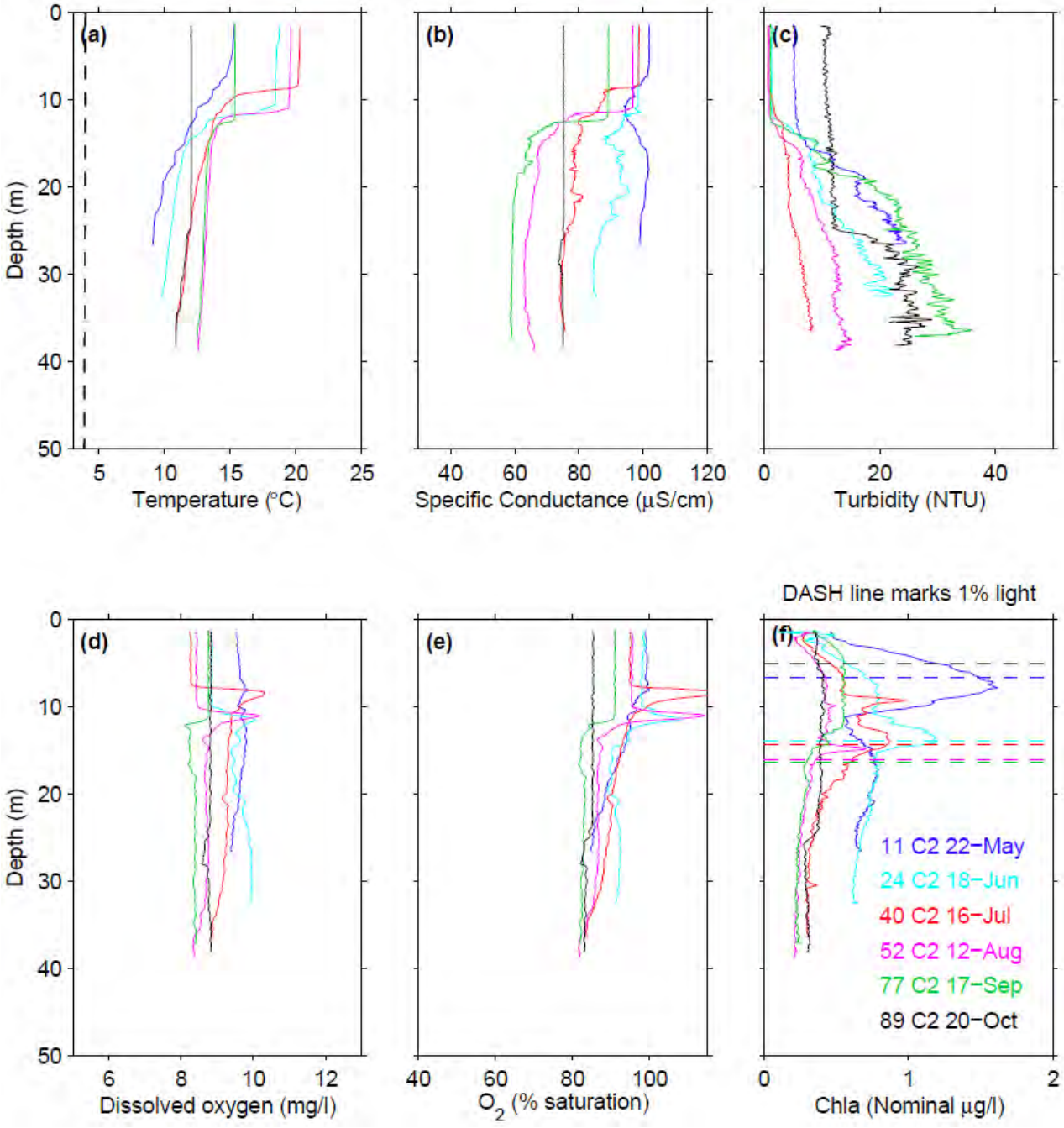

Figure 43. (a) Temperature, (b) conductivity, C25, (c) turbidity, (d) dissolved oxygen, (e) dissolved oxygen as percent saturation, and (f) nominal chlorophyll profiles collected at Carpenter Reservoir station C2, May to October, 2015. The legend in the last panel gives the cast number, station and date. In (f), the dash lines marks the bottom of the photic zone (the 1% light level).

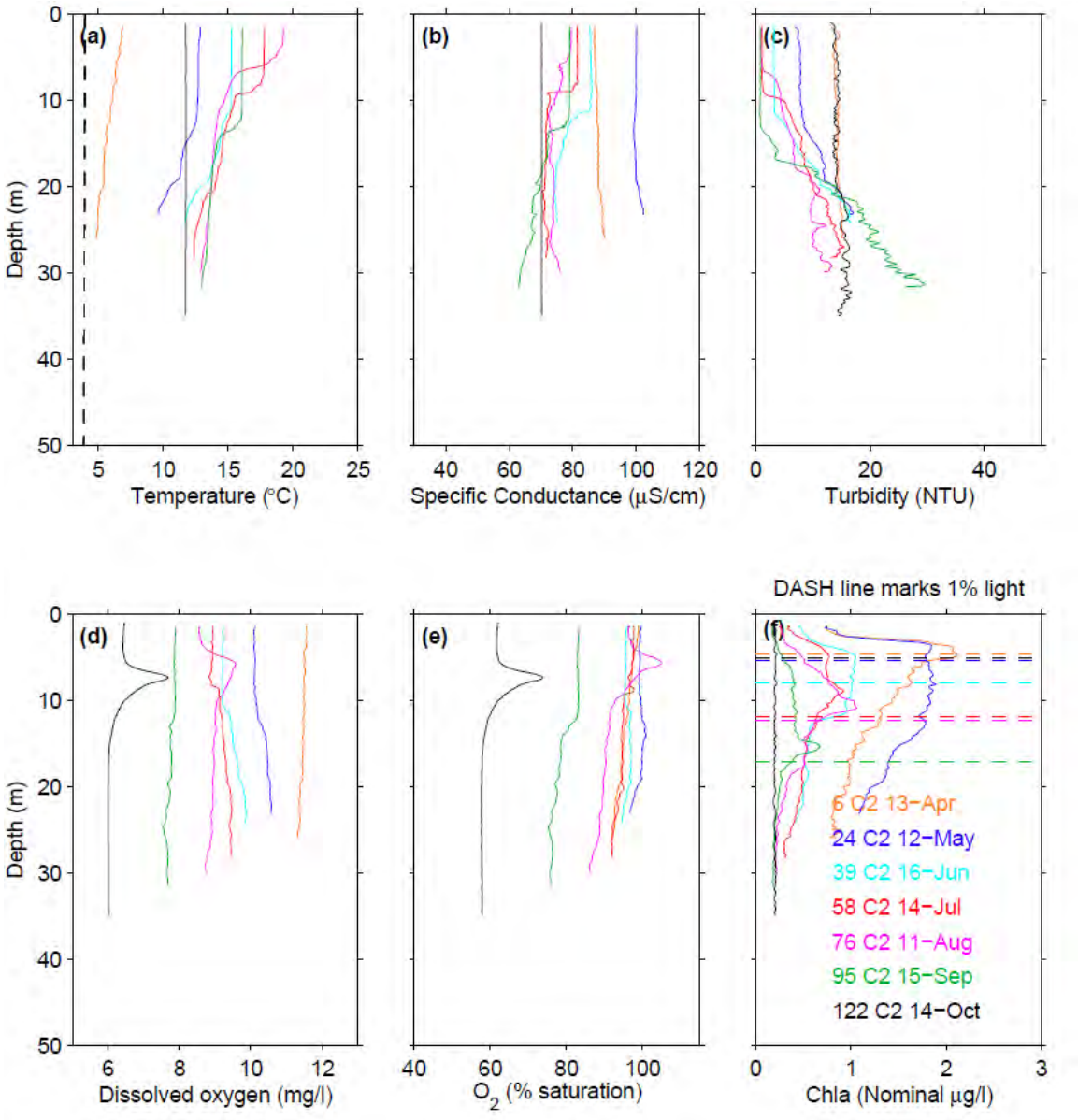

Figure 44. (a) Temperature, (b) conductivity, C25, (c) turbidity, (d) dissolved oxygen, (e) dissolved oxygen as percent saturation, and (f) nominal chlorophyll profiles collected at Carpenter Reservoir station C2, Apr to October, 2016. The legend in the last panel gives the cast number, station and date. In (f), the dash lines marks the bottom of the photic zone (the 1% light level).

3.4.7 Mooring

3.4.7.1 Temperature, April to October 2015

The water temperature data measured by the instruments hung from the log boom in 2015 are shown in Figure 45, along with wind speed, air temperature, solar radiation and inflow, shown for reference.

The water temperature is shown as both a line plot (Figure 45e) and a contour plot (Figure 45f). In the line plot, each line of a given color plots the temperature at a

given depth. From 22 May to 18 June 2015, the deepest temperature sensor was removed as part of repair of the turbidity wiper.

In the contour plot, the color gives the temperature. Note, the contour program interpolates data between the measured depths. For example, the contour plot shows a smooth gradient between the data from the sensor at 10 m to that at 15 m depth. However, through most of the summer, there is a sharp gradient in temperature at the thermocline, located at 12 to 14 m depth as seen in the Seabird profiles (Figure 43a); this is not resolved in the contour plot. Additional sensors were added in 2016 to better resolve the thermocline.

At the start of the mooring period on 16 April 2015, the reservoir had just begun to stratify with temperature ranging from 5.5 to 7.4 °C. The reservoir reached maximum stratification during the exceptionally hot period from 26 June to 10 July 2015, with a surface layer temperature well above 20 °C and temperature at 0.5 m peaking at 24.9 °C during a period of low wind on 3 July 2015 (day 184). The temperature of the deep water also increased over the summer, reaching a maximum of about 13 °C in late August 2015 (Figure 45).

In September, the surface cooled steadily and deepened to 15 m on 20 September 2015 (day 263). By mid-October, little stratification remained with temperature ranging from 11.3 to 12.2 °C on 20 October 2015 (Figure 45).

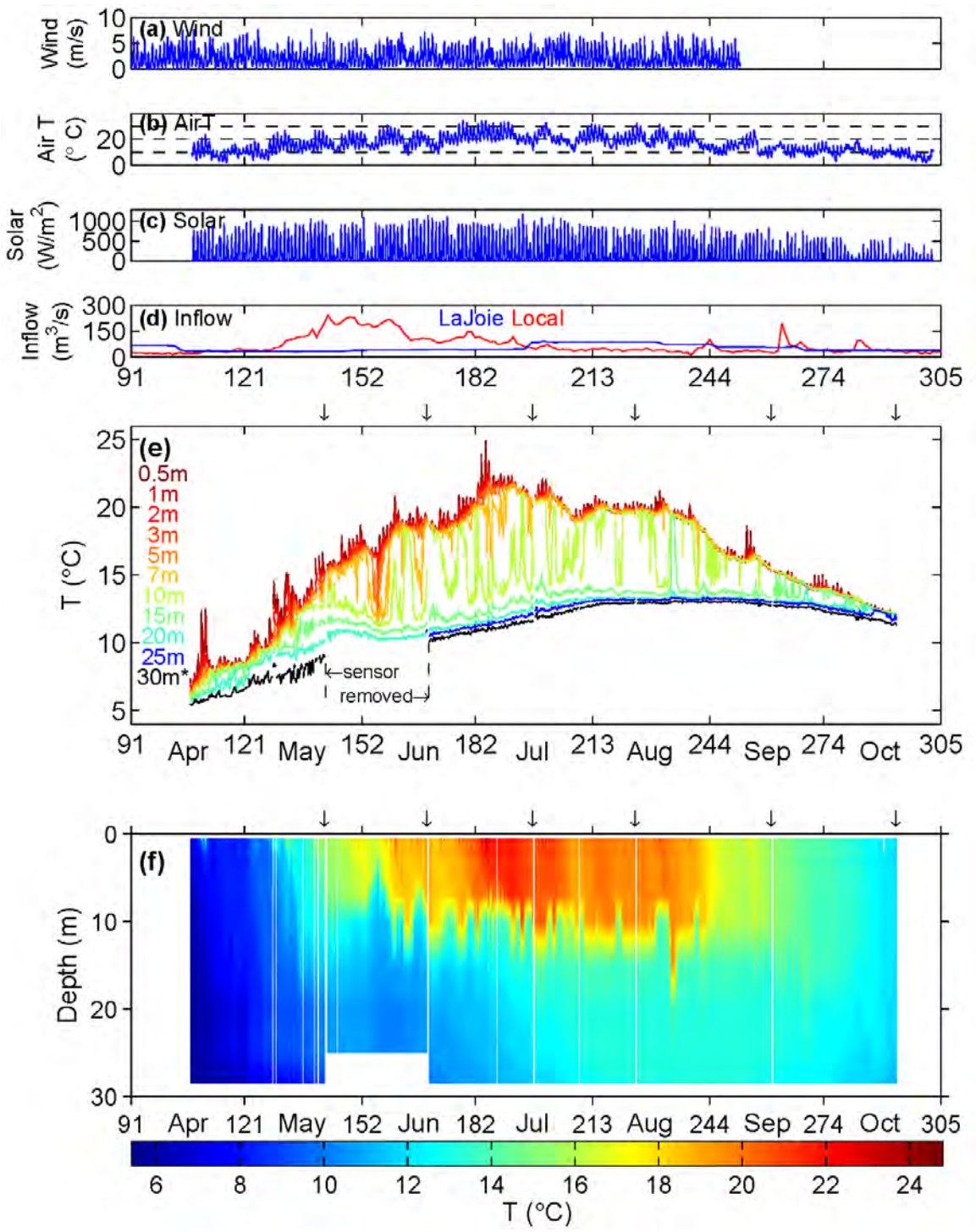

Figure 45. (a) Wind speed at Fivemile, (b) air temperature at Terzaghi Dam, (c) solar radiation at Terzaghi Dam, (d) inflows and (e,f) water temperature at log boom in Carpenter Reservoir, 16 April to 20 October 2015. From 22 May to 18 June, the deepest sensor was removed for repair of the turbidity wiper. Arrows mark the times of the sampling surveys.

3.4.7.2 Temperature, October 2015 - April 2016

On 20 October 2015, the mooring hanging from the log boom in Carpenter Reservoir was replace with three temperature recorders at depths of 0.5, 5 and 10 m for the winter. When the temperature sensors were installed, the top 10 m was well mixed at 12 °C (Figure 46). Based on the data from the previous mooring removed on 20 October 2015, there was little temperature stratification and fall turnover likely began in late October. The top 10 m cooled steadily and remained well mixed throughout the fall; during this time both wind and cooling contributed to mixing.

The reservoir reached the temperature of maximum density (T_{MD} = 3.98 °C) on 24 December 2015 (day 358), after which it alternated between brief periods of mixing and reverse stratification. Below T_{MD}, cooling gives rise to less dense and stable water, which resists mixing by the wind. The data suggests ice-on was likely complete around 3 January 2016 (day 368) when the water stopped cooling, and a period of relatively steady temperature began.

Relatively steady water temperature ended around 6 February 2016 (day 402), when the 0.5 m sensor began to warm; the 0.5 m sensor reached the temperature of the 5 m sensor on 8 February 2016 (day 404), and that of the 10 m sensor on 14 February 2016 (day 410). From this it is hard to pinpoint when ice-off occurred, though it likely happened by late February.

From late-February through March, the top 10 m of the reservoir warmed toward T_{MD}; during this time both wind and warming contributed to mixing. There was a strong diurnal cycle at 0.5 m, with strong cooling at night (stable) and occasional warming during the day (unstable). The top 10 m reached T_{MD} on 30 March 2016 (day 455). As the surface continued to warm, there were periods of stable temperature stratification and periods of mixing. While it is hard to tell when the summer temperature stratification began from just the top 10 m, it probably started in early April, and had definitely occurred by 13 April 2016, when the deeper moorings were installed (Figure 47).

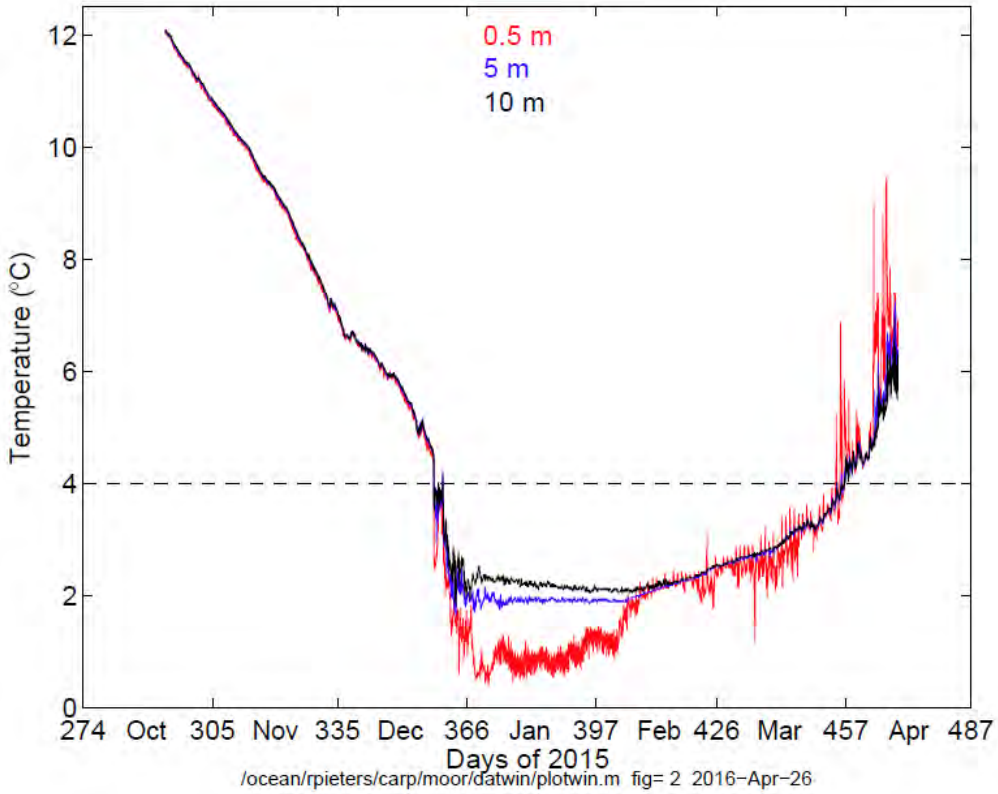

Figure 46. Temperature at 0.5, 5 and 10 m at the log boom in Carpenter Reservoir, 20 October 2015 to 13 April 2016. The dash line marks the temperature of maximum density, T_{MD} = 3.98 °C.

3.4.7.3 Temperature, April - October 2016

In 2016, two moorings were deployed, one hung from the log boom (top 20 to 25 m) and one moored on the bottom near the log boom (bottom 12 m). Account was taken of the gradual deepening of the bottom mooring as the water level increased, and the data from both moorings were interpolated to 1 m depths. The interpolated temperatures are shown in Figure 47, along with wind speed, air temperature, solar radiation and inflow, shown for reference.

At the start of the mooring period on 13 April 2016, the reservoir had just begun to stratify with temperature ranging from 4.6 to 7.3 °C. Unlike 2015, when the maximum temperature stratification occurred from the end of June to early July (during a period of prolonged hot weather), in 2016 the maximum stratification occurred from late July to early August, with the temperature at 0.5 m peaking to 22.9 °C on 28 July 2016 (day 575) and to 23.2 °C on 12 August 2016 (day 590). The temperature of the deep water also increased over the summer, with the temperature at 30 m reaching a maximum of 13.6 °C in early September 2016.

In September, the surface cooled steadily and deepened to 10 m by 8 September 2016 (day 617), and to 20 m by 8 October 2016 (day 647). By mid-October, little stratification

remained with temperature ranging from 11.5 to 11.9 °C on 14 October 2016, when the mooring was recovered.

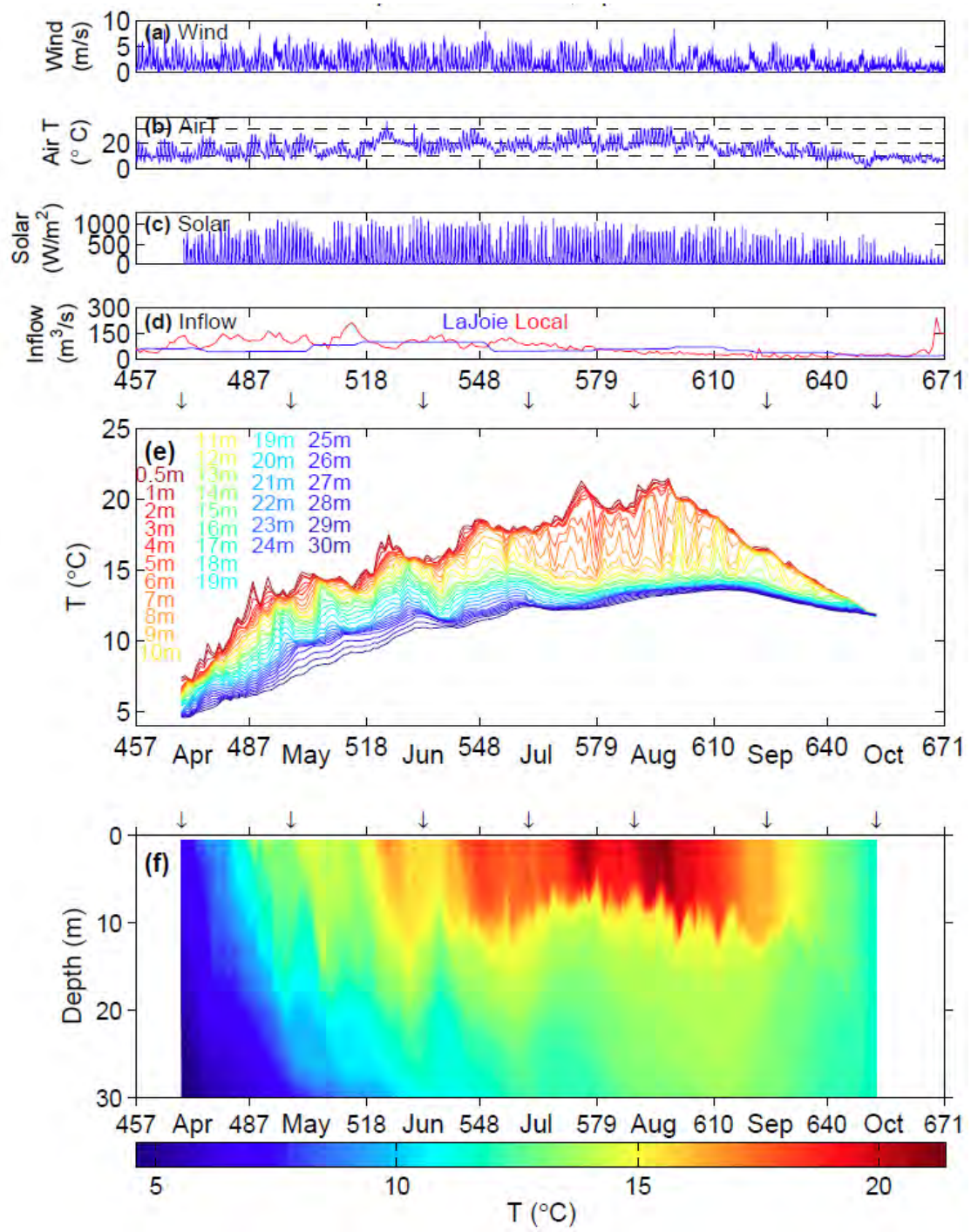

Figure 47. (a) Wind speed at Fivemile, (b) air temperature at Terzaghi Dam, (c) solar radiation at Terzaghi Dam, (d) inflows and (e,f) water temperature (2 hour average) in Carpenter Reservoir, 13 April to 14 October 2016. Data from both the boom and subsurface moorings were interpolated to 1 m depths. Arrows mark the times of the sampling surveys. Time is in days of 2015.

3.4.7.4 Turbidity, April to October 2015

A continuous record of turbidity was measured in the deep water of the reservoir from April to October in both 2015 and 2016. In 2015, the turbidity recorder was attached at approximately 30 m depth to the mooring at the log boom, see Figure 48. In 2016, the turbidity recorder was attached 1.8 m above the bottom on the subsurface mooring, see Figure 49. In both years, the turbidity was high, varying from 10 to 40 NTU.

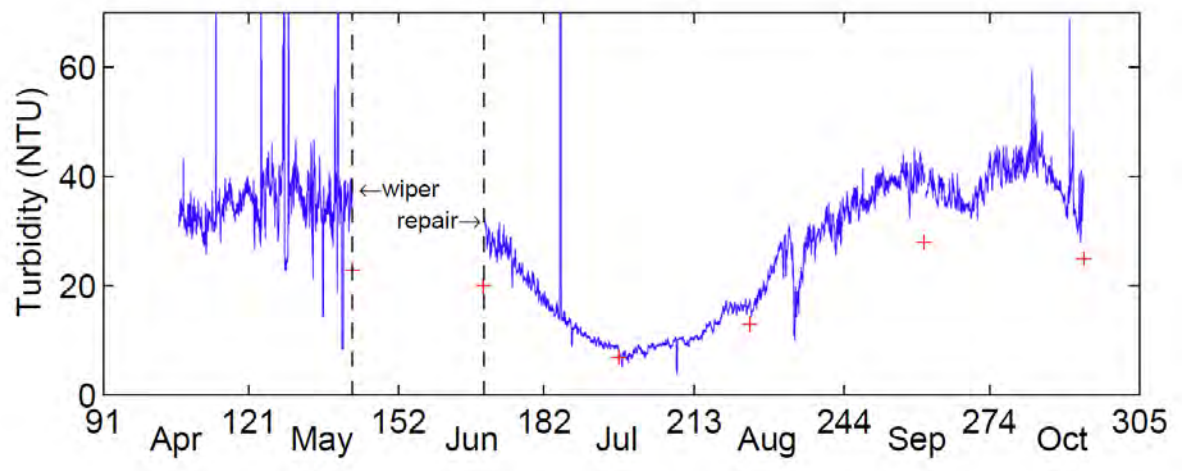

Figure 48. Turbidity data recorded at the log boom in Carpenter Reservoir, 16 April to 20 October, 2015. The recorder was at 27.5 m depth before 18 June 2015, and at 30 m depth thereafter. The red + signs give the turbidity measured at 30 m by the Seabird at Station C2.

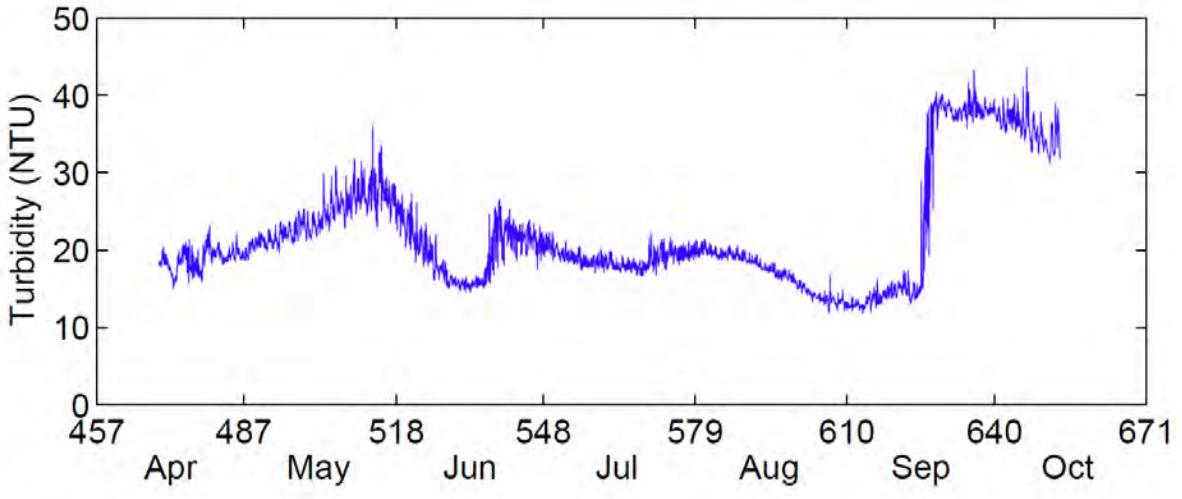

Figure 49. Turbidity data recorded at the log boom in Carpenter Reservoir, 13 April to 14 October, 2016. The recorder was at located 1.8 m above the bottom on the subsurface mooring approximately 1 km downstream of the log boom. At the start of the mooring period the turbidity recorder was at a depth of 30.9 m. As the water level rose, the depth of water above the turbidity recorder increased to 43.6 m by the end of the mooring period.

3.4.8 CE-QUAL-W2 Model

3.4.8.1 Model scenarios

Three model scenarios are presented. The first two scenarios are for 2015 (Scenario 1) and 2016 (Scenario 2), which are used to validate the model against the field data. For 2015 and 2016, the model was run from the first to the last of the sampling dates for the given field season.

Scenario 3 was set up using the flow and water level data from 2009; it was selected as an example because 2009 had very low inflow and water level in contrast to 2015 and 2016. Note that Scenario 3 (2009) used the meteorological forcing and tributary water quality from 2015 since these data were not available for 2009. Table 17 summarizes the time intervals and reservoir conditions for each scenario.

Table 17. CE-QUAL-W2 model scenarios summary.

Scenario	Year	Start	End	La Joie Outflow	Local Inflow	Water level
1	2015	22-May	20-Oct	High	Average	High
2	2016	12-May	14-Oct	Very High	Average	Average
3	2009	22-May	20-Oct	Low	Very Low	Very Low

Figure 50 compares the inflows, outflows and water level of Carpenter Reservoir for each of the three scenarios. The main inflow is defined as the combined outflow from La Joie Dam and the Hurley River (Figure 50a). Tributary inflow is defined as the local inflow minus the Hurley River Figure 50b).

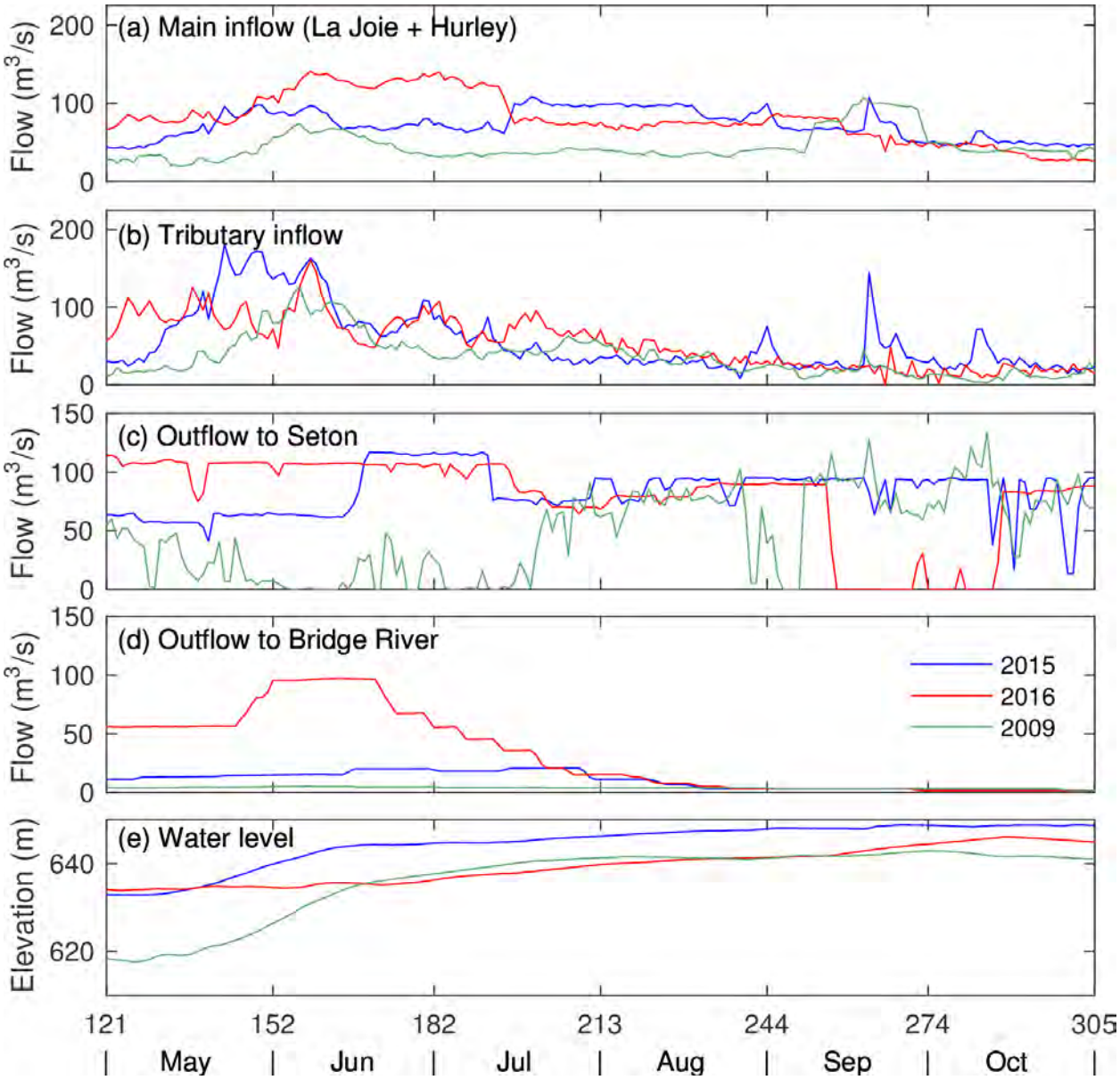

Figure 50. (a-d) Flow boundary conditions, and (e) the resulting water level for each scenario.

For each scenario, model results are shown in two different formats. The first format consists of time series plots of the model data at Station C2 (model segment 53). Model temperature, total dissolved solids (TDS), turbidity, and two nutrients (TDP and NO_3) will be shown. This location is important because it is close to the moorings, close to the deepest in the reservoir, and close to the intakes feeding the Bridge powerhouses on Seton Lake.

The second format consists of snapshots along the whole reservoir, which are shown at the times of the field sampling campaigns. These snapshots show temperature, turbidity, and total dissolved solids (TDS), and give an idea of the processes happening along the length of the reservoir.

3.4.8.2 Model Scenario 1 (2015)

3.4.8.2.1 Water temperature

Water temperature computed by the model is shown as both line and contour plots in Figure 51a-b, and can be compared with the moored data in Figure 45. Another way to compare the model and measured temperature is to plot the temperature data for individual depths as shown in Figure 52. The modelled temperature shows general agreement with the moored temperature. However, the model surface temperature is slightly warmer than observed and the thermocline is somewhat shallower. A sensitivity analysis will be conducted to assess the relative importance of model parameters and factors such as wind on the thermal stratification.

Water temperature can also be seen from the snapshots (column 1, Figure 53). The seasonal evolution of the thermocline can be seen as the epilimnion warms into summer and then cools and deepens in the fall. In addition, there are times when the depth of the thermocline varied along the length of the reservoir.

Both the moor and model data show oscillations in the depth of the thermocline, separating the warmer epilimnion (surface layer) from the cooler hypolimnion (deep water). These oscillations have a period of 4 to 6 days, and likely results from prolonged variations of the wind on the surface of the reservoir. For example, wind from the west will push the warm surface layer toward Terzaghi Dam, deepening the layer of warm water near the dam. When the wind ends, the warm layer near the dam will become shallower again.

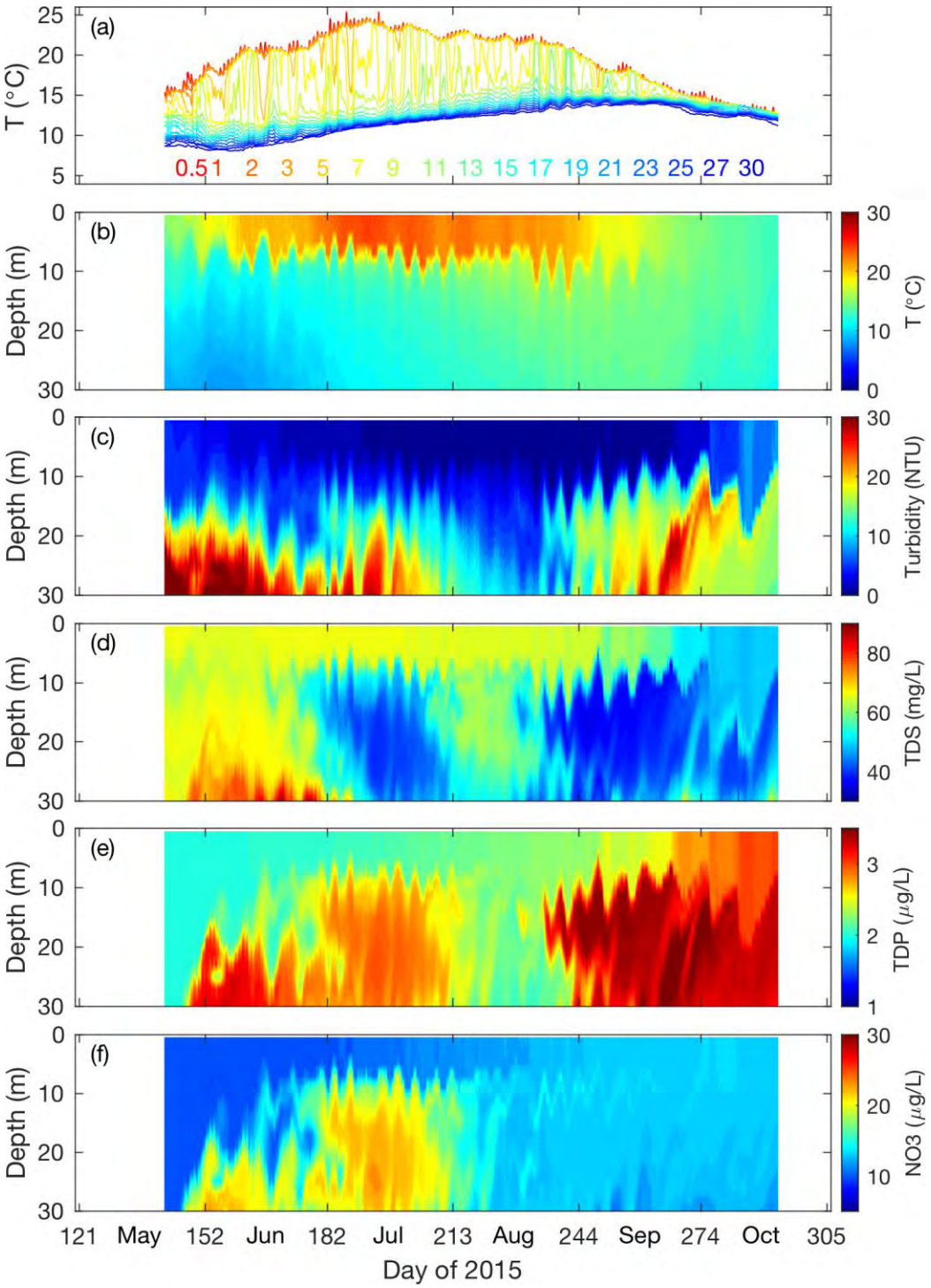

Figure 51. Scenario 1 (2015). Modelled water quality parameters at segment 53 (station C2).

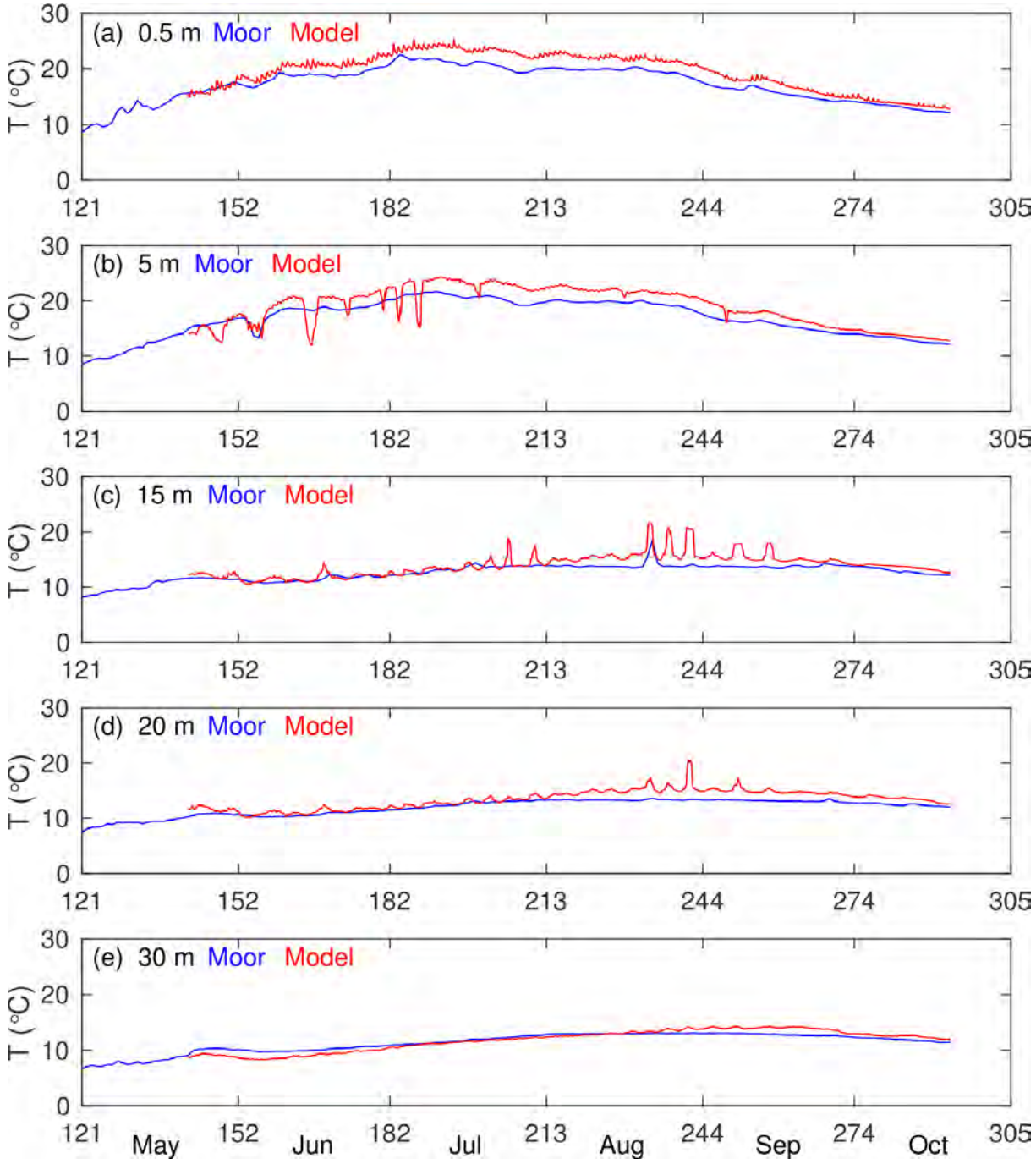

Figure 52. Scenario 1 (2015). Comparison of the temperature measured at the log boom (blue) and the temperature from segment 53 (station C2) of the model (red) at depths of (a) 0.5, (b) 5, (c) 15, (d) 20 and (e) 30 m.

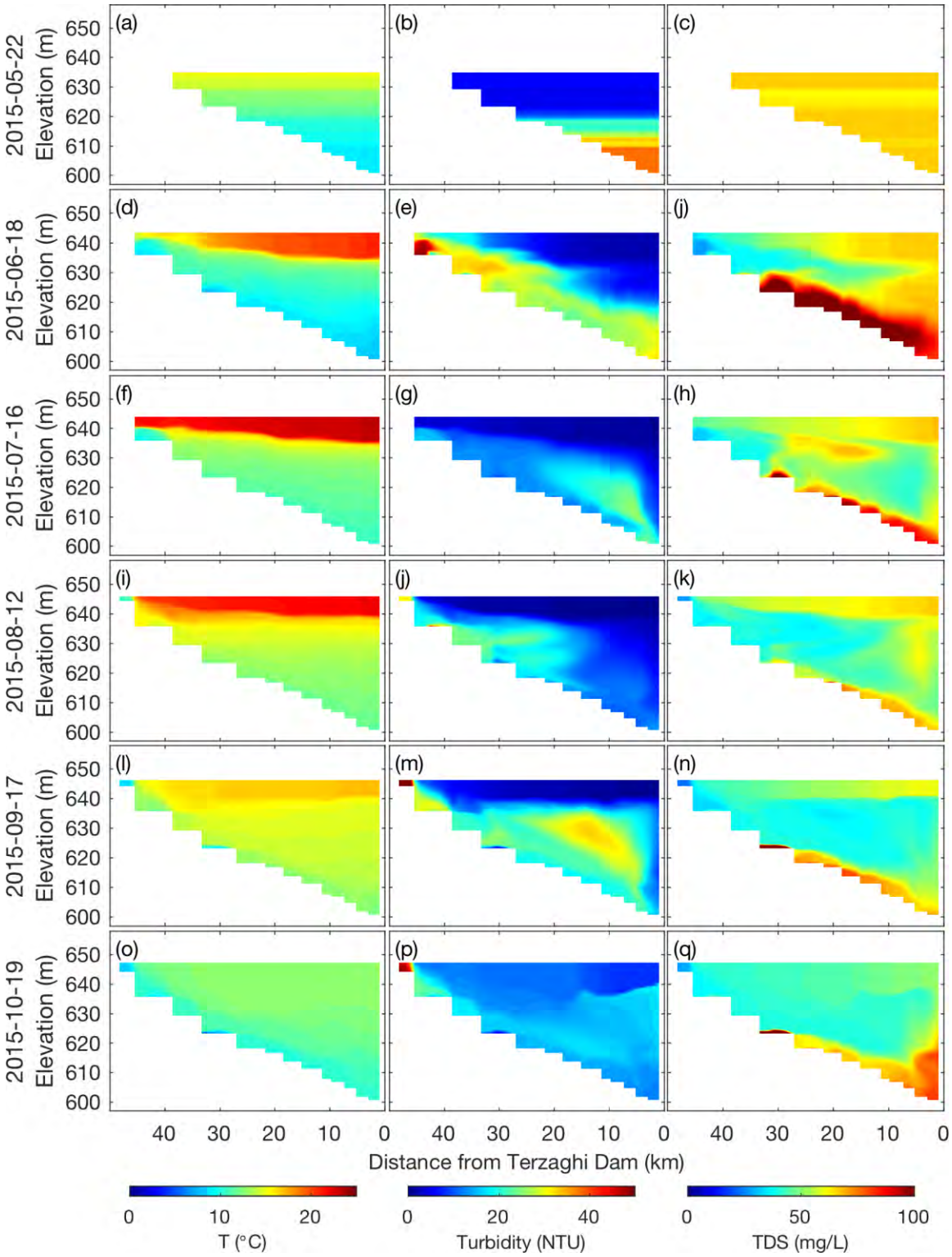

Figure 53. Scenario 1 (2015). Time sequence showing snapshots of modelled temperature, turbidity and TDS.

3.4.8.2.2 Water quality

The modelled turbidity is shown as a time series in Figure 51c. The initial turbidity in the reservoir was set to the Seabird turbidity measurements at station C2 on 22 May 2015 (Figure 43c). The initial turbidity was approximately 5 NTU in the top 10 m, increasing to approximately 20 NTU in the deepest water (> 20 m). The turbidity in both the main inflow and the tributary inflow were around 50 NTU at the start of the simulation; they both declined to ≤10 NTU in June, but then the turbidity in the main inflow rose again (Figure 36g).

The effect of these inflows can be seen in the reservoir: plunging of cold turbid inflow initially increased the turbidity of the deep water of the reservoir (below 15 m, until mid-July, Figure 51c). During this time, the turbidity of the top 10 m was relatively unaffected. After mid-July, the turbidity of the deep water started to decline due to the declining turbidity of the inflows. However, from late August onward, the turbidity in the deep water increased again, reflecting the increasing turbidity in the main inflow. This pattern of the declining and then rising turbidity of the deep water was also observed in the Seabird profiles (Figure 36c).

Total dissolved solids (TDS) is a measure of the dissolved ions of the water, and is a useful tracer given the contrasting TDS of the inflows. The initial TDS of the reservoir was 70 mg/L (May 22, Figure 51d), while the main inflow had lower TDS (≈40 mg/L, Figure C-5g in APPENDIX C). In contrast, the tributary inflow had, on average, higher TDS (≥70 mg/L, Figure C-6 in APPENDIX C).

In the reservoir, the TDS of the deep water first increased slightly during freshet (May to early June), reflecting tributary inflows with higher TDS concentrations. However, from July onward, the TDS of the deep water generally declined as a result of the plunging of cold main inflow with lower TDS (Figure 51d). The TDS of the surface water remained relatively steady through summer, and began to decline in the fall. The declining TDS of the deep water was also observed in the C25[1] from the Seabird profiles (Figure 43b).

The inflow of high TDS water from tributaries can also be seen at the bottom of the reservoir in the snapshot of 18 June 2015 (Figure 53j). Note how water with lower TDS water from the main inflow slots in above this.

Total dissolved phosphorus (TDP) concentration from the model is shown in Figure 51e. The initial TDP was at the detection limit of 2 µg/L; the tributary inflow was also at or close to the detection limit. TDP in the main inflow was somewhat higher, reaching 4.7 µg/L in August 2015 (Figure C-3g in APPENDIX C).

The effect of the higher TDP in the main inflow can be seen at depth, through June and July. During this time, the TDP concentration in the surface layer remained relatively constant. In September and August, the TDP generally increased at most

[1] Electrical conductivity, corrected to 25 °C (C25) is used to measure TDS; TDS[mg/L] ≈ 0.7 * C25 [µS/cm].

depths. This suggests that resupply of TDP to the surface layer does not occur until the fall, and that TDP from the main inflow may 'short circuit' to the deep outlet without being available to the photic zone.

The model results for nitrate (NO_3) are shown in Figure 51f. The initial concentration of nitrate in the reservoir was very low (10 µg/L). The concentration of nitrate in the tributary inflow was also very low, and that in the main inflow was modestly higher for the first part of the summer (Figure C-5g in APPENDIX C).

Plunging of the main inflow resulted in increasing nitrate at depth in June and early July, while nitrate in the surface layer remained relatively constant until mid-August when it also begins to rise (Figure 51f). As with TDP, nitrate in the inflow is not made available for early season productivity.

3.4.8.2.3 Tracers

Tracers – the transport of inert scalars - were added to the model to track (1) the fraction of water in the reservoir at the start of the model run, (2) the fraction of water coming from the main inflow (flow from La Joie Reservoir and the Hurley River) and (3) the fraction of local flow (not including the Hurley River). Tracers can help in understanding various mechanisms including the transport of plunging inflows, transport from the hypolimnion to the epilimnion, and the residence times of specific inflows.

The three tracers for Scenario 1 (2015) are shown in Figure 54. The contours show the fraction of water originating from (a) the initial water in the reservoir, (b) the main inflow, and (c) the tributary inflow, all shown at station C2 (segment 53). At each depth and for each time, the sum of the values in panels a, b and c is equal to one.

At the beginning of the simulation, the fraction of initial water was one, and the fraction of water originating from the main and tributary inflows were both equal to zero (May 22, Figure 54). During freshet (May to mid-June), the inflows plunged deep into the reservoir and replaced almost all the initial water below 20 m. By July, almost all the initial water in the hypolimnion was replaced by the inflows. As the summer progressed and tributary inflow decreased, the water in the hypolimnion was largely replaced with that from the main inflow. From mid-August to mid-September, the lens of tributary water around 10 m depth suggests insertion of tributary water to the thermocline with the cooler main inflow below.

Very little water from the inflows entered the surface layer before September. This result suggests that, for most of the productive season, the turbidity in the surface layer depends on the initial turbidity in the reservoir rather than on the higher inflow turbidity. Seabird profiles showed a decrease in turbidity in the surface layer, each month, from May to September (Figure 43), despite high inflow turbidity. In October, the Seabird profiles showed a large increase in turbidity in the surface layer. The tracer results show that by October, most of the initial water in the surface layer was replaced by turbid water from the main inflow, in agreement with Seabird profile observations.

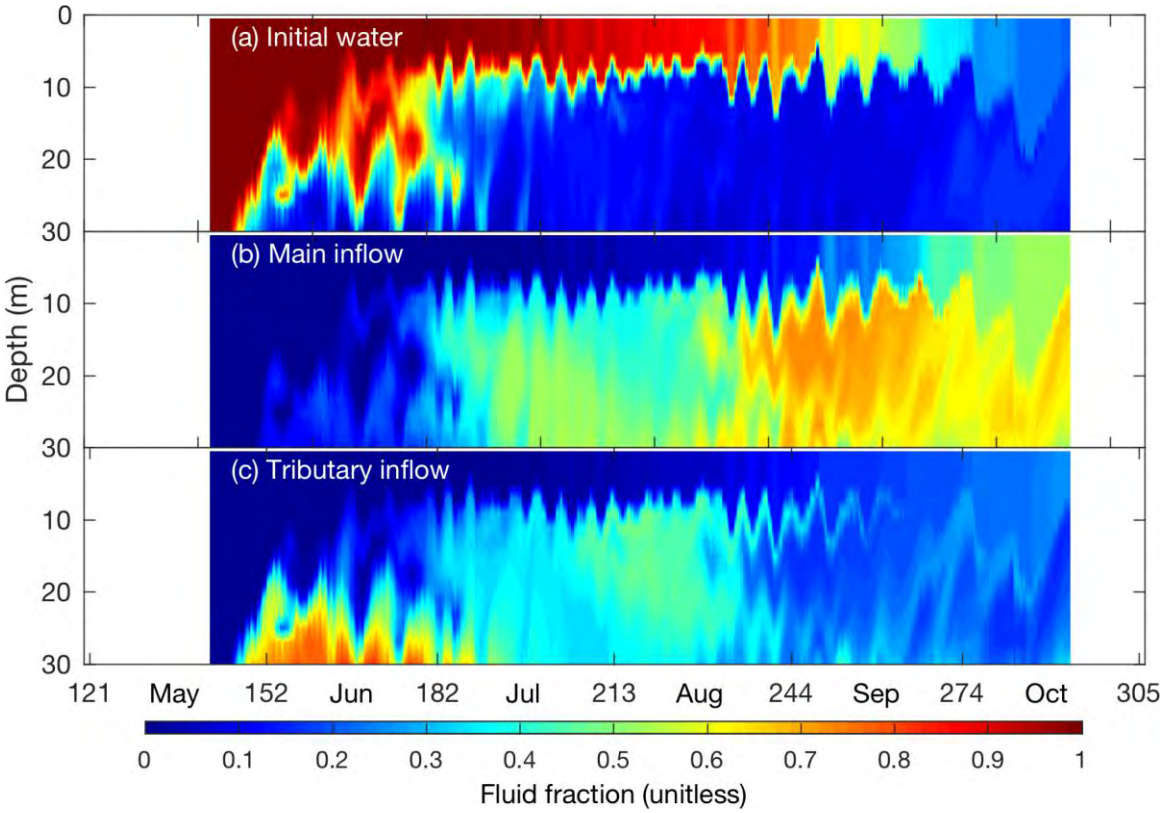

Figure 54. Scenario 1 (2015). Passive conservative tracers at segment 53 (station C2) from (a) Initial water in the reservoir, (b) Main inflow, (c) Tributary inflow.

3.4.8.3 Model Scenario 2 (2016)

3.4.8.3.1 Water temperature

Modelled water temperature for 2016 is shown as both a line and contour plot in Figure 55a-b, which can be compared with the moored data in Figure 47. Modelled and measured temperature data are compared for selected depths in Figure 56. The modelled temperature shows general agreement with the moored temperature. Discrepancies between the observed and modelled data are similar to those seen in Scenario 1 for 2015: the surface temperature is slightly warmer than observed and the thermocline is somewhat shallower.

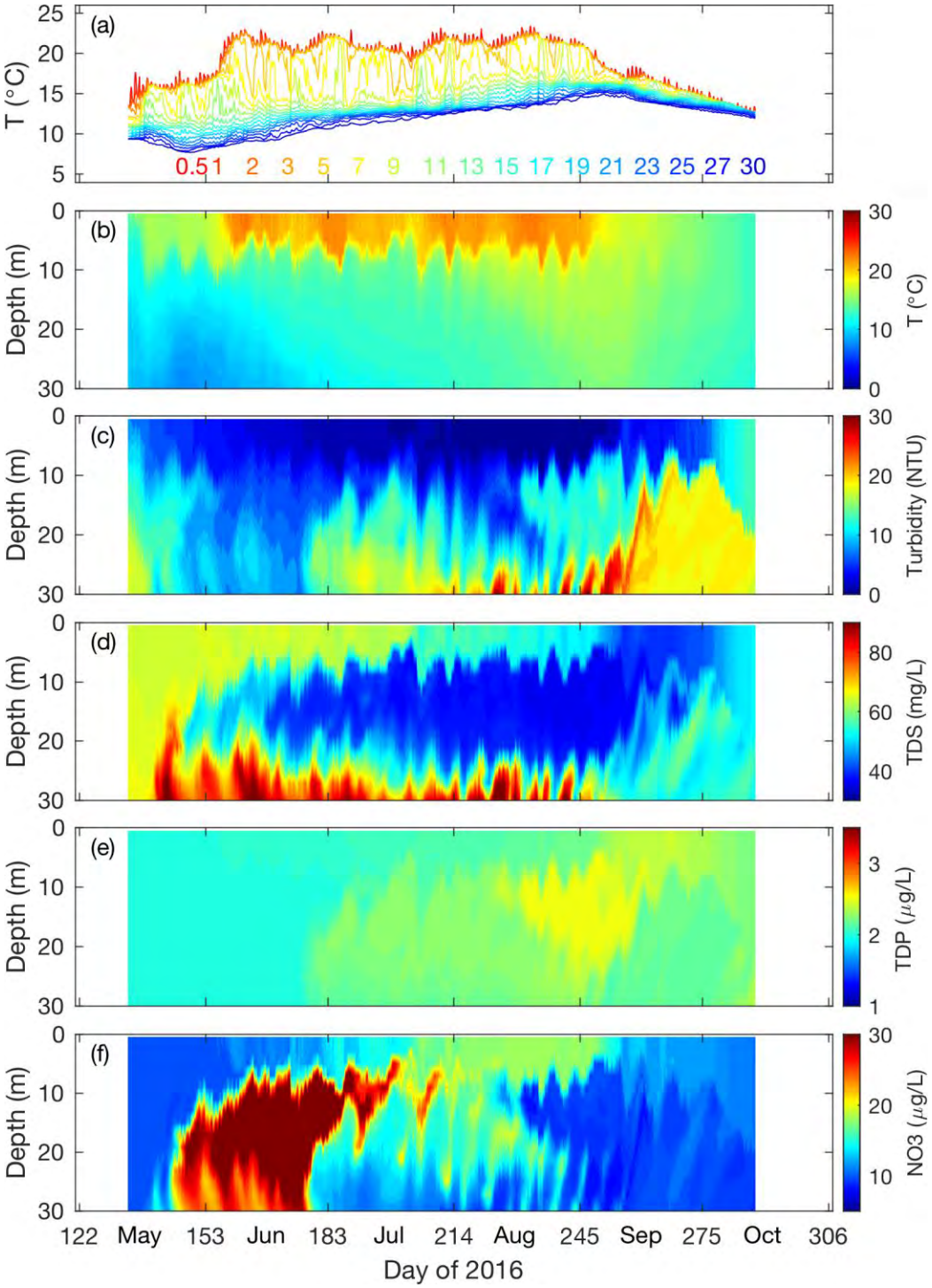

Figure 55. Scenario 2 (2016). Modelled water quality parameters at segment 53 (station C2).

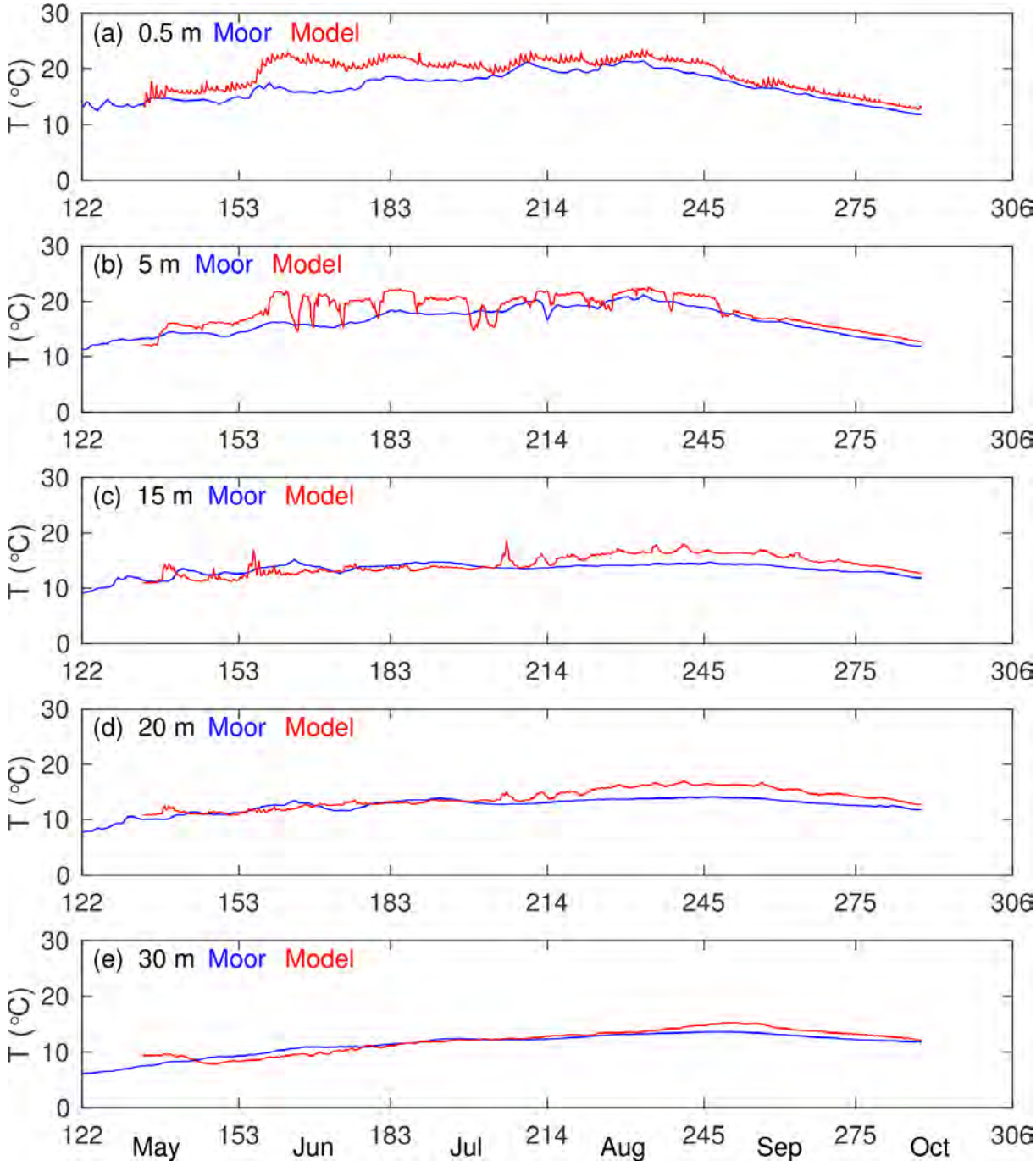

Figure 56. Scenario 2 (2016). Comparison of the temperature measured at the log boom (blue) and the temperature from segment 53 (station C2) of the model (red) at depths of (a) 0.5, (b) 5, (c) 15, (d) 20 and (e) 30 m.

3.4.8.3.2 Water quality

The modelled turbidity is shown in Figure 55c. The initial turbidity in the reservoir was set to the Seabird turbidity measurements at station C2 on 12 May 2016 (Figure 44c). The turbidity was 8 NTU in the top 10 m, and increased to 16 NTU in the deepest water (> 20 m). At the start of the simulation, the turbidity in the main inflow was approximately 10 NTU, significantly lower than in 2015. The turbidity in the tributary inflow was <10 NTU at the start of the simulation, also significantly lower than in 2015 (Figure 36 and Figure 37).

As a result of lower turbidity in the inflows in 2016, the plunging of cold turbid inflow in May and June 2016 (Figure 55c) is less apparent than in 2015 (Figure 51c) due to the low initial turbidity of the inflows. Though it is hard to see in these figures, the model results for 2016 show the onset of higher turbidity in the surface layer earlier in the productive season than in 2015 (see Figure 57). The modelled changes in turbidity in the surface layer over the productive season follow the same trend as the Seabird profiles (Figure 44c).

TDS, TDP, and NO_3 showed similar patterns to Scenario 1 for 2015, with several exceptions. First, TDS in the surface layer declined earlier in 2016 (Figure 55d) than in 2015 (Figure 51d). Second, TDP was lower over the whole simulation period in 2016 compared to 2015. The lower TDP is consistent with the lower tributary measurement used as inflow boundary conditions in the model (Figure C-1 and C-2 in APPENDIX C). Third, the main inflow delivered higher concentrations of nitrate, which entered the surface layer earlier in 2016 (Figure 55f) than in 2015 (Figure 51f).

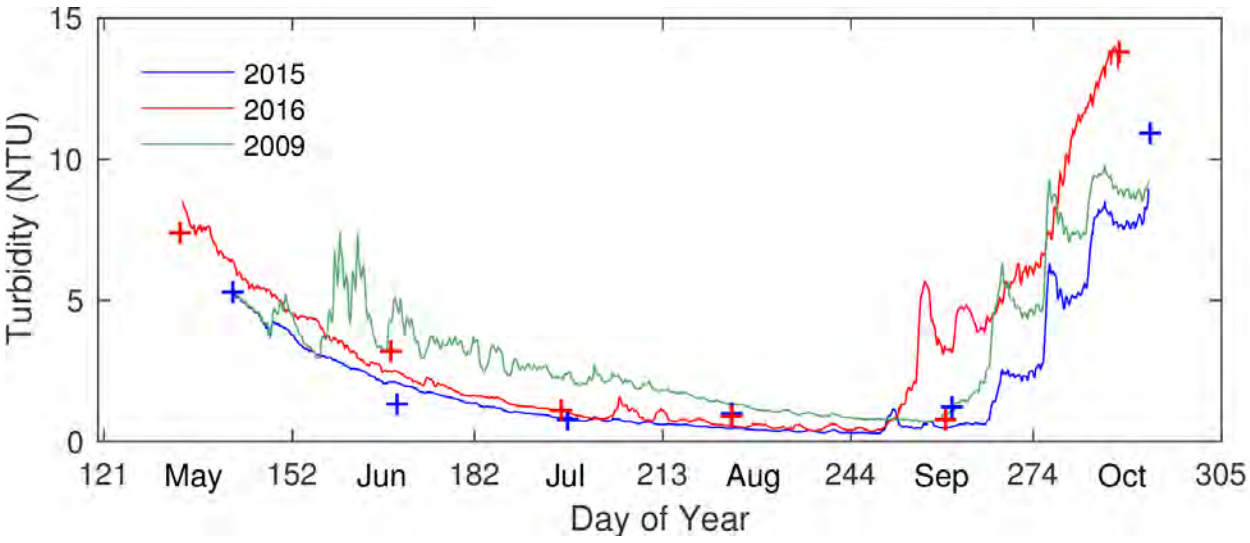

Figure 57. Comparison of measured and modelled surface turbidity at segment 53 (station C2). (solid lines), modelled turbidity at 1 m depth; (+), measured turbidity from the Seabird profiles at 1 m depth.

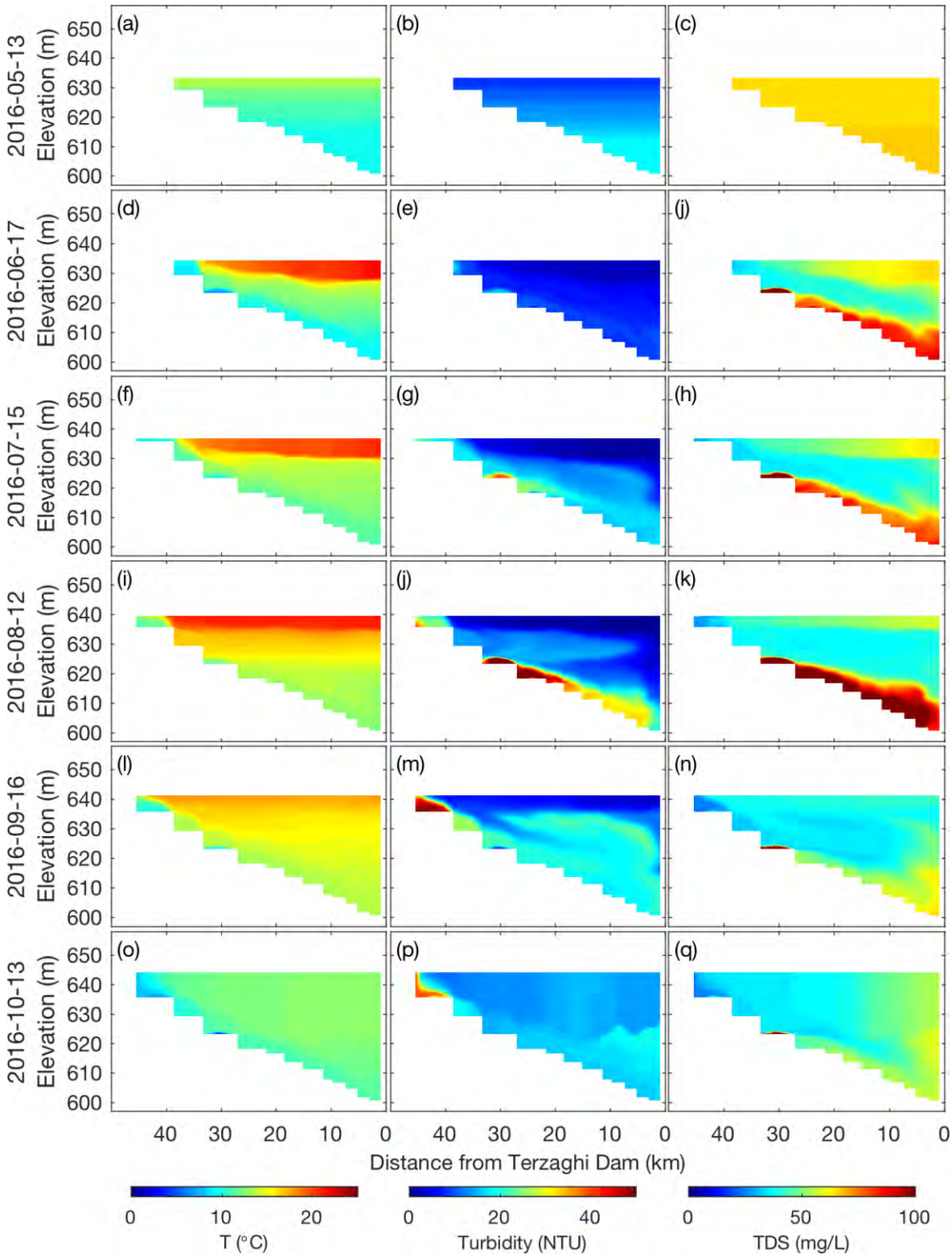

Figure 58. Scenario 2 (2016). Time sequence showing snapshots of modelled temperature, turbidity and TDS.

3.4.8.3.3 Tracers

The modelled tracers for 2016 are shown in Figure 59. Compared to 2015, both higher outflows from La Joie and Terzaghi Dams in June resulted in an earlier replacement of the initial water in the hypolimnion. In addition, water originating from the main and tributary inflows entered the surface layer earlier in the productive season.

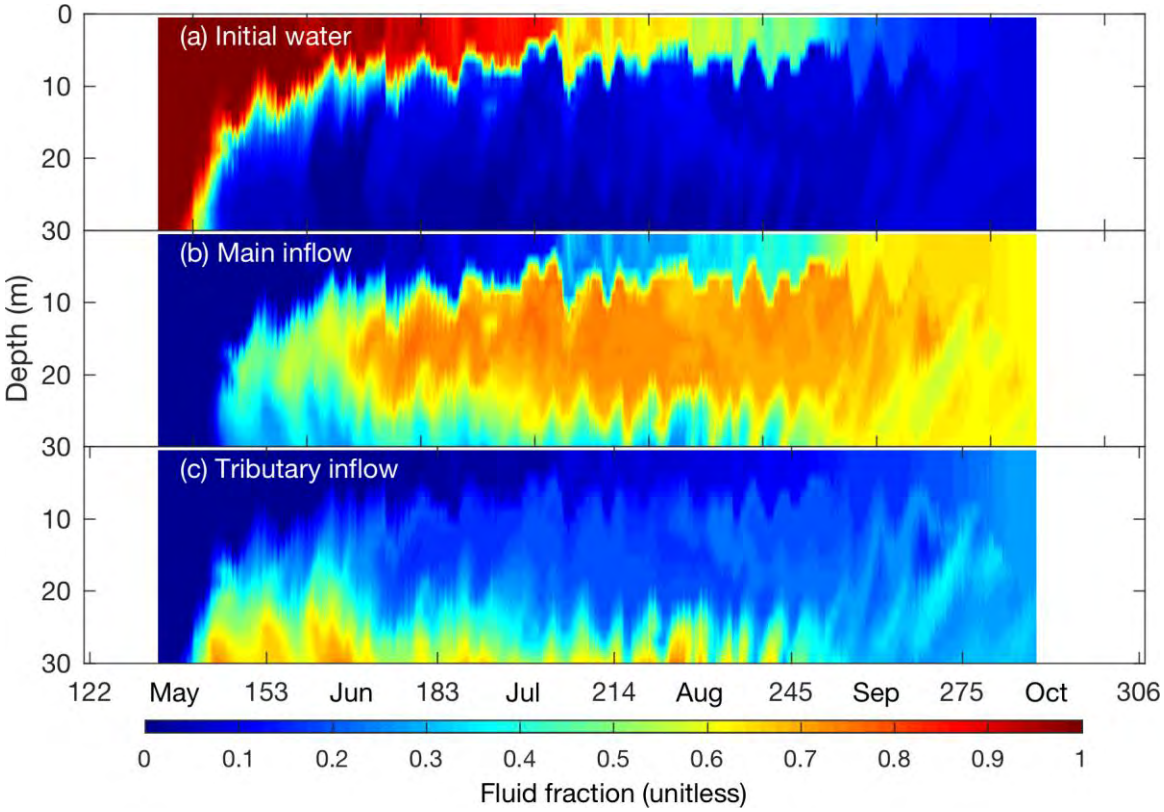

Figure 59. Scenario 2 (2016). Passive conservative tracers at segment 53 (station C2) from (a) Initial water in the reservoir, (b) Main inflow, (c) Tributary inflow.

3.4.8.4 Model Scenario 3

Recall, Scenario 3 was set up with flows from 2009, using meteorological forcing and tributary water quality from 2015; as a result, Scenarios 1 and 3 differ only by their flows and water levels. Scenario 3 is given as one example of a reservoir operation scenario; future work includes assessing a wide range of scenarios.

3.4.8.4.1 Water temperature

Modelled water temperature for 2009 is shown in Figure 60a-b. The model results for Scenario 3 show the same general seasonal cycle as observed in 2015 and 2016. Compared to Scenario 1 (2015), the surface layer is slightly warmer and the deep water remains slightly cooler through much of the summer, both consistent with low flow conditions. Note the initial water level was lower, and as a result the reservoir was less

than 30 m depth at the start of the simulation, accounting for the steps at the bottom of the contour plots in the first month of the simulation (Figure 60b-f).

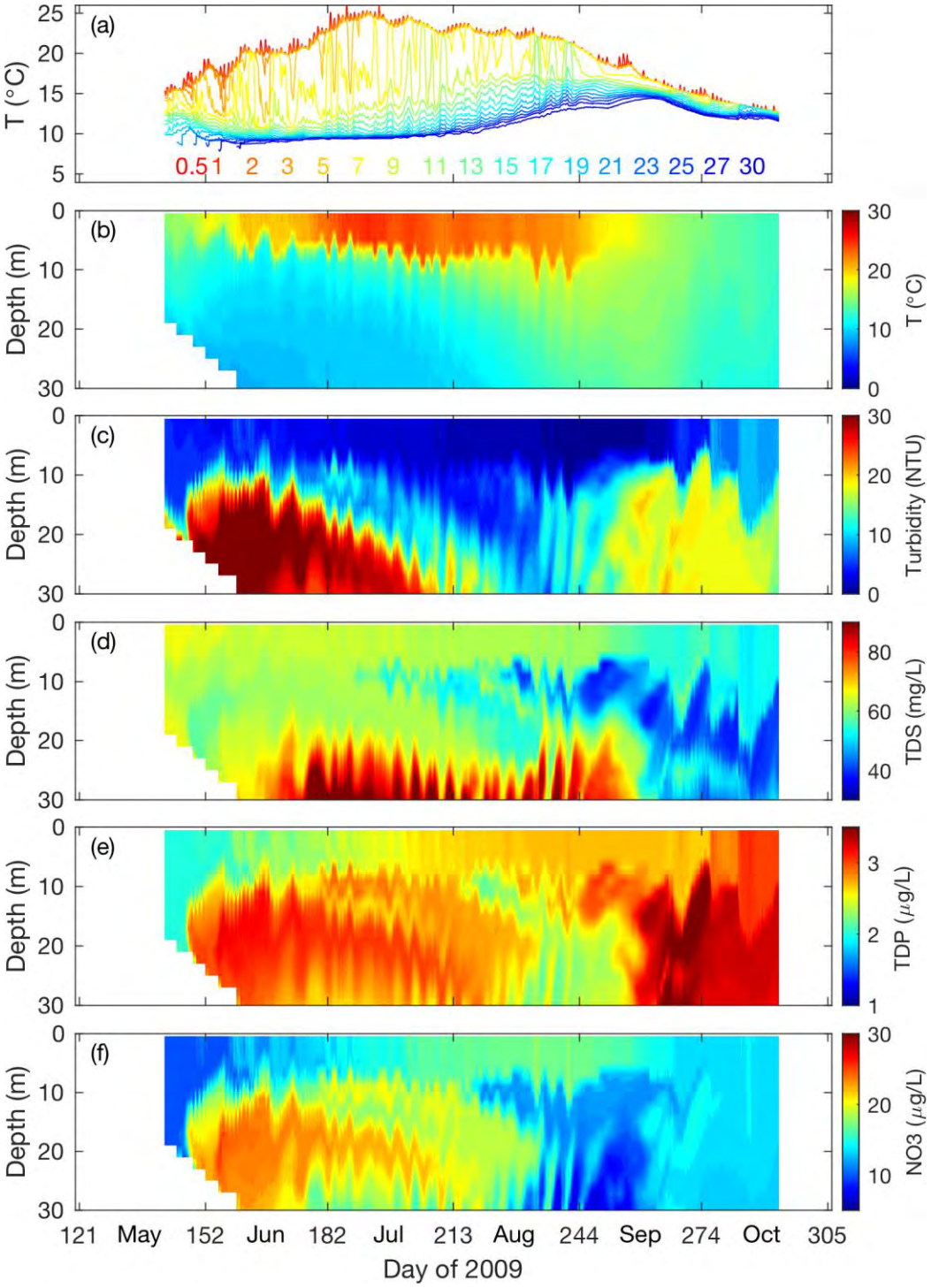

Figure 60. Scenario 3 (2009). Modelled water quality parameters at segment 53 (station C2).

3.4.8.4.2 Water quality

The modelled turbidity is shown in Figure 60c. As in the previous scenarios, plunging of the cold inflows transports turbidity to depth (Figure 61, second column).

Also, there is more transport of turbidity into the surface layer than in 2015 or 2016, which can best be seen in Figure 57.

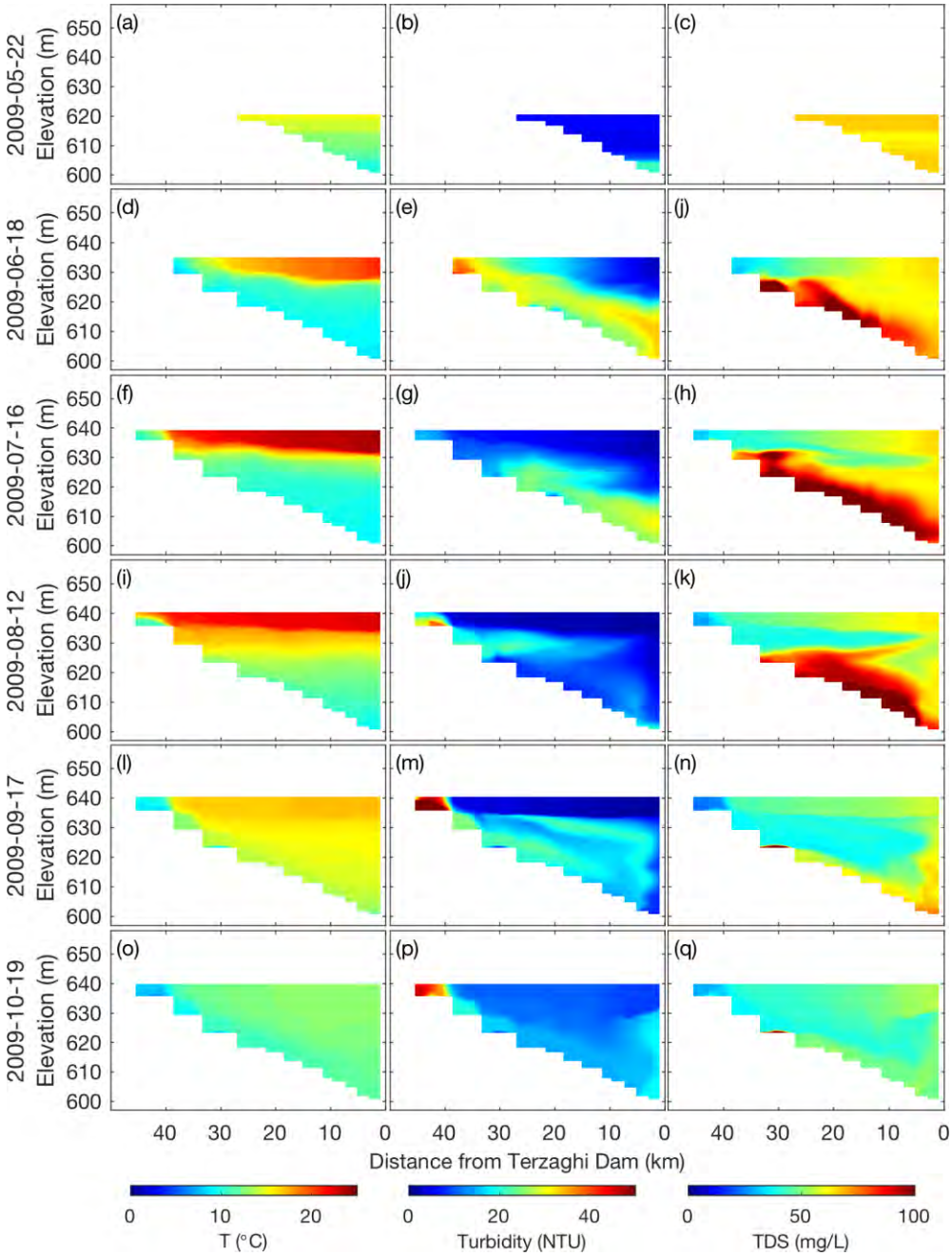

Figure 61. Scenario 3 (2009). Time sequence showing snapshots of modelled temperature, turbidity and TDS.

3.4.8.4.3 Tracers

The modelled tracers show the main inflow inserting at the thermocline instead of plunging into the hypolimnion (Figure 62). This results in more transport of the main inflow into the surface layer compared to Scenarios 1 and 2.

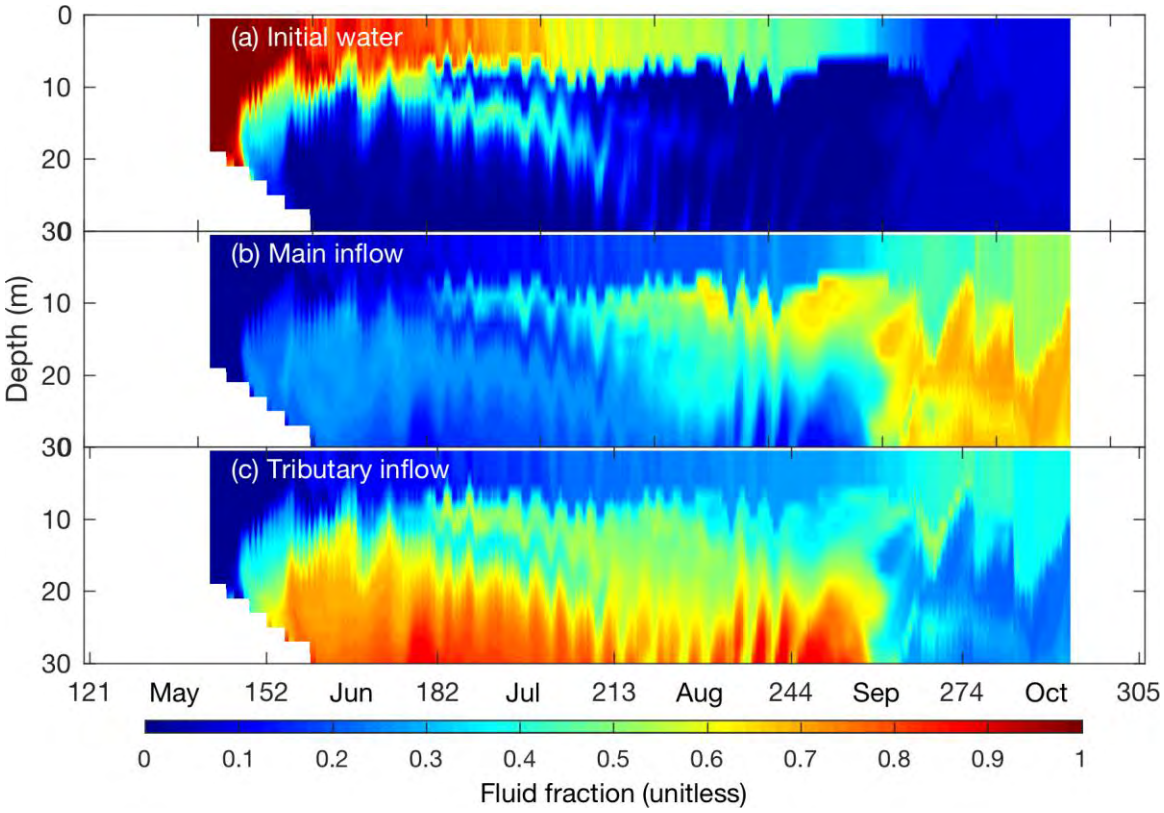

Figure 62. Scenario 3 (2009). Passive conservative tracers at segment 53 (station C2) from (a) Initial water in the reservoir, (b) Main inflow, (c) Tributary inflow.

3.4.8.5 Chlorophyll-a Regression Analysis with CE-QUAL-W2 model outputs

We employed a similar modelling approach as with phytoplankton primary productivity and biomass, discussed in Section 3.3.2, when we regressed phytoplankton biomass (chlorophyll-a) with the CE-QUAL-W2 output for the three scenarios described above (Table 17). The purpose of this exercise was to validate the regression results using the modeled parameters from CE-QUAL-W2 against the model parameters for the actual data collected from Carpenter, Anderson and Seton.

The top model out of 64 had an r^2 of 0.61 and a model weight of 0.78 suggesting a high degree of support for this model, which meant that model averaging was not required (Table B-7 in APPENDIX B). Equation 10 shows the unstandardized coefficients with the standardized coefficients presented in

Table 18.

$$\log_{10}\text{Chlorophyll-a} = -1.33 - 0.01*\text{Temperature} - 0.01*\text{Turbidity} - 3.33 \times 10^{-4}*\text{PAR} + 0.14*\text{DIN} + 0.21*\text{SRP} - 0.46*\text{Water Residence Time}$$

Equation 10

Table 18. Model statistics for 2015 and 2016 phytoplankton chlorophyll-a modeled with CE-QUAL for Carpenter Reservoir.

Variable	Standardized Coefficient	Estimate	t-value
(Intercept)	0.00	-1.33	-4.05
Temperature	-0.26	-0.01	-3.65
Turbidity	-0.33	-0.01	-5.27
PAR	-0.13	-3.33×10^{-4}	-2.28
DIN	1.57	0.14	5.36
SRP	0.28	0.21	3.46
Water Residence Time	-0.46	0.00	-7.28

Note: Estimate is the unstandardized coefficients that are presented in Equation 10.

The magnitude of the coefficients was different in all but one case. The standardized coefficient for PAR using the actual data was -0.132 (Table 14) and was -0.130 with the CE-QUAL-W2 output (Table 18). This could be a spurious result given the other coefficients did not match but it could also reflect a good approximation by CE-QUAL-W2 of PAR conditions. The direction of the model parameters was the same to the averaged model presented in Section 3.3.2.3 (Equation 7) with two notable differences, DIN and SRP. Chlorophyll-a, using the CE-QUAL-W2 model output, increased in cooler less turbid water, with less light and shorter water residence times but increased with more DIN and SRP, the opposite of what we found with the actual 2015 and 2016 data (Table 14).

There are two reasons for the discrepancies in this initial trial. First, the model presented in this section, includes modeled data from 2009, which would change the estimates for the predictor variables. Second, the chlorophyll-a modeled in Section 3.3.2.3 included data from Carpenter, Anderson and Seton, which covers a wider swath of values for each predictor variable in the model (e.g. wider range in PAR and turbidity). The results in this section only include data from Carpenter. The high model fit and weight for Equation 10 in this section is further evidence that data from Anderson Lake and Seton Lake could be biasing the results in Sections 3.2 and 3.3.

We will explore the statistical implications of removing data from Anderson Lake and modeling data from Carpenter Reservoir and Seton Lake separately as well as refining the CE-QUAL-W2 model. These changes should address some of the differences observed between the results in this section and Section 3.3.2.3. Despite the discrepancies observed, the potential for using CE-QUAL-W2 to assist in predicting

outcomes for response variables from management decisions is improving. This section briefly shows how CE-QUAL-W2 modelled parameters such as PAR, will be validated against actual data.

3.5 Question 4: Can suspended sediment transport into Seton be altered by changes in Carpenter Reservoir Operations?

We will be refining the regression and CE-QUAL-W2 models in 2017 and 2018 and will use the output from these models to fully answer this question.

4 CONCLUSIONS

The purpose of this project is to determine if light is the primary regulating factor for biological production in Carpenter Reservoir and how flow management decisions might affect PAR and other environmental variables. The results will ultimately inform how to best manage Carpenter Reservoir to benefit fish populations and their prey.

Based on our current findings, PAR is an important driver of littoral periphyton production on stony substrates and phytoplankton primary productivity in the pelagic habitat. Both increased with increasing percent of surface PAR. However, PAR did not describe as much variation in periphyton growing on sand and was negatively correlated with phytoplankton biomass in the pelagic zone. The algal community found on the sand samples in Carpenter were mostly motile species suggesting these organisms were not directly associated with the sand but likely captured from the water column as the samples were drawn up to the surface. This would decouple the relationship between algal biomass on sand and PAR at the sample depths. This also highlights the importance of analyzing the community assembly for each of the response variables.

The negative relationship between phytoplankton biomass and PAR may be due to the availability of other growth limiting factors such as nutrients. Primary production is limited by nitrogen and phosphorus (Stockner and Shortreed 1978, Perrin et al. 1987, Bothwell 1988, Suttle and Harrison 1988) therefore primary production can increase in areas with higher concentrations of limiting nutrients so long as they are within the euphotic zone (1% or more of total surface PAR) (Wetzel 2001).

PAR was not included in the zooplankton regression analysis but given the smaller size class of phytoplankton was an important determinant in zooplankton biomass, PAR can influence zooplankton production indirectly by influencing the biomass of phytoplankton. Urabe et al. (2002) also found that herbivores such as *Daphnia* spp., the dominant cladoceran in Carpenter, Anderson and Seton, were more abundant in low light conditions. This is counter-intuitive but occurred because the nutrient content in phytoplankton increased relative to carbon, which meant the phytoplankton became a higher quality food source for the zooplankton.

Zooplankton biomass increased with water residence time, a measure that can be managed by increasing or decreasing the outflow in Carpenter Reservoir. As a cursory check, we looked at how change in water residence time would affect zooplankton biomass during the coolest and warmest months in the reservoir. Using Figure 63, we identified May-June as the coolest months and August-September as the warmest with mean temperatures of 11.13 °C and 13.90 °C, respectively.

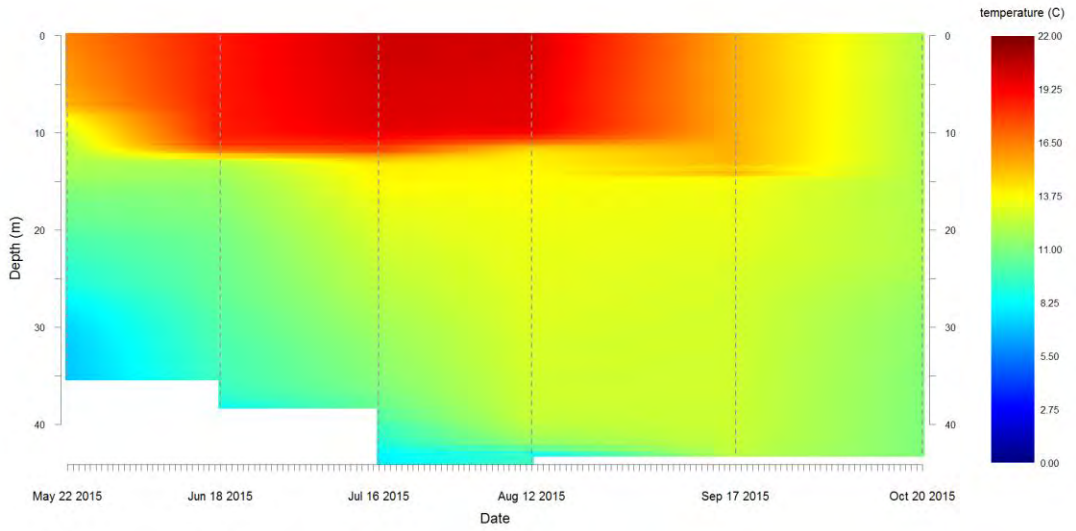

Figure 63. Temperature profile for Carpenter Reservoir by sampling date as indicated by the vertical dashed lines.

A doubling of mean water residence time from 57 days to 113 days resulted in a 4% increase in zooplankton biomass of 71 mg dry weight/m^2 for both temperature regimes (Figure 64). However, an increase in mean temperature from 11.13 to 13.90 °C resulted in a 77% increase in zooplankton biomass of 1,432 mg dry weight/m^2, regardless of mean water residence time. This is a substantial difference but this correlation may be due to the seasonal changes in species development rather than driven by environmental variables. This trend will need to be further explored in subsequent analyses.

From Figure 64 and the regression results in Sections 3.3.3.2 and 3.3.3.3 we can see that temperature had a much larger effect on zooplankton biomass than water residence time.

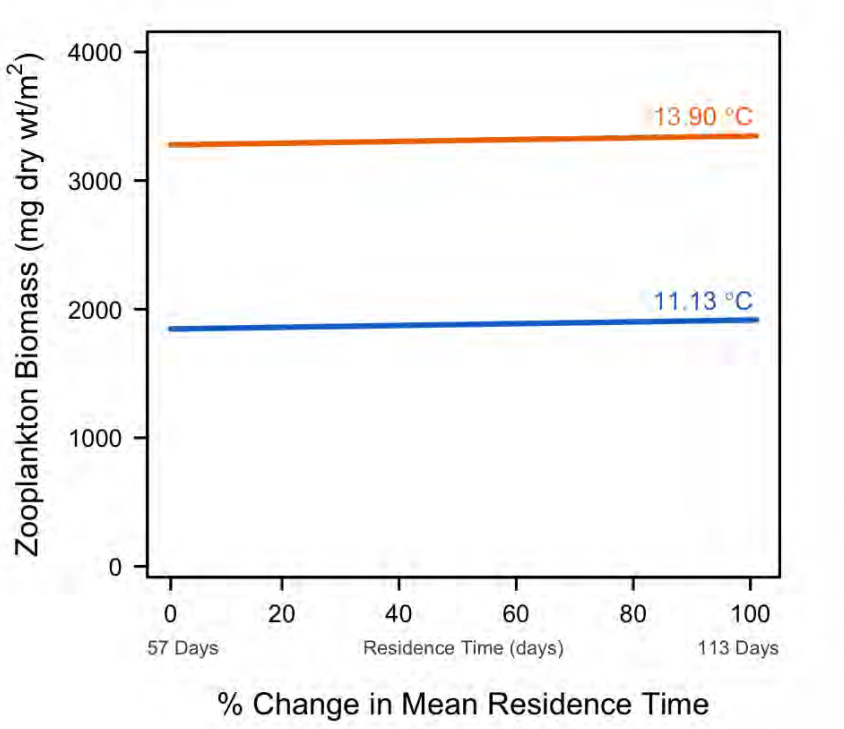

Figure 64. Zooplankton biomass as a function of percent change in mean residence time. The range extends from the minimum mean recorded residence time during the sampling period in 2015 (0% change or 57 days) to 100% change or twice as long (113 days).

We also found that water temperature, turbidity and dissolved inorganic nitrogen were significant determinants of periphyton and zooplankton production. These factors along with PAR are endpoints from the CE-QUAL-W2 model, which is performing well with the 2015 and 2016 data. An emerging picture of links between physical and chemical attributes in the reservoir and biological production is as follows. Relatively warm water having low turbidity favouring zooplankton is restricted to the top 10m of the water column in May through September. Bottom water is cold and turbid in relation to inflows sinking according to density gradients, mainly in May through mid-July. After July, inflow turbidity declines as does the bottom turbidity in the reservoir but the bottom water remains cool. The change in inflow turbidity is likely related to declining flows and less erosion by glacial headwaters that leads to reduced transport of fines. As temperature rises among inflows late in the summer, some entrainment of inflow in reservoir surface waters is apparent with accompanying increasing turbidity. The strong influence of rising temperature over more of the water column than earlier in the growing season has a strong effect by favouring conditions for zooplankton despite the rising turbidity. Increasing concentrations of TDP and NO_3-N late in the growing season in Carpenter Reservoir resulted in increasing export to Seton Lake with peak transport of TDP in the fall (Figure 65) and peak DIN in the early summer, followed by more

moderate increases in the fall (Figure 66). These increases will favour phytoplankton and periphyton production with the boost in phytoplankton production favouring zooplankton. These interactions show that fall is an optimum time for biological production in Carpenter Reservoir and potentially Seton Lake. Combinations of suitable temperature and rising nutrient concentrations will drive metabolic activity. Light does not appear to be the main story of the modeling so far.

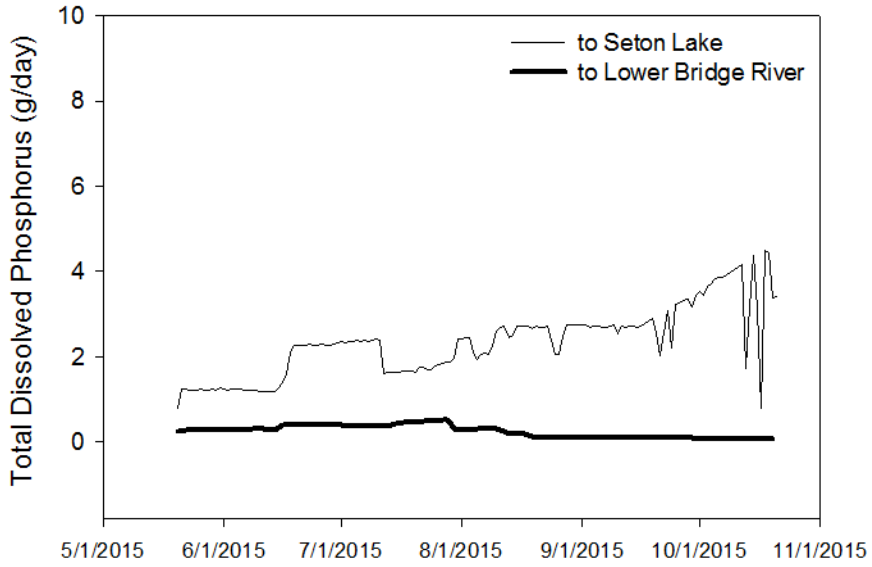

Figure 65. Total dissolved phosphorus (TDP) transport from Carpenter Reservoir to Seton Lake (thin line) and Lower Bridge River (bold line) from 1 May to 1 November, 2015.

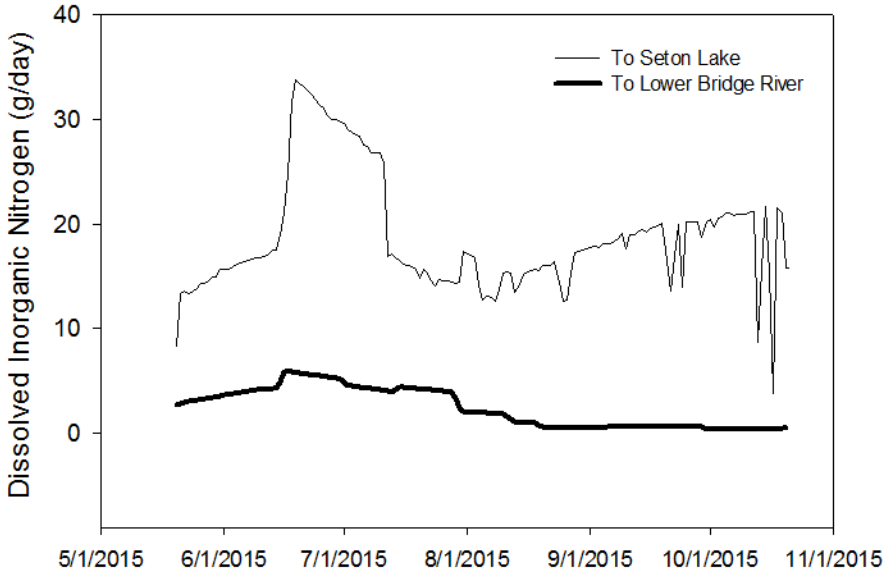

Figure 66. Dissolved inorganic nitrogen (DIN) transport from Carpenter Reservoir to Seton Lake (thin line) and Lower Bridge River (bold line) from 1 May to 1 November, 2015.

Further development of the modeling will include a closer link between CE-QUAL-W2 and the statistical models. This link will facilitate simulations to show implications of change in a water management strategy on biological endpoints including periphyton accrual that is an indicator of benthic production in littoral habitat and phytoplankton and zooplankton that are indicators of biological production in pelagic habitat. This approach can be particularly valuable in exploring potential change to biological production with respect to unforeseen events as is presently occurring with need to release more water in the spring and for ongoing periods in face of safety precautions needed in the Bridge system (Ministry of Forest, Lands and Natural Resource Operations, 2016). The linked CE-QUAL-W2 and regression modelling will prove very useful in predicting changes to biological production in Carpenter Reservoir should similar or different scenarios occur in the future.

5 NEXT STEPS

5.1 Biological production and environmental variables

All the periphyton, phytoplankton and zooplankton samples have been collected along with water chemistry, light, CTD profiles for PAR, turbidity, temperature and other measures of suspended and dissolved material, which have increased the dataset for and predictive power of the regression models. We will update the periphyton analysis with the 2016 data and continue to refine the phytoplankton and zooplankton analyses. This will include exploring the weak model fit for periphyton and phytoplankton. Increasing model fit (and our confidence in their predictive power) may be achieved by removing data collected from Anderson and modelling data from Carpenter Reservoir and Seton Lake separately.

We will also incorporate the output from CE-QUAL-W2 for key scenarios with the periphyton and phytoplankton data to cross-validate the modeled output against the actual data collected in 2015 and 2016. This process will help hone the CE-QUAL-W2 modeling strategy and lend confidence to the final CE-QUAL-W2 model results for future scenarios.

5.2 CE-QUAL-W2 modelling strategy

The modelling strategy consists of the following steps:

1. **Model setup:** CE-QUAL-W2 has been setup to simulate conditions during the productive season of 2015 and 2016.
2. **Model calibration:** We have begun a systematic comparison of the model to the measured field parameters, including temperature, TDS, turbidity, PO_4, TDP, TP, and NO_3. A sensitivity analysis of important

model parameters and factors such and wind, will also be completed. The model will be calibrated by adjusting the tributary boundary conditions and model parameters to give the best results for 2015.

3. **Model validation**: The model will be validated by comparing the results to the field data for 2016.

6 LIST OF REFERENCES CITED

Armantrout, N.J. 1998. *Glossary of Aquatic Habitat Inventory Terminology*. American Fisheries Society. Bethesda, MD.

Akaike, H. (1974). New Look at Statistical Model Identification. IEEE Transactions on Automatic Control. AC19(6): 716–723.

Allan, J. D., and M. M. Castillo. 2007a. Nutrient dynamics. In Stream Ecology: structure and function of running waters (2nd ed.). Dordrecht, The Netherlands: Springer.

Allan, J. D., and M. M. Castillo. 2007b. Primary producers. In Stream Ecology: structure and function of running waters (2nd ed.). Dordrecht, The Netherlands: Springer.

Allan, J. D., and M. M. Castillo. 2007c. The abiotic environment. In Stream Ecology: structure and function of running waters (2nd ed.). Dordrecht, The Netherlands: Springer.

Bartoń, K. 2015. Multi-model inference. R package version 1.15.6

Basu, B. K., and F. R. Pick. 1996. Factors regulating phytoplankton and zooplankton biomass in temperate rivers. Limnology and Oceanography. 41(7): 1572–1577.

Bates, D, M. Maechler, B. Bolker, S. Walker, R. H. B. Christensen, H. Singmann, B. Dai, G. Grothendieck and P. Green. 2016. Lme4: Linear Mixed-Effects Models using 'Eigen' and S4. R package version 1.1-12

BC Hydro. 1995. Dam Safety Investigations. Terzaghi Dam deficiency investigation. Summary report and appendices. BC Hydro. Maintenance, Engineering and Projects. Report No. H2479.

Behrenfeld, M.J., E. Boss, D.A. Siegel, and D.M. Shea. 2005. Carbon-based ocean productivity and phytoplankton physiology from space. Global Biogeochemical Cycles. 19: 1-14.

Benke, A.C. and A.D. Huryn. 2006. Secondary production of macroinvertebrates. In F.R. Hauer and G.A. Lamberti (eds.). *Methods in Stream Ecology*. New York, NY: Academic Press. 691-710pp.

Berry, H. A., and C. A. Lembi. (2000). Effects of temperature and irrandiance on the seasonal variation of a Spirogyra (Chlorophyta) population in a midwestern lake (USA). Journal of Phycology. 36: 841–851.

Biggs, B.J.F. 2000. Eutrophication of streams and rivers: dissolved nutrient-chlorophyll relationships for benthic algae. Journal of the North American Benthological Society. 19: 17-31.

Bothwell, M.L. 1988. Growth rate responses of lotic periphytic diatoms to experimental phosphorus enrichment: The influence of temperature and light. Canadian Journal of Fisheries and Aquatic Sciences. 45: 261-270.

Bothwell, M.L. 1989. Phosphorus – limited growth dynamics of lotic periphyton diatom communities: Areal biomass and cellular growth rate responses. Canadian Journal of Fisheries and Aquatic Sciences. 46: 1293-1301.

Bridge River WUP CC. 2003. Bridge River Water Use Plan Consultative Committee Report (WUP CC). Compass Resource Management and BC Hydro. A report produced for BC hydro Water Use Planning group. (Executive Summary available on website: http://www.bchydro.com/content/dam/hydro/medialib/internet/documents/environment/pdf/wup_bridge_river_executive_summary_pdf.pdf

Burks, R. L., D. M. Lodge, E. Jeppesen, and T. L. Lauridsen. 2002. Diel horizontal migration of zooplankton: costs and benefits of inhabiting the littoral. Freshwater Biology. 47: 343–365.

Burnham, K. P., and D. R. Anderson. 2002. Model selection and multimodel inference: a practical information-theoretic approach (2nd ed., pp. 1–515). New York, NY: Springer.

Canter-Lund, H. and J.W.G. Lund. 1995. *Freshwater Algae – Their Microscopic World Explored*. BioPress Ltd. Bristol, U.K.

Clarke, L.R. and D.H. Bennett. 2007. Zooplankton production and planktivore consumption in Lake Pend Oreille, Idaho. Northwest Science. 81: 215-223.

Clarke, K.R., and R.N. Gorley. 2006. PRIMER v6: User Manual/Tutorial. PRIMER-E: Plymouth. UK.

Cloern, J.E., C. Grenz, and L. Vidergar-Lucas. 1995. An empirical model of the phytoplankton chlorophyll:carbon ratio – the conversion factor between productivity and growth rate. Limnology and Oceanography. 40: 1313-1321.

Cole T. M. and S. A. Wells. 2015. CE-QUAL-W2: A Two-Dimensional, Laterally Averaged, Hydrodynamic and Water Quality Model, Version 3.72, User Manual. Department of Civil and Environmental Engineering, Portland State University, Portland, Oregon. 797pp.

Cyr, H., and M. L. Face. 1993. Magnitude and patterns of herbivory in aquatic and terrestrial ecosystems. Nature. 361: 148–150.

Effron, B. and R. Tibshirani. 1993. An introduction to the bootstrap. Mongraphs on Statistics and Applied Probability No. 57. Chapman and Hall. London, U.K.

Geen, G.H. and F.J. Andrew. 1961. Limnological changes in Seton Lake resulting from hydroelectric diversions. International Pacific Salmon Commission Progress Report 8.

Goldman, J.C. and E.J. Carpenter. 1974. A kinetic approach to the effect of temperature on algal growth. Limnology and Oceanography. 19: 756-766.

Griffiths, R.P. 1999. Assessment of fish habitat and production in Carpenter Lake

Reservoir relative to hydroelectric operations. Report prepared by R.P. Griffith and Associates for BC Hydro. 202pp.

Guadayol, Ó, F. Peters, C. Marrassé, J. M. Gasol, C. Roldán, E. Berdalet, R. Massana and A. Sabata. 2009. Episodic meteorological and nutrient-load events as drivers of coastal planktonic ecosystem dynamics: a time-series analysis

Marine Ecology-Progress Series. 381: 139-155.

Guildford, S.J. and R.E. Hecky. 2000. Total nitrogen, total phosphorus, and nutrient limitation in lakes and oceans: Is there a common relationship? Limnology and Oceanography. 45: 1213-1223.

Harrell, F. E. 2001. Regression modelling strategies. New York, New York, USA: Springer.

Haven, K. E., J. Hauxwell, A. C. Tyler, S. Thomas, K. J. McGlathery, and J. Cebrian. 2001. Complex interactions between autotrophs in shallow marine and freshwater ecosystems: implications for community responses to nutrient stress. Environmental Pollution, 113, 95–107.

Healey, F.P. 1985. Interacting effects of light and nutrient limitation on the growth rate of *Synechococcus linearis* (Cyanophyceae). Journal of Phycology 21:134-146.

Ichimura, S., T.R. Parsons, M. Takahashi and H. Seki. 1980. A comparison of four methods for integrating ^{14}C-primary productivity measurements per unit area. J. Oceanogr. Soc. Jap. 36: 259-262.

Jeppesen, E., J. P. Jensen, M. Søndergaard, and T. Lauridsen. 1999. Trophic dynamics in turbid and clearwater lakes with special emphasis on the role of zooplankton for water clarity. Hydrobiologia, 408/409, 217–231.

Korpelainen, H. 1986. The effects of temperature and photoperiod on life history parameters of Daphnia magna (Crustacea: Cladocera). Freshwater Biology, 16, 615–620.

Lamberti, G. A., and A. D. Steinman. 1997. A comparison of primary production in stream ecosystems. Journal of the North American Benthological Society, 16(1), 95–104.

Leland, H. V. 1995. Distribution of phytobenthos in the Yakima River basin, Washington, in relation to geology, land use and other environmental factors. Canadian Journal of Fisheries and Aquatic Sciences, 52(5): 1108–1129.

Lewis Jr., W. M. 1984. The diatom sex clock and its evolutionary significance. The American Naturalist. 123(1): 73-80.

Li, Q. P., P. J. S. Franks, M. R. Landry, R. Goericke, and A. G. Taylor. 2010, Modeling phytoplankton growth rates and chlorophyll to carbon ratios in California coastal and pelagic ecosystems, Journal of Geophysical Research. 115: G04003.

Liess, A, C. Faithful, B. Reichstein, O. Rowe, J. Guo, R. Pete, G. Thomsson, W. Uszko, and S. N. Francoeur. 2015. Terrestrial runoff may reduce microbenthic net community productivity by increasing turbidity: a Mediterranean coastal lagoon mesocosm experiment. Hydrobiologia, 753(1): 205-218.

Limnotek. 2017. Seton Lake aquatic productivity monitoring (BRGMON6): Final report. . 215pp.

Marcarelli, A. M., C. J. Huckins, and S. L. Eggert. 2015. Sand aggradation alters biofilm standing crop and metabolism in a low-gradient Lake Superior tributary. Journal of Great Lakes Research, 41(4), 1052–1059. http://doi.org/10.1016/j.jglr.2015.09.004

McCauley E. 1984. The estimation of the abundance and biomass of zooplankton in samples. In J.A. Downing and F.H. Rigler (eds.). *A Manual on Methods for the Assessment of Secondary Productivity in Fresh Waters*. Oxford, U.K.: Blackwell Scientific Publications. 228-265.

Ministry of Forest, Lands and Natural Resource Operations. 2016. Section 93 Order – Terzaghi Target Flow Release and Annual Water Budget dated May 20, 2016. File: 76975-35/Bridge.

Nürnberg, G. K. and B. D. LaZerte. 2001. Predicting lake water quality. In: C. Holdren, W. Jones and J. Taggart. Ed. Managing lakes and reservoirs. North American Lake Management Society, Madison, WI. Terrene Institute in cooperation with Office of Water Assessment Watershed Protection Division U.S.-EPA, p. 139-163.

Parsons, T.K., Y. Maita and C.M. Lalli. 1984. A Manual of Chemical and Biological Methods for Seawater Analysis. Pergamon Press, Oxford. 173 pp.

Pawlowicz, R. 2008. Calculating the conductivity of natural waters. Limnology and Oceanography: Methods. 4: 489–501.

Perrin, C.J., M.L. Bothwell and P.A. Slaney. 1987. Experimental enrichment of a coastal stream in British Columbia: effects of organic and inorganic additions on autotrophic periphyton production. Canadian Journal of Fisheries and Aquatic Science. 44:1247-1256.

Perrin, C. J., & Richardson, J. S. 1997. N and P limitation of benthos abundance in the Nechako River, British Columbia. Canadian Journal of Fisheries and Aquatic Science. 54: 2574–2583.

Perrin, C.J. and R.H. Macdonald. 1999. A phosphorus budget and limnology in Carpenter Lake Reservoir, 1995-96. Report prepared by Limnotek Research and Development Inc., Vancouver, B. C., for R.P. Griffith & Associates, Sidney, B.C. 72 pp.

Pieters, R. and G.A. Lawrence. 2011. Plunging inflow and the summer photic zone in reservoirs. Water Quality Research Journal of Canada 47(3-4): 268-275. doi: 10.2166/wqrjc.2012.143

Potapova, M. and P. Snoeijs. 1997. The natural life cycle in wild populations of *Diatom moniliformis* (Bacillariophyceae) and its disruption in an aberrant environment. Journal of Phycology. 33:924-937.

Prescott, G.W. 1978. *How to Know the Freshwater Algae*. 3rd Edition. Wm. C. Brown Company. Dubuque, IA.

R Development Core Team. 2016. R: a language and environment for statistical computing. R Foundation for Statistical Computing, Vienna, Austria. https://www.R-project.org/

Rhee, G. Y. 1978. Effects of N:P atomic ratios and nitrate limitation on algal growth, cell composition, and nitrate uptake. Limnology and Oceanography. 23: 10-25.

Rhee, G. Y., and I.J. Gotham. 1980. Optimum N:P ratios and coexistence of planktonic algae. Journal of Phycology. 16: 486-489.

Rempel, L.L., J.S. Richardson, and M.C. Healey. 2000. Macroinvertebrate community structure along gradients of hydraulic and sedimentary conditions in a large gravel-bed river. Freshwater Biology. 45: 57-73.

Riemann, B. P. Simonsen, and L. Stengaard. 1989. The carbon and chlorophyll content of phytoplankton from various nutrient regimes. Journal of Plankton Research. 11: 1037-1045.

Rosemond, A. D., P. J. Mulholland, and J. W. Elwood. 1993. Top-down and bottom-up control of stream periphyton: effects of nutrients and herbivores. Ecology. 74(4): 1264–1280.

Schwartz, S. S., and R. E. Ballinger. 1980. Variations in life history characteristics of Daphnia pulex fed different algal species. Oecologia. 44(2): 181–184. http://doi.org/10.1007/BF00572677

Shelson, A.L. and G.K. Meffe. 1995. Path analysis of collective properties and habitat relationships of fish assemblages in coastal plain streams. Canadian Journal of Fisheries and Aquatic Science. 52: 23-33.

Shortreed, K. S., K. F. Morton, K. Malange, and J. M. B Hume. 2001. Factors Limiting Juvenile Sockeye Production and Enhancement Potential for Selected BC Nursery Lakes. Canadian Science Advisory Secretariat. Research Document 2001/098. http://www.dfo-mpo.gc.ca/CSAS/Csas/DocREC/2001/RES2001_098e.pdf

Shuter, B.J. and K.K. Ing. 1997. Factors affecting the production of zooplankton in lakes. Canadian Journal of Fisheries and Aquatic Science. 54: 359-377.

Steemann Nielsen, E. 1952. The use of radioactive carbon (^{14}C) for measuring organic production in the sea. Journal du Conseil International pour l'Exploration de la Mer. 18: 117-140.

Stockner, J. G., and K. Shortreed. 1978. Enhancement of autotrophic production by

nutrient addition in a coastal rainforest stream on Vancouver Island. Journal of the Fisheries Board of Canada 35:28–34.

Suttle, C. A., and P. J. Harrison. 1988. Ammonium and phosphate uptake rates, N:P supply ratios, and evidence for N and P limitation in some oligotrophic lakes. Limnology and Oceanography 33:186–202.

SYSTAT 13 Software, Inc. 2009. Chicago, IL.

Thorp, J.H. and A.P Covich. 1991. Ecology and classification of north American freshwater invertebrates. Academic Press.

Urabe, J., M. Kyle, W. Makino, T. Yoshida, I. T. Andersen, and J. J. Elser. 2002. Reduced light increases herbivore production due to stoichiometric effects of light/nutrient balance. Ecology. 83(3): 619-627.

Utermohl, H. 1958. Zur Vervollkommnung der quantitativen Phytoplankton methodik. Int. Verein. Limnol. Mitteilungen No. 9.

Wallace, J.B. and N.H. Anderson. 1996. Habitat, life history, and behavioural adaptations of aquatic insects. p12 – 28. In: R.W. Merritt and K.W. Cummins (Ed.). An Introduction to Aquatic Insects of North America. Kendall Hunt Publ. Dubuque Iowa. 862pp.

Water Act Order. 2011. Province of British Columbia Water Act Order. Water Act Sections 87 and 88. License file numbers 0212289, 0115688, 0161431, 0210947, 0202694, 0265200, 0199585, 3005073, 3005075, 3005074.

Wetzel, R.G. 2001. *Limnology.* Academic Press. San Diego.

Wu, L., and D. A. Culver. 1992. Ontogenetic diet shift in Lake Erie age-0 yellow perch (Perca flavescens): A size related response to zooplankton density. Canadian Journal of Fisheries and Aquatic Science. 49(9): 1932–1937.

Yentsch, C.S. and V.W. Menzel. 1963. A method for the determination of phytoplankton chlorophyll-a and phaeophytin by fluorescence. Deep-Sea Research. 10: 221-231.

Zuur, A. F., E. N. Ieno, and C. Elphick, C. 2010. A protocol for data exploration to avoid common statistical problems. Methods in Ecology and Evolution. 1:3–14.

7 APPENDIX A

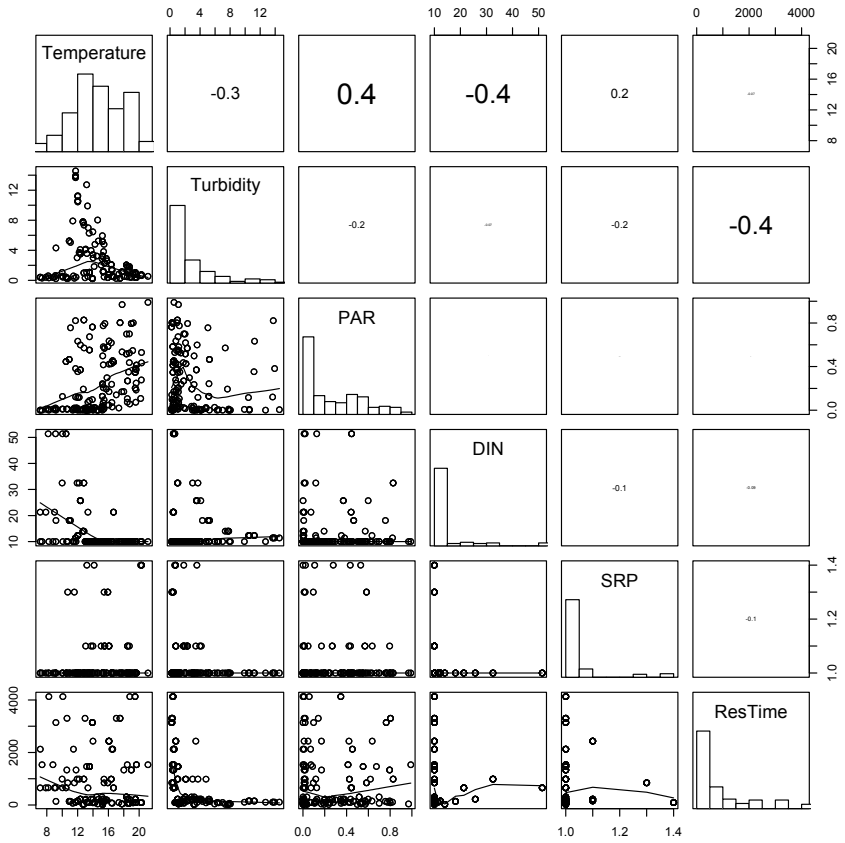

Figure A-1. Correlation coefficients for final variable set used in the phytoplankton and chlorophyll-a analyses. ResTime is the daily value for water residence time for each watershed. The smaller the coefficient the smaller the font displaying the coefficient. The smallest font corresponds to a correlation coefficient < 0.1 (e.g. DIN and Residence Time = -0.09) and where none is displayed the correlation = 0.

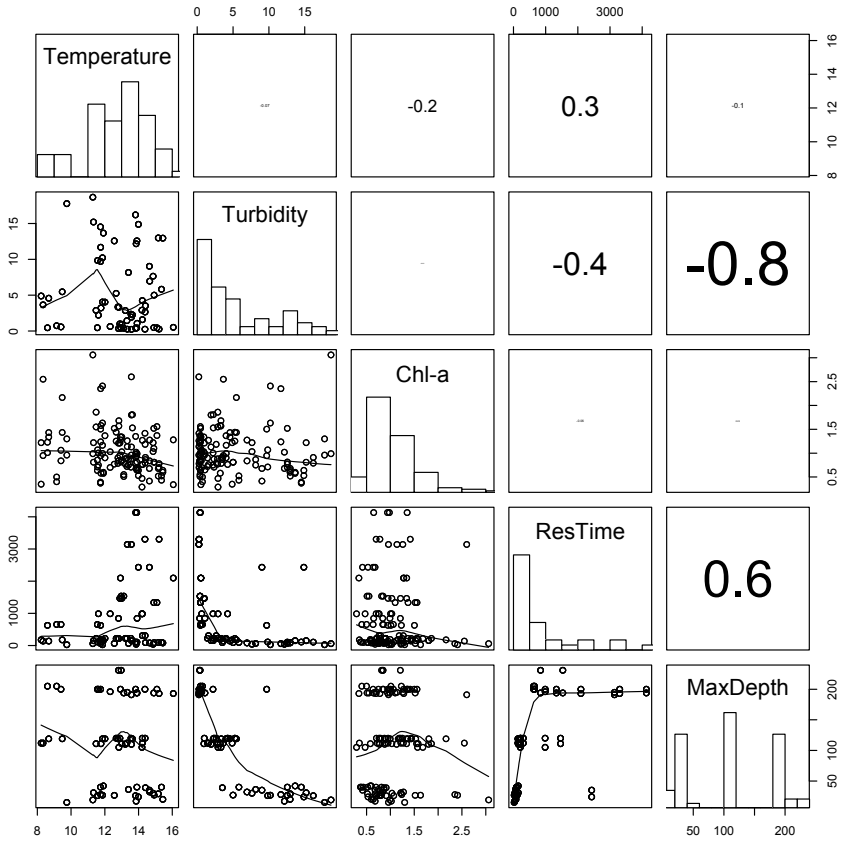

Figure A-2. Correlation coefficients for the predictor variables considered for the zooplankton analysis. The high correlation coefficient for turbidity and maximum reservoir depth we excluded maximum water depth from the final analysis. See Section 2.3.5 and Figure for the final variable set included in the zooplankton analysis.

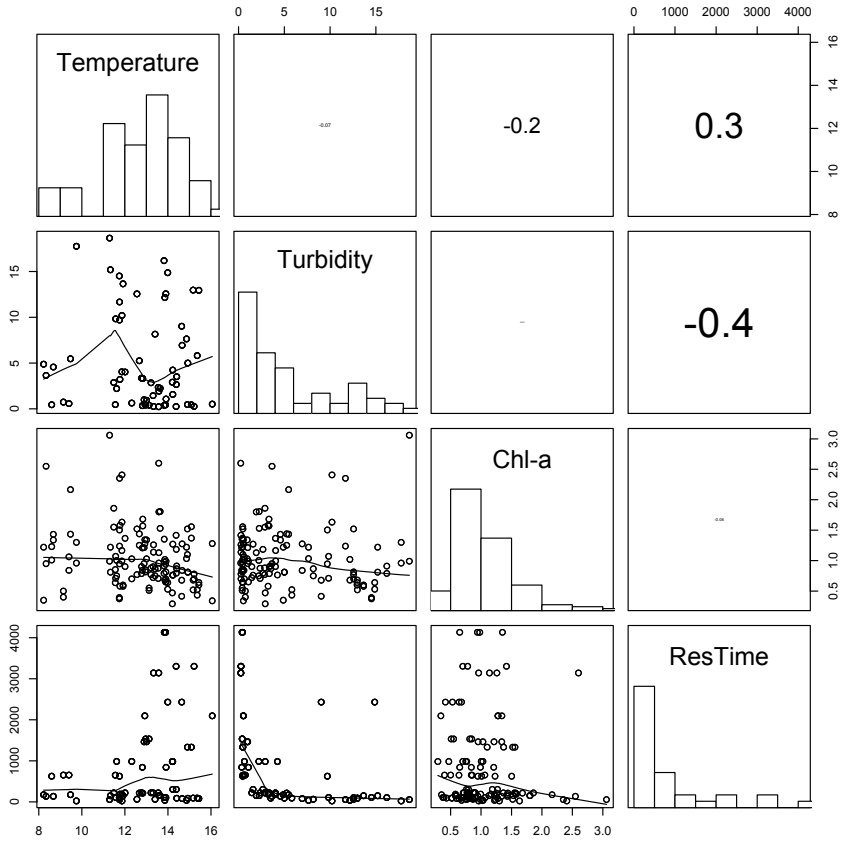

Figure A-3. Correlation coefficients for final variable set used in the zooplankton analysis. Chl-a is chlorophyll-a measured from the phytoplankton samples and ResTime is the mean 78-day residence time for each watershed.

8 APPENDIX B

Table B-1. Periphyton biovolume in 2015, measured as $\mu m^3 \times 10^9 \bullet m^{-2}$ by lake, substrate and incubation period (series) separated by major taxa. SD is the standard deviation when the mean of two samples was calculated.

Substrate	Lake	Series	Blue Green	Diatoms	Chlorophytes	Chryso - Cryptophytes	Dinoflagellates	Euglenoids	Total Mean Biovolume	SD
Polystyrene balls	Carpenter	Spring	72	1,398	2,651	-	-	-	4,121	529
		Summer	40	1,003	2,651	-	-	-	3,694	-
		Fall	13	1,038	7,085	-	25	51	8,212	-
	Anderson	Spring	92	1,272	-	-	-	-	1,364	932
		Summer	21	451	1,444	-	-	-	1,916	-
		Fall	76	2,306	4,629	-	-	-	7,011	-
	Seton	Spring	34	823	7	-	-	-	864	23
		Summer	95	1,437	1,609	-	-	-	3,142	294
		Fall	358	1,986	3,153	430	-	-	5,927	3,561
Sand pails	Carpenter	Spring	-	-	-	93	-	-	93	131
		Summer	-	54	-	-	-	-	54	76
		Fall	-	57	4	387	-	-	447	481

Table B-2. Phytoplankton biovolume by year, station and month separated by major taxa.

Station	Year	Month	Diatoms (um^3 x $10^3 \cdot L^{-1}$)	Green Algae (um^3 x $10^3 \cdot L^{-1}$)	Flagellates (um^3 x $10^3 \cdot L^{-1}$)	Blue Green Algae (um^3 x $10^3 \cdot L^{-1}$)	Dinoflagellates (um^3 x $10^3 \cdot L^{-1}$)	Euglenoids (um^3 x $10^3 \cdot L^{-1}$)	Other (um^3 x $10^3 \cdot L^{-1}$)	Total Biovolume (um^3 x $10^3 \cdot L^{-1}$)	SD 2015
C2	2015	May	216.05	31.01	288.82	7.18	26.36	0.00	21.61	591.05	18.90
		June	23.79	8.24	152.53	0.00	46.98	0.64	24.44	256.62	29.74
		July	6.76	13.95	117.75	0.00	102.72	0.00	13.47	254.64	151.13
		August	1.35	24.04	131.66	0.99	46.58	0.00	36.91	241.53	47.48
		September	19.61	22.93	171.60	7.98	18.54	0.48	24.94	266.07	17.85
		October	5.56	21.93	135.95	0.00	5.75	3.84	17.46	190.48	27.55
	2016	May	252.14	7.98	598.35	0.00	9.59	2.40	52.37	922.82	244.85
		June	91.85	330.00	203.28	0.00	4.79	0.96	10.81	641.69	163.84
		July	210.60	26.18	258.25	0.00	5.51	0.00	22.44	523.00	0.33
		August	89.92	3.98	160.48	0.00	3.60	0.00	20.26	278.23	70.51
		September	155.79	7.55	164.37	0.00	1.44	0.96	21.63	351.73	175.80
C6	2015	May	186.24	11.97	281.27	0.00	36.49	0.00	50.37	566.35	51.80
		June	21.84	16.02	212.27	0.00	18.22	0.96	33.92	303.22	4.69
		July	0.00	10.65	111.43	0.00	8.11	0.00	14.91	145.10	17.59
		August	12.64	0.00	81.41	0.29	26.05	0.32	26.39	147.11	35.80
		September	5.03	30.41	125.22	0.00	11.98	1.44	13.72	187.80	52.89
		October	4.41	26.38	196.02	0.29	3.60	4.31	28.68	263.69	21.95
	2016	May	32.14	0.00	507.28	0.00	0.00	0.00	34.91	574.33	20.91
		June	1.15	251.38	377.76	0.00	1.44	0.00	29.93	661.65	131.64
		July	163.24	6.16	237.29	0.00	5.75	0.00	14.96	427.40	87.22
		August	88.03	28.84	143.14	0.00	1.44	0.00	27.43	288.88	33.83

Station	Year	Month	Diatoms (um^3 x $10^3 \cdot L^{-1}$)	Green Algae (um^3 x $10^3 \cdot L^{-1}$)	Flagellates (um^3 x $10^3 \cdot L^{-1}$)	Blue Green Algae (um^3 x $10^3 \cdot L^{-1}$)	Dinoflagellates (um^3 x $10^3 \cdot L^{-1}$)	Euglenoids (um^3 x $10^3 \cdot L^{-1}$)	Other (um^3 x $10^3 \cdot L^{-1}$)	Total Biovolume (um^3 x $10^3 \cdot L^{-1}$)	SD 2015
		September	109.63	10.76	145.54	0.00	0.72	0.00	16.21	282.86	8.36
		October	51.02	0.00	83.25	0.00	1.20	0.00	9.14	144.62	32.34
A1	2015	May	19.97	92.60	143.78	0.00	12.16	0.00	27.93	296.44	142.96
		June	0.48	2.07	11.28	0.00	0.72	0.48	2.00	17.02	1.12
		July	13.65	153.29	98.82	14.55	14.19	0.00	10.31	304.82	256.75
		August	113.29	36.47	246.18	5.13	8.11	0.00	19.20	428.37	100.24
		September	35.19	46.24	112.88	0.03	3.60	3.36	10.10	211.38	28.92
	2016	May	40.42	77.57	98.55	12.25	2.16	12.16	23.94	267.05	107.40
		June	52.11	68.92	114.84	0.00	0.72	1.92	13.72	252.22	28.74
		July	61.20	66.38	123.87	0.00	5.03	0.96	18.95	276.39	6.08
		August	245.67	9.98	132.72	0.00	14.38	3.84	19.19	425.77	28.44
		September	203.72	15.93	98.12	0.24	0.00	1.20	11.84	331.04	12.57
		October	73.35	14.34	67.56	0.12	1.92	0.48	8.73	166.50	30.60
A2	2015	May	47.75	76.22	194.00	15.71	32.44	0.00	20.03	386.15	138.93
		June	1.22	2.67	11.37	0.00	0.00	0.08	4.01	19.35	5.90
		July	24.99	41.01	66.79	2.53	0.00	0.00	9.64	144.96	18.07
		August	87.31	121.16	116.93	0.65	16.22	0.00	84.79	427.07	76.05
		September	14.19	128.30	106.09	0.11	22.53	2.40	16.21	289.83	148.37
	2016	May	62.84	121.41	98.98	0.49	7.55	0.96	27.18	319.41	12.51
		June	31.07	15.49	109.53	0.00	0.00	0.00	18.70	174.79	28.01
		July	46.59	174.61	130.34	0.00	4.79	1.92	19.07	377.32	74.60
		August	156.87	22.82	163.63	0.00	10.79	1.92	28.68	384.71	100.9

Station	Year	Month	Diatoms (um^3 x $10^3 \cdot L^{-1}$)	Green Algae (um^3 x $10^3 \cdot L^{-1}$)	Flagellates (um^3 x $10^3 \cdot L^{-1}$)	Blue Green Algae (um^3 x $10^3 \cdot L^{-1}$)	Dinoflagellates (um^3 x $10^3 \cdot L^{-1}$)	Euglenoids (um^3 x $10^3 \cdot L^{-1}$)	Other (um^3 x $10^3 \cdot L^{-1}$)	Total Biovolume (um^3 x $10^3 \cdot L^{-1}$)	SD 2015
											6
		September	207.02	18.78	133.67	0.00	2.40	0.00	20.77	382.63	159.08
		October	15.34	30.24	75.07	0.00	1.31	0.00	17.87	139.83	25.53
S4	2015	May	176.14	230.98	177.74	1.20	12.16	0.00	20.20	618.42	
		June	104.49	61.30	236.71	0.10	20.37	8.11	35.41	466.49	
		July	149.30	41.11	185.07	0.32	37.44	5.41	22.19	440.84	
		August	109.48	111.26	233.70	2.89	72.98	10.81	44.14	585.26	
		September	3.45	8.20	120.33	0.00	4.31	0.48	20.37	157.14	
	2016	May	232.40	30.69	257.68	3.65	23.97	4.79	39.40	592.58	
		June	51.12	16.69	221.32	0.00	0.00	0.48	6.23	295.84	
		July	70.65	21.98	184.95	0.00	1.20	0.00	22.44	301.22	
		August	35.41	8.58	217.18	0.00	7.19	3.60	34.91	306.87	
		September	10.81	13.94	131.90	0.00	1.44	0.00	22.45	180.54	
		October	56.90	3.51	87.85	0.00	0.72	0.00	13.72	162.70	
S5	2015	May	116.65	11.43	258.92	7.78	52.71	0.00	37.41	484.90	
		June	127.12	79.95	230.39	11.16	93.26	0.00	43.64	585.52	
		July	128.95	25.66	251.95	0.08	20.27	8.11	23.44	458.47	
		August	182.02	34.73	257.01	0.39	48.66	0.00	28.18	550.98	
		September	14.99	27.91	117.53	1.58	4.31	0.00	16.21	182.54	
	2016	May	278.46	36.10	306.44	3.65	7.91	0.96	44.39	677.92	
		June	240.60	25.90	282.90	0.00	0.00	0.00	39.90	589.30	
		July	154.89	44.77	238.53	0.00	14.32	0.96	32.42	485.89	
		August	44.34	7.80	184.84	0.00	5.75	0.48	32.00	275.22	

Station	Year	Month	Diatoms (um^3 x $10^3 \cdot L^{-1}$)	Green Algae (um^3 x $10^3 \cdot L^{-1}$)	Flagellates (um^3 x $10^3 \cdot L^{-1}$)	Blue Green Algae (um^3 x $10^3 \cdot L^{-1}$)	Dinoflagellates (um^3 x $10^3 \cdot L^{-1}$)	Euglenoids (um^3 x $10^3 \cdot L^{-1}$)	Other (um^3 x $10^3 \cdot L^{-1}$)	Total Biovolume (um^3 x $10^3 \cdot L^{-1}$)	SD 2015
		September	6.14	0.54	179.28	0.24	0.72	0.00	24.94	211.86	
		October	81.26	0.52	90.61	0.00	0.00	0.00	15.59	187.98	

Table B-3. Results from the model selection process for the top 10 of 40 models using AICc for periphyton production on polystyrene balls anchored in the littoral habitat. PAR is photosynthetically active radiation, DIN is dissolved inorganic nitrogen measured as the sum of NH_4-N and NO_3-N, and SRP is soluble reactive phosphorus measured as PO_4-P.

Model	Adjusted r^2	*k*	logLik	ΔAICc	w_i	ER
PAR * Temperature + DIN	0.38	6	6.30	0.00	0.30	1.00
PAR * Temperature	0.37	5	4.88	0.51	0.23	1.29
PAR * Temperature + DIN - SRP	0.38	7	6.67	1.64	0.13	2.27
PAR * Temperature + DIN + Turbidity	0.38	7	6.37	2.26	0.10	3.09
PAR * Temperature - SRP	0.36	6	5.04	2.51	0.09	3.50
PAR * Temperature - Turbidity	0.36	6	5.02	2.56	0.08	3.59
PAR * Temperature + DIN - SRP + Turbidity	0.37	8	6.72	4.00	0.04	7.37
PAR * Temperature - SRP - Turbidity	0.36	7	5.23	4.53	0.03	9.62
PAR + Temperature - SRP	0.24	5	-2.73	15.73	0.00	2602.72
PAR + Temperature + DIN - SRP	0.24	6	-2.02	16.63	0.00	4084.94

Note: Adjusted r^2 is the r^2 of the linear regression model adjusted for the number of variables in the model,

k is the number of parameters in each model including the intercept and error terms

logLik is the log-likelihood,

ΔAICc is the difference between the top model AICc value and subsequent model AICc values,

w_i is the model weight for each model

ER is the evidence ratio for each model, which measures the likelihood that the top model is better than model *i.*

Table B-4. Results from the model selection process for the top 10 of 27 models using AICc for periphyton production in sand pails. SRP is soluble reactive phosphorus measured as PO_4, DIN is dissolved inorganic nitrogen measured as the sum of NH_4 and NO_3 and PAR is photosynthetically active radiation.

Model	Adjusted. r^2	*k*	logLik	ΔAICc	w_i	ER
Temperature - SRP	0.54	4	11.96	0.00	0.25	1.00
DIN - Turbidity	0.54	4	11.84	0.24	0.22	1.13
DIN - Turbidity - Temperature	0.59	5	13.57	0.72	0.17	1.43
DIN - Turbidity - SRP	0.59	5	13.48	0.90	0.16	1.57
Temperature - SRP - PAR	0.52	5	12.13	3.59	0.04	6.01
Temperature - SRP - Turbidity	0.52	5	12.06	3.73	0.04	6.45
Temperature - SRP + DIN	0.51	5	11.97	3.92	0.03	7.09
DIN - Turbidity + PAR	0.51	5	11.89	4.08	0.03	7.69
DIN	0.35	3	8.15	4.26	0.03	8.42
DIN + Temperature	0.35	4	8.84	6.26	0.01	22.86

Note: Adjusted r^2 is the r^2 of the linear regression model adjusted for the number of variables in the model,

k is the number of parameters in each model including the intercept and error terms

logLik is the log-likelihood,

ΔAICc is the difference between the top model AICc value and subsequent model AICc values,

w_i is the model weight for each model

ER is the evidence ratio for each model, which measures the likelihood that the top model is better than model *i.*

Table B-5. The candidate model set for phytoplankton primary roduction in Section 3.3.2.2.

Model	Adjusted r^2	*k*	logLik	ΔAICc	w_i	ER
PAR + Temperature - Turbidity - Water Resident Time	0.21	10	-79.25	0.00	0.19	1.00
PAR + Temperature - Turbidity - SRP - Water Resident Time	0.21	11	-78.49	0.62	0.14	1.37
PAR - Turbidity - Water Resident Time	0.20	9	-80.88	1.13	0.11	1.76
- DIN + PAR - Turbidity - Water Resident Time	0.20	10	-79.87	1.24	0.10	1.86
- DIN + PAR + Temperature - Turbidity - Water Resident Time	0.21	11	-79.05	1.76	0.08	2.41
- DIN + PAR - Turbidity - SRP - Water Resident Time	0.21	11	-79.20	2.06	0.07	2.80
PAR - Turbidity - SRP - Water Resident Time	0.20	10	-80.35	2.20	0.06	3.01
- DIN + PAR + Temperature - Turbidity - SRP - Water Resident Time	0.21	12	-78.28	2.38	0.06	3.29
PAR + Temperature - Water Resident Time	0.19	9	-82.19	3.74	0.03	6.49
PAR + Temperature - Turbidity	0.19	9	-82.28	3.94	0.03	7.16
PAR + Temperature	0.18	8	-83.62	4.49	0.02	9.45
PAR + Temperature - SRP - Water Resident Time	0.19	10	-82.06	5.62	0.01	16.60
PAR + Temperature - Turbidity - SRP	0.19	10	-82.07	5.64	0.01	16.81
- DIN + PAR + Temperature - Water Resident Time	0.19	10	-82.12	5.74	0.01	17.60
PAR - Turbidity	0.18	8	-84.26	5.77	0.01	17.87

Note: Adjusted r^2 is the r^2 of the linear regression model adjusted for the number of variables in the model,

k is the number of parameters in each model including the intercept and error terms

logLik is the log-likelihood,

ΔAICc is the difference between the top model AICc value and subsequent model AICc values,

w_i is the model weight for each model

ER is the evidence ratio for each model, which measures the likelihood that the top model is better than model *i.*

Table B-6. The candidate model set for phytoplankton biomass measured as chlorophyll-a in Section 3.3.2.3

Model	Adjusted r^2	*k*	logLik	ΔAICc	w_i	ER
- DIN - PAR - Temperature - Turbidity	0.30	10	401.60	0.00	0.31	1.00
- DIN - PAR - Temperature	0.30	9	400.04	1.01	0.19	1.66
- DIN - PAR - Temperature - Turbidity - SRP	0.30	11	401.77	1.77	0.13	2.42
- DIN - PAR - Temperature - Turbidity - Water Resident Time	0.30	11	401.63	2.04	0.11	2.77
- DIN - PAR - Temperature - SRP	0.30	10	400.09	3.02	0.07	4.52
- DIN - PAR - Temperature - Water Resident Time	0.30	10	400.07	3.07	0.07	4.63
- DIN - PAR - Temperature - Turbidity - SRP - Water Resident Time	0.30	12	401.80	3.82	0.05	6.75
- DIN - PAR - Temperature - SRP - Water Resident Time	0.30	11	400.12	5.07	0.02	12.63

Note: Adjusted r^2 is the r^2 of the linear regression model adjusted for the number of variables in the model,

k is the number of parameters in each model including the intercept and error terms

logLik is the log-likelihood,

ΔAICc is the difference between the top model AICc value and subsequent model AICc values,

w_i is the model weight for each model

ER is the evidence ratio for each model, which measures the likelihood that the top model is better than model *i.*

Table B-7. The candidate model set for phytoplankton biomass measured as chlorophyll-a modeled with CE-QUAL output data in Section 3.4.8.5.

Model	Adjusted r^2	*k*	logLik	ΔAICc	w_i	ER
DIN - PAR - Temperature - Turbidity + SRP - Water Resident Time	0.61	11	254.39	0.00	0.78	1.00

Note: Adjusted r^2 is the r^2 of the linear regression model adjusted for the number of variables in the model,

k is the number of parameters in each model including the intercept and error terms

logLik is the log-likelihood,

ΔAICc is the difference between the top model AICc value and subsequent model AICc values,

w_i is the model weight for each model

ER is the evidence ratio for each model, which measures the likelihood that the top model is better than model *i.*

Table B-8. Zooplankton biomass by year, station and month separated by major taxa.

Station	Year	Month	Cladocera ($mg \cdot m^{-2}$)	Cyclopoid ($mg \cdot m^{-2}$)	Calanoid ($mg \cdot m^{-2}$)	Total Biomass ($mg \cdot m^{-2}$)
C2	2015	May	178.07	140.99	18.83	337.88
		June	661.54	425.27	142.57	1229.37
		July	2417.43	266.46	714.71	3398.60
		August	1775.32	110.16	309.77	2195.25
		September	1296.63	70.54	113.19	1480.35
		October	226.96	70.34	16.92	314.22
	2016	May	112.79	628.04	106.82	847.66
		June	457.05	16282.55	320.43	17060.03
		July	200.46	338.12	46.82	585.39
		August	427.46	359.24	51.75	838.44
		September	3138.42	251.13	55.70	3445.25
		October	221.64	18.39	5.85	245.88
C6	2015	May	11.98	19.68	4.74	36.39
		June	332.13	202.41	29.19	563.72
		July	1926.53	138.54	263.49	2328.56
		August	3020.73	77.23	406.32	3504.28
		September	643.01	84.03	190.91	917.96
		October	127.32	43.35	32.23	202.90
	2016	May	4.92	10.85	1.55	17.32
		June	7.57	23.14	1.86	32.57
		July	99.76	98.91	2.46	201.13
		August	1032.87	316.40	59.35	1408.62
		September	2753.72	249.42	155.58	3158.72
		October	478.66	74.98	16.09	569.73

Station	Year	Month	Cladocera ($mg \cdot m^{-2}$)	Cyclopoid ($mg \cdot m^{-2}$)	Calanoid ($mg \cdot m^{-2}$)	Total Biomass ($mg \cdot m^{-2}$)
A1	2015	May	795.23	1135.72	19.64	1950.58
		June	3364.96	544.94	30.34	3940.24
		July	4774.86	373.03	37.54	5185.43
		August	2914.73	590.82	56.12	3561.68
		September	847.15	601.16	8.21	1456.52
	2016	May	435.05	794.37	33.39	1262.81
		June	4781.48	232.11	14.54	5028.12
		July	2405.58	385.91	1.41	2792.90
		August	917.16	351.24	15.33	1283.73
		September	766.62	585.18	21.80	1373.60
		October	1157.30	300.05	5.69	1463.03
A2	2015	May	871.82	1270.85	12.47	2155.14
		June	3028.55	539.43	21.88	3589.86
		July	1310.68	327.67	52.58	1690.93
		August	1532.90	666.36	41.71	2240.97
		September	1732.33	724.16	3.00	2459.49
	2016	May	1174.64	856.04	16.13	2046.80
		June	7456.95	127.95	79.05	7663.95
		July	2633.09	341.81	29.30	3004.19
		August	644.48	545.18	8.03	1197.68
		September	565.53	541.88	12.59	1119.99
		October	1529.60	550.58	3.12	2083.29
S4	2015	May	27.52	796.55	49.25	873.32
		June	382.88	628.76	28.48	1040.12
		July	632.51	231.64	33.79	897.94

Station	Year	Month	Cladocera ($mg \cdot m^{-2}$)	Cyclopoid ($mg \cdot m^{-2}$)	Calanoid ($mg \cdot m^{-2}$)	Total Biomass ($mg \cdot m^{-2}$)
		August	753.13	211.07	63.68	1027.87
		September	1044.47	128.08	21.29	1193.83
	2016	May	9.77	811.16	9.26	830.18
		June	215.91	362.28	26.15	604.34
		July	469.97	177.27	45.59	692.82
		August	1349.81	131.82	23.13	1504.76
		September	1626.74	174.75	24.68	1826.16
		October	313.13	201.41	7.85	522.38
S5	2015	May	25.74	574.22	81.95	681.91
		June	801.84	609.58	69.93	1481.34
		July	891.90	288.78	14.06	1194.74
		August	718.39	199.78	49.46	967.63
		September	722.99	188.82	15.61	927.42
	2016	May	8.34	693.29	7.38	709.01
		June	225.68	148.65	21.72	396.05
		July	528.42	93.78	45.90	668.10
		August	786.36	104.57	38.75	929.67
		September	652.47	130.74	27.51	810.72
		October	578.60	98.19	7.14	683.93

Table B-9. The candidate model set for zooplankton biomass including chlorophyll-a sampled with a 0.20 µm filter in Section 3.3.3.2.

Model	Adjusted r^2	*k*	logLik	ΔAICc	w_i	ER
- Chlorophyll-a + Temperature - Turbidity	0.49	8	-35.29	0.00	0.41	1.00
- Chlorophyll-a - Turbidity	0.48	7	-36.64	0.43	0.33	1.24
- Chlorophyll-a + Mean Water Residence Time + Temperature - Turbidity	0.49	9	-35.20	2.14	0.14	2.91

Note: Adjusted r^2 is the r^2 of the linear regression model adjusted for the number of variables in the model,

k is the number of parameters in each model including the intercept and error terms

logLik is the log-likelihood,

ΔAICc is the difference between the top model AICc value and subsequent model AICc values,

w_i is the model weight for each model

ER is the evidence ratio for each model, which measures the likelihood that the top model is better than model *i.*

Table B-10. The candidate model set for zooplankton biomass including chlorophyll-a sampled with a 0.75 µm filter in Section 3.3.3.3.

Model	Adjusted r^2	*k*	logLik	ΔAICc	w_i	ER
- Chlorophyll-a + Temperature - Turbidity	0.48	8	-37.79	0.00	0.38	1.00
- Chlorophyll-a + Mean Water Residence Time + Temperature - Turbidity	0.48	9	-36.96	0.67	0.27	1.40
- Chlorophyll-a - Turbidity	0.46	7	-39.66	1.47	0.18	2.09
- Chlorophyll-a + Mean Water Residence Time - Turbidity	0.46	8	-39.24	2.91	0.09	4.29
- Turbidity	0.43	6	-42.90	5.71	0.02	17.37

Note: Adjusted r^2 is the r^2 of the linear regression model adjusted for the number of variables in the model,

k is the number of parameters in each model including the intercept and error terms

logLik is the log-likelihood,

ΔAICc is the difference between the top model AICc value and subsequent model AICc values,

w_i is the model weight for each model

ER is the evidence ratio for each model, which measures the likelihood that the top model is better than model *i.*

9 APPENDIX C

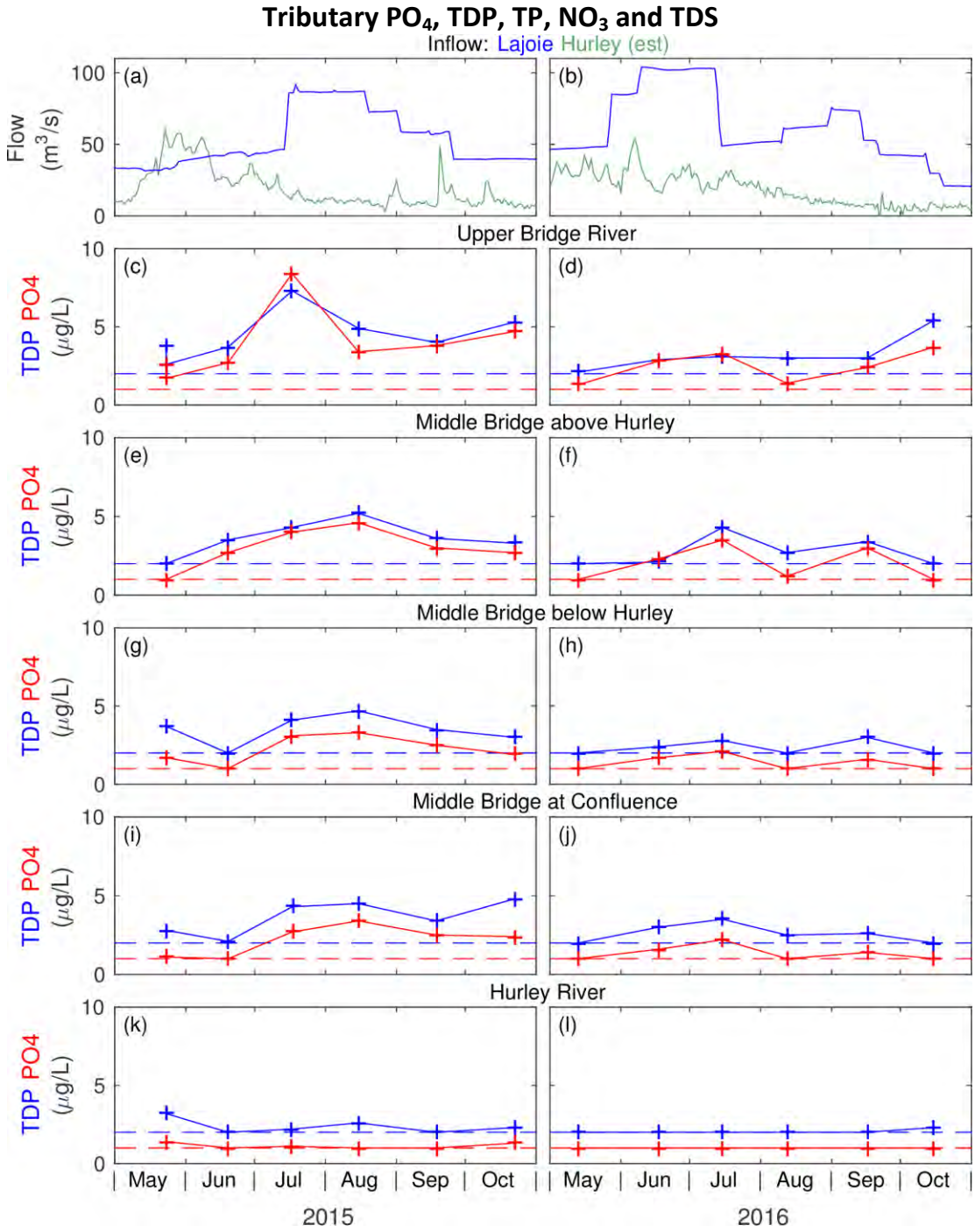

Figure C-1. (a) Outflow from La Joie Dam, and inflow from the Hurley River (estimated as 25% of the local flow). (b-f) Phosphate (PO4) and total dissolved phosphorus (TDP), May to October, 2015 and 2016.

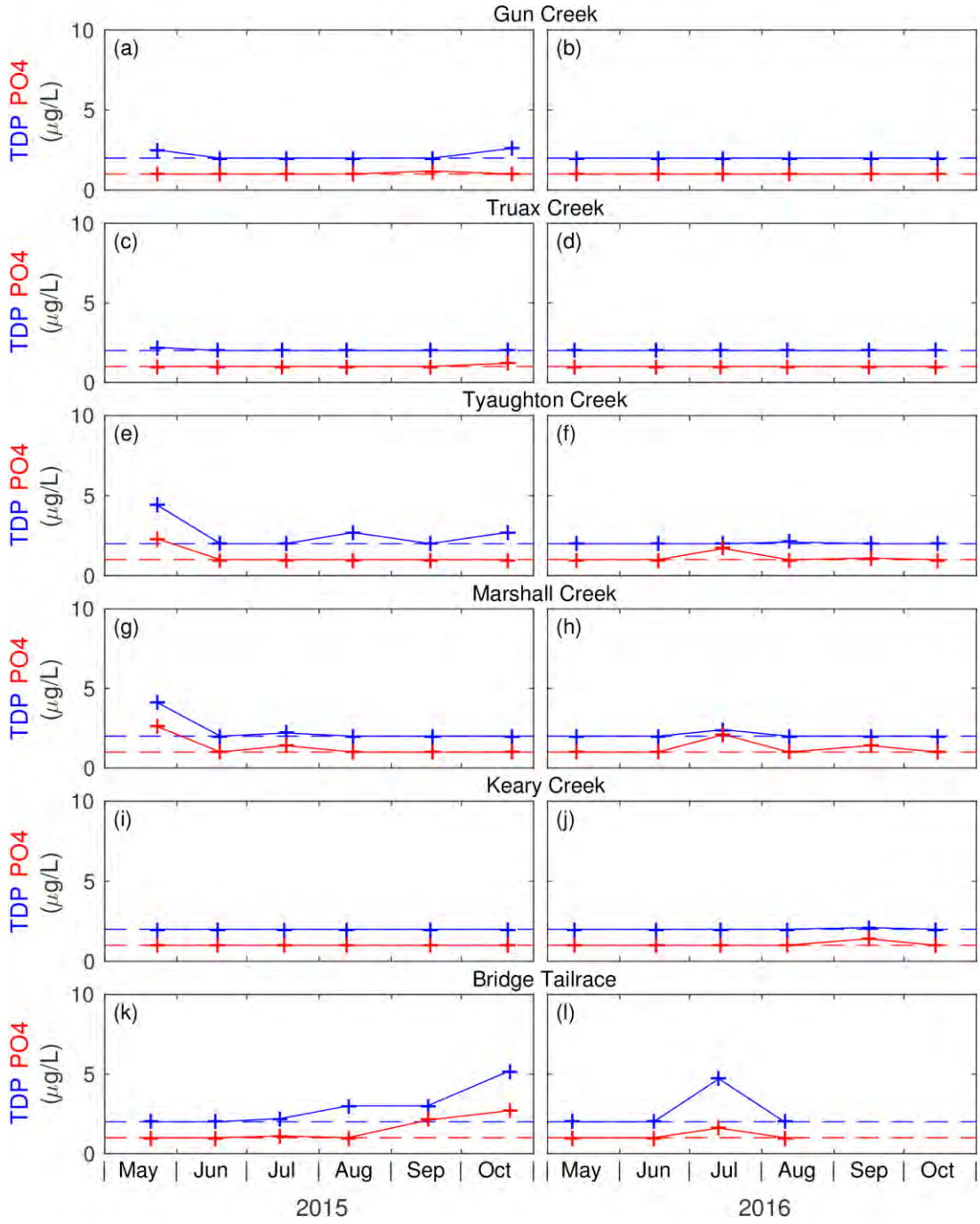

Figure C-2. (a-f) Phosphate (PO4) and total dissolved phosphorus (TDP), May to October, 2015 and 2016.

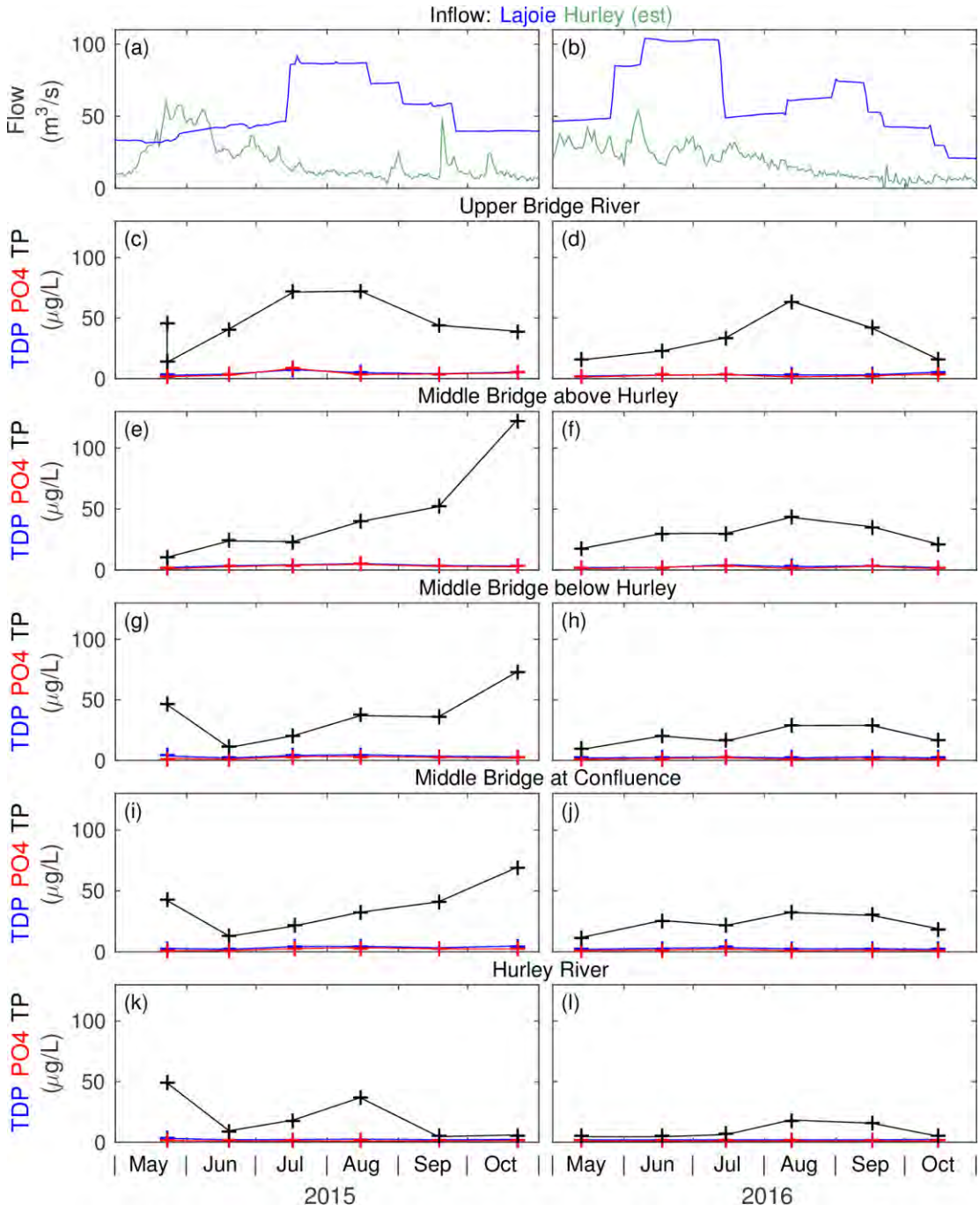

Figure C-3. (a) Outflow from La Joie Dam, and inflow from the Hurley River (estimated as 25% of the local flow). (b-f) Total phosphorus (TP), May to October, 2015 and 2016.

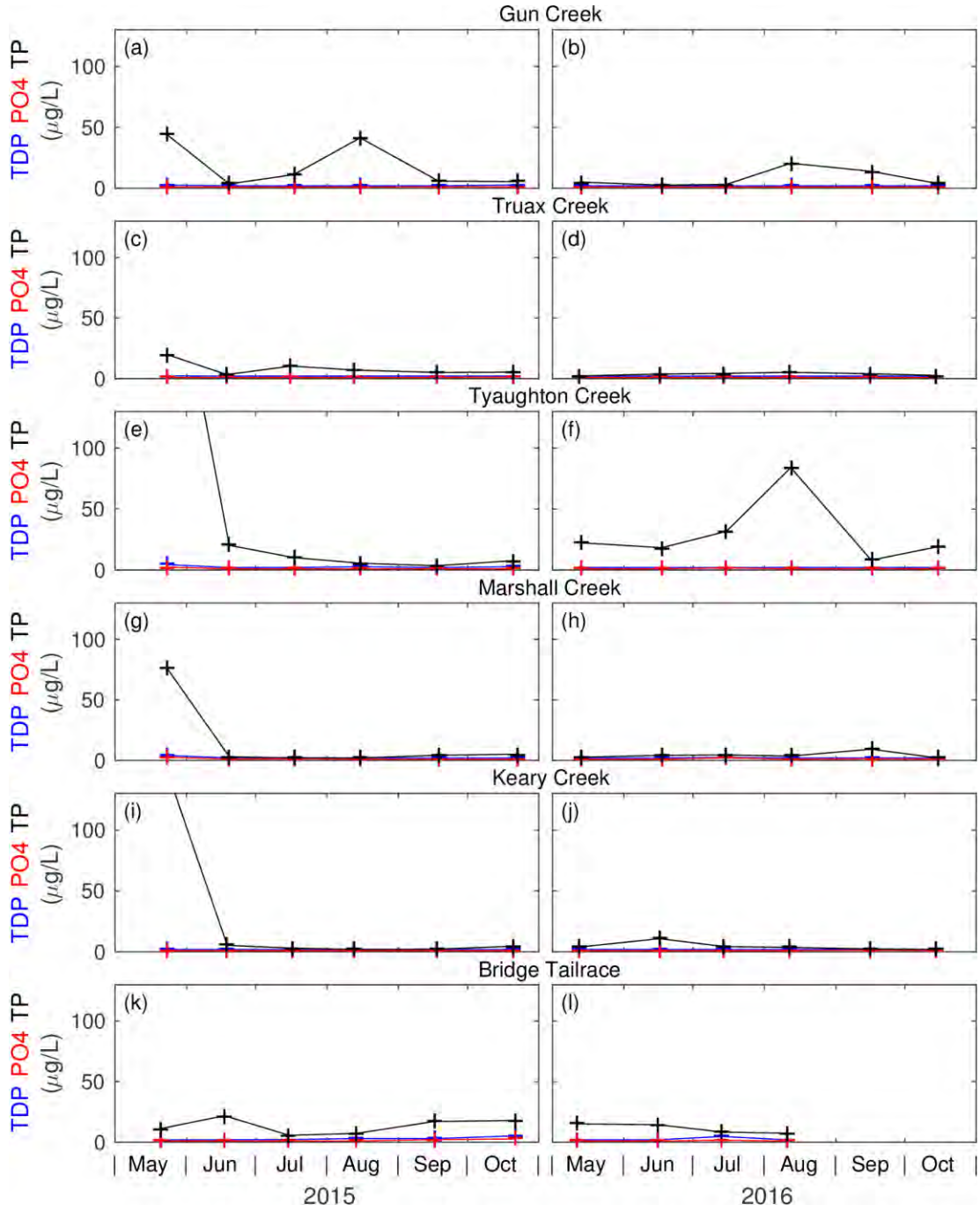

Figure C-4. (a-f) Total phosphorus (TP), May to October, 2015 and 2016.

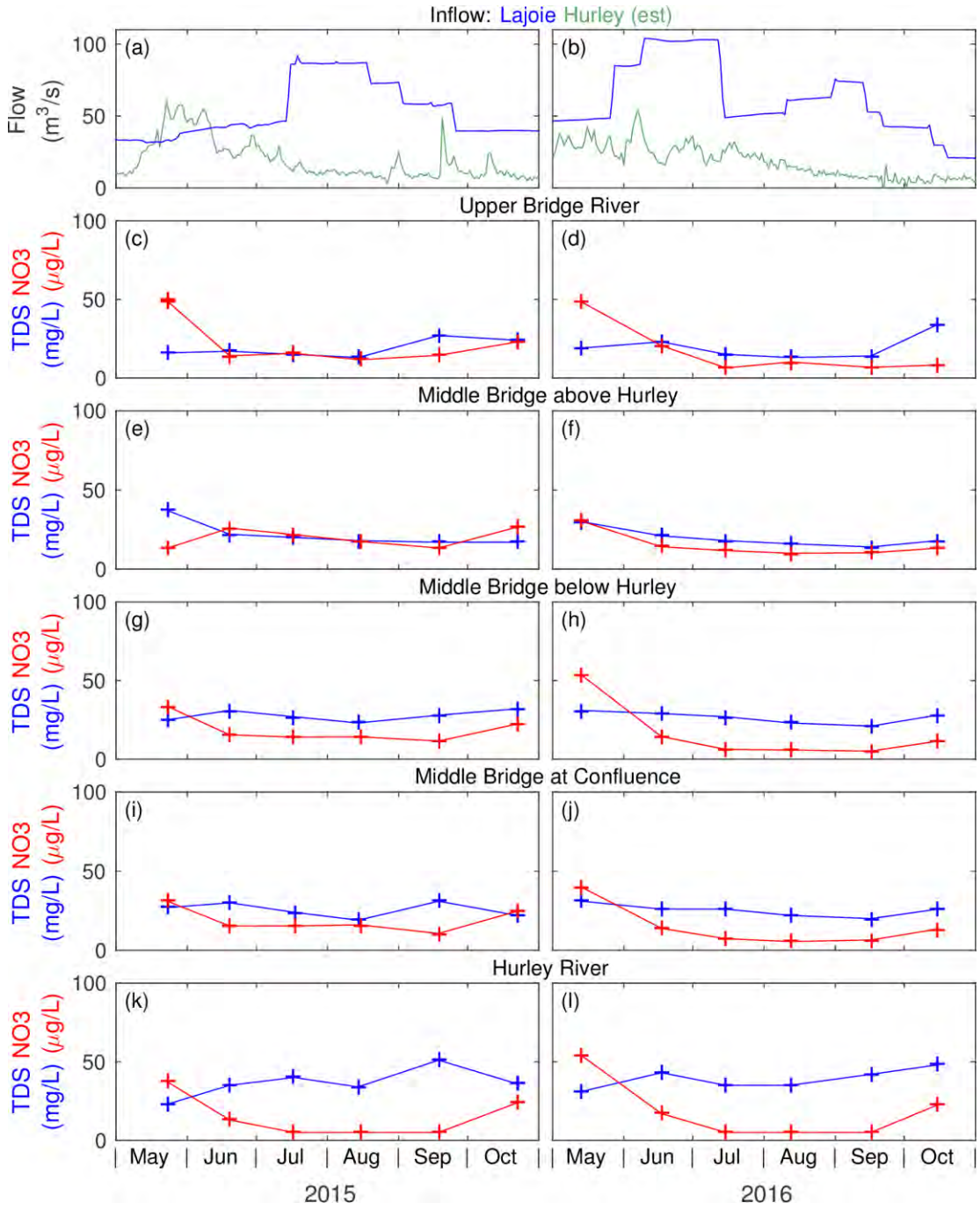

Figure C-5. (a) Outflow from La Joie Dam, and inflow from the Hurley River (estimated as 25% of the local flow). (b-f) Nitrate (NO3) and total dissolved solids (TDS), May to October, 2015 and 2016.

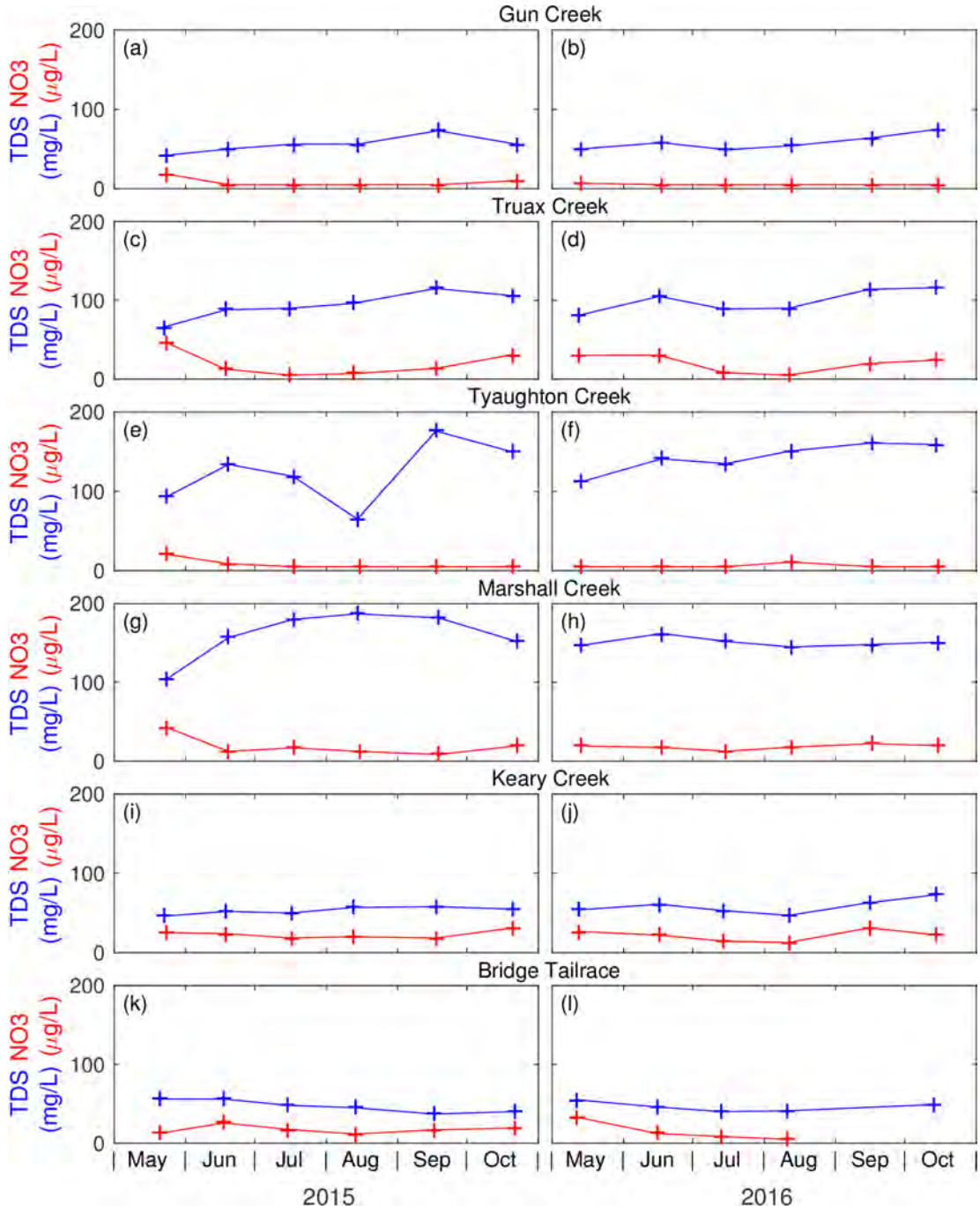

Figure C-6. (a-f) Nitrate (NO3) and total dissolved solids (TDS), May to October 2015 and 2016.